The Dissertation Committee for Colin O'Mara Hayes Certifies that this is the approved version of the following dissertation:

Directly-Patternable Benzocyclobutene Dielectric Materials

Committee:

Carlton Grant Willson, Supervisor

Christopher Ellison

Guangbin Dong

Stephen F. Martin

Christopher Mack

Directly-Patternable Benzocyclobutene Dielectric Materials

by

Colin O'Mara Hayes, B.A.

Dissertation

Presented to the Faculty of the Graduate School of

The University of Texas at Austin

in Partial Fulfillment

of the Requirements

for the Degree of

Doctor of Philosophy

The University of Texas at Austin

May 2016

Dedication

Mark and Ann Marie Hayes

Acknowledgements

My journey would be nothing without the people I came to know, work and live with here in Austin. First and foremost I need to thank Prof. Willson, who took a chance on me in my first year: On that day I promised I wouldn't let you down; I hope I succeeded. Prof. Willson gave me tremendous freedom to grow and learn as a graduate student: a luxury not everyone has during a PhD. Under another advisor's tutelage I doubt I would have become half the graduate. I also have to thank Donna Martin, Kathleen Sparks, and Mindy Maloney for their hard work keeping the group running and fighting the bureaucracy.

I never would have made it this far without the love and support from my parents and family. I don't think anyone has more loving and supportive parents who gave me every opportunity to succeed. Thank you, Mark and Ann Marie. Thanks are also owed to my brother and sister, Ryan and Kelsey: your support and enthusiasm have been invaluable.

I also must thank many Willson group alumni who have had a significant impact on my life here. Thank you to Drs. Michael Maher and Chris Bates. Their energy and drive inspired me to be a better student. I will never forget these two covalently bound at the hip. Many thanks to Dr. Ryan Mesch who provided many points on the arts of synthesis and craft brewing. Thank you Kensuke Matsuzawa and Kazu "Tin Man" Mori: your companionship and friendship were invaluable. Lastly, Dr. William Bell, you taught me many things. Palling around, photo lithography, how to identify a metal band in under ten seconds, how long can a human listen to the Star Wars Cantina Band song

before going bananas, to name a few. The journey would not have been the same without you.

I have many wonderful contemporaries in the Willson group as well. Team Packaging: Andrew Dick and Phillip Liu have seen our dielectric journey come a long way. Austin "Plane" Lane and Ben "Soft Serve" Cassidy, you formed a dynamic gauntlet few would cross. Xiaohan Wang, Anthony Engler, Jeff Self and Greg Blachut, Yusuke Asano and Nobu Someya were all tremendous colleagues. And of course, Paxton "Pax the Destroyer" Thedford: your affinity for destroying glassware was only matched by your ability to ROMP (and stomp). Your energy and enthusiasm were tremendous. I must also thank my colleagues during my summer at Intel Corporation. Dr. Brandon Rawlings and Dr. Tao Wu in particular expanded my horizons on microelectronics manufacturing.

This thesis would not be complete without the tremendous help of my collaborators at Georgia Tech. Many thanks to Prof. Paul A Kohl, Dr. Brennen Mueller and Jared Schwartz. Without your help the world would never know what some of these materials could do. Besides the Kohl group, Prof. Chris Ellison and his group have also been instrumental in my research. Many additional thanks to Reika Katsumata and Sunshine Zhou for the insight and friendship, and thanks to Dr. Dustin Janes for his wisdom, humor and excellent original music compositions. This list must go on: Prof. Guangbin Dong and Penghao Chen must also be acknowledged for their welcoming group and essential assistance. Without their help, the low temperature BCB project would still be a pipe dream.

Lastly, some of the most important people to this work my friends in Austin. Alex Goodenough, Danny Klosowski, Laura McCaslin, Zachary Kasun, John Ketchum, Aarkarsh Saxena, and Rohan Khade all provided perhaps the most important thing to a

graduate student: friendship. Many thanks to Janine Elliott and Kovu, I would have had a fraction of the fun here in Austin living with anyone else. A special thanks belongs to Nik Savage, who I had the pleasure of beginning my career in chemistry with at College of the Holy Cross, and the privilege of following to Austin. I wouldn't be here without you. Finally, the person who shaped these years the most: Victoria Garza. I don't know if I could have made it through these years without your support. A separate thesis could be written on why you were instrumental to my success, but for now these words will have to do.

Directly-Patternable Benzocyclobutene Dielectric Materials

Colin O'Mara Hayes, Ph.D.

The University of Texas at Austin, 2016

Supervisor: Carleton Grant Willson

Silicon Valley, America's bastion of innovation is named for the tiny pieces finely patterned silicon transistors that are the "brains" of all modern computational devices. However, without the ability to protect these valuable chips and translate their electrical signals to other hardware, silicon transistors are useless to the world. The demand for these microelectronic packages to perform better, cost less and be made in high yield is perhaps the next great challenge in the microelectronics industry.

This dissertation covers several approaches to next generation packaging materials. In chapter two, the design, synthesis and characterization of long wavelength photobase generators for patterning polyimides is discussed. The rest of the dissertation focuses understanding and applying benzocyclobutene (BCB) thermosets to a packaging application. BCB materials have been combined with polyhedralsilsesquioxane (POSS), ring opening metathesis polymerization (ROMP) norbornenes, and addition polymer norbornenes to produce several original resins with interesting and attractive properties. New chemistry has been employed to understand the relationship of the BCB electrocyclic ring opening and Diels Alder crosslink.

Table of Contents

List of Tables

List of Figures

Chapter 1: Introduction to Photolithography

1.1 Ab Initio

A computer is any machine with physical components that can carry out mathematical or logical operations quickly and automatically. A discussion of what a computer truly is and where it began could stretch back to the abacus, however the modern era of computing (and therefore the shape and form of the world as we know it today) began with Moore's Law. Gordon Moore, then an employee of Fairchild Semiconductor, predicted that number of components on an integrated circuit "chip" would double every year[1]. This observation has since been applied to microprocessors and memory components, however the takeaway has been this: Moore's prediction has become a self-fulfilling prophecy, the Stockdale Paradox of the industry. The entire electronics industry strives to match the fervent pace of Moore's Law to this day, and the result has been to place an exponential growth in computing power at the disposal of mankind. The key to driving this progress has historically been the process of photolithography, which has allowed device dimensions to shrink continuously through innovation.

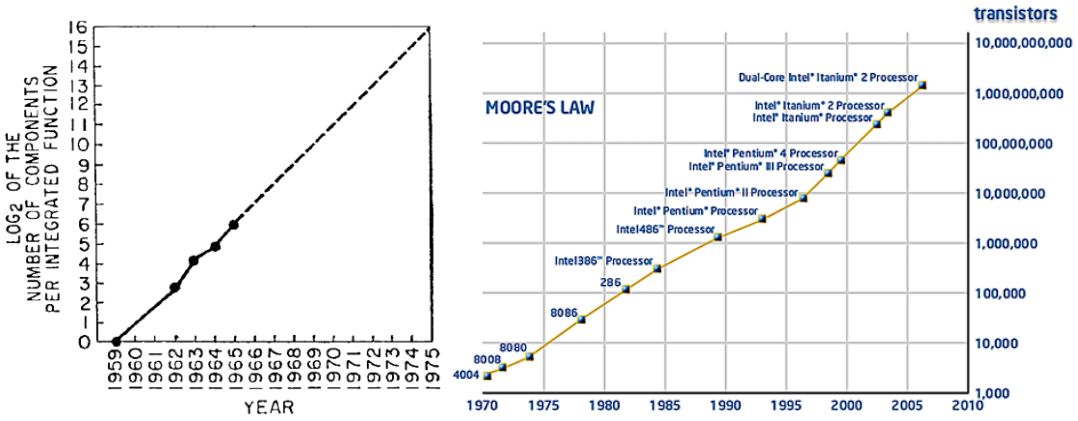

Figure 1.1: Moore's initial observation (left) and Intel microprocessors from 1971 to 2006 (right). *Copyright 1998, IEEE.*

1.2 PHOTOLITHOGRAPHY

The key process that defines the physical dimensions of the circuit elements on a silicon chip, photolithography operates very similarly to simple photography. While photography creates an image based on how light reflects off of an object, photolithography creates an image when light passes through a pre-defined mask. Both processes rely and photochemical operations to distinguish one region of an image from another. Depending on the type of chemistry employed, the regions exposed in photolithography can either be rendered insoluble or soluble in a subsequent development step, resulting in positive or negative tone images (Figure 1.2), replicating the patterns on the mask.

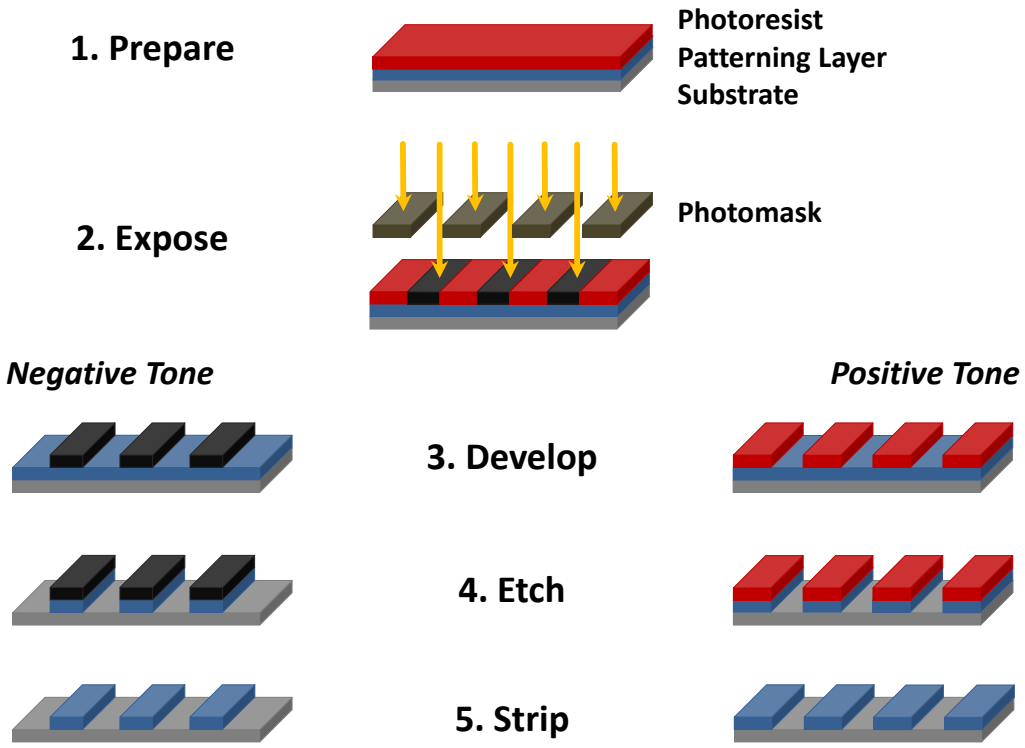

Figure 1.2: Depiction of the photolithographic process. Photoresist (red) is coated onto a patterning layer (blue) supported by a substrate (light gray). The film is exposed through a photomask (dark gray), creating a chemical change in the exposed area. This alters the solubility of the polymer, which either is removed (positive tone, right) or remains (negative tone, left).

The photolithographic process is performed, (for example) on silicon wafers which contain a thin layer of native silicon dioxide bearing terminal silanol (-OH) groups. It is commonplace to employ adhesion promoters which are typically silanes with the general formula $RSiX_3$ or hexamethyl disilazane (HMDS). The use of adhesion promoters can (predictably) improve the adhesion of the photoresist to the wafer surface and its uniform coating. The specific and controlled thickness of the photoresist is managed with a process known as spin coating. After the photoresist is deposited, the wafer is spun very quickly on the order of 2000 to 3000 rotations per minute (rpm). The

result is an exceptionally uniform film with an edge bead that can be removed with a wet process. The exact thickness desired for a given resist is often determined experimentally and is inversely proportional to the square root of the spin speed (ω) (Equation 1.1).

$$Thickness \propto \frac{1}{\sqrt{\omega}} \tag{1.1}$$

After spin coating, the wafer is usually subject to a post-apply bake (PAB) to remove residual solvent. This is done for several reasons, in general to "stabilize" the film, making it less susceptible to particle contamination and to improve adhesion. The photoresist is then exposed through either proximity, contact (used exclusively in this thesis), or projection lithography. Contact lithography offers good resolution, but particles on the mask can create defects in the underlying photoresist, thus the process is not suitable for large throughput. Proximity printing solves this problem but at the cost of a severe decrease in resolution. Modern fabrication facilities (fabs) rely exclusively on projection printing. The maximum achievable resolution for projection lithography is defined by the Raleigh Criterion[2] (Equation 1.2).

$$R = k_1 \frac{\lambda}{NA} \tag{1.2}$$

Where R is defined as the resolution, λ is the wavelength of the light source, NA is the numerical aperture ($NA = n \sin \theta$), and k_1 is a constant determined by specific lithographic techniques. The minimization of resolution is the focus of great research in the microelectronics industry, however this thesis focuses on dielectric and package level materials, where desired resolution (on the order of 5 μm half pitch) at this level is easily obtained through available techniques and the minimization of resolution will not be discussed prominently.

Regardless of printing method, the photoresist chemistry must be designed so that upon exposure a solubility switch is induced (a more in depth discussion on photoresist chemistry will follow later). When this switch is induced, the photoresist is immersed in a

solvent called a developer. The solvent must be chosen so that it selectively dissolves either the exposed or unexposed region, creating an image. The solvent is often a basic aqueous solution (such as tetramethyl ammounium hydroxide) in the case of positive tone resists and a blend of organic hydrocarbons in the case of negative tone resists.

Once the regions of an image have been defined by development, the image is transferred into the underlying substrate with another step. Two prominent patterning processes are "fluoride etching" and ion implantation. In fluoride etching, hydrofluoric acid is used, which dissolves the underlying inorganic silicon but is blocked by the organic photoresist, thus replicating the photoresist pattern in the substrate. In ion implantation, controlled bursts of silicon dopants such as atomic boron are targeted at the wafer, creating selectively doped regions in the silicon and thus the physical basis of transistors. Lastly the resist is stripped using a suitable solvent, leaving a finely patterned silicon wafer behind.

1.3 EARLY PHOTORESIST CHEMISTRY

In 1954, Kodak introduced a high performance negative tone resist marketed as Kodak Thin Film Resist (KTFR). Cyclized isoprene as the resin was formulated with the bis-azide 2,6-bis(4-azidobenzylidene)-4-methylcyclohexanone (BACM, Figure 1.3).

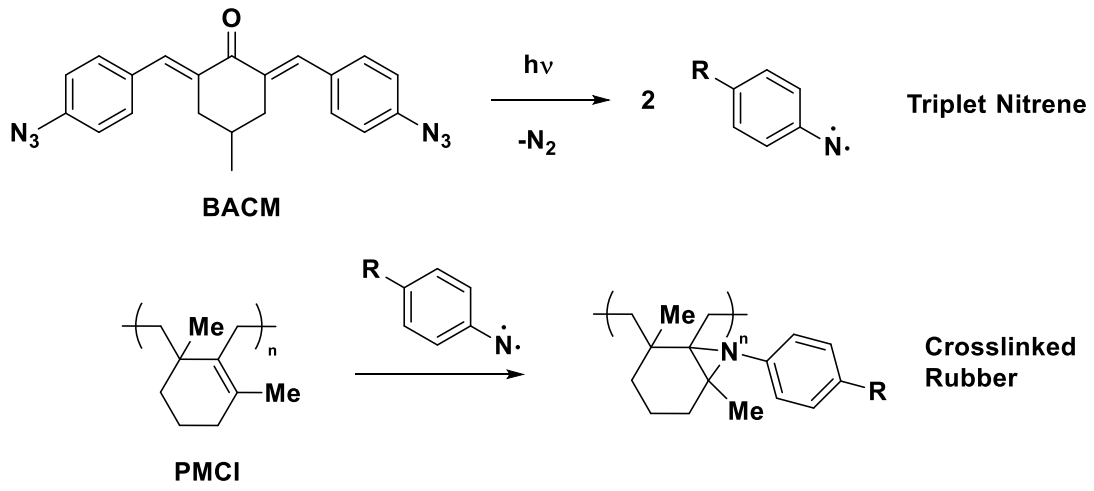

Figure 1.3: Schematic representation of KTFR chemistry. A bifunctional azide reacts under exposure to form the triplet nitrene, which can insert into double bonds to form aziridines, thus creating a cross-link.

This material became the lithographic work horse of the semiconductor industry for the next decade due to its reliability and ability to form well defined features on the ten micron length scale[3]. However, KTFR hit a wall as features approached single micron dimensions. The solubility switch in the resist is based on a change in molecular weight. The drawback of this approach is that any developer that dissolves the unexposed region will also slightly prefer to swell the exposed region, as the higher molecular weight material still contains functional groups compatible with the developer. At micron length scales and aspect ratios approaching 1.0, the consequence is dramatic swelling and deformation of the remaining resist. The swollen features are not useful for substrate pattern transfer due to their excessive line-edge roughness (Figure 1.4).

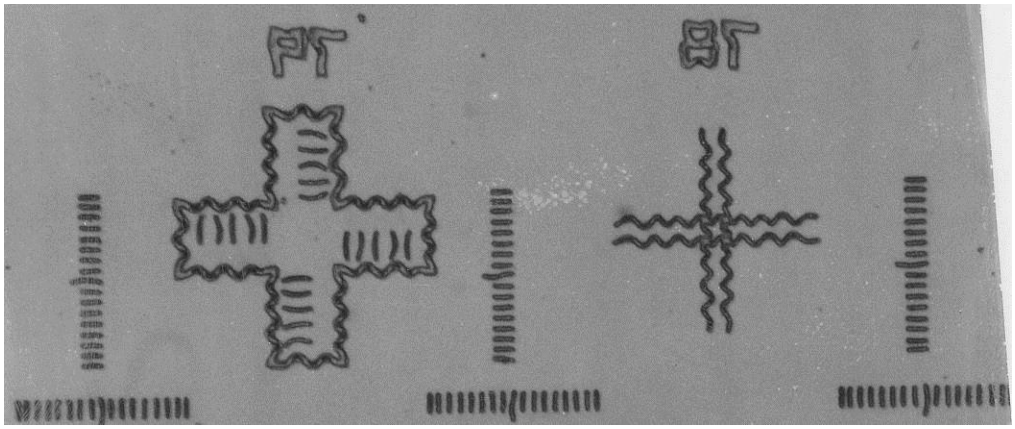

Figure 1.4: Swelling in KTFR.

An alternative to KTFR had already been developed by Kalle AG in a material known as Ozatec. Ozatec used a novolac based resin (phenol and formaldehyde condensation polymer) mixed with a photoactive compound diazonaphthoquinone (DNQ). When exposed to light, DNQ outgasses nitrogen and creates an alpha-carbenoid species, which undergoes the Wolff rearrangement to form the ring-contracted ketene. The ketene is hydrolyzed by water to the corresponding carboxylic acid. This transformation had the profound effect of creating a vast difference in the dissolution rates between exposed and unexposed regions of DNQ-Novolac in aqueous base, creating a robust positive tone resist with fine patterning abilities exceeding that of KTFR.

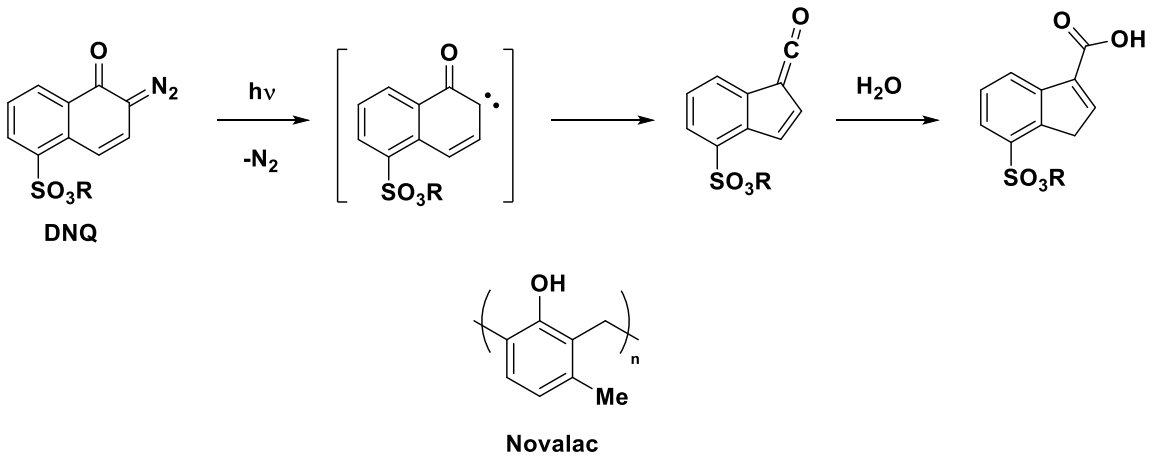

Figure 1.5: Wolff rearrangement of DNQ upon light exposure and structure of resin novolac.

DNQ-Novolac photoresists continued to be an industry standard from the early 1970's until the 1980's. Resists were adapted as light sources shifted from g-line (436 nm) to the shorter wavelength h-line (405 nm) and i-line (365 nm) to increase feature resolution (in accordance with the Raleigh Criterion). Because of its high pattern fidelity and excellent etch resistance, DNQ-Novolac continues to be used in various lower resolution applications to this day. However, as the industry sought to continue Moore's Law and to push resolution well into the nanometer domain, a new chemistry needed to be developed.

1.4 Chemical Amplification

In order to supersede DNQ-Novolac resists, a new paradigm of resist chemistry had to be developed. Once more based off of the novolac resin, the concept of an acid labile protective group for the phenol functional group emerged. The first positive-tone photoresist based on this concept was developed by G. H. Smith of 3M in 1973. Smith used a tetrahydropyranyl (THP) protective formulated with a sulfonium salt based photoacid generator[4] (PAG, Figure 1.6). The catalytic approach resulted in many

solubility changing events on the resin with a single photon, a concept later referred to as "chemical amplification." 3M, however, chose not to capitalize on this resist chemistry.

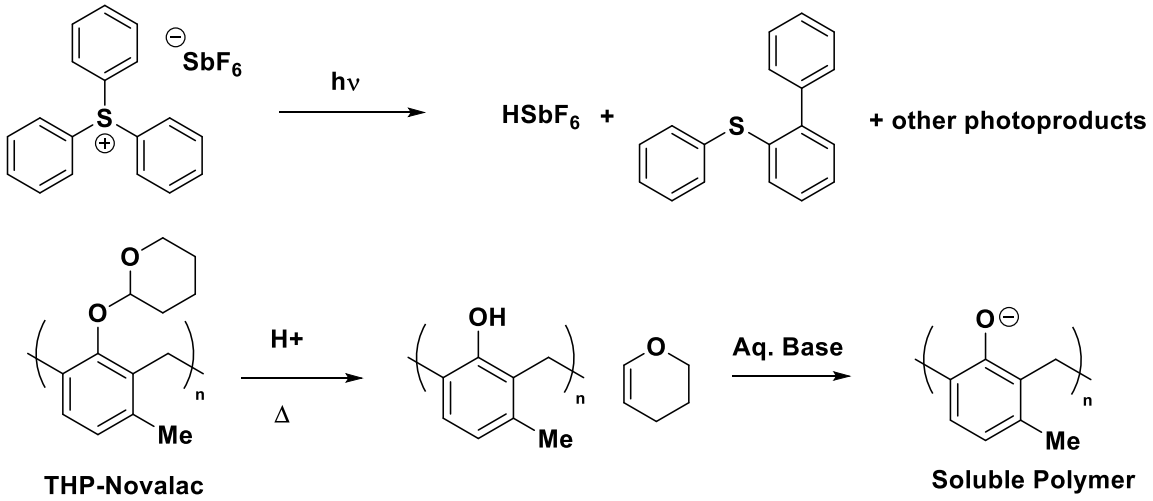

Figure 1.6: Scheme of 3M's chemically amplified photoresist THP-Novalac.

In the early 1980's, Grant Willson, Jean Fréchet and Hiroshi Ito at IBM developed the first chemically amplified positive tone resist that would change the process of lithography for the foreseeable future[5]. The group used a similar design to that of Smith, but instead of novolac as a resin, poly(para-hydroxy styrene) was exploited due to its superior transparency in the deep UV region of the electromagnetic spectrum. By protecting the phenol with a tert-butyl carbonate, acid catalyzed deprotection could occur in the same general manner as Smith's resist (Smith's resist design also required one equivalent of water per deprotection event, where the tert-butyl carbonates do not) (Figure 1.7).

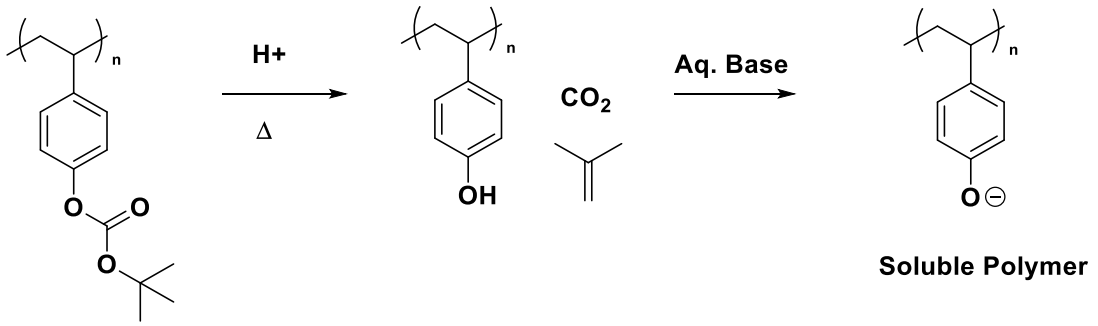

Figure 1.7: The Willson et al. chemically amplified resist strategy based on para-hydroxy polystyrene.

The PAG in the resist formulation was also sulfonium salt derived. The resist proved to be very effective: patterning could be achieved at sensitivities as low as 1 mJ/cm^2 at 254 nm irradiation, a two order of magnitude improvement over DNQ-novalac resists. Willson et al. also found that the formulation could form a positive tone image if developed in aqueous base or a negative tone image if nonpolar organic developers such as anisole were used. The primary drawback to this technique is that the process is highly and adversely affected by even parts per billion basic amine contaminations, eroding image quality with "T-topping" of the image. Amine contaminants can be eliminated through rigorous carbon filtration of air in a fab.

Since the Willson et al. development of the chemically amplified resist, there have been many subsequent generations that have optimized the resist chemistry. Resists have utilized various monomers in the backbone such as norbornenes and maleic anhydrides, and the protective group has also been varied. However, none of these represent a complete shift in resist strategy, which still consists of an acid catalyzed deprotection event that drastically chances a polymer's solubility.

1.5 INTERCONNECT DELAY

While the advances of lithography and chemical amplification allowed the number of transistors per chip to reach billions in count, an integrated circuit does not function until all the transistors are connected to one another and the outside world. As photolithography enabled more and more transistors per chip, the challenge of connecting all of these logic devices in the "Back End of the Line" (BEOL) processes magnified considerably. Further, the interconnects became a limiting factor in the performance of an integrated circuit. Major challenges of modern electrical engineering include the obstacles of Place and Route. Place is the challenge of where to put transistors in an IC, and Route is the challenge of how to connect them in the shortest, most efficient way possible. Modern ICs use more than one layer of metallization to optimize Place and Route, allowing for more flexibility in routing wires at the tradeoff of additional cost.

The clock speed of a chip is a function of both how fast a transistor can be switched on and off as well as how quickly this signal can propagate along a wire. There is a slight delay of each signal as a transistor switches on or off, and this is called τ, or the RC time constant.

$$\tau = RC = \rho_m \varepsilon_d \frac{L^2}{t_m t_d} \tag{1.3}$$

The RC time constant is described in equation 1.3. The constant is equal to Resistance (R) times Capacitance (C), which is equivalent to the resistivity of the metal in question (ρ_m) times the dielectric constant of the insulator (ε_d) times the square of the length of the wire divided by the product of the thicknesses of the metal and insulator. It is evident from equation 1.3 that there are several ways one could minimize interconnect delay[6]. The first is to switch to a metal with lower resistivity, which the IBM did in 1997 when they moved to copper ($1.7*10^{-6}$ Ω cm) from aluminum ($2.8*10^{-6}$ Ω cm). You could also solve the challenges of Place and Route to minimize wire length; however the

problem is so complex with billions of transistors that it's considered impossible to be sure that Place and Route are globally optimized. This leaves the dielectric constant of an insulating material.

The industry has long stuck to silicon dioxide (K = 3.9, $\varepsilon_d = K\varepsilon_0$) as its insulator of choice at the chip level, and organic polymers with oxide fillers (varying K) at the packaging level (the absolute minimum value of K = 1 for a vacuum). While it is very difficult to develop a material with a low dielectric constant, this represents a great opportunity to develop materials to tackle the challenge of minimizing interconnect delay. With new chemistry, polymer resins could be developed that take K to new lows.

1.6 Packaging and Coefficient of Thermal Expansion

While most of this chapter has been dedicated to manufacturing processes responsible for transistor formation (the die), most of this thesis will focus on materials developed for applications in microelectronics packaging, which connect chips to one another and the outside world. The package is the interface between the die and motherboard, effectively translating the logic computations to the rest of the computer hardware, and bringing power to the processors. The package continues to build on the metallization layers of the die, except now metallization occurs on the micron to millimeter length scale (as opposed to nanometer scales on the die). As such, packaging is also subject to the concerns of Place and Route, however at fewer metallization layers and much larger interconnects, the problem is therefore simpler to optimize.

A parameter of principle concern at the packaging level is the coefficient of thermal expansion (CTE) of the insulating material. First generations of packaging materials were constructed from inorganic ceramic materials, which achieved the goals of very small CTE, but these materials were costly and often had substandard dielectric

properties. Current generation packaging insulation is constructed of cheap organic polymeric materials, which suffer from high (100-200 ppm/K) CTEs, but typically have a low dielectric constant, mechanisms for patternability, and low cost. The primary consequence of a high CTE is warpage during soldering, curing, or heat shock reliability testing. Warpage of the package can lead to delamination of metallization layers and cracking, thence total device failure.

$$\alpha_L = \frac{1}{L}\frac{dL}{dT} \tag{1.4}$$

CTE of a given linear direction is given by equation 1.4. It is a function of the instantaneous change in length per unit of temperature normalized by the initial dimensions. While many think that a single number can describe the CTE of a material that is often not the case. Indeed, many materials are isotropic, and one number can describe the CTE in any direction, but more often than not, materials are unexpectedly anisotropic. Many factors can contribute to anisotropy, such as asymmetrically crystalline materials. Long, rigid, ladder-like polymers often lie preferentially in the plane of a film, creating anisotropy. Even perfectly isotropic materials can have anisotropy induced through an anisotropic deposition method, such as spin coating. All this means that one must think critically about the thermal expansion of a material when designing for a microelectronic device. Expansion in the plane of each metal layer ($CTE_{xy} = \alpha_{xy}$) primarily leads to warpage and the aforementioned consequences. However, one cannot ignore the expansion out of the plane of each metal layer ($CTE_z = \alpha_z$), which can lead to delamination and thus another mechanism of device failure.

The CTE of a material can be thought of at the atomic level as the change in average interatomic distance normalized for dimensions. This can be best understood by an examination of the Morse Potential, which describes the asymmetric relationship of interatomic distance as a function of different quantized energy states. The lowest energy

state at the trough minimum is for the case where T = 0 K, and subsequent increased in temperature increase the average bond length. The Morse potential relationship is given by equation 1.5.

$$V(r) = D_e(1 - e^{-a(r-r_e)})^2 \quad (1.5)$$

Where V represents the energy of the system, r is the internuclear separation, r_e is the equilibrium bond distance, D_e is the well depth (also referred to as Bond Dissociation Energy or BDE). When comparing two hypothetically isotropic crystalline materials, the material with the greater BDE will have a deeper, narrower well, and thus a lower average interatomic distance over a range of temperatures (and thus a lower CTE).

Figure 1.8 shows such a case:

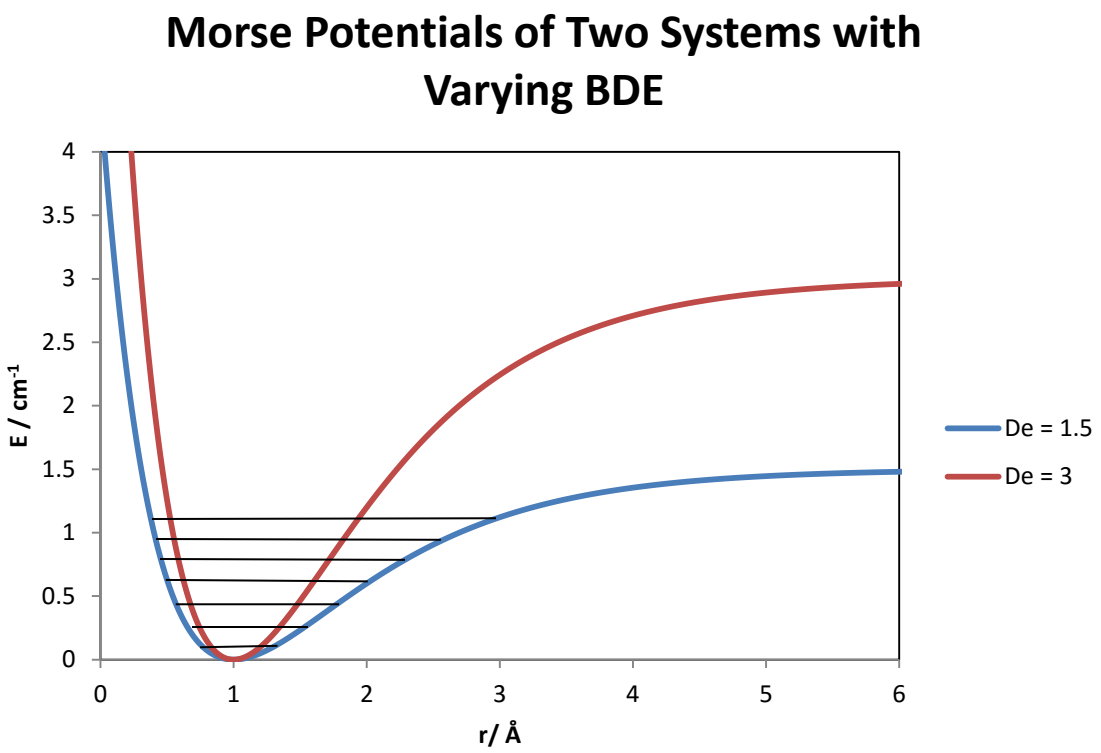

Figure 1.8: A Morse Potential of two systems with a factor of two differences in BDE. The resulting shape and depth of the well corresponds to the CTE of the materials in a two hypothetically identical, isotropic crystalline materials. The lines drawn in the well represent hypothetical different quantized states in increasing energy (and increase interatomic distance).

By creating two different Morse potential energy wells with BDE's arbitrarily differing by a factor of two, one can clearly see the effect of BDE on the shape and depth of the resulting energy well. In the case of the red (deeper) well, increasing the energy of the system raises the population of atoms in higher energetic states, thus increase the average interatomic distance and CTE of the material. However, in the shallower (blue) well, it can be clearly seen that the energy that raises the system to the same quantized state results in a greater average interatomic distance, and thus a larger system CTE. The

conclusion from this relationship is that overall, stronger bonds should be designed into a low CTE material.

In sum, there are three major design challenges to the insulating material of a modern packaging device. The material must have a low dielectric constant (ideally less than 3.0) (and low dielectric loss). Two: match CTE to a value as close to Silicon (3 ppm/K) as possible. Three: be inherently patternable, thereby cutting down on process steps. The goal of this work is to solve these materials challenges.

DISSERTATION STRUCTURE

Chapter one provides a brief history of photolithography and background to the challenges of designing dielectric materials, low CTE materials and packaging. The central goal of this thesis is to design, develop and demonstrate materials that can meet all of these challenges. Chapter 2 discusses the synthesis and characterization of a photobase generator designed to enable direct patternability of commercial polyimide materials. Chapter 3 examines unusual hybrid materials based on polyhedral silsesquioxanes and benzocyclobutene. Chapter 4 relates a new chemical method developed in order to access derivatives of benzocyclobutene that thermoset at a greatly reduced temperature. Chapter 5 examines new benzocyclobutene-norbornene crosslinkable polymers and the effects of crosslinker density on CTE in ring opening metathesis polymerized polynorbornenes. Chapter 6 highlights optimized palladium-based methods for the addition polymerization of polynorbornenes, including new, rigid, dielectric polymers. Lastly, Chapter 7 summarizes work done towards the synthesis of high T_g top coats for block copolymer lithography (although not necessarily germane to the thesis as a whole, the work exploits synthetic techniques developed for the packaging project). Together, this thesis expands upon the versatility and understanding of

properties and potential of benzocyclobutene based thermosets for packaging applications.

Chapter 2: Synthesis and Characterization of a Visible Wavelength PBG

2.1 INTRODUCTION

When considering a candidate for dielectric materials for packaging, a logical first candidate would be polyimides. Polyimides are a ubiquitous class of step growth polymers made from condensation of a diamine and a dianhydride to yield polyamic acid, which under thermal treatment eliminates water to form polyimide. Polyimides tend to be rigid, rod-like structures that possess excellent thermal stability, low thermal expansion, high tensile strength, and moderately low dielectric properties[7]. Polyimide has already found many applications, including connecting the circuit board to the monitor in laptop computers, high temperature adhesive tape, and even the solar sails of the Japanese IKAROS spacecraft.

One of the most widely used commercial polyimides is the DuPont product Kapton®, the condensation product of 4,4'oxydiphenylamine (ODA) and pyromellitic dianhydride (PMDA, Figure 2.1).

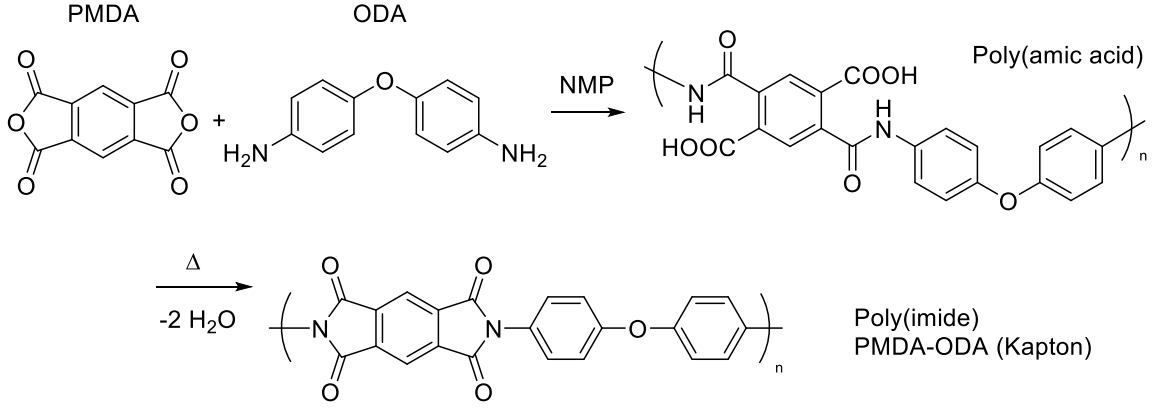

Figure 2.1: Synthesis of step growth polyamic-acid Kapton precursor and the imidized polyimide Kapton.

The resulting step growth polymer is a polyamic acid. Upon thermal treatment, imidization occurs, removing two equivalents of water per monomer repeat unit. Kapton has reasonably low CTE (about 20 ppm/K in the xy plane), and a dielectric constant of about 3.1, but its real benefit lies in its availability and relatively low cost. However, Kapton is not directly patternable. Major efforts have been made to render polyimides photosensitive. The earliest successful efforts focused on replacing the acid groups with hydroxy-ethyl methacrylate (HEMA, Figure 2.2). The mechanism of patterning is a radical initiated methacrylate polymerization, resulting in a negative tone photoresist. This mechanism successfully produces high resolution, high aspect ratio images, although it comes with a cost. During the imidization process, the HEMA groups are eliminated and volatilized. The result is dramatic shrinkage of the film on the order of 50% of original dimensions. This level of shrinkage highly limits the dimensions of the polymer and can cause layer to layer stress, inducing warpage. As such, this mechanism of patterning is not viable for modern packaging devices.

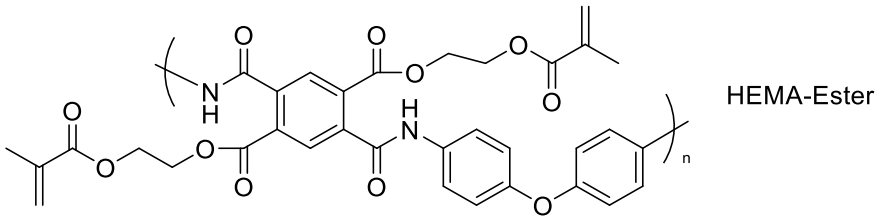

Figure 2.2: A polyamic acid HEMA precursor. The acrylates undergo a high resolution lithographic step to form desired features, but are volatilized upon curing, creating significant and undesired shrinkage.

A different method of rendering polyimides photosensitive was developed at IBM in the early 1990s. It was noticed than amine impurities in the casting solvent N-Methyl-2-Pyrrolidone (NMP) caused “premature” imidization of polyimide prepolymer. As a

result, it was realized organic amines could be exploited as an organocatalyst for imidization[8,9]. Frechét also discovered that rate of imidization scales with increasing basicity of a given amine[10], indicating general base catalysis.

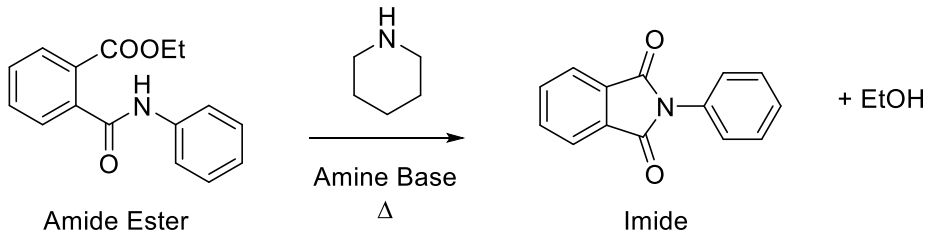

Figure 2.3: Amine catalyzed imidization of an amide ester.

This knowledge was leveraged to create the first chemically amplified, negative tone, photopatternable polyimides using ortho-nitro carbamates as photobase generators.[11,12]. This process benefits from greatly reduced shrinkage compared to the HEMA based system, and can resolve intermediate feature sizes in thin films[13]. A problem with the ortho-nitro carbamate chemistry, however, is that these compounds are only active in the ultraviolet regions of the spectrum[14], meaning that patterning can only be done with light sources such as i-line lamps (365 nm)[15]. While this is not a problem for thin films, most polyimides have very high absorption at shorter wavelengths so light cannot penetrate the thicker films required for packaging applications (on the order of 15-30 μm). Figure 2.4 shows a UV-vis spectrum of PAETE, the para-ethyl ester of Kapton precursor.

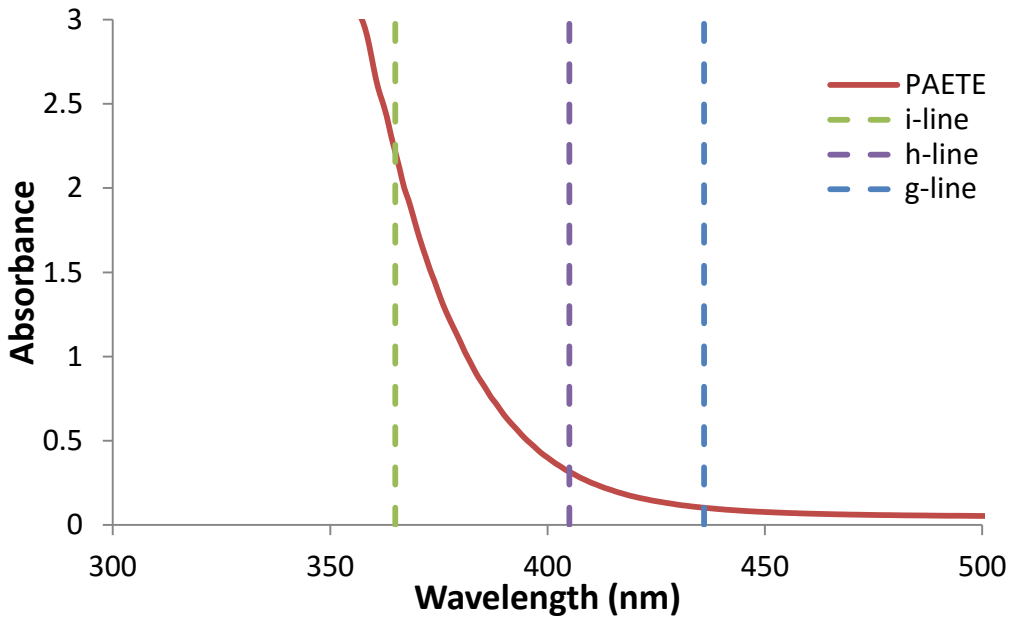

Figure 2.4: UV-vis spectrum of a 7 µm thick film of Kapton® ethyl ester precursor

While Kapton® precursor has significant absorbance at i-line, there is minimal absorbance at g and h-line. Thus, if it were possible to red shift the activity of the photobase, it might be possible to pattern thick films of Kapton® for packaging.

Several problems occur when attempting to red shift the photobase generator[16]. Functionalization of the *o*-nitrocarbamates with electron donating methoxy groups does move the activity of the photobase closer to i-line, but at the cost of significant loss of quantum efficiency and thermal stability whilst still not being sufficiently red shifted[17,18,19]. A new chromophore, recently developed by BASF as a photoacid generator (PAG)[20], demonstrated excellent photoactivity based on a phenylnitrile thiophene scaffold. It was proposed that by repurposing the chromophore to serve as a carbamate, one could photochemically release amines at visible wavelengths, thus enabling thick film patterning of commercially available Kapton®. This chapter

describes the synthesis and characterization of a new photobase generator with the direction of elucidating the mechanisms of the chromophore.

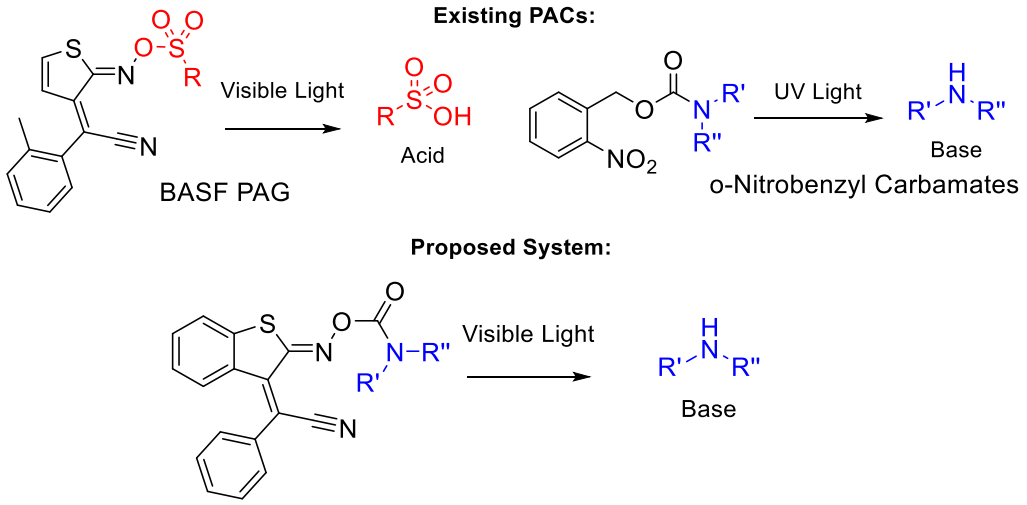

Figure 2.5: Scheme of existing BASF PAG, o-Nitrobenzyl carbamates and proposed compound.

2.2 SYNTHESIS

As shown in Scheme 2.1, Compounds **2.6a-8a** were synthesized in five steps from commercially available benzothiophene (**2.1**). Compound **2.1** was brominated using NBS in THF to give 3-bromobenzothiophene (**2.2**). Compound **2.2** was subsequently nitrated and then deprotected to give 2-nitrobenzothiophene over two steps (compound **2.4**). Then, using benzyl cyanide and basic conditions, oxime **2.5** was synthesized via Michael Addition, and the Z-isomer was isolated via recrystallization and confirmed via X-ray crystallography.

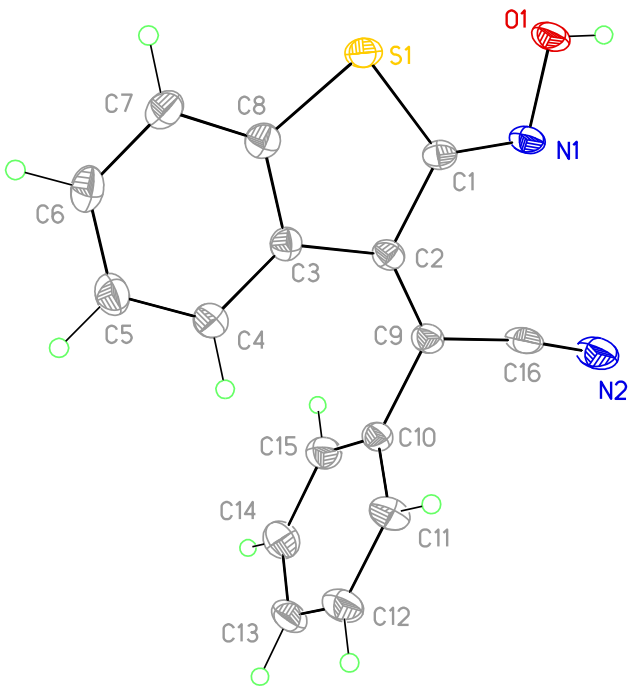

Figure 2.6: X-ray crystal structure of oxime 2.5, confirming Z-isomer.

It should be noted that while the first crop of crystals contained exclusively Z-isomer, subsequent crops contained an intractable mixture of E and Z-isomers. Deprotonation of oxime **2.5** and reaction with corresponding carbamoyl chlorides gave carbamates **2.6a-8a**: the dipentyl, dibenzyl and piperdinyl carbamates.

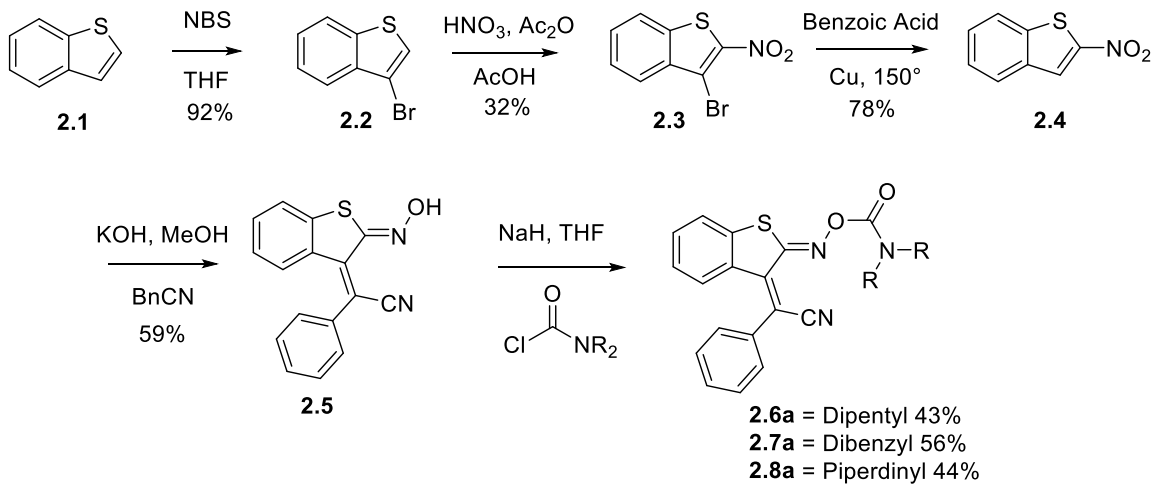

Scheme 2.1: Synthesis of benzothiophene carbamates. The "protect-deprotect" strategy using bromination provided the cleanest products in an easily saleable method.

It should also be noted to the interested chemist that this route requires no chromatography, and most steps were performed on very large (~100g) scale. This route is readily amenable to scaling up.

2.3 Evaluation of Photochemistry

First, in order to evaluate the photochemistry of the benzothiphene chromophore, a UV-vis photobleaching experiment was performed. A solution of the dipentylamine PBG **2.6a** in acetonitrile (7 mM) was exposed to iterative doses of 405 nm light, and the response was measured using UV-visible spectroscopy. The results of the experiment are highlighted in figure 2.7.

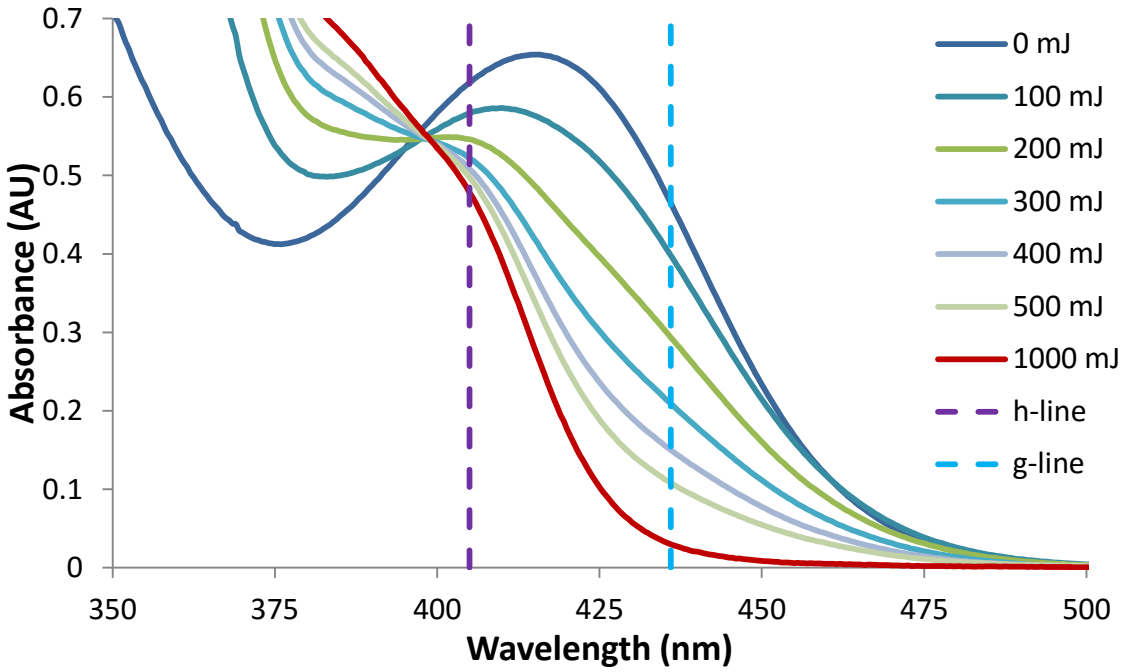

Figure 2.7: UV-vis photobleaching study of compound 2.6a. Doses are in 405 nm irradiation. Absorbance decreases at g-line as a function of dose.

Figure 2.6 highlights both h-line (405 nm) and g-line (436 nm) as potential wavelengths of a light source for this compound. While absorbance increases slightly at h-line, the compound bleaches considerably at g-line, which suggests that this compound is an excellent candidate for a g-line lithography process. The bleaching is particularly important for thick film patterning, as extensive bleaching leads to superior penetration of light through the film. Another major conclusion of the photobleaching experiment is that the benzothiophene chromophore has a large number of isosbestic points (wavelengths at which the total absorbance does not chance over the course of a reaction) across the full UV-vis spectrum, which is a hallmark of clean photochemistry (few side products).

Next, an NMR photolysis study[21] was performed to ascertain whether compound **2.6a** was producing the desired amine under exposure. Compound **2.6a** was dissolved in deuterated acetonitrile (7 mM) and exposed to iterative doses of 405 nm light in a quartz NMR tube. At each interval, the NMR tube was shielded from light and then a proton spectrum was recorded. Figure 2.7 highlights the results of the NMR study.

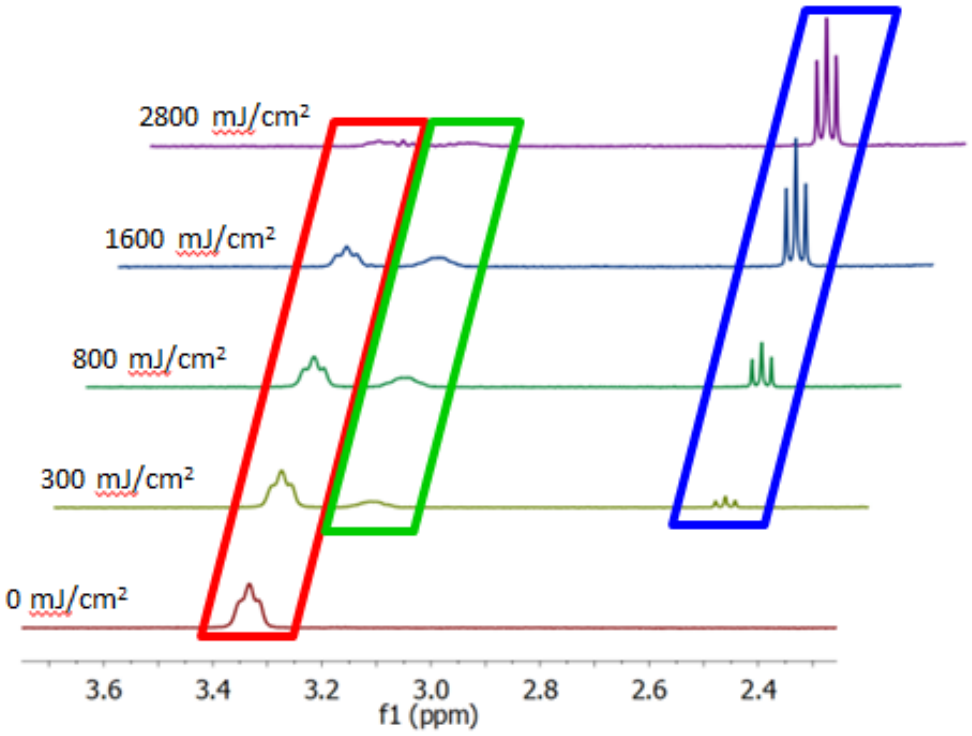

Figure 2.8: NMR photolysis study of compound **2.6a** at doses of 405 nm light. Amide protons at 3.35 ppm disappear and dipentylamine protons at 2.5 ppm appear. A transient resonance is noticeable at 3.15 ppm (green).

Several resonances are highlighted in figure 2.8. The first (in red, 3.35 ppm) are the amide protons of compound **2.6a**, which gradually decrease in intensity as a function of dose as expected. The third (in blue, 2.5 ppm) corresponds to the furthest downfield triplet of dipentylamine (confirmed by internal standard). This is a promising result, indicating that the chromophore is photochemically releasing amine as intended. Of

great interest, however, is the intermediate resonance that appears at 3.2 ppm (green) after 300 mJ/cm^2, yet is absent upon complete conversion. It is proposed that compound **2.6a** is not the active compound that releases amine, but rather is converted to an active intermediate, which releases amine in a second photochemical event. It is further proposed that this active intermediate is the *E* isomer of the phenyl-nitrile alkene (**2.6b**)[22].

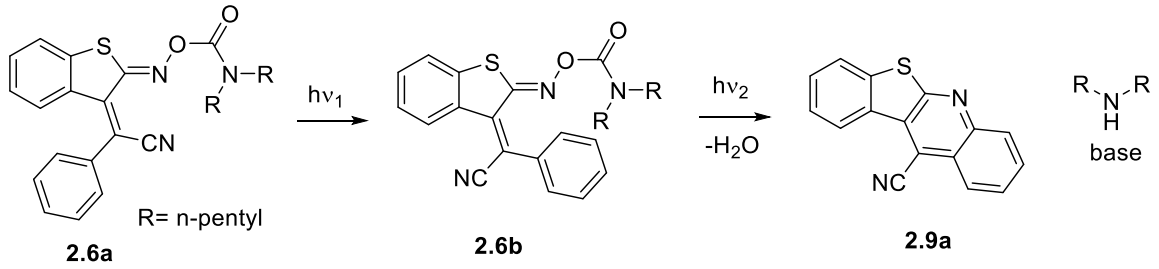

2.6a **2.6b** **2.9a**

Scheme 2.2: Proposed photolysis pathway of compound 2.6a.

Further evidence of the *E* isomer as the active intermediate was found during an LC/MS study of compound **2.7a**. The dibenzyl amine analogue compound **2.7a** was chosen as the corresponding amine product could be easily detected by the liquid chromatograph's UV-vis detector. Compound **2.7a** was dissolved in acetonitrile and exposed to 405 nm light. The solution was examined by LC/MS at various intervals, one of which is shown in figure 2.9.

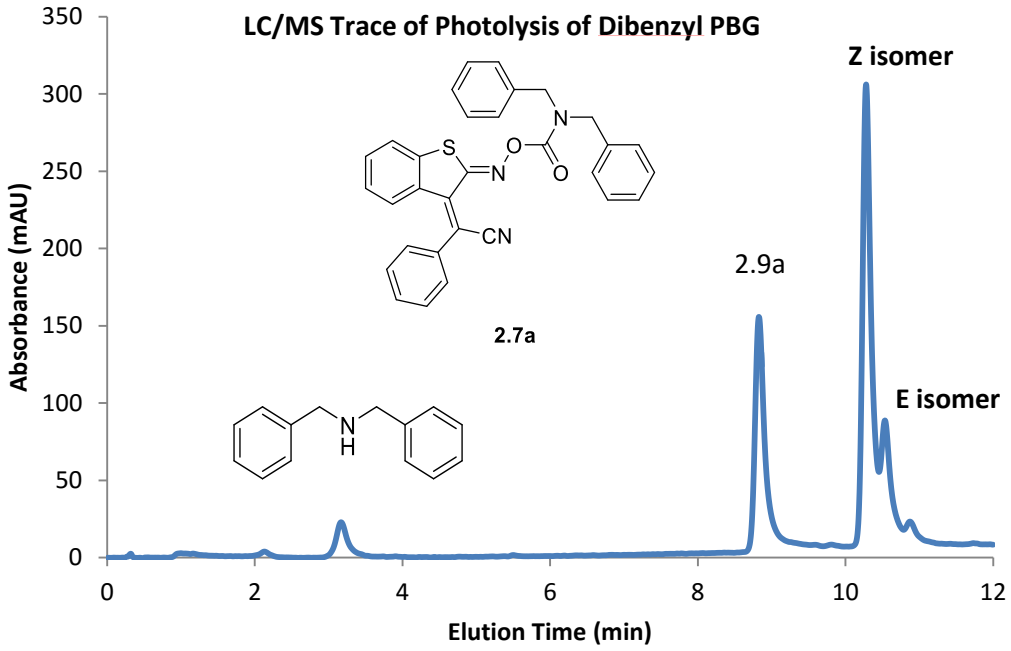

Figure 2.9: Sample LC/MS trace of compound **2.7a** at intermediate exposure dose, showing **2.7a** and all three photoproducts.

At intermediate exposure, compound **2.7a** and three photoproducts can be seen. The first product to appear is a shoulder on the starting material peak, which has the each same m/z (mass to charge ratio): (524, M+Na), as **2.7a**, which strongly suggests an isomer. Also present is the expected dibenzyl amine at 3.0 minutes of elution time, and an initially unknown photoproduct assigned as **2.9a**. At complete conversion, both isomers disappear, leaving only dibenzyl amine and the final product **2.9a**.

Photolysis of the oxime provided further evidence of the proposed pathway. The benzothiophene oxime **2.5a** was subjected to the same LC/MS photolysis study of compound **2.7a**, and it gave similar results[23].

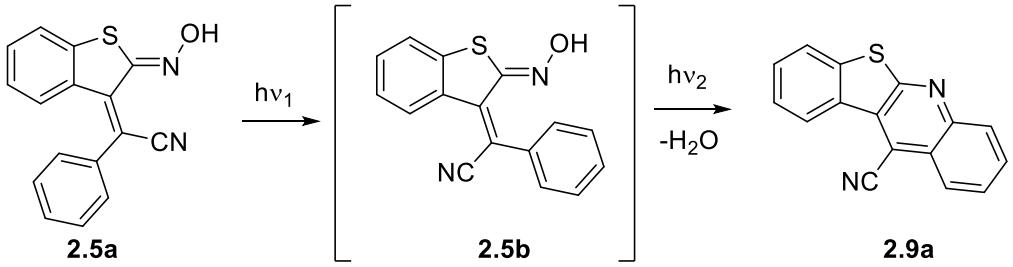

Scheme 2.3: Proposed photochemical pathway of oxime skeleton, including initial isomerization then conversion to benzothiophene-quinoline photoproduct.

The proposed pathway of photolysis is shown in Scheme 2.3. Once again, the first photochemical event is the isomerization of the phenyl-nitrile alkene bond from *Z* to *E*. Evidence for this transformation is shown in Figure 2.10.

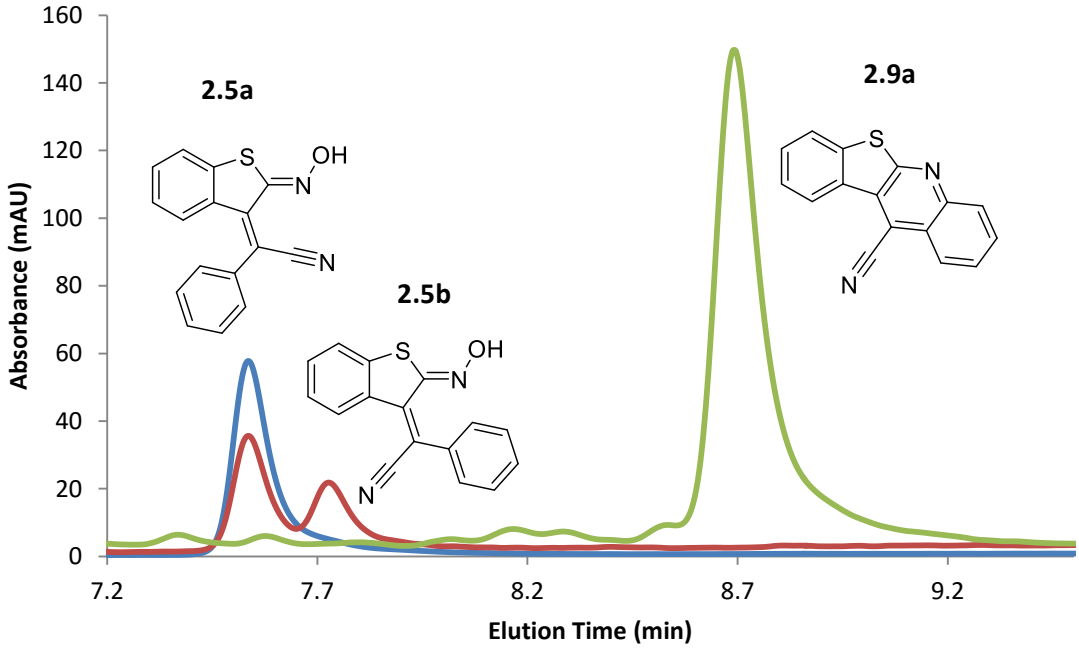

Figure 2.10: LC/MS traces of photolysis of oxime skeleton 2.5a. Curves correspond to unexposed (blue), partially exposed (red) and completely converted (green).

After a small amount of exposure, a second peak appeared of identical m/z (279, M+H), very close to the starting material. This peak was assigned as the *E* isomer **2.5b**. Also, note that at complete conversion, the only product on the LC/MS trace is the heterocycle **2.9a**, registering at the exact same elution time and m/z as in the dibenzyl amine photolysis experiment. This means that the photochemistry of the oxime skeleton is very similar to that of the corresponding carbamates. Further, the results demonstrate that the oxime **2.5a** is a "photo-water generator" (the only byproduct of the photoreaction being that of water).

In order to confirm the identity of the photoproduct **2.9a**, a sample of dipentyl carbamate **2.6a** was dissolved in acetonitrile (7 mM), and exposed at 405 nm until complete conversion was achieved by NMR (~30 minutes). Upon examining the reaction flask, it was observed that the bleached solution contained a small amount of needle-shaped, crystalline precipitate, which unfortunately was not of sufficient size to yield a crystal structure. The precipitate was filtered, dried and subject to a series of 1D and 2D NMR studies to confirm its identity. H^1, C^{13}, COSY, HSQC and HMBC spectra suggested two separate aromatic proton systems, as well as the still present nitrile functionality (also seen in the FTIR). COSY was used to identify which proton resonances corresponded to which aromatic ring system, and complete assignment of all resonances could then be completed through HSQC and HMBC spectra. High resolution mass spectrometry confirmed that the photoproduct **2.9a** has the same m/z as the signals seen in LC/MS experiments. Further, the isolated **2.9a** was resubmitted to LC/MS; it has the same elution time and mass to charge ratio, confirming its identity in the previous photolysis experiments.

One more interesting observation can be gleamed from NMR studies. During the NMR photolysis study of the dipentyl amine carbamate, at complete conversion it was

observed that the proton resonances matched those of heterocycle **2.9a**, except that one resonance was integrated at 50% intensity. Using the previously discussed 2D NMR techniques, particularly COSY and HMBC, this resonance was assigned to compound **2.9b** as shown in Scheme 2.4.

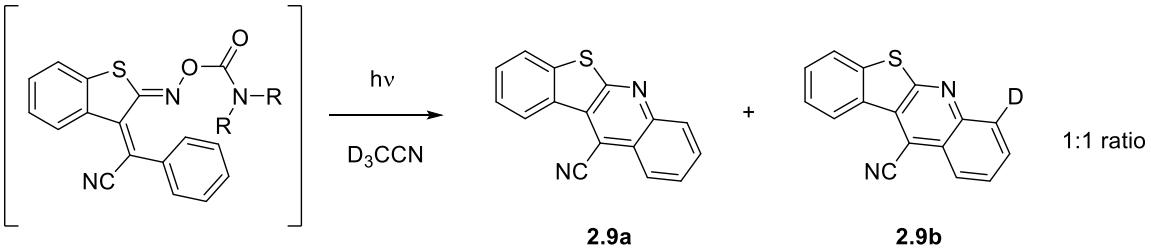

Scheme 2.4: NMR deuterium labeling experiment. Running the photoreaction in deuterated acetonitrile results in a 1:1 ratio of products as shown.

The results suggest that there is some unexpected proton abstraction from the position beta to the quinoline nitrogen in products **2.9a-b**. It is generally accepted that this type of compound proceeds through hemolysis of the oxime N-O bond, followed by addition into the proximal aryl group[24]. The reaction is completed when the now free amine abstracts a proton from the proximal aryl system, reestablishing aromaticity. In the BASF PAG derivative, a methyl group on the proximal phenyl system is scrambled to 1:1 beta:epsilon from the quinoline nitrogen, which suggests a radical spirocyclic intermediate. While one might take a 1:1 incorporation of deuterium into the photoproducts as a sign of a similar spirocyclic intermediate, not enough data is currently present to support that conclusion.

It is proposed here that the reaction follows a radical-nucleophilic aromatic substitution pathway (S_{RN1}). Photochemical oxime N-O bond homolysis and subsequent aryl addition is not an unprecedented reaction, and the two common pathways of the

radical addition have been proposed to be the 6-endo-trig product (**2.10**, Scheme 2.5) and a radical spirocycle (**2.11**, Scheme 2.5).

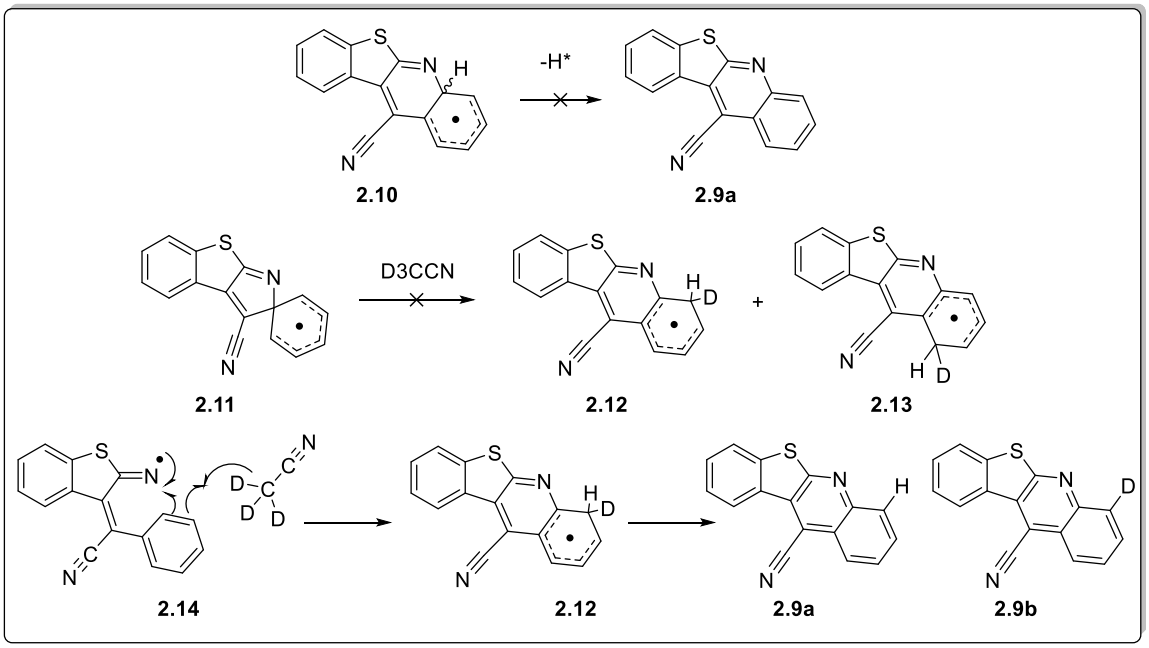

Scheme 2.5: Proposed pathway leading to a 1:1 mixture of photoproducts when the photoreaction is carried out in deuterated acetonitrile. A concerted pathway leading to key intermediate 2.12 is proposed. Products isolated are not consistent with 6-endo-trig intermediate 2.10 or a spirocyclic intermediate 2.11.

It is proposed that the key intermediate that must exist in light of a 1:1 ratio of deuterated products (**2.9a** and **2.9b**) is **2.12**, which has an enantiotopic hydrogen and deuterium β to the quinoline nitrogen. If either intermediate **2.10** or **2.11** were to form[25], one would either expect to observe exclusively **2.9a** (no deuteration), or a mixture of deuterium incorporated on the opposite sides of the quinoline aryl ring in the case of a spirocylic intermediate. Thus, it is proposed that the deuterium is incorporated in a concerted step that leads to intermediate **2.12**. It is assumed that the transition states for

either proton or deuterium abstraction to form **2.9b** and **2.9a**, respectively, are approximately equal in energy, leading to a 1:1 distribution of products.

2.4 Conclusions and Outlook

In order for this series of photobase generators to be viable for long wavelength patterning of polyimides, the compounds not only have to demonstrate efficient photolysis but also must survive a post exposure bake step of about 160˚C in order to complete imidization. Unfortunately, when the thermal stability of these compounds was evaluated using thermogravimetric analysis (TGA), it was found that decomposition occurred before the target 160˚C in all cases. The mechanism of thermolysis was proposed to be a loss of amine and carbon dioxide, which matched well with relative weight loss data. For a more detailed discussion of these TGA experiments, the interested reader should peruse the thesis of Dr. William Bell.

These compounds were ultimately unsuccessful for a polyimide patterning application, but a great deal has been learned about this benzothiophene chromophore as an amine protecting group, and it could have applications in total synthesis. Firstly, the compounds described in this chapter very cleanly release amine upon 400 nm irradiation, which is very rare for amine PBGs. The mechanism has been explored, and the data suggest a subsequent two stage mechanism in which the first photochemical event is the isomerization of the phenyl-nitrile double bond, and the second is homylsis of the oxime N-O bond resulting in release of carbon dioxide, amine, and the unusual quinoline **2.9a**.

There are several reasons why these benzothiophene compounds have a future as an amine protecting group. Firstly is that synthesis of these compounds is very scalable as no chromatography is required in any step. Secondly since these compounds protect amines in a similar manner as benzyl carbamates, they are likely to be less susceptible to

reduction and have a unique mode of deprotection (visible light). Thirdly, the deprotection of these compounds is extremely easy. Indeed, solvation in acetonitrile followed by 30 minutes of light exposure cleanly releases amine while the byproduct (compound **2.9a**), which is itself insoluble in acetonitrile, is easily removed by filtration. Lastly, it is a well-established strategy in total synthesis to protect finished compounds in order to obtain crystal structures. While the author only obtained a crystal structure of the oxime **2.5a**, it should be noted that all protected amines could be purified by recrystallization, including the "greasy" protected dipentylamine **2.6a**. These data suggest that even highly lipophilic compounds could have crystalline derivatives when protected with this chemistry, which could lead to facile structural determination through crystallography.

Ultimately, the benzothiophene compounds in this chapter possess interesting and very clean photochemistry. The synthesis is facile and scaleable; the derivatives are crystalline and easy to purify. While this series must be unfortunately ruled out for polyimide patterning, there are many potential advantages of using these benzothiophene as general amine protecting groups.

2.5 EXPERIMENTAL

General Methods and Materials

All solvents and reagents were obtained from Sigma-Aldrich and were used without further purification except where noted. TEA was distilled from CaH_2 while THF was distilled from sodium/benzophenone. Reactions were run in flame-dried glassware and under an atmosphere of nitrogen unless otherwise noted. Photosensitive

reactions were protected from ambient light by wrapping reaction flasks with aluminum foil. ^{1}H and ^{13}C NMR spectra were recorded on a Varian Unity Plus 400 MHz instrument. Chemical shifts are reported in ppm downfield from TMS using residual protonated solvent as an internal standard (DMSO-d_6, ^{1}H 2.49 ppm and ^{13}C 39.5 ppm or $CDCl_3$, ^{1}H 7.26 ppm and ^{13}C 77.0 ppm). Coupling constants are expressed in Hz. HRMS (CI) was obtained on a VG analytical ZAB2-E instrument while HRMS (ESI) was obtained on an Ion Spec FT-ICR (7 Tesla) instrument. IR data was recorded on a Nicolet Avatar 360 FT-IR using either a KBr pellet or thin film on a NaCl disc. Melting points were recorded using a Mel-Temp II and are uncorrected. Thermogravimetry was performed using a TA Instruments Q500 TGA.

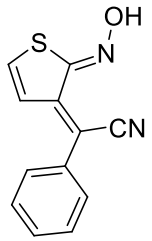

Synthesis of (Z)-2-((Z)-2-(hydroxyimino)thiophen-3(2H)-ylidene)-2-phenylacetonitrile. Potassium hydroxide (10.844 g, 193.26 mmol) was dissolved in 50 mL of methanol and added to a 250 mL round-bottom flask. This solution was cooled to 0 °C and benzyl cyanide (5.711 g, 48.75 mmol) was added dropwise. 2-nitrothiophene (6.214 g, 48.12 mmol) was then dissolved in 50 mL of methanol and added to the reaction over a 25 minute period. The solution rapidly became dark orange, and then gradually faded to deep brown/black. After 20 minutes, the reaction was quenched with 50% acetic acid/water at 0 °C and diluted with ethyl acetate. This solution was washed with water and brine, dried with $MgSO_4$, filtered and concentrated to obtain approximately 11 grams of a black, tarry substance. This material was purified by

column chromatography (20% ethyl acetate in hexanes) and crystallization from toluene to yield a deep brown solid (2.983 g, 27% yield). MP: 168-170 °C (dec); ^{1}H NMR (400 MHz, DMSO-d6): δ 6.56 (d, *J* = 6.6 Hz, 1H), 7.38 (d, *J* = 6.6 Hz, 1H), 7.53 – 7.41 (m, 5H), 13.24 (s, 1H); ^{13}C NMR ($CDCl_3$): δ 104.29, 119.28, 122.58, 129.10, 129.12, 129.41, 134.55, 136.25, 145.63, 151.92; HRMS $[M+H]^+$ calcd. = 229.0436, found = 229.0435; FTIR ν = 3220 (br), 3008, 2955, 2835, 2215, 1525, 1492, 1428, 1334, 1285, 1258, 1230, 1112, 989, 839 cm^{-1}.

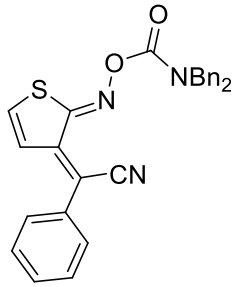

Synthesis of (Z)-2-((Z)-2-(dibenzylcarbamoyloxyimino)thiophen-3(2H)-ylidene)-2-phenylacetonitrile. To a 25 mL round-bottom flask added **3.1** (0.337 g, 1.48 mmol), dry THF (10 mL) and dibenzylcarbamyl chloride (1.299 g, 5.00 mmol). This solution was cooled to -78 °C and NaH (0.028 g, 60% mineral oil dispersion—0.694 mmol) was added in one portion. The reaction was then shielded from light and warmed to room temperature. Stirring was continued for 4 hours, after which the reaction was quenched with water and diluted with ethyl acetate (50 mL). This extract was washed three times with water and once with brine, dried over $MgSO_4$, filtered and concentrated. The crude material was purified by column chromatography (30% ethyl acetate in hexanes), followed by crystallization from toluene to yield the product as a yellow solid (0.401 g, 60%). MP: 140-142 °C; ^{1}H NMR (400 MHz, $CDCl_3$): δ 7.24-7.52(m, 15H), 6.816(d, *J*=6.4, 1H), 6.626(d, *J*=7.6, 1H), 4.55(s, 2H), 4.45(s, 2H); ^{13}C-NMR (100 MHz, CDCl3):

δ 153.07, 144.26, 136.43, 134.43, 132.68, 130.06, 129.43, 129.02, 127.77, 123.15, 118.01, 111.2, 50.31, 49.27; HRMS $[M+H]^+$ calcd. = 452.1433 found = 452.1432; FTIR ν = 3109, 2207, 1740, 1521, 1494, 1453, 1410, 1323, 1263, 1198, 1086, 1010, 943, 866, 778 cm^{-1}.

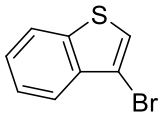

Synthesis of 3-bromobenzo[b]thiophene. Benzo[b]thiophene (5.051 g, 37.64 mmol) was dissolved in 120 mL THF and added to a 250 mL round-bottom flask. The solution was cooled to 0 °C and NBS (10.147 g, 57.01 mmol) was added portionwise. The mixture was stirred for 30 minutes at 0 °C, then warmed to room temperature and stirred for an additional 48 hours. The reaction was quenched with aqueous $Na_2S_2O_3$ and extracted with ether. The extracts were combined and washed, dried with $MgSO_4$, filtered and concentrated to obtain approximately 10 grams of crude material. This was purified by column chromatography (hexanes), yielding a clear oil (7.373 g, 92%). ^1H NMR (400 MHz, $CDCl_3$): δ 7.91 – 7.79 (m, 2H), 7.56 – 7.35 (m, 3H); ^{13}C NMR (101 MHz, $CDCl_3$): δ 138.40, 137.33, 125.14, 124.88, 123.36, 122.89, 122.57, 107.57; HRMS $[M]^+$ calcd. = 211.9295 found = 211.9294; FTIR ν = 3104, 3058, 1492, 1453, 1429, 1316, 1253, 1145, 1060, 1017, 929, 820 cm^{-1}.

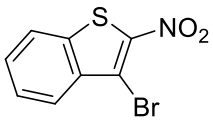

Synthesis of 3-bromo-2-nitrobenzo[b]thiophene. To a 500 mL round bottom flask was added 3-bromobenzo[b]thiophene (12.795 g, 60.045 mmol) and 200 mL of acetic anhydride. The solution was cooled to 0 °C and a mixture of 25 mL of nitric acid and 20

mL of acetic acid was added dropwise with vigorous stirring. A yellow precipitate began to form after several minutes. Once the addition was complete, the ice bath was removed and the reaction stirred for two hours at room temperature. The mixture was then poured into ice water and the resulting precipitate collected by filtration. The solid was washed with water and crystallized from ethanol, yielding a fluffy golden solid (4.926 g, 32%). Only the first crop of material contains the desired product. MP: 160-162 °C; ^{1}H NMR (400 MHz, DMSO-d6) δ 7.65 (ddd, *J* = 8.2, 7.2, 1.1 Hz, 1H), 7.73 (ddd, *J* = 8.4, 7.2, 1.3 Hz, 1H), 7.99 (ddd, *J* = 8.2, 1.2, 0.7 Hz, 1H), 8.16 (ddd, *J* = 8.2, 1.4, 0.9 Hz, 1H); ^{13}C NMR (101 MHz, DMSO-d6): δ 111.89, 123.79, 126.29, 127.26, 130.72, 136.45, 136.60, 145.96; HRMS $[M+H]^+$ calcd. = 257.9224, found = 257.9220; FTIR ν = 3074, 1591, 1552, 1520, 1484, 1334, 1303, 1243, 917, 867, 803, 761, 740, 727, 710 cm^{-1}.

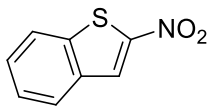

Synthesis of 2-nitrobenzo[b]thiophene. 3-bromo-2-nitrobenzo[b]thiophene (4.313 g, 16.71 mmol) and benzoic acid (7.555 g, 61.87 mmol) were added to a 3-neck 100 mL round bottom flask. The solids were mixed thoroughly with a magnetic stir bar and the reaction was purged 3 times before heating to 150 °C. Under a cone of nitrogen, copper powder (5.159 g, 81.19 mmol) was then added to the melt. The reaction was stirred for an additional 30 minutes at 150 °C, then slowly cooled to room temperature. The resulting solid was suspended in dichloromethane and the residual copper was removed by gravity filtration. The DCM solution was washed three times with saturated $NaHCO_3$, once with water and once with brine. This was then dried over $MgSO_4$, filtered and concentrated to obtain a golden power (2.326 g, 78%). MP: 109-112 °C; ^{1}H NMR (400 MHz, $CDCl_3$): δ 8.20 (d, J = 3.3 Hz, 1H), 7.88 (ddd, J = 38.1, 8.1, 2.6 Hz, 2H), 7.53 (dtd,

J = 15.0, 7.2, 2.9 Hz, 2H); ^{13}C NMR (101 MHz, $CDCl_3$): δ 151.32, 140.33, 136.08, 129.13, 127.00, 126.11, 125.61, 122.89; HRMS $[M]^+$ calcd. = 179.0041 found = 179.0044; FTIR ν = 3098, 1594, 1558, 1516, 1496, 1451, 1424, 1346, 1315, 1250, 1190, 1160, 1126, 1081, 1052, 872, 849, 802, 757 cm^{-1}.

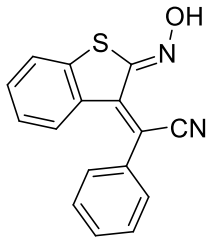

Synthesis of (Z)-2-((Z)-2-(hydroxyimino)benzo[b]thiophen-3(2H)-ylidene)-2-phenylacetonitrile. Potassium hydroxide (0.530 g, 9.44 mmol) was dissolved in 10 mL of methanol and added to a 50 mL round-bottom flask. The solution was then cooled to 0 °C and benzyl cyanide (0.276 g, 2.36 mmol) was added dropwise. 2-nitrobenzo[b]thiophene (0.422 g, 2.36 mmol) was dissolved in 25 mL of methanol and added dropwise to the reaction vessel. The solution immediately became brilliant yellow and gradually darkened to a vibrant orange color. The reaction was then protected from light by covering the flask with aluminum foil and stirred overnight at room temperature. Upon completion as determined by TLC, the reaction was poured into 200 mL of water, then acidified with 50% acetic acid/water. The resulting suspension was extracted 3 times with ethyl acetate. The extracts were combined, washed with water and brine, dried with $MgSO_4$, filtered and concentrated to obtain 0.62 grams of crude material. Purification by column chromatography (20% ethyl acetate in hexanes) yielded the product as a yellow powder (0.389 g, 59%). MP: 184-185 °C (dec; sample darkened at 175 °C without melting); ^{1}H NMR (400 MHz, DMSO-d6): δ 13.15 (s, 1H), 7.70 – 7.48 (m, 6H), 7.39 – 7.30 (m, 1H), 6.89 (ddd, J = 8.4, 7.4, 1.2 Hz, 1H), 6.38 (dd, J = 8.2, 0.5 Hz, 1H); ^{13}C NMR (101 MHz, DMSO-d6): δ 150.94, 142.23, 139.12, 134.36, 132.32,

131.78, 130.11, 128.83, 128.70, 126.63, 125.30, 123.83, 119.38, 106.56; HRMS $[M+H]^+$ calcd. = 279.0592 found = 279.0590; FTIR ν = 3325, 3061, 2201, 1583, 1546, 1487, 1445, 1363, 1308, 1286, 1261, 1211, 1166, 988, 892, 766 cm^{-1}.

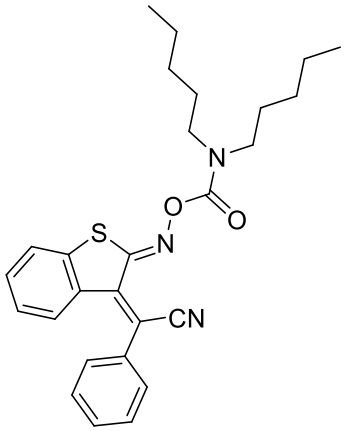

Synthesis of (Z)-2-((Z)-2-(dipentylcarbamoyloxyimino)benzo[b]thiophen-3(2H)-ylidene)-2-phenylacetonitrile. To a 5 mL round-bottom flask added the corresponding oxime (0.109 g, 0.392 mmol), dry THF (3 mL) and dipentylcarbamyl chloride (0.315 g, 1.43 mmol). This solution was cooled to -78 °C and NaH (0.037 g, 60% mineral oil dispersion—0.925 mmol) was added in one portion. The reaction was then shielded from light and warmed to room temperature. Stirring was continued for 3 hours, at which point all starting material was consumed, as determined by TLC. The reaction was then quenched with water and diluted with ethyl acetate (50 mL). This was washed three times with water and once with brine, dried over $MgSO_4$, filtered and concentrated to obtain 0.286 grams of crude material. Crystallization from hexanes yielded the product as a yellow solid (0.077 g, 43%). MP: 106-108 °C (dec; pronounced outgassing from the melt was observed, suggesting carbamate thermolysis); ^1H NMR (400 MHz, CD_3CN): δ 7.66 – 7.46 (m, 5H), 7.42 (d, J = 7.9 Hz, 1H), 7.34 (t, J = 7.6 Hz, 1H), 6.88 (dd, J = 8.2, 7.3 Hz, 1H), 6.50 (d, J = 8.3 Hz, 1H), 3.33 (t, J = 7.1 Hz, 4H), 1.65 (d, J = 27.1 Hz, 4H),

1.38 (s, 8H), 0.94 (s, 6H); ^{13}C NMR (101 MHz, CD_3CN): δ 159.54, 153.20, 142.84, 139.16, 135.45, 133.43, 132.76, 131.27, 131.09, 129.41, 128.13, 126.77, 124.30, 119.46, 111.93, 49.10, 48.58, 29.84, 29.64, 29.28, 28.30, 23.16, 14.36; HRMS $[M+Na]^+$ calcd. = 484.2029 found = 484.2039; FTIR ν = 2956, 2927, 2858, 2199, 1739, 1584, 1538, 1489, 1460, 1440, 1414, 1312, 1272, 1232, 1204, 1139, 1010, 972, 859, 757 cm^{-1}.

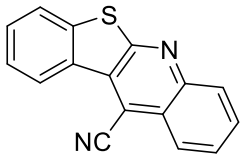

Formation of photoproduct benzo[4,5]thieno[2,3-b]quinoline-11-carbonitrile.

To quartz cuvette was added (Z)-2-((Z)-2-(dipentylcarbamoyloxyimino)benzo[b]thiophen-3(2H)-ylidene)-2-phenylacetonitrile (22.6mg, 0.056 mmol) in acetonitrile (8 ml, 7 mM), and exposed for 30 minutes through a 405 nm bandpass filter. Upon completion, a solid had precipitated in solution, which was filtered and washed with hexanes to give a pale yellow solid identified as benzo[4,5]thieno[2,3-b]quinoline-11-carbonitrile (11.7 mg, 92%). MP: 208-213°C 1H NMR (500 MHz, cdcl3) δ 9.01 (ddd, J = 7.9, 1.3, 0.6 Hz, 1H), 8.44 (ddd, J = 8.4, 1.4, 0.6 Hz, 1H), 8.25 (ddd, J = 8.5, 1.2, 0.6 Hz, 1H), 7.96 – 7.90 (m, 2H), 7.81 (ddd, J = 8.2, 6.9, 1.2 Hz, 1H), 7.69 (td, J = 7.6, 1.3 Hz, 1H), 7.64 (ddd, J = 7.9, 7.3, 1.3 Hz, 1H). 13C NMR (126 MHz, cdcl3) δ 162.8, 146.6, 139.8, 130.8, 130.4, 130.3, 129.2, 128.9, 128.1, 125.8, 125.14, 125.08, 124.1, 123.3, 115.3, 109.8. HRMS (ESI-TOF) (M+) calcd. for $C_{16}H_8N2S$: 260.0408, found 260.0408. FT-IR (neat): 2923, 2360 (strong), 1736, 1599, 1454, 1367, 1216, 1115, 844, 754 cm-1. 2D NMR spectra appended at the end of the experimental section.

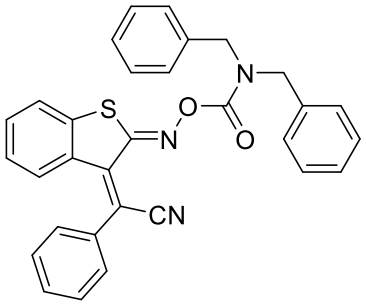

Synthesis of (Z)-2-((Z)-2-(((dibenzylcarbamoyl)oxy)imino)benzo[b]thiophen-3(2H)-ylidene)-2-phenylacetonitrile. To a 25 mL round-bottom flask added (Z)-2-((Z)-2-(hydroxyimino)benzo[b]thiophen-3(2H)-ylidene)-2-phenylacetonitrile (0.370 g, 1.329 mmol), dry THF (13 mL) and dibenzylcarbamyl chloride (1.208 g, 4.652 mmol). This solution was cooled to -78 °C and NaH (0.080 g, 60% mineral oil dispersion—3.3 mmol) was added in one portion. The reaction was then shielded from light and warmed to room temperature. Stirring was continued for 3 hours, at which point all starting material was consumed, as determined by TLC. The reaction was then quenched with water and diluted with ethyl acetate (50 mL). This was washed three times with water and once with brine, dried over $MgSO_4$, filtered and concentrated to obtain 0.880 grams of crude material. Crystallization from hexanes yielded carbamate as a yellow solid (0.373 g, 56%). MP: 172-175 °C. ^{1}H NMR (400 MHz, $cdcl_3$) δ 7.58 – 7.17 (m, 17H), 6.83 (ddd, J = 8.4, 7.1, 1.5 Hz, 1H), 6.59 (d, J = 8.1 Hz, 1H), 4.49-4.62 (m, 4H). ^{13}C NMR (101 MHz, $cdcl_3$) δ 158.6, 153.2, 141.6, 138.3, 136.5, 133.9, 132.1, 131.7, 130.3, 129.9, 128.8, 128.7, 127.8, 127.7, 127.3, 125.7, 123.0, 118.4, 112.0, 50.2, 49.3. HRMS (ESI-TOF)

$[M+H]^+$ calcd. For $C_{31}H_{24}N_3O_2S$ = 502.1584 found = 502.1585. FTIR ν = 3268, 3142, 2422, 1727, 1373, 1219, 1056 cm-1.

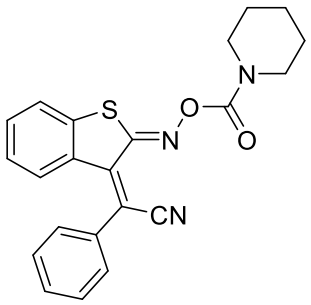

Synthesis of (Z)-2-phenyl-2-((Z)-2-(((piperidine-1-carbonyl)oxy)imino)benzo[b]thiophen-3(2H)-ylidene)acetonitrile. To a 25 mL round-bottom flask added (Z)-2-((Z)-2-(hydroxyimino)benzo[b]thiophen-3(2H)-ylidene)-2-phenylacetonitrile (0.213 g, 0.765 mmol), dry THF (11 mL) and dibenzylcarbamyl chloride (0.335ml, 2.678 mmol). This solution was cooled to -78 °C and NaH (0.076 g, 60% mineral oil dispersion—1.9 mmol) was added in one portion. The reaction was then shielded from light and warmed to room temperature. Stirring was continued for 3 hours, at which point all starting material was consumed, as determined by TLC. The reaction was then quenched with water and diluted with ethyl acetate (50 mL). This was washed three times with water and once with brine, dried over $MgSO_4$, filtered and concentrated to obtain 0.411 grams of crude material. Crystallization from hexanes yielded carbamate as a yellow solid (0.131 g, 44%). MP: 163-166 °C ^{1}H NMR (400 MHz, $cdcl_3$) δ 7.58 – 7.38 (m, 5H), 7.26 (dd, *J* = 8.0, 4.5 Hz, 2H), 6.89 – 6.78 (m, 1H), 6.60 (d, *J* = 8.2 Hz, 1H), 3.52-3.60 (m, 4H), 1.65 (s, 6H). ^{13}C NMR (101 MHz, $cdcl_3$) δ 157.8, 151.6, 141.7, 138.5, 134.0, 132.0, 131.8, 130.2, 129.8, 128.7, 127.2, 125.6, 123.0, 118.4, 111.8, 45.5,

24.2. HRMS (ESI-TOF) $[M+Na]^+$ calcd. for $C_{22}H_{19}N_3O_2SNa$ = 412.1095 found = 412.1090. FTIR ν = 3388, 3259, 3208, 1925, 1575, 1364, 1278, 1168, 1138 cm-1.

Photobleaching

UV/Visible spectra were collected using a Cary 1E spectrophotometer (Varian). A 9E-5 M stock solution of **2.6a** was prepared in acetonitrile. Solutions were *not* degassed prior to exposure. Samples were irradiated in a quartz cell using a Novacure 2100 spot curing system (Lumen Dynamics) at a 5 inch distance. The source was filtered using a 405 nm bandpass filter (A_{405}: 1.571; 20 nm FWHM). The resulting intensity was 0.55 mW/cm^2, as measured using a PowerMax PM3 thermopile (Coherent) connected to a Field Max II power meter (Coherent). The full dataset can be seen below.

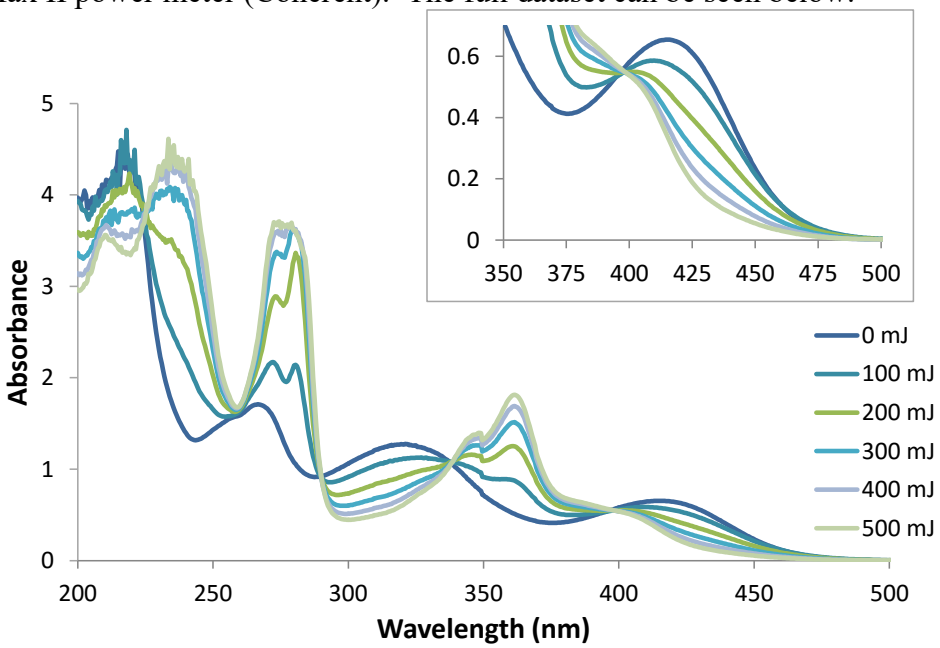

NMR Photolysis

^{1}H NMR spectra were collected using a Varian Unity Plus 400 MHz instrument. Photobases were dissolved in CD_3CN to a concentration of 7 mM. The solutions were *not* degassed prior to exposure. Samples were irradiated using a Novacure 2100 spot curing system (Lumen Dynamics) at a 5 inch distance. The source was filtered using a 405 nm bandpass filter (A_{405}: 1.571; 20 nm FWHM). The resulting intensity was 0.46 mW/cm^2, as measured using a PowerMax PM3 thermopile (Coherent) connected to a Field Max II power meter (Coherent).

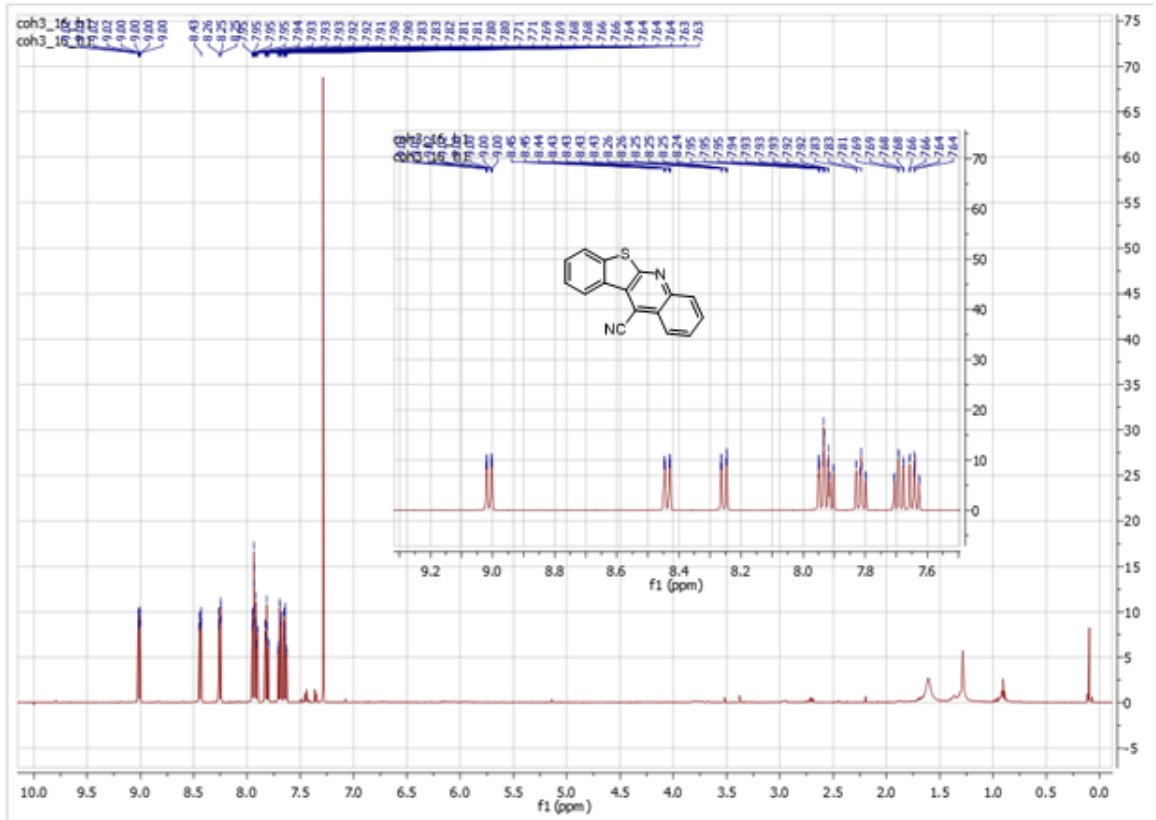

Proton Spectrum of 2.9a.

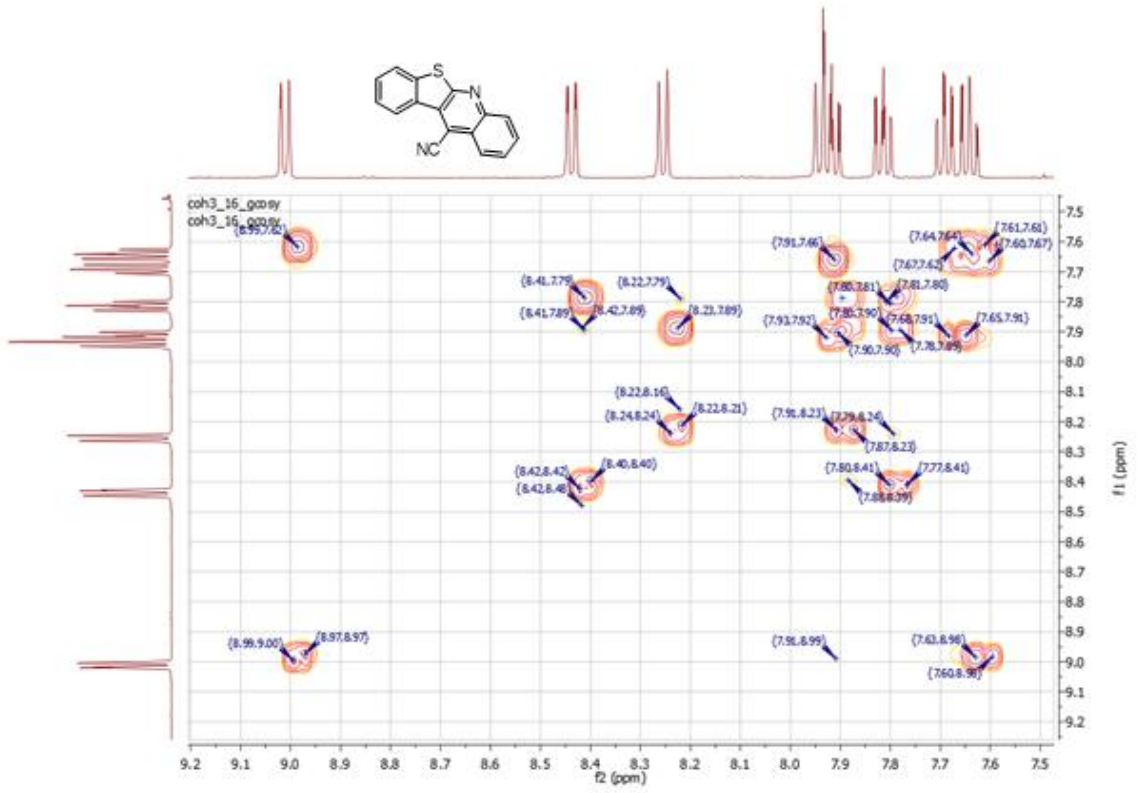

COSY spectrum of 2.9a.

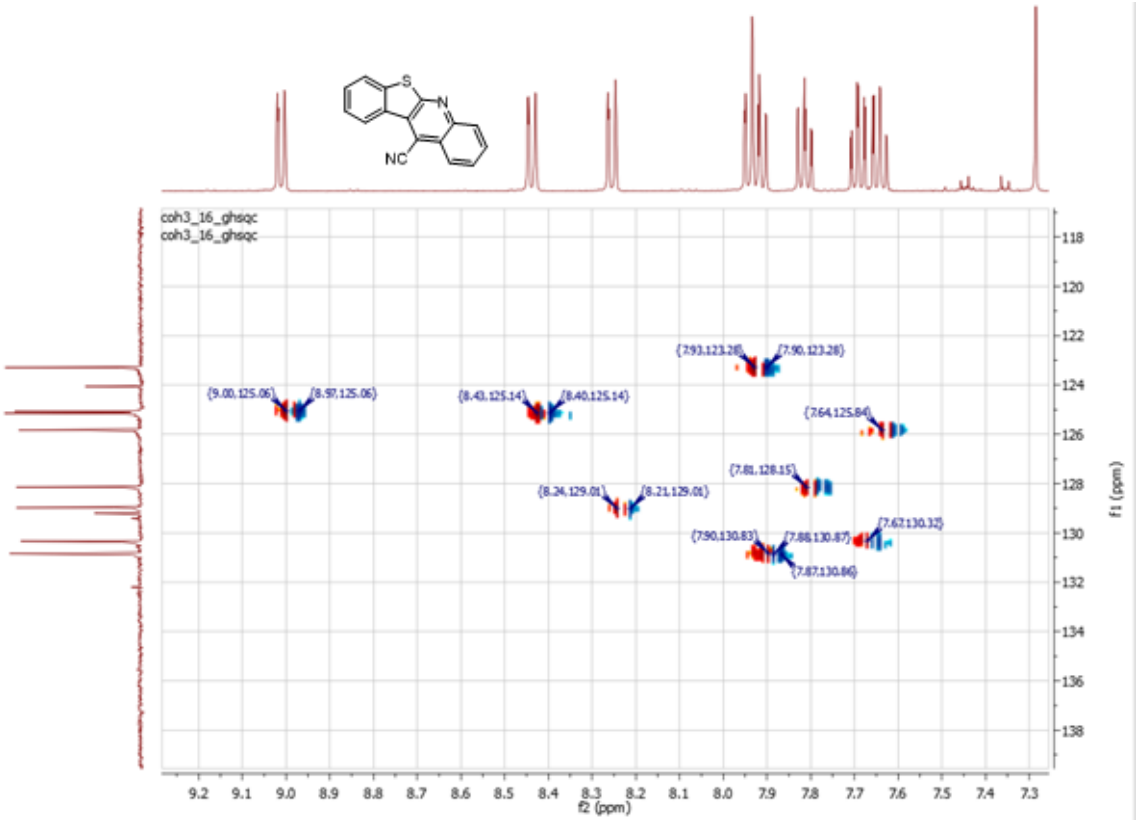

HSQC spectrum of 2.9a.

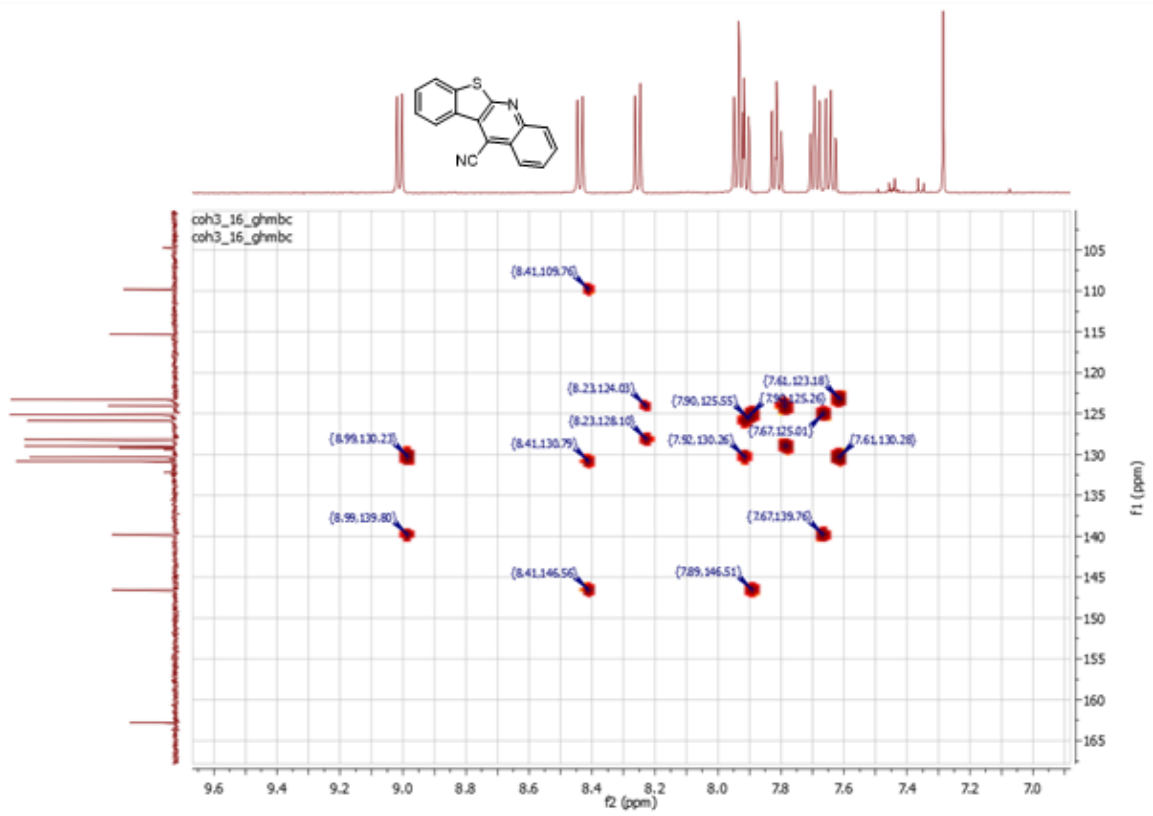

HMBC spectrum of 2.9a.

Chapter 3: Directly Patternable Polyhedral Silsesquioxane and Benzocycobutene Materials for Microelectronics Packaging

3.1 Introduction

While great emphasis is often placed on the manufacturing of transistors on chips, perhaps equally important is the analogous process of packaging chips at the back end (connecting those transistors to each other and to the outside world). The package is responsible for protecting the silicon chip, dissipating heat and providing cost-effective electrical interconnections to the motherboard. This wiring, like all other components of the computing device, is shrinking consistently from generation to generation. Current generation packaging circuits are defined with sacrificial photoresists or laser ablation, which adds additional process steps and can contain etch processes that lead to copper via delamination and device failure[26]. An inherently photosensitive and patternable dielectric material has the opportunity to save process steps, improve device yield, and ultimately cut costs for future generation packages. However, in addition to direct patternability with resolution on the order of five micron lines and spaces, an ideal functional resist would also possess a low dielectric constant (ε_d < 3.0), a low coefficient of thermal expansion (CTE, $\propto_{xy}$ < 30 ppm/K), and a cure temperature below 200˚C to be compatible with current infrastructure and minimize thermal stress on the package. Altogether, this unique combination of materials requirements presents a lofty challenge.

Polyhedral oligomeric silsesquioxanes (POSS) are a class of functional materials with the general formula $R_nSi_nO_{1.5n}$ that represent the smallest conceivable nanoparticle of SiO_2[27]. SiO_2 nanoparticles are a common filler in microelectronic packaging applications[28,29], given their exceptionally low CTE of 0.5 ppm/K[30-32]. POSS materials were selected as they represent the interface between inorganic SiO_2 particles and organic functional silicones in nomenclature[33], which often have useful chemistry but suffer in

CTE (common organic polymers typically have CTEs on the order of 100-300 ppm/K)[34-36]. POSS materials have another advantage: they are easy to functionalize substituents at each corner of the cube[37]. POSS particles are also very small, on the order of 1.2-1.4 nm in diameter, which mitigates any kind of light scattering in a lithography process. POSS resins often have interesting optical[38], thermal and mechanical properties in films[39], and can often be used to augment the properties of polymers due to the material's high surface area to volume ratio and thus excellent dispersability in a matrix[40].

Benzocyclobutene (BCB) chemistry has numerous advantages for microelectronic applications. The Dow Chemical product Cyclotene® is a BCB based silicone thermoset that has a reported dielectric constant of 2.65, a CTE of 42-55 ppm/K, and some reports of patternability down to 20 μm full pitch[41-43]. BCB resins crosslink[44,45] through a thermal 4-π electrocyclic ring opening and subsequent Diels-Alder [4+2] cycloaddition reaction, or through the "forbidden" [4+4] cycloadduct (~30% of products) which likely proceeds through the joining of two diradical BCB species[46] (Figure 3.1).

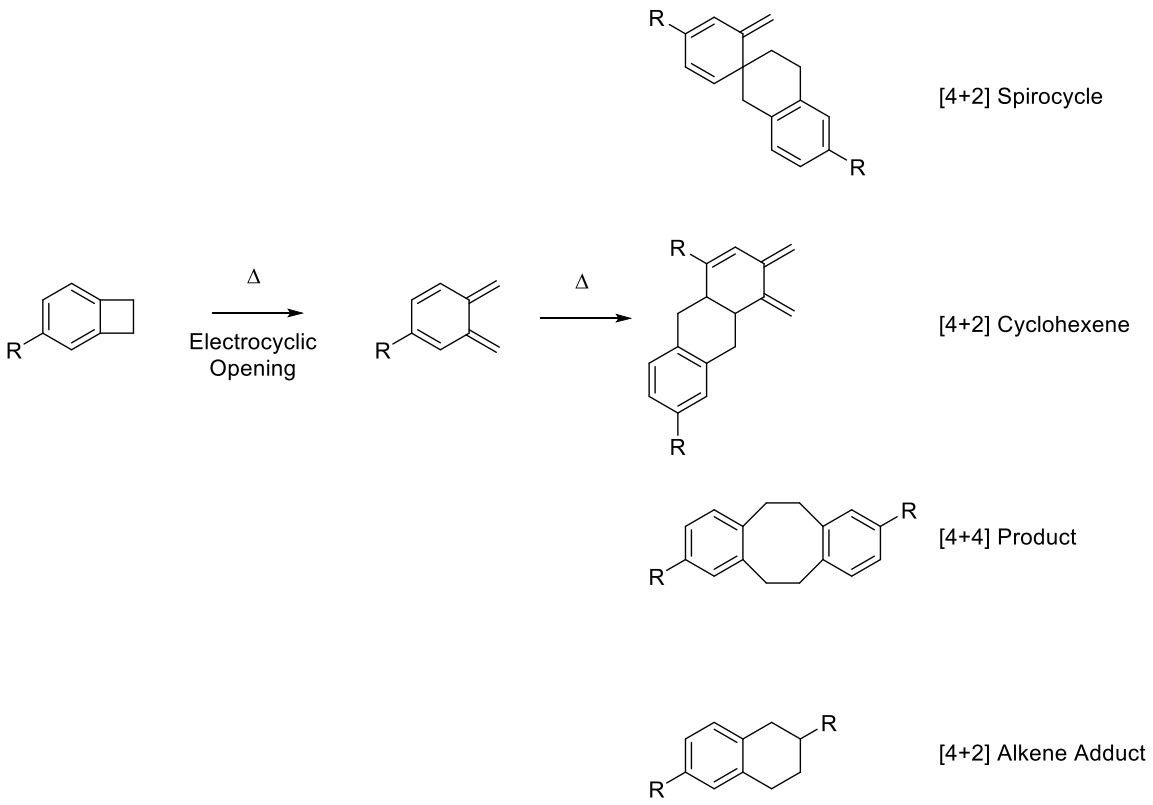

Figure 3.1: Scheme of four major products of BCB resin crosslinking.

BCB chemistry is also attractive for a packaging application since BCB resins have minimal shrinkage[47], low copper diffusion[48], do not require any small molecule additives to complete a cure and do not release any small molecules or gasses during cure[49]. BCB is often difficult to synthesize on a lab scale, which represents a sufficient barrier to prevent most materials scientists from investigating the potential of BCB resins. However, on an industrial scale, BCB can be mass manufactured via flash vacuum pyrolysis (FVP), which can produce ordinary and 1-substituted BCBs in high yield on kilogram scale.

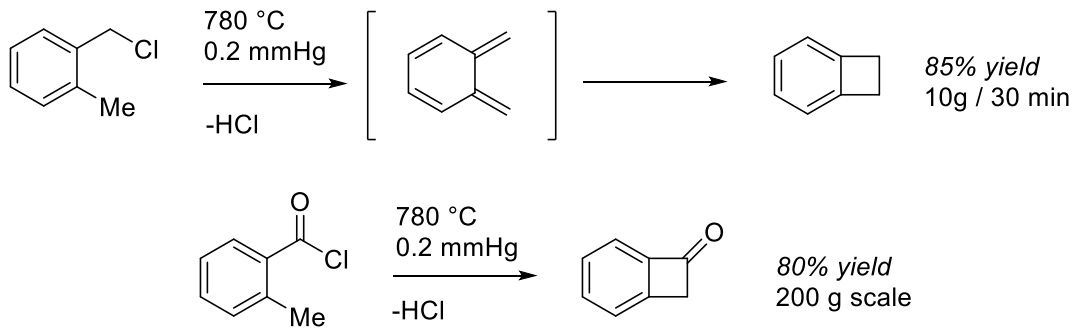

Figure 3.2: Large scale synthesis of BCBs via FVP.

In this chapter, three dually functionalized POSS resins have been synthesized and evaluated for their application as resins for microelectronics packaging. The first resin is a dually functionalized POSS containing both allyl BCB and dimethyl benzyl alcohol moieties, which eliminate one water molecule and crosslink as α-methyl styrene upon exposure to acid. The second resin is dually functionalized POSS based on a minimum amount of allyl methyl methacrylate to yield photosensitivity along with allyl BCB. The third and final POSS contains all BCBs with an internal *E* alkene as a functional group for nitrene based crosslinking.

3.2 MATERIALS CHARACTERIZATION

In Chapter 3 and subsequent chapters, novel dielectric materials and polymers are characterized for their application in microelectronics packaging. To calculate the in-plane CTE, the change in the radius of curvature of the sample (a silicon wafer coated with the cured polymer) was measured on a Flexus Tencor F2320 equipped with a temperature-controlled hotplate and a He-Ne laser. All in-plane CTE measurements were done at Georgia Tech in collaboration with Dr. Brennen Mueller, Jared Schwartz and Dr. Paul Kohl. The stress at each temperature was calculated using Stoney's equation, Equation 3.1, where $E_s/1-\nu_s$ is the biaxial elastic modulus of the substrate, t_s is the

thickness of the substrate, t_f is the film thickness and R is the change in radius of curvature, given by Equation 3.2[50]. R_1 is the radius of curvature of the bare silicon wafer before processing, and R_2 is the radius of curvature after processing (cure of 250˚C for one hour). The stress as a function of temperature was fit by ordinary least-squares (OLS) linear regression to calculate $\partial\sigma/\partial T$. Final values for all properties measured are reported with their 95% confidence intervals. Equation 3.3 was then used to calculate the in-plane CTE, α_{xy}, where α_s is the CTE of the substrate, and ν_f is the Poisson's ratio of the film, estimated to be 0.33.

$$\sigma = \left(\frac{E_s}{1-\nu_s}\right)\frac{t_s^2}{6Rt_f} \tag{3.1}$$

$$\frac{1}{R} = \frac{1}{R_2} - \frac{1}{R_1} \tag{3.2}$$

$$\frac{\partial\sigma}{\partial T} = \left(\frac{E_f}{1-\nu_f}\right)[\alpha_{xy} - \alpha_s] \tag{3.3}$$

Through-plane CTEs were measured on a Woollam M-2000D ellipsometer equipped with a HCS 402 temperature-controlled stage with a liquid nitrogen pump. Ellipsometric measurements were made from 370 to 988.8 nm at an incident angle of 60 degrees. The sample was heated to 200°C and then ramped to room temperature at a rate of -5°C/min. The optical constants were defined by Cauchy models, as shown in Equation 3.4, where n is the refractive index, K_1, K_2, and K_3 are fitted coefficients, and λ is the wavelength. The temperature of the substrate was taken into account by modeling the Si wafer with the Si Temp JAW model. The as-collected values of polymer CTE, α_z, were corrected for expansion in the z-direction due to being constrained on the substrate by use of Equation 3.5, where α_z is the corrected through-plane CTE of the polymer.

This correction accounts for the in-plane contributions to the through-plane volume change due to the constraint of the Si wafer[51-53].

$$n(\lambda) = K_1 + K_2\lambda^{-2} + K_3\lambda^{-4} \tag{3.4}$$

$$\alpha_{z,measured} = \alpha_z + \left(\frac{2\nu_f}{1-\nu_f}\right)[\alpha_{xy} - \alpha_s] \tag{3.5}$$

Indents were performed with a cube corner diamond tip (Northstar, tip radius ~40 nm) and calibrated against quartz and polycarbonate standards. All nanoindentation data were also taken at Georgia Tech. The corrected tip geometry was defined by Equation 3.6. Step times for each indent were held constant, while the peak force was varied. The tip was loaded over a 10s period of time, held at the peak force for 10s to allow for time-dependent relaxations, and unloaded over a 4 s period of time. Hardness, H, was calculated at the maximum load, P_{max}, divided by the projected contact area, $A(h_c)$, Equation 3.7. The contact area was estimated using the Oliver Pharr model in Equation 3.8, where h_{max} is the maximum indent depth, ε is a geometrical constant, and S is the stiffness[54]. The stiffness was defined as the initial slope of the unloading curve, and the reduced modulus was calculated using Equation 3.9, where β is a geometrical constant[55].

$$A(h_c) = 2.598h_c^2 + C_1h_c^1 + C_2h_c^{1/2} + \cdots + C_8h_c^{1/128} \tag{3.6}$$

$$H = \frac{P_{max}}{A(h_c)} \tag{3.7}$$

$$h_c = h_{max} - \frac{\varepsilon P_{max}}{S} \tag{3.8}$$

$$E_r = \frac{\sqrt{\pi}}{2\beta}\frac{S}{\sqrt{A(h_c)}} \tag{3.9}$$

$$\frac{1}{E_r} = \frac{(1-\nu_f^2)}{E_f} + \frac{(1-\nu_i^2)}{E_i} \tag{3.10}$$

3.3 DIMETHYL BENZYL ALCOHOL OR "ITO" POSS

The first silsesquioxane developed was inspired by work from Hiroshi Ito, who developed a (dimethyl benzyl alcohol) styrene system as a dielectric functional resist. The resist system relies on using established and highly efficient photoacid generators (PAGs) as the photo-active compound in the formulation. The strategy exploits photogenerated acid to eliminate water to form an alpha-methyl styrene, which initiates a cationic polymerization of the elimination product which renders the exposed areas insoluble (Figure 3.3).

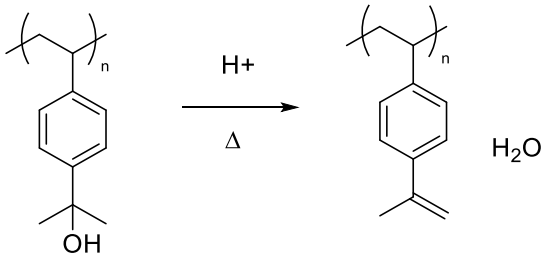

Figure 3.3: Hiroshi Ito dielectric negative tone resist.

Firstly, a BCB moiety suitable for hydrosilylation on a POSS was synthesized. The synthesis is outlined in Scheme 3.1.

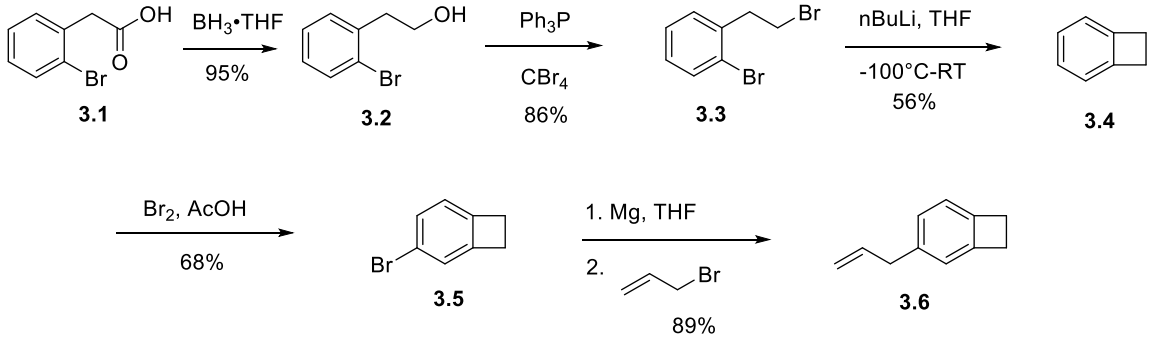

Scheme 3.1: Synthesis of allyl benzocyclobutene.

Starting with commercially available 2-bromophenyl acetic acid, reduction to the primary alcohol was achieved with stoichiometric borane-THF complex in high yield. Conversion to the primary alkyl bromide using the Appel Reaction, followed by lithiation to create the four membered BCB ring via a 4-exo-tet cyclization. It should be noted that the synthesis of BCB **3.4** is extremely sensitive to temperature; reactors were cooled to -100˚C with pentane and liquid nitrogen before addition of n-butyl lithium. Reactor bath temperature was monitored throughout the course of the reaction with a mercury thermometer. When temperatures rose above -78˚C, elimination of the primary alkyl bromide forming the corresponding styrene dominated the reaction mixture. Further, the styrene was extremely difficult to separate from desired **3.4** via fractional distillation. Nevertheless, under rigorously cold conditions, BCB can be obtained at large scale in reasonable yield after distillation. Mild electrophilic aromatic substitution was performed using bromine in glacial acetic acid to obtain the brominated BCB **3.5**. Finally, after formation of the aryl Grignard reagent, reaction with an excess of allyl bromide (as an electrophile) afforded the desired allyl BCB **3.6** in excellent yield.

An allyl Ito derivative was targeted instead of a styrene derivative in order to match the kinetics of the forthcoming hydrosilylation reaction. Synthesis of the desired molecule was facile from available materials and is outlined in Scheme 3.2.

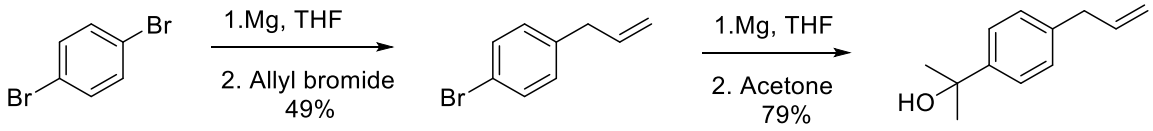

3.7 **3.8** **3.9**

Scheme 3.2: Synthesis of tertiary alcohol **3.9**.

Synthesis began with readily available and inexpensive 1,4-dibromobenzene **3.7.** By applying a stoichiometric amount of magnesium, the mono-aryl Grignard reagent was formed. Subsequent reaction with allyl bromide afforded the 1,4-allylbromobenzene **3.8**. Another Grignard reaction using acetone as the electrophile provided the desired Ito target **3.9** upon mildly acidic workup. With both targets in hand, a dually functionalized Ito-POSS was synthesized.

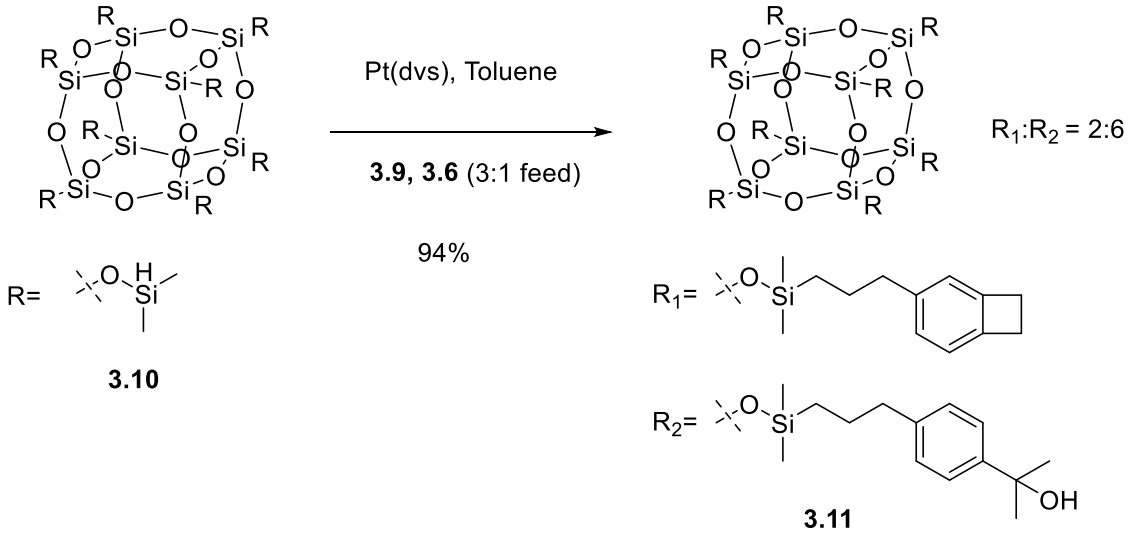

Scheme 3.3: Synthesis of Ito-POSS.

A dimethyl silane POSS **3.10** can be synthesized[56] or obtained commercially. Using Karstedt's catalyst[57] (platinum divinyl siloxane or Pt(dvs)), Ito-POSS **3.11** could be synthesized containing a statistical ratio of allyl compounds that matched the feed by H^1NMR[58]. It should be noted, however, that not every cube has exactly two BCB units and six alcohol units, rather a distribution is obtained, which was characterized by MALDI-TOF mass spectrometry and described in the experimental section of this chapter.

The isolated Ito POSS was formulated with mesitylene and 5 wt% of triphenylsulfonium triflate PAG and spin coated on a bare silicon wafer to obtain a film 320 nm thick after a post exposure bake of one minute. Contact lithography was performed using a Ronchi Ruling mask with a 25 μm full pitch, at 217 mJ/cm^2 at 254 nm. A post exposure bake of 130˚C for 1 minute was followed by development in isopropyl alcohol for 20s to provide an image. An optical microscope (Figure 3.4), shows that the Ito POSS system is capable of forming discrete images; however initial tests suggest that this system lacks the contrast of its polystyrene counterpart. Qualitatively, it was observed that these images suffered from line edge roughness and considerable sloping. Furthermore, attempts to scale resolution down to the target 10 μm full pitch were unsuccessful, suggesting that this lithography is inadequate to meet the demands of next generation packaging materials.

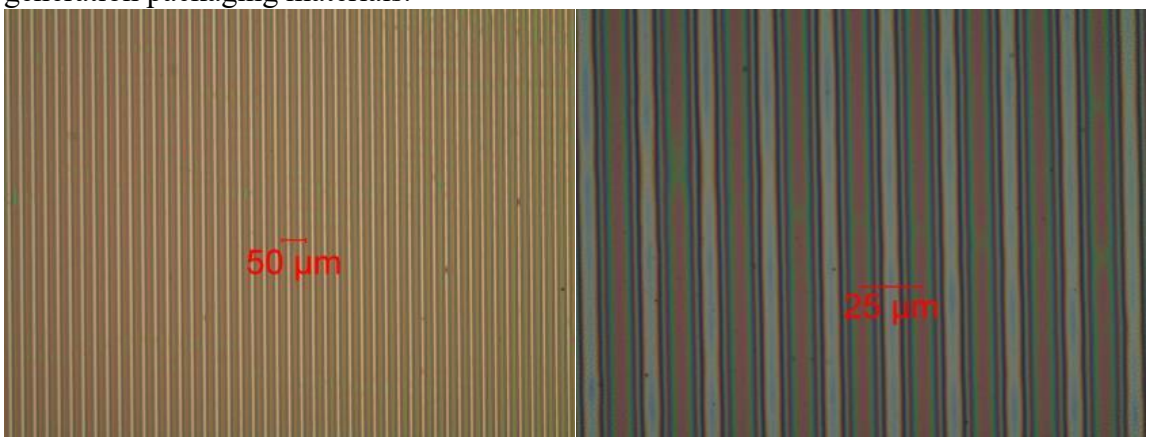

Figure 3.4: Optical micrographs of patterned Ito POSS. While images can be reliably formed at 25 micron full pitch, considerable sidewall sloping can be observed in the optical micrographs.

An initial materials evaluation of dielectric constant and coefficient of thermal expansion was performed on Ito POSS. The dielectric constant of the material was estimated to be 2.19 based on the square of the refractive index (which was obtained by

spectroscopic ellipsometry), which is well within the requirements for a next generation packaging material. However, thermomechanical evaluations deemed the material to be less promising. In collaboration with Georgia Tech and Drs. Paul Kohl and Brennen Mueller, optical wafer bow stress tests and in plane coefficient of thermal expansion measurements were performed. A formulation of Ito POSS at 5 wt% triphenylsulfonium triflate was coated on a bare silicon wafer and exposed, after which a residual stress of -12.21 ± 0.79 MPa was observed. The wafer was cured in a vacuum oven under nitrogen at 250˚C for two hours, after which a residual stress of +23.85 ± 0.37 MPa was observed. Measuring the residual stress as a function of temperature produced a linear relationship. The slope, dσ/dT, was used to obtain an in plane CTE α_{xy} of 53.5 ± 3.9 using Equation 3.3, which suggests that the few BCB units in the resin provide insufficient crosslinking density to provide the desired sub 30 ppm/K value for CTE. The results are depicted in Figure 3.5.

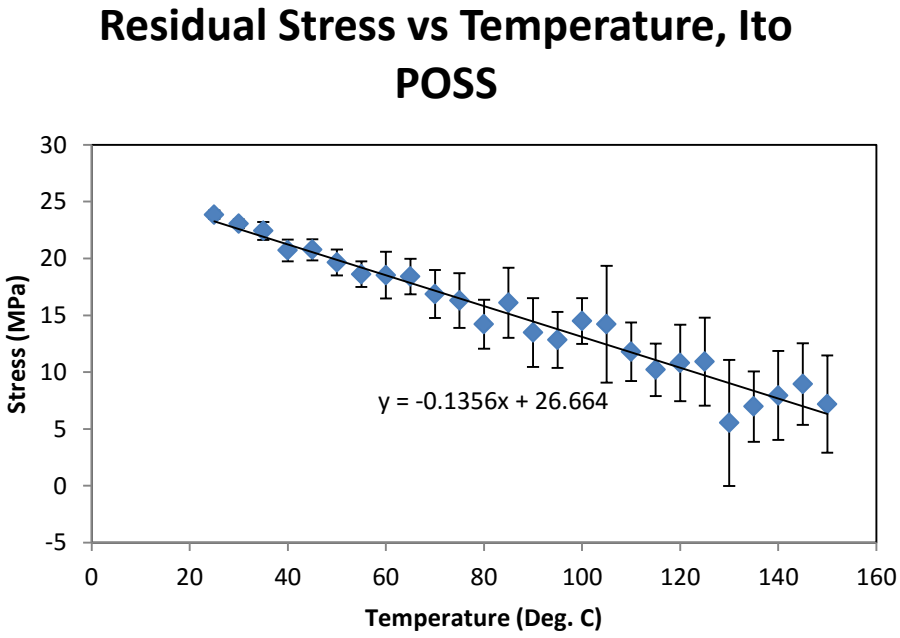

Figure 3.5: Stress as a function of temperature for cured Ito POSS on silicon.

The out of plane CTE, α_z was measured using heated state ellipsometry with a substrate temperature dependent Cauchy model. The true value for α_z was calculated using Equation 3.5, informed by the in plane CTE data to produce a value of 203 ± 1 ppm/K, which is on the order of Cyclotene.

In summary, the Ito POSS resin developed for next generation microelectronics packaging possesses a few interesting traits (outlined in Table 3.1), but is ultimately insufficient for the application. The resin possesses patternability, but poor contrast. With a dielectric constant of 2.19 at optical frequencies, the material is a suitable insulator. However, CTE values both in and out of plane are disappointing, especially considering the high SiO_2 content. In order to surpass the limitations of this resin, two new POSS cubes were designed to drastically increase BCB content in order to decrease CTE, and new photoresist chemistries were explored.

Table 3.1	n	n^2	E_z (Gpa), assumed	α(xy) ppm/K	α(z) ppm/K
Ito POSS	1.48	2.19	1.8	53.5 ± 3.9	203±1

Table 3.1: Summary of Ito POSS material properties. Good dielectric properties are overshadowed by mediocre CTE and inadequate lithographic contrast.

3.4 Dually Functionalized (DF) and Octovinyl BCB (OVBCB) POSS

While the first generation Ito POSS resin proved to be ultimately insufficient for the demands of next generation packaging materials, the versatility of the silsesquioxane platform provided access to new chemistries in order to increase BCB concentration, as well as other mechanisms for photopatternability. Two new mechanisms of crosslinking were explored: firstly, radical initiated acrylate polymerization, and secondly, bis-azide nitrene insertion.

A Dually Functionalized POSS (DF POSS) was envisioned, possessing both an acrylate functional group for photopatterning via a radical polymerization and a BCB functional group to impart a thermoset with high thermal stability. While the acrylates are known to make excellent photo-definable patterns, these materials suffer from low thermal stability and shrinkage upon curing. While the BCB functionality is not inherently photopatternable, the moiety has a minimum amount of shrinkage: the acrylate patterns could be vitrified by the BCB thermoset[59].

Using previously synthesized allyl BCB **3.6**, a mixed hydrosilylation reaction was performed along with allyl methacrylate[60]. A ratio of three acrylates to five BCBs was chosen as three acrylates proved the minimum amount in order to render the resin sufficiently photosensitive. Acrylates typically suffer from high shrinkage and low thermal stability, so it is desirable to minimize their contribution to the resin from a design standpoint. The resulting Dually Functionalized POSS (DF POSS) **3.12** was isolated in high yield following column chromatography. It was found that the feed of acrylates to BCB matched the composition by proton NMR. Further, the allyl alkenes were selectively hydrosilylated over the available acrylate alkenes, which are more sterically encumbered and electron deficient.

In order to achieve the maximum amount of BCB incorporation into a POSS resin yet still maintain photosensitivity, an Octo-vinyl BCB POSS (OVBCB POSS) **3.15** was synthesized. The photosensitivity in this resin is based on a bis-azide nitrene insertion into the alkene moiety, to achieve a dissolution difference based on change in molecular weight. The required alkynyl BCB **3.14** was synthesized via Corey-Fuchs Homologation protocol from the corresponding aldehyde **3.13**. The *E* selective hydrosilylation used to synthesis cube **3.15** was accomplished with tritertbutyl phosphine as a ligand on platinum[61]. During the reductive elimination, alkene stereochemistry is set as *E* due to

sterics of the ligand [62]

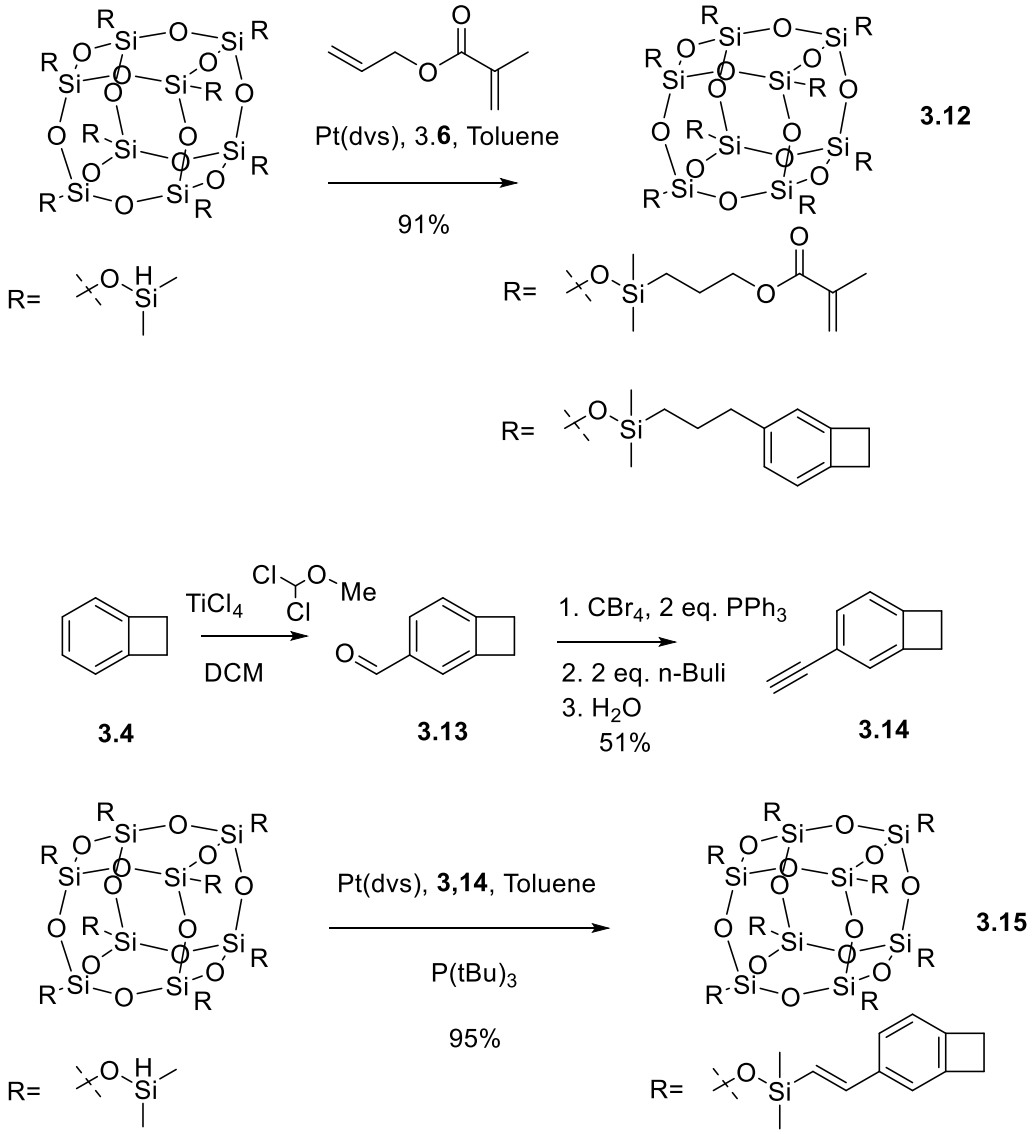

Scheme 3.4: Synthesis of OVBCB POSS and DF POSS.

While both of these cubes could be synthesized in high yields, both molecules were of too low molecular weight in order to be deposited on silicon wafers via spin coating solutions. In order to increase the molecular weight of the resin, both **3.12** and **3.15** were B-staged (an industry term meaning partial polymerization, or oligomerization, stopping

short of a complete cure, i.e. gelation of the resin).

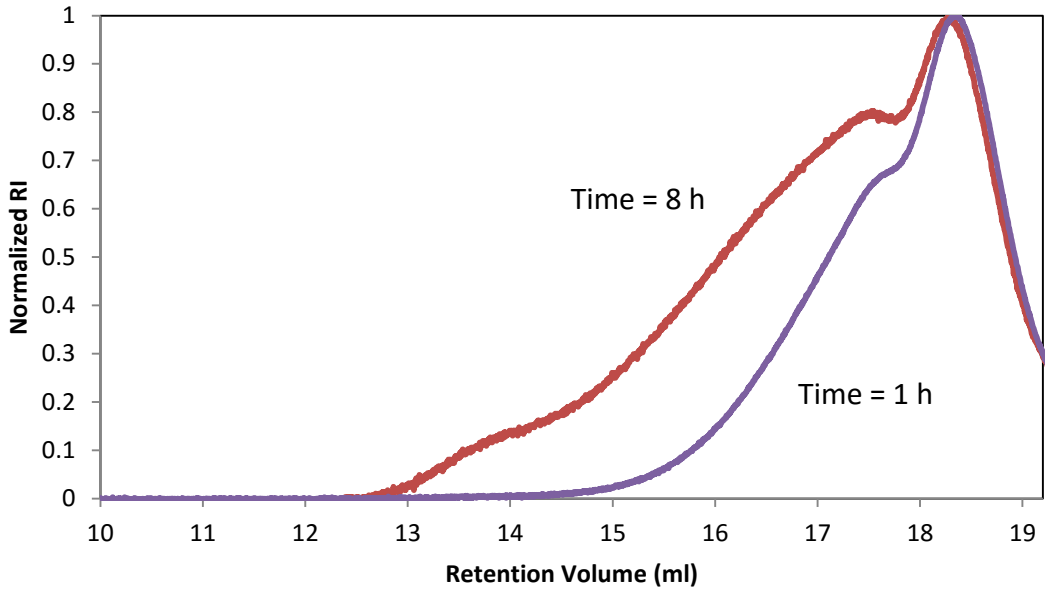

Figure 3.6: Size exclusion chromtapgraphs of B-Stages DF POSS samples.

It was found that the B-stage of POSS resins proceeded at a manageable pace when 25 weight percent solutions were heated at 160˚C over time. Figure 3.6 shows that the B-stage proceeds in an uncontrolled manner, with very high molecular weight cube oligomers forming preferentially.

Interestingly, the rate of polymerization for the two POSS resins differed substantially. Figure 3.7 shows DF POSS polymerizes rapidly and it appears to be second order kinetics. In contrast, OVBCB POSS increases its molecular weight in a much slower and linear (first order) fashion. This result is likely due to the acrylate moieties attached to DF POSS, which are excellent dienophiles. Since the polymerization occurs via Diels Alder reaction, the faster cycloaddition is no doubt an addition to the acrylates. Unfortunately, this also means that the photosensitive acrylates are being consumed

during the course of the B-stage, an undesirable result leading to decreased lithographic sensitivity, as will be seen later.

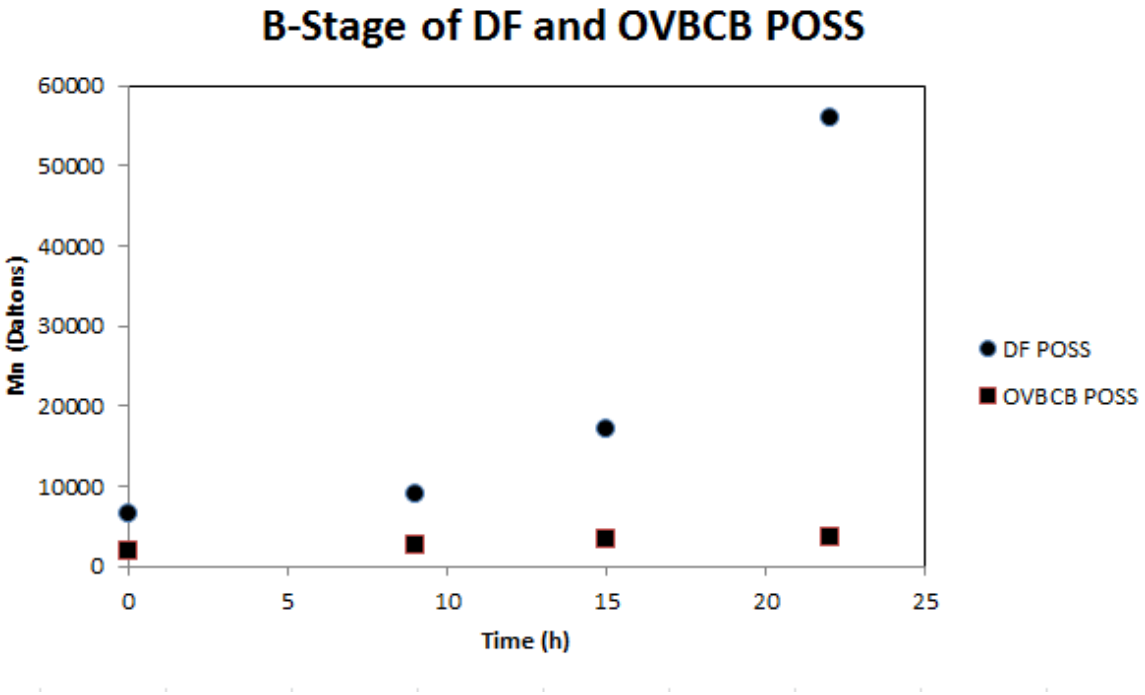

Figure 3.7: Molecular weight changes over time during a B-Stage process for OVBCB POSS and DF POSS (25 wt% in mesitylene, 160˚C).

The B-stage process was successful in producing resins with suitable viscosity and molecular weight for spin coating on silicon, as long as a suitable adhesion promoter (amino-triethoxy propylsilane (APTES)) was used. Unfortunately, more often than not, the B-stage process resulted in gelation of the resin or incorporation of difficult to remove gel particles, rendering the material useless. The B-stage process proved to be the ultimate downfall of these materials for potential technology transfer, yet several successful batches were used in order to complete materials evaluation.

Lithographically, both materials readily met the project resolution requirements of five microns. B-staged resins were formulated with 5 wt% of their respective photoactive

compounds in mesitylene, coated and exposed using a contact lithography tool at i-line (365 nm) exposure. The results were promising, and representative micrographs are found in Figure 3.8.

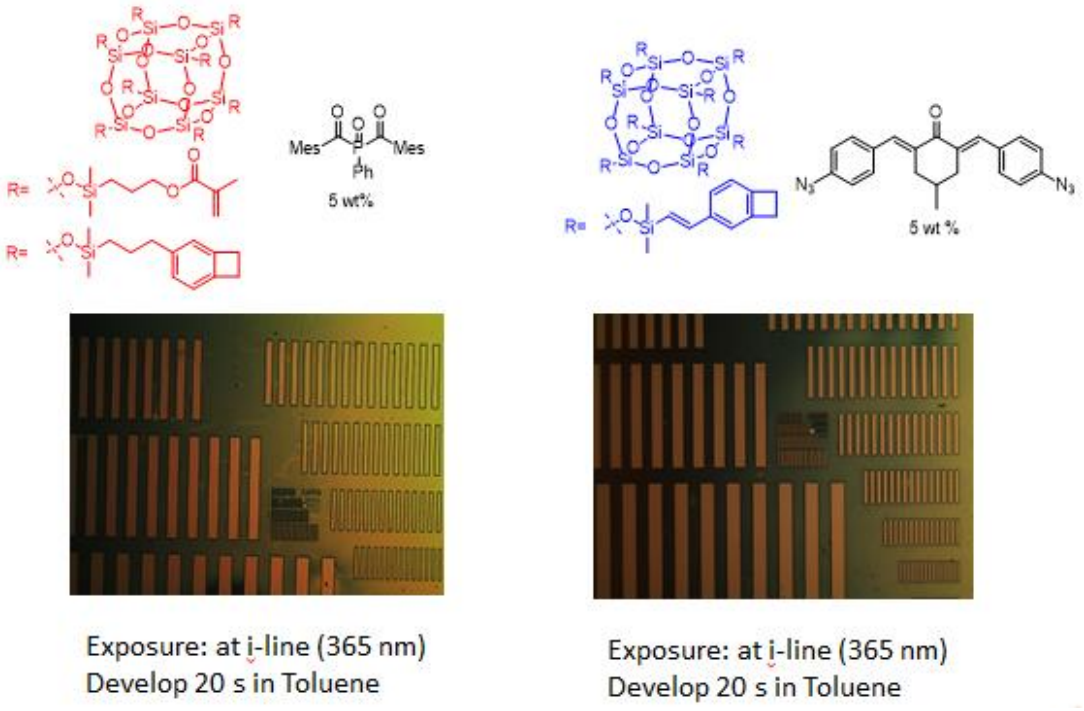

Figure 3.8 Lithographic evaluation of DF POSS and OVBCB POSS. Ten micron full pitch resolved. Largest features (bottom left of each image) are 100 micron half pitch.

Both materials produced five micron critical dimensions at i-line exposure. It should be noted that lithography experiments were performed in relatively thin (about half a micron) films due to limited material availability. It is important for next generation packaging materials to provide high aspect ratio (about 3:1) features, but the lithographic proof of concept is promising nonetheless. It should also be noted it is important to obtain thick films for this application: typical packaging dielectric layers are on the order of fifteen to one hundred microns thick. To demonstrate that these materials can be cast

thick films, concentrated formulations were spun that produced twenty five micron thick films, confirmed by profilometry.

Material evaluation provided impressive results. The in plane CTE α_{xy} was evaluated in collaboration with Dr. Brennen Mueller at Georgia Tech via a wafer bow flexus measurement. As explained previously, the residual stress of a substrate is measured optically as a function of temperature, then the CTE in plane is obtained with knowledge of the substrate CTE (3 ppm/K for Si), reduced modulus (obtained through nanoindentation) and poisson's ratio (here assumed to be 0.33). Both resins were found to have excellent in plane values (results outlined in Figure 3.9).

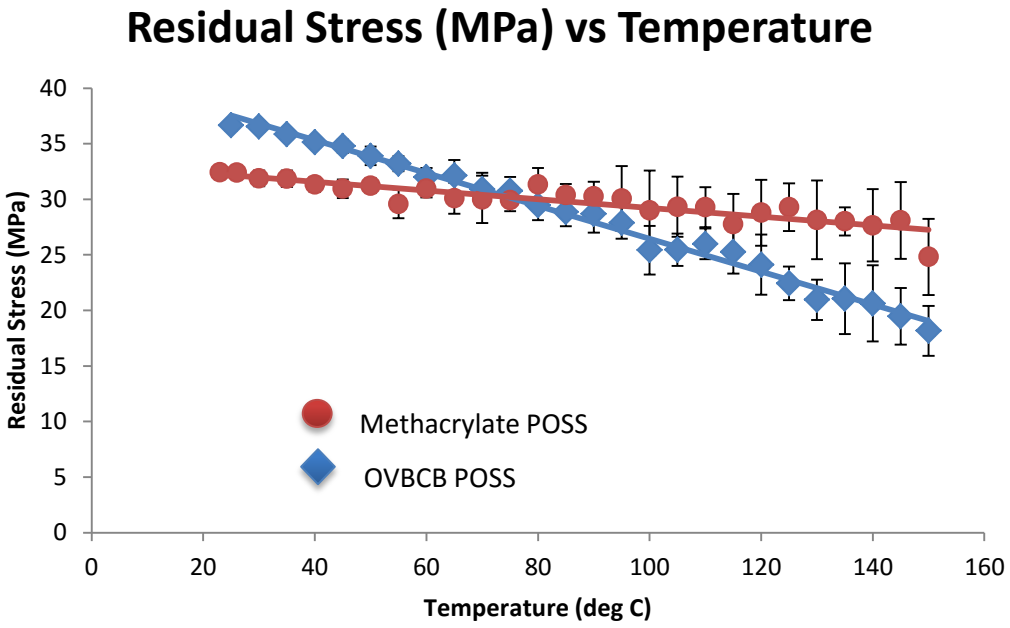

Figure 3.9: Residual stress curves of OVBCB POSS and DF POSS on silicon.

OVBCB POSS was found to have an in plane CTE of 12.7 ± 0.9 ppm/K, while DF POSS was found to have an in plane CTE of 6.0 ± 1.3 ppm/K. While it is easy to conclude that these results are simply excellent and worthy of incorporation into a microelectronic

device, one must consider the implication of DF POSS's in plane CTE being approximately a factor of two smaller. In order to understand CTE at an atomic level, recall from chapter one that CTE is related to the average interatomic distance over a material, dictated by the shape of the Morse Potential of atomic bonds. The stronger the bonds on average, the lower the CTE will be. The difference between DF POSS and OVBCB POSS is the presence of acrylates, which are likely consumed via Diels Alder over the course of the B-stage and cure. It is proposed here that the [4+2] Diels Alder adduct of BCB with a simple alkene electrophile (other than BCB itself) leads to a product with stronger bonds, or at least less free volume. This results in a lower CTE. More evidence for this "[4+2] hypothesis" will be found in subsequent chapters.

Despite excellent in-plane CTE values, both POSS materials demonstrated significant anisotropy. Out-of-plane CTEs α_z were obtained as before using heated stage ellipsometry. It was found that DF POSS had an out of plane CTE of 216 ± 9 ppm/K, while OVBCB POSS's value was found to be 105 ± 4 ppm/K, this time a factor of two difference in favor of OVBCB POSS. In this case, it is proposed that the differences stem from the differences in molecular weight obtained during the B-stage. During deposition via spin coating, shear is applied to linear chains of oligomerized cubes, preferentially orienting them in the plain of the wafer. This method of deposition is believed to be the source of surprising differences bewtween CTEs in the plane versus out of the plane. While all α_z measurements were done at the center of each wafer, it is proposed that if one measured the CTE closer to the edge, one would find an increased value proportional to the shear applied. The results of the out of plane measurements are illustrated in Figure 3.10.

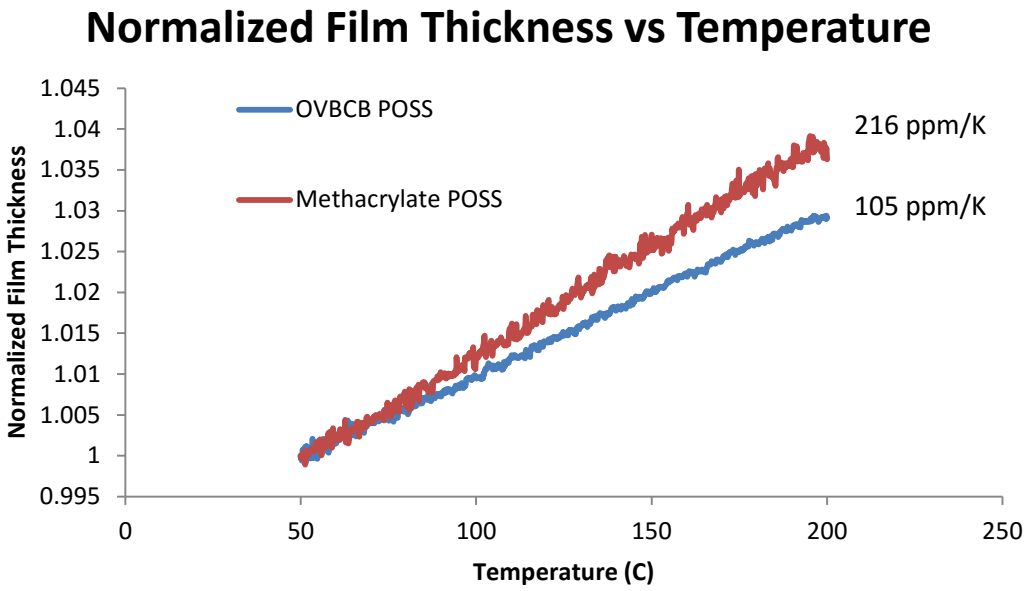

Figure 3.10: Out of plane CTE measurements of DF POSS and OVBCB POSS.

In conclusion, two very unique and promising resins have been developed for application in microelectronics packaging. Both have very low dielectric constants as outlined in Table 3.2 (2.0 for DF POSS and 2.2 for OVBCB POSS, at optical frequencies). Both possess good photosensitivity and can be patterned down to five micron half pitch using i-line contact lithography, and both have excellent CTEs in the plane, well below the target of 30 ppm/K. Unfortunately, the downfall of these materials is the uncontrollable B-stage process. While the B-stage was able to produce several samples for evaluation, the B-stage process produced gels or gel particles in the majority of experiments, even when run to identical time points. The high fail rate of this process suggests that as stand-alone resins, these materials will never make it to market. However, since the cubes themselves (non-B-staged **3.12** and **3.15**) can be synthesized in high yield and appear to possess exceptional properties, they may have an application as polymer additives in future dielectric materials.

Table 3.2	M_n (Daltons)	n	n^2	E_r (Gpa)	α(xy) ppm/K	α(z) ppm/K
DF POSS	9100	1.41	2.00	3.91 ± 0.44	6.0 ± 1.3	216 ± 9
OVBCB POSS	2700	1.49	2.22	4.59 ± 0.15	12.7 ± 0.9	105 ± 4

Table 3.2: Summary of materials properties for DF POSS and OVBCB POSS. B-staged resins had excellent dielectric properties and CTE, although both demonstrated significant anisotropy.

3.5 Experimental Section

2-(2-bromophenyl)ethanol

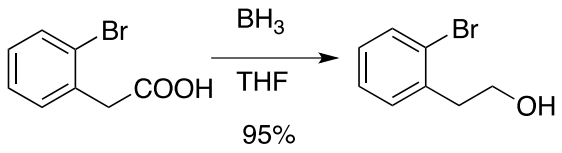

A 2L 3-neck round bottom flask equipped with a magnetic stir bar, condenser and addition funnel, was flame dried and purged with dry argon. To the vessel, 2-(2-bromophenyl)acetic acid (100 g, 465 mmol, 1 eq) was added. The solid was dissolved in 300 mL of dry THF, and 600 mL of 1M borane (1.3 eq) in THF was added dropwise over 4 hours. The solution was stirred overnight, then refluxed for 3 hours, cooled to room temperature, and quenched with 100 mL of water. The THF was removed by rotary evaporation, and the solution was diluted to 500 mL with water. The aqueous phase was extracted with 200 mL of ethyl ether three times. The organic phases were combined and washed with equivolume amounts of water, sat. aq. $NaHCO_3$ (2x), and twice with brine. The solution was filtered through a short plug of silica, and the ether was removed via rotary evaporation to yield 2-(2-bromophenyl)ethanol (88 g, 95% yield) as a colorless oil. ^{1}H-NMR (400 MHz; $CDCl_3$): δ 7.55 (dd, *J* = 7.9, 1.0 Hz, 1H), 7.29-7.23 (m, 2H), 7.10 (m, 1H), 3.87 (s, 2H), 3.05-3.01 (m, 2H), 3.88 (d, *J* = 13.4 Hz, 2H), 3.05-3.01 (m, 2H),

1.57-1.54 (bs, 1H). ^{13}C-NMR (100 MHz; $CDCl_3$): δ 137.9, 133.1 , 131.4, 128.35, 127.6, 124.8, 62.2, 39.5. HRMS: $C_8H_9O^{79}Br$ calculated: 199.9837, found: 199.9838.

1-bromo-2-(2-bromoethyl)benzene

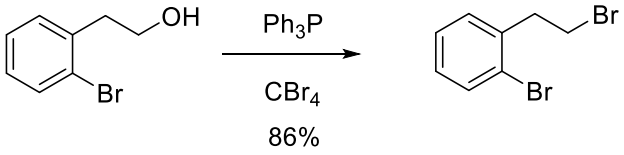

Under argon, 2-(2-bromophenyl)ethanol (23.0 g, 115 mmol ,1 eq) was added to a round bottom flask equipped with a magnetic stir bar and was dissolved in 350 mL of dry dichloromethane. The resulting solution was cooled to 0 ˚C in an ice bath. Triphenylphosphine (30.0 g, 115 mmol , 1 eq) was added to the solution. Carbon tetrabromide (38 g, 115 mmol, 1 eq) was added portionwise to the solution, and the solution was warmed to room temperature and stirred overnight. The solvent was reduced by rotary evaporation, and the yellow oil was passed through a short plug of silica with DCM as the eluent. Removal of the solvent and purification via distillation yield the product as a clear and colorless oil (21.1 g, 86% yield). ^{1}H-NMR (400 MHz; CDCl3): δ 7.71-7.64 (m, 1H), 7.57-7.52 (m, 1H), 7.46 (dddd, *J* = 8.2, 5.6, 2.9, 1.2 Hz, 1H), 7.16-7.12 (m, 1H), 3.60 (t, *J* = 7.6 Hz, 2H), 3.31 (t, *J* = 7.6 Hz, 2H). ^{13}C-NMR (100 MHz; CDCl3): δ 138.2, 133.2, 131.3, 128.9, 127.7, 124.4, 39.7, 31.2. HRMS: $C_8H_8{}^{79}Br_2$ calculated 261.8993, found 261.8994.

Bicyclo[4.2.0]octa-1,3,5-triene

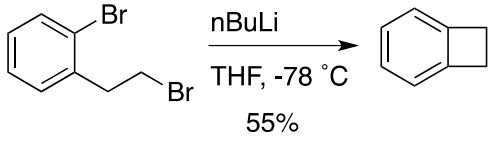

In a 2 L flask equipped with a stir bar, 1-bromo-2-(2-bromoethyl)benzene (61.5 g, 233 mmol, 1 eq) was dissolved in 760 mL of dry THF. The vessel was cooled to -78˚ C and 102 mL of n-butyllithium (2.5 M in hexanes, 1.1 equivalents) was added dropwise. The reaction vessel was warmed to room temperature over the course of 1 hour after complete addition of n-butyllithium. The reaction was quenched with 400 mL of water. The solution was extracted with ether (3x 250 mL), and the combined ether layers were dried over $MgSO_4$. The ether was removed via rotary evaporation and a pale yellow oil was obtained. Distillation yielded the desired product (b.p. 60˚C at 65 mmHg) as a colorless oil in 55% yield. ^{1}H-NMR (400 MHz; CDCl3): δ 7.21-7.18 (m, 2H), 7.07-7.04 (m, 2H), 3.19 (s, 4H). ^{13}C-NMR (100 MHz; CDCl3): δ 145.6, 126.6, 121.2, 29.4. HRMS: C_8H_8 calculated 104.0626, found 104.0628.

Bicyclo[4.2.0]octa-1,3,5-triene-3-carbaldehyde

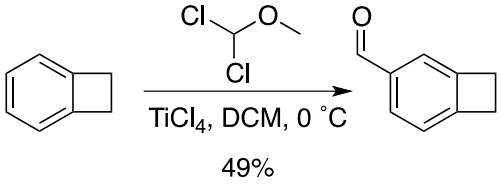

49%

In a flame dried round bottom flask equipped with a stir bar, benzocyclobutane (4.776 g, 45.8 mmol, 1 eq) was dissolved in 60 mL of dry dichloromethane under argon. The reaction vessel was cooled to 0 ˚C in an ice bath. Titanium tetrachloride (17.5 g, 91.9 mmol, 2 eq.) was added slowly over the course of 10 minutes. A solution of 1,1-dichloromethyl methyl ether (5.5 g in 12 mL of dry DCM, 47.8 mmol, 1.05 eq.) was then added dropwise, and the reaction was stirred at 0 ˚C for 1.2 hours. The contents of the reaction vessel were poured over 100 mL of ice and water and the product was extract with ethyl acetate (3x 100 mL). The combined organics were washed with water, then brine, and dried over Na_2SO_4. Removal of the solvent yielded 5.2 g of crude product that

was purified using flash chromatography (10% ethyl acetate/hexanes). The purified product was obtained as a slight yellow oil (2.95 g, 49%). ^{1}H-NMR (400 MHz; $CDCl_3$): δ 9.95 (s, 1H), 7.72 (ap. d, *J* = 7.5 Hz, 1H), 7.57 (ap. s, 1H), 7.20 (ap. d, *J* = 7.5 Hz, 1H), 3.25-3.21 (m, 4H).^{13}C-NMR (10 MHz; $CDCl_3$): δ 192.7, 153.9, 146.8, 135.9, 130.6, 123.1, 123.0, 30.2, 29.4. HRMS: C_9H_8O calculated 132.0575, found 132.0573.

3-vinylbicyclo[4.2.0]octa-1,3,5-triene

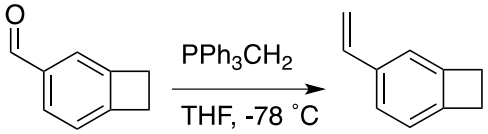

55%

In a flame dried round bottom flask equipped with a stir bar, triphenylphosphonium iodide (11.3 g, 27.8 mmol, 1.2 eq) was added to 50 mL of dry THF. The slurry was cooled to -78 ˚C and 12.7 mL of n-butyllithium (2.5 M in hexanes, 1.2 eq) was added dropwise. The slurry turned bright yellow, and was warmed to room temperature. The solution became dark orange after complete dissolution, and the reaction vessel was cooled back to -78 ˚C. Bicyclo[4.2.0]octa-1,3,5-triene-3-carbaldehyde (3.44 g, 23.2 mmol, 1 eq) dissolved in 13 mL of dry THF and was added slowly to the solution. A gummy precipitate appeared during the addition. The reaction was warmed to room temperature and stirred for 2 hours. The solution was filtered, and the solvent was removed via rotary evaporation. Then, the crude material was passed through a short column of silica and further purified by column chromatography (pentanes) to yield the product (1.88g, 55% yield) as a colorless oil. ^{1}H-NMR (400 MHz; $CDCl_3$): δ 7.22 (dd, *J* = 7.6, 1.3 Hz, 1H), 7.16 (ap. s, 1H), 7.01 (dd, *J* = 7.5, 0.8 Hz, 1H), 6.70 (dd, *J* = 17.6, 10.9 Hz, 1H), 5.67 (dd, *J* = 17.6, 1.0 Hz, 1H), 5.15 (dd, *J* = 10.9, 1.0 Hz, 1H), 3.17-3.16 (m, 4H). ^{13}C-NMR (100 MHz; $CDCl_3$): δ 146.2, 145.8, 137.9, 136.6,

125.7, 122.7, 119.9, 112.5, 29.6, 29.4. HRMS: $C_{10}H_{10}$ calculated 130.0783, found 130.0783.

3-ethynylbicyclo[4.2.0]octa-1,3,5-triene

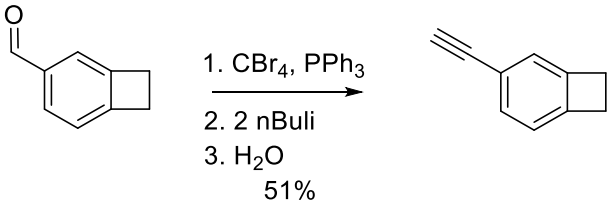

In a flame dried round bottom flask equipped with a stir bar, Bicyclo[4.2.0]octa-1,3,5-triene-3-carbaldehyde (1.165 g, 8.81 mmol, 1 eq) and triphenylphosphine (9.243 g, 35.2 mmol, 4 eq) were dissolved in 40 mL of distilled DCM and cooled to 0˚ C. Carbon tetrabromide (5.846 g, 17.6 mmol, 2 eq) was added to the flask as a solution in 15 ml DCM, and the reaction was stirred for 30 minutes until starting material had been consumed by TLC. Then, ether was added to the solution and the reaction was run through a short plug of silica with hexanes and concentrated as a light yellow oil, then used in the next step without purification. The crude material was dissolved in distilled THF and cooled to -78˚C. Then n-butyllithium (13.8 ml, 1.3M, 2.1 eq) in hexanes was added slowly to the solution over fifteen minutes. The reaction was allowed to stir at -78˚C for 2 hours, then warmed to room temperature over 15 minutes at which point distilled water was added. The product was extracted with ether (2x25ml), then the combined organic layers were washed with brine (25 ml) then dried over $MgSO_4$, concentrated and chromatographed on silica with hexanes to yield the product (576 mg, 51% yield) as a pale yellow oil. 1H-NMR (400 MHz; $CDCl_3$): δ 7.34 (ap. d, J=7.4 Hz 1H), 7.18 (s, 1H), 7.00 (ap. d, *J* = 7.5 Hz, 1H), 3.20-3.15 (m, 4H), 3.01 (s, 1H) ^{13}C-NMR (100 MHz; $CDCl_3$): δ146.8, 131.1, 126.0, 122.5, 120.2, 104.9, 84.6, 75.9 29.8, 29.4.

HRMS: $C_{10}H_8$ calculated 128.0626, found 128.0624. FT-IR (neat) 3293, 2969, 2933, 2826, 2105, 1468, 1427, 1205, 885, 827 cm-1.

3-bromobicyclo[4.20]octa-1,3,5 triene

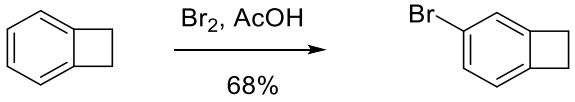

Benzocyclobutene (0.46 g, 4.4 mmol, 1.0 eq.), and glacial acetic acid (5ml) were added to a 10 mLround bottom flask and immersed in an ice bath. Bromine (0.72 g, 4.5 mmol, 1.0 eq.) was slowly added dropwise by a syringe into the flask. The resulting mixture was stirred for 16 hrs. Aqueous sodium bisulfate solution was then added and the aqueous layer was extracted with diethyl ether twice. The combined organic layer was washed with brine, dried with magnesium sulfate, filtered and the solvent was removed under reduced pressure. The residue was purified by column chromatography with hexanes on silica gel. The product 0.548 g, 68 % was recovered as a clear liquid. 1H NMR (400 MHz, CDCl3): δ 7.353 (ap. d, J = 7.6 Hz, 1H), 7.211 (ap. s, 1H), 6.938 (ap. d, J = 8 Hz, 1H), 3.190- 3.126 (m, 4H). 13C-NMR (100 MHz, CDCl3): δ 147.2, 144.1, 129.8, 125.9, 124.3, 120.5, 29.4, 29.4, 29.2, 29.1. HRMS ([M+1]+) calcd. for C8H8Br: 182.9809, found 182.9809.

3-allylbicyclo[4.20]octa-1,3,5 triene

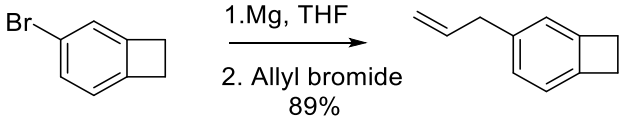

Ground magnesium (0.09 g, 3.6 mmol, 1.1 eq.) and one spatula tip of NaH along with one crystal of iodine were added to a 50 mL three-necked round-bottom flask equipped with a magnetic stir bar and a reflux condenser. The setup was stirred under

vacuum for approximately 60 minutes before nitrogen gas was added. 4-bromo-benzocyclobutene (0.59 g, 3.2 mmol, 1.0 eq.) was added in a solution of distilled THF (20 ml) and the reaction was stirred for 30–60 min at room temperature, at which point solution turned green. The reaction vessel was immersed in an ice bath at 0 ºC and allyl bromide (2.178 g, 18 mmol, 5.0 eq.) was slowly added by syringe. The resulting mixture was removed from the ice bath and warmed to room temperature then heated to reflux for 60 minutes. The solvent was evaporated under reduced pressure and the remaining liquid was poured into cold DI water, extracted with diethyl ether, and the organic layer was washed with brine, dried over magnesium sulfate and concentrated on a rotary evaporator. The product was isolated by column chromatography with hexanes on silica gel as a clear liquid 0.15 g, 32%. 1H NMR (400 MHz, CDCl3): δ 6.993–7.240 (m, 2H), 6.936 (ap. s, 1H), 5.938–6.039 (m, 1H), 5.050–5.129 (m, 2H), 3.387 (d, J = 6.8 Hz 2H), 3.171 (s, 4H). 13C-NMR (100 MHz, CDCl3): δ 145.9, 143.4, 138.6, 138.1, 127.0, 122.8, 122.4, 115.3, 40.9, 29.3, 29.2. FT-IR (neat): 3075, 3002, 1602, 1203 (weak), 2963, 2829, 802, 705 (medium), 2928, 1638, 1473, 1432, 993, 826 cm-1 (strong). HRMS ([M+1]+) calcd. for C11H13: 145.1017, found 145.1017.

1-allyl-4-bromobenzene

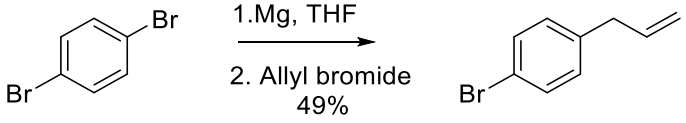

1,4-dibromobenzene (22.2 g, 94 mmol, 1 eq) in distilled THF (100 ml) was added to flame dried magnesium (2.277 g, 93.7 mmol, 0.99 eq) and a spatula tip of NaH in a 250 ml round bottom flask with reflux condenser and magnetic stir bar. The solution was stirred at room temperature for 30 minutes before solution turned green, at which point it was cooled to 0˚C and was cannula transferred into a solution of allyl bromide (7.78 ml,

92 mmol, 0.95 eq) in THF (50 ml). The reaction was stirred at reflux for 1 hour, cooled to room temperature then poured into ice and extracted with diethyl ether (2x100 ml), dried over $MgSO_4$ and concentrated, then purified by column chromatography in hexanes to yield product (9.08 g 49%). 1H NMR (400 MHz, CDCl3) δ7.40 (t, J=8.4 Hz, 2H), 7.05 (d, J=8.4 Hz, 2H) 5.87–5.97 (m, 1H), 5.03–5.09 (m, 2H), 3.33 (d, J=6.8 Hz, 2H). 13C NMR (100 MHz, CDCl3) 142.3 136.4, 131.6, 129.9, 129.1, 127.2 116.5, 39.7. Spectral data matched literature: Maegawa et al. Tet. Lett. 69, 5312-5318.

2-(4-allylphenyl)propan-2-ol

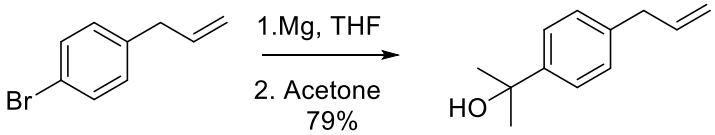

1-allyl-4-bromobenzene (3.4 g, 17.3 mmol, 1 eq) in distilled THF (50 ml) was added to flame dried magnesium (0.503 g, 20.7 mmol, 1.2 eq) and a spatula tip of NaH in a 100 ml round bottom flask with reflux condenser and magnetic stir bar. Reaction was stirred at 40˚C for 3 hours until solution turned green, at which point it was cooled to 0˚C and acetone (4.5 ml, 3 eq) was added and stirred at room temperature overnight. The solution was then poured into ice and extracted with ethyl acetate (3x30 ml), washed brine (30 ml) and dried over $MgSO_4$. The extract was concentrated in vacuo and purified by column chromatography (1:1 hexanes:ethyl acetate) to give the product (2.4g, 79%). 1H NMR (400 MHz, DMSO): δ 7.331-7.386 (m, 2H), δ 7.061-7.101 (m, 2H), δ 5.915 (ddt, J = 16.8, 10.0, 6.8 Hz, 1H), δ 4.992-5.081 (m, 2H) δ 4.913 (s, 1H), δ 3.050 (d, J = 6.8 Hz) δ 1.387 (s, 6H). 13C-NMR (100 MHz, DMSO): δ 148.7, 138.3, 137.6, 128.1, 125.0, 124.9, 116.0, 70.9, 32.4. HRMS (M+) calcd. for C12H16O: 176.1201, found

176.1200. FT-IR (neat) 3391 (broad), 2976, 2929, 1638, 1511, 1364, 1257, 1170, 1096, 995, 955 cm-1.

Preparation of Q8H

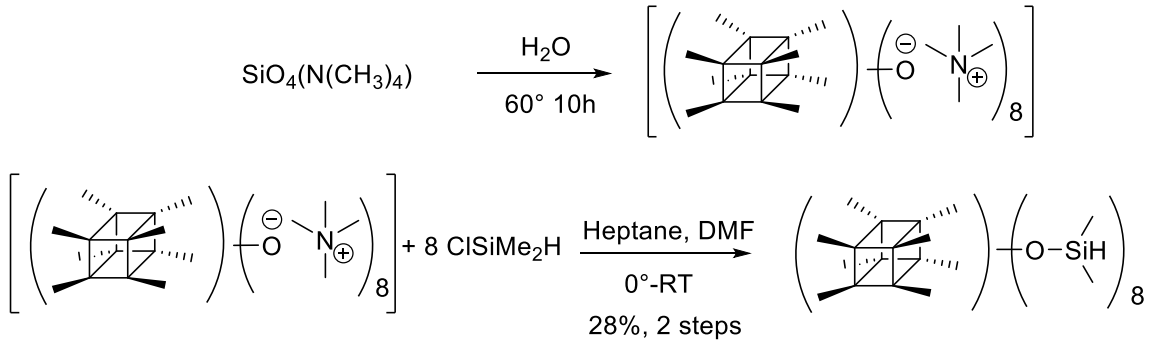

Tetramethyl ammonium silicate solution 87 ml (10 wt% in H_2O) was stirred and heated in a round bottom flask at 60˚ for 10 hours. After 10h, the solution was cooled in an ice bath and resulting solid was filtered out as crude tetramethylammounium silicate salt of POSS and directly carried into the next step without further purification. A mixture of dried heptane (200 mL), dimethylformamide, (400 mL), and dimethylchlorosilane (200 mL, 188.6 g, 2 mol) was prepared in a 2 L single necked round-bottom flask equipped with a septum and a magnetic stir bar. The mixture was stirred for about 15 min. at room temperature and then cooled to 0 °C before crude tetramethylammonium silicate salt of POSS (9.528 g, 0.0084 mol) was added slowly to the mixture. The resulting mixture was stirred for 15 min. before ~1 L of chilled distilled water was added drop wise through an addition funnel at a rate of a few drops/s. The organic layer was separated from the aqueous layer, then washed with distilled water (3x400 mL) until the organic layer was neutralized. The solvent was removed under reduced pressure at 50 °C to leave a white solid that was purified by crystallization from hexanes and isolated to yield 2.435 g (28%) of product sublimes between 166-245 °C. 1H

NMR (400 MHz, CDCl3): δ 4.710 (sep., J = 2.8 Hz, 8H), 0.24-0.22 (m, 48H). 13C-NMR (100 MHz, CDCl3): δ 0.042. FT-IR (KBr): 2963, 2361, 2359, 837 (m), 2144, 1096, 901, 771, 552 cm-1 (s). HRMS ([M-1]+) calcd. for C16H55O20Si16: 1014.9595, found = 1014.9595.

Octo-nPropyl-Benzocyclobutene-POSS

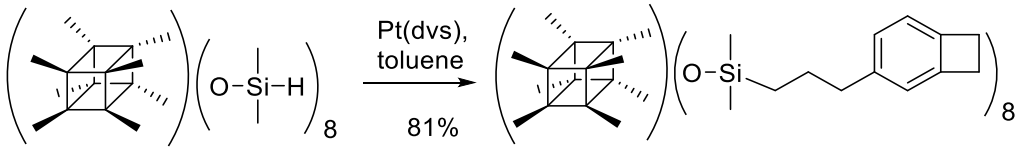

Q8 OSiH (0.563 g, 0.35 mmol, 1.0 eq.), freshly distilled toluene (5 mL) 3-allylbicyclo[4.20]octa-1,3,5 triene (0.813 g, 5.6 mmol, 16 eq.), and Karstedt's catalyst (0.45 mL, 0.06 eq) were combined in a 25 mL round bottom flask with a stir bar under nitrogen at 0˚C. The reaction was allowed to warm to RT over 12 h and then filtered through celite, concentrated in vacuo then purified by column chromatography hexanes to ethyl acetate gradient. The product 0.777 g was obtained in 81% as a slightly yellowish oil. 1H NMR (400 MHz, CDCl3): δ 6.812- 6.887 (dd, J = 15.3 Hz, J = 7.5 Hz, 16H), 6.759 (ap s, 8H), 3.006 (s, 32H), 2.463-2.501 (t, J = 7.6 Hz, 16H), 1.484-1.564 (m, 16H), 0.484-0.526 (m, 16H), 0.000-0.015 (br. s, 48H). 13C-NMR (100 MHz, CDCl3): δ 145.5, 142.7, 141.3, 126.9, 122.6, 122.2, 40.4, 29.3, 29.1, 25.9, 17.9, 0.7, 0.2. ^{29}Si-NMR (100 MHz, CDCl3): δ -18.3, -109.7. FT-IR (neat): 2858, 1475, 1410, 704 (w), 2960, 2926 (m), 1259, 1112, 1056, 846, 802 (s), 446 cm-1 (br). HRMS, MALDI calcd. for C104H152O20Si16 = 2168.7185 found = 2168.7187)

Dually Functionalized Methacrylate-BCB POSS

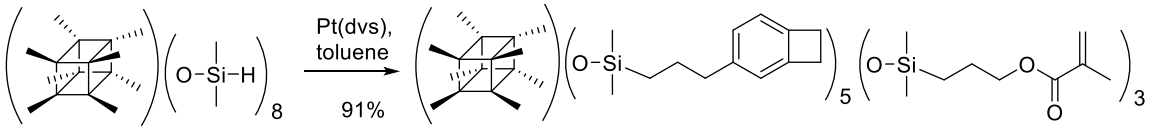

To a solution of flame dried silane terminated POSS (141 mg 1 eq) in 40 ml freshly distilled toluene was added 3-allylbicyclo[4.20]octa-1,3,5 triene (200 mg, 10 eq) and allyl methacrylate (105 mg, 6 eq) in a 100 ml rbf equipped with a magnetic stir bar and flushed with nitrogen. The solution was cooled to 0˚ C, then Pt(dvs) solution (2 wt% Pt) in xylenes (0.18 ml, 0.06 eq) was added. The reaction warmed to room temperature and stirred for 12h. The reaction was then filtered through celite, concentrated in vacuo and the purified by column chromatography using a gradient from hexanes to ethyl acetate. A distribution of isomers was isolated as a dark viscous oil. 1H-NMR showed broad peaks that integrated to give a 5:3 average of BCB to methacrylate. Characterization was performed by MALDI mass spec which showed M+Na peaks for ratios of isomers from 2:6 BCB:Methacrylate to 6:2 BCB:Methacrylate.

Methacrylate POSS MALDI				
(BCB+Methacrylate) x+y = 8				
BCB (x)	Methacrylate (y)	M	M+Na	
0	8	2025	2048	Not Observed
1	7	2043	2066	Not Observed
2	6	2061	2084	Observed
3	5	2079	2102	Observed
4	4	2097	2120	Observed
5	3	2115	2138	Observed

6	2	2136	2159	Observed
7	1	2151	2174	Not Observed
8	0	2169	2192	Not Observed

Representative spectrum:

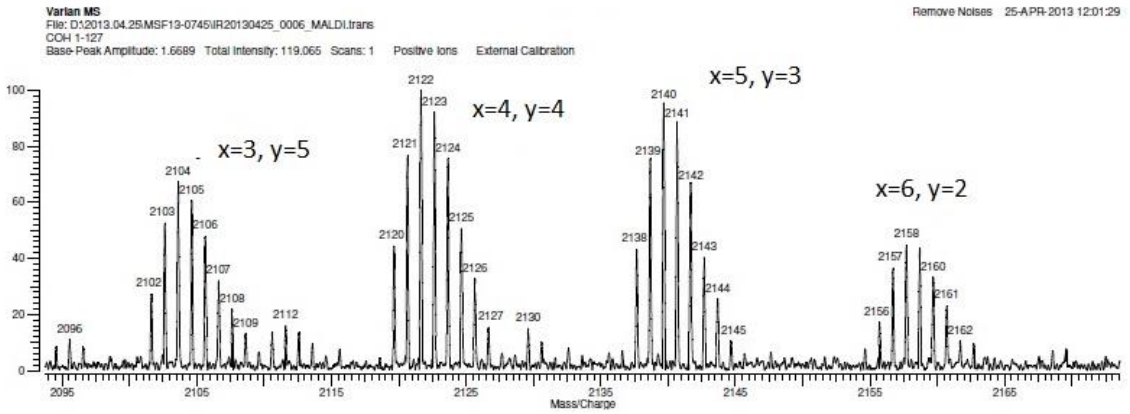

Ito POSS: Dually Functionalized BCB and t-Benzylic Alcohol

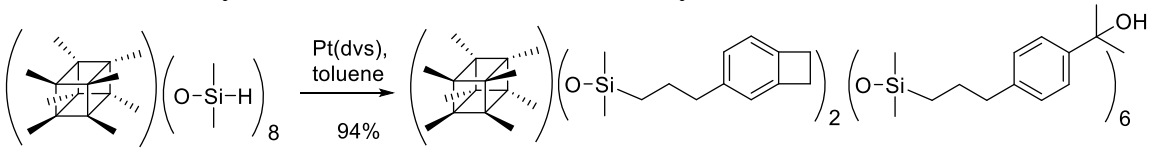

To a solution of flame dried Q8H (735 mg 1 eq) in 100 ml freshly distilled toluene was added 3-allylbicyclo[4.20]octa-1,3,5 triene (205 mg, 4 eq) and 2-(4-allylphenyl)propan-2-ol (735 mg, 12 eq) in a 250 ml rbf equipped with a magnetic stir bar and flushed with nitrogen. The solution was cooled to 0˚ C, then Pt(dvs) solution (2 wt% Pt) in xylenes (0.48 ml, 0.06 eq) was added. The reaction was allowed to warm to room temperature and stirred for 12h. The reaction was then filtered through celite, concentrated in vacuo and the purified by column chromatography running a gradient from hexanes to ethyl acetate. A distribution of isomers was isolated as a dark viscous

oil. 1H-NMR showed broad peaks that integrated to give a 2:6 average of BCB to alcohol. Characterization was performed by MALDI mass spec which showed M+ peaks for ratios of isomers from 0:8 BCB:Alcohol to 5:3 BCB:Alcohol.

Ito POSS MALDI			
(BCB+Alcohol) x+y=8			
BCB (x)	Alcohol (y)	M+	
0	8	2425	Observed
1	7	2393	Observed
2	6	2361	Observed
3	5	2329	Observed
4	4	2297	Observed
5	3	2265	Observed
6	2	2233	Not Observed
7	1	2201	Not Observed
8	0	2169	Not Observed

Representative Spectrum:

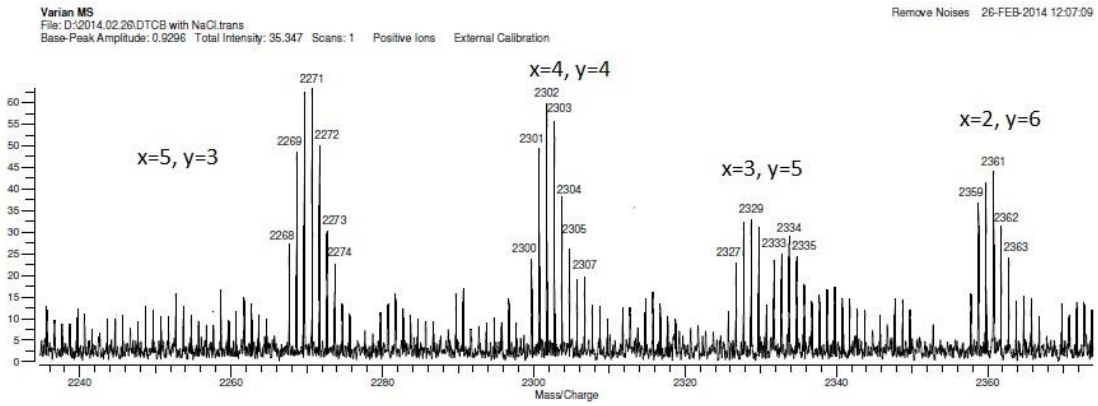

Octovinyl-Benzocyclobutene-POSS

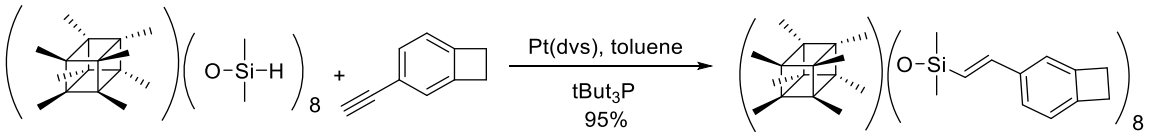

A solution of Pt(dvs) (2 wt% Pt) in xylenes (1.097 ml, 0.06 eq) was added to a solution of tri-tertbutylphosphine (29.6 mg, 0.18 eq) in freshly distilled toluene (30 ml) and allowed to stir at room temperature for 30 minutes. This solution was cannula transferred into a solution of Q8H (830 mg, 1 eq), 3-thynylbicyclo[4.2.0]octa-1,3,5-triene (1.0g, 12 eq) and freshly distilled toluene (120 ml) in a 250 ml rbf equipped with a magnetic stir bar under nitrogen at 0˚C. The reaction warmed to room temperature and stirred for 12h, while monitoring aliquots by crude 1H NMR. After 12h, the solution was filtered through celite, concentrated in vacuo and chromtaographed on silica gel using a gradient from hexanes to ethyl acetate to give a dark viscous oil (1.7g, 95%). 1H-NMR (400 MHz; $CDCl_3$): δ 7.17 (ap. d, J=7.5 Hz 1H), 7.10 (s, 1H), 6.91 (ap. d, J = 7.5 Hz, 1H), 6.90 (d, J=19.2 Hz), 6.26 (d, J=19.2 Hz) 3.12-3.05 (m, 4H), 0.25-0.18 (br. s, 48H) 13C-NMR (100 MHz; $CDCl_3$): δ145.8, 137.1, 126.3, 125.1, 122.4, 120.1, 117.8, 106.0, 29.4, 29.2, 0.3. HRMS: C96H120O20Si16 calculated (M+Na) 2063.4579, found 2063.4612. FT-IR (neat): 2927, 2877, 1613, 1575, 1470, 1416, 1331, 1252, 1196, 1034, 986, 846, 802 cm-1.

Nanoindentation Impact Curves for DF POSS:

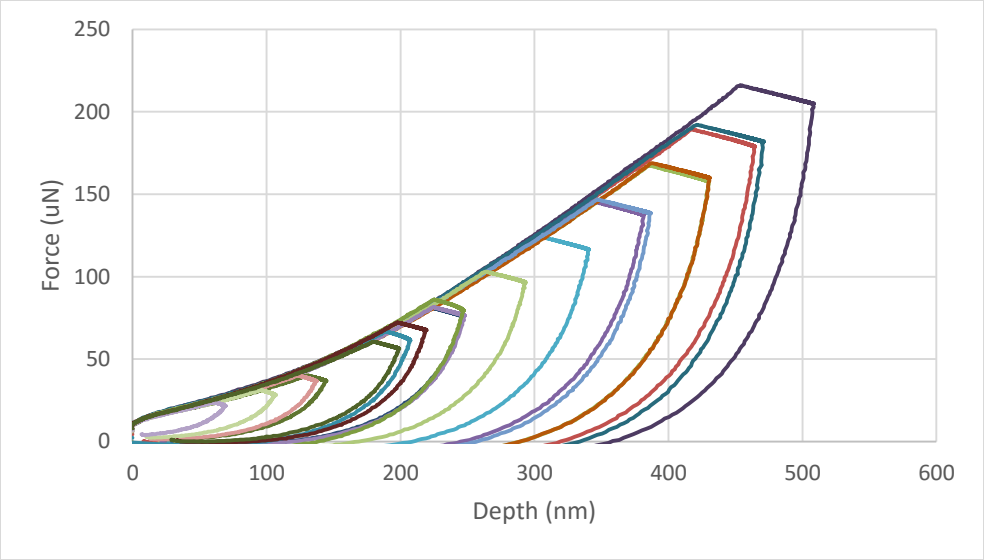

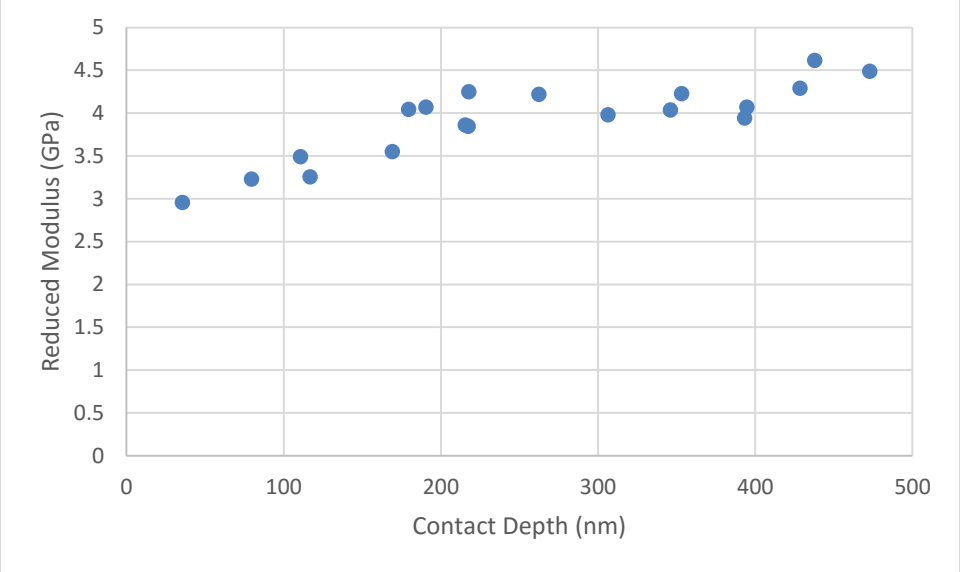

Nanoindentation Impact Curves for OVBCB POSS:

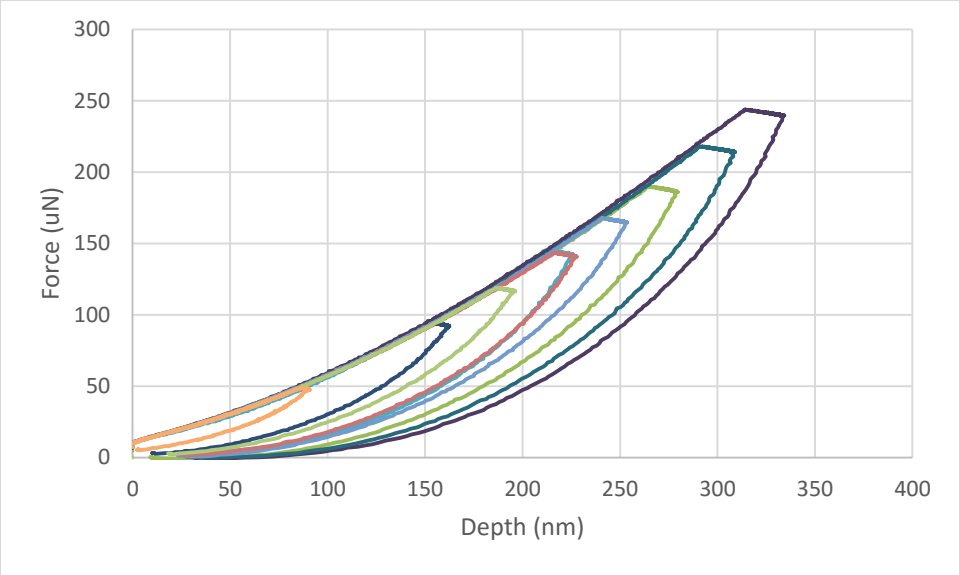

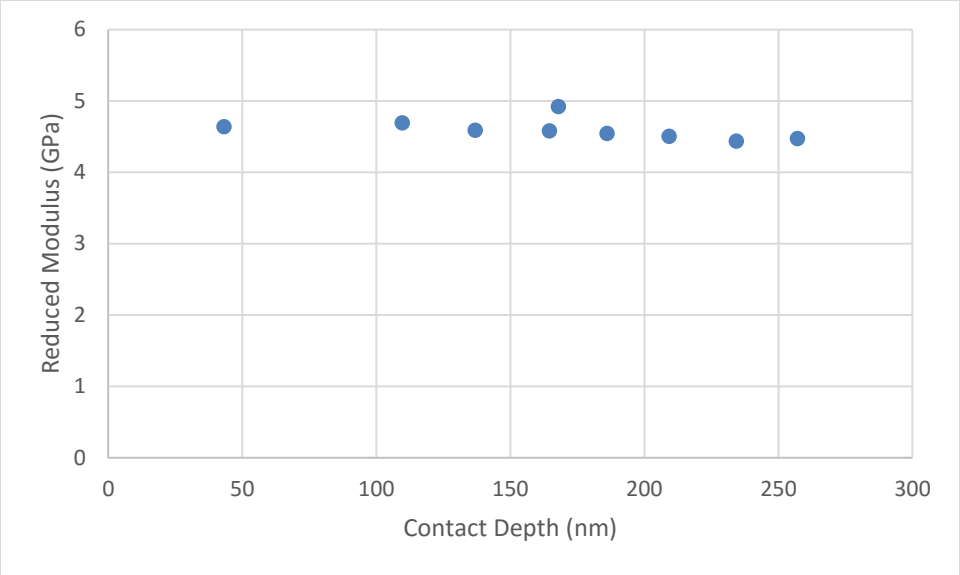

Chapter 4: Lowering the Reaction Temperature of Benzocyclobutene Thermosets

4.1 Introduction

As discussed in Chapter 3, benzocyclobutene (BCB) chemistry has a number of applications[63], including crosslinking thin films, well defined nanoparticles[64], and dielectric materials that can be cured with almost no shrinkage. While originally employed in total synthesis as a latent Diels Alder diene[65], BCB chemistry is most widely used today in dielectric materials. The Dow Chemical Company produces large amounts of BCB via flash vacuum pyrolysis for microelectronics applications. However, a major shortcoming of BCB chemistry is its relatively high cure temperature, 250˚C for one hour, which is incompatible with many sensitive processes and functional groups. Furthermore, a minimal amount of thermal stress should be induced on a microelectronic device during an ideal fabrication process in order to maximize yield. Lowering the reaction temperature of a BCB thermoset has the potential to make BCB chemistry viable for more sensitive and demanding processes[66].

There are two notable works in the field of lowering the reaction temperature of BCB for a macromolecular applications. The first is the synthesis of 3-vinylbicyclo[4.2.0]octa-1,3,5-triene by Pugh et al., wherein the key step is an ortho-diazonium carboxylate salt as a benzyne precursor[67,68]. While this route reportedly produced a monomer that was polymerizable and crosslinked at reduced temperature, the chemistry was restricted to styrenes, the yield of the BCB forming step was low and the use of diazonium carboxylates are potentially dangerous at large scales. The second notable work was published by Dobish et al., who synthesized 2-(bicyclo[4.2.0]octa-1,3,5-trien-7-yloxy)ethan-1-amine which crosslinked at reduced temperature, but required an undesireable “grafting onto” approach which requires available carboxylic acid groups

on a resin, and also began their synthesis from commercially available, but expensive 1-bromobenzocyclobutene[69].

An efficient route is described in this chapter that allows for the formation of a benzocyclobutenone phenol that can be derivatized to provide virtually any desired polymeric moiety, and the ketone can be altered to enable a range of ring opening temperatures. These reactions were examined via differential scanning calorimetry (DSC). A most surprising result occurred when the Mitsunobu reaction with a benzocyclobutenol was attempted in tetrohydrofuran (THF). A new and interesting THF insertion product was produced. To the best of the author's knowledge, no such solvent insertion has been reported under Mitsunobu conditions of this sort. The THF inserted product was observed to have an exothermic transition with a maximum at 148˚C, over a hundred degrees lower than ordinary BCB. Polystyrene and polynorbornene copolymers containing the THF inserted BCB were prepared and studied in thin films. Both were rendered insoluble at greatly reduced temperatures.

4.2 Results and Discussion

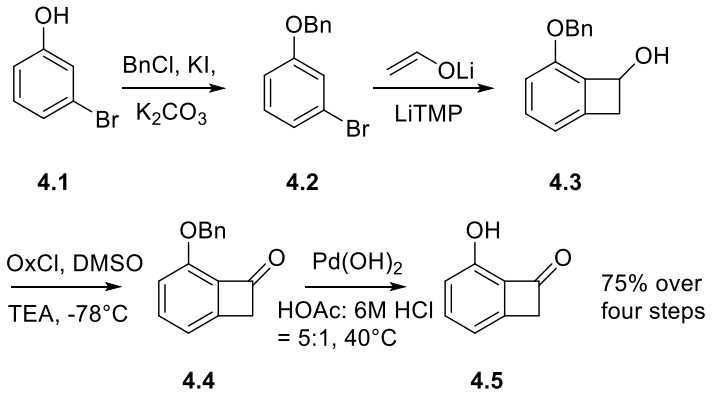

Scheme 4.1: Ten gram scale synthesis of benzocyclobutenone phenol.

From a retrosynthetic perspective, it is easy to envision a 1-functionalized BCB deriving from benzyne as an intermediate[70,71]. While there are many ways to generate benzyne and multiple potential nucleophiles to consider,[72] Chen et al. at the University of Texas optimized the transformation from the benzyl ether **4.2** to give the alcohol **4.3**, where the enolate of acetaldehyde is generated from lithiation of THF[73]. Benzyne is generated via elimination of the aryl bromide using lithium tetramethyl piperdine as the base. It should also be noted that the alkylation from phenol **4.1** to **4.2** is nearly quantitative and the starting material **4.1** is extremely cheap (26¢ per gram from Oakwood Chemical, at time of writing). Swern conditions produced the ketone **4.4**, and deprotection of the benzyl ether was achieved either via hydrogenation as shown or by treatment of boron trichloride in dichloromethane to produce the free phenol **4.5** in large scale and 75% overall yield over four steps.

The phenol **4.5** was envisioned as a divergent point in the synthesis upon which any desirable polymerizable moiety could be tethered. Three such examples were chosen to demonstrate the versatility of this method and they are outlined in Scheme 4.2.

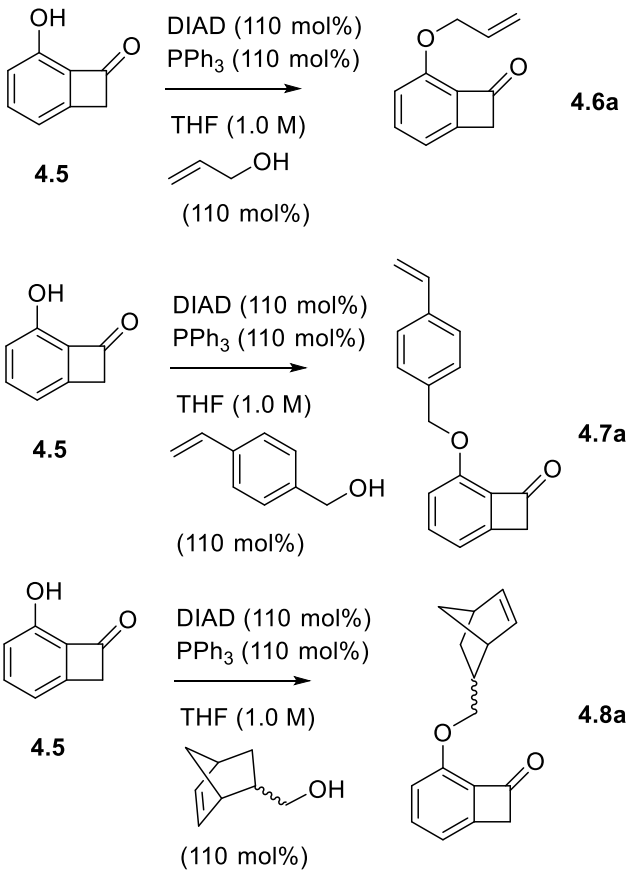

Scheme 4.2: Synthesis of allyl, styrenyl, and norboryl-benzocyclobutenones.

The allyl derivative **4.6a** was synthesized as a potential coupling partner to the POSS resins from Chapter 3 via hydrosilylation; the thermal behavior of allyl derivatives could also be studied via DSC without fear of any auto-polymerization reactions showing competitive signals. Styrenyl and norbornyl derivatives were chosen as two common monomeric functional groups with broad applications in polymer sciences. Norborne based BCB thermosets are also of interest as ROMP materials for next generation packaging materials; these will be discussed in more detail in Chapter 5.

Reduction of the ketone was accomplished through ordinary $NaBH_4$ and MeOH conditions to give the BCB-ol **4.6b** (Scheme 4.3). An easy way to investigate a steric

effect in BCB ring opening was to add silyl protecting groups of differing size. To that end, TBS and TBDPS protected benzocyclobutenols **4.9** and **4.10** were synthesized in high yield using the Corey protocol.

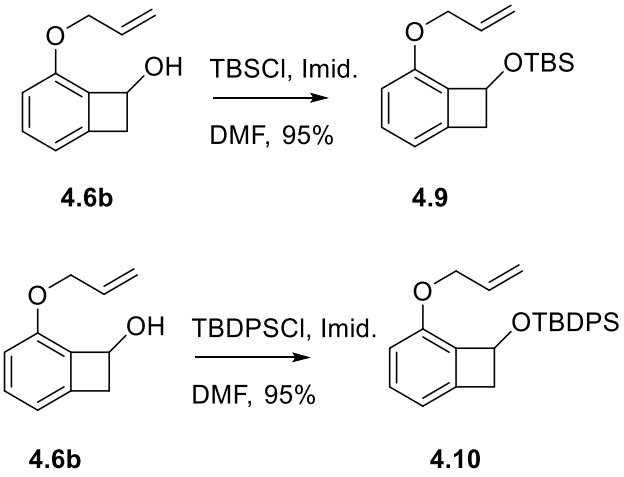

Scheme 4.3: Synthesis of silyl-protected 1-BCBs.

It was found that **4.6b** could not be alkylated using a typical Williamson ether synthesis protocol. A variety of bases and temperatures all produced the same result: the deprotonated BCB underwent electrocyclic ring opening followed by tautomerization to the *o*-methylbenzaldehyde[74,75]. Due to the availability of relatively acidic fluorinated alcohols in the Willson Labs, Mitsunobu reactions were attempted using these unusual coupling partners[76].

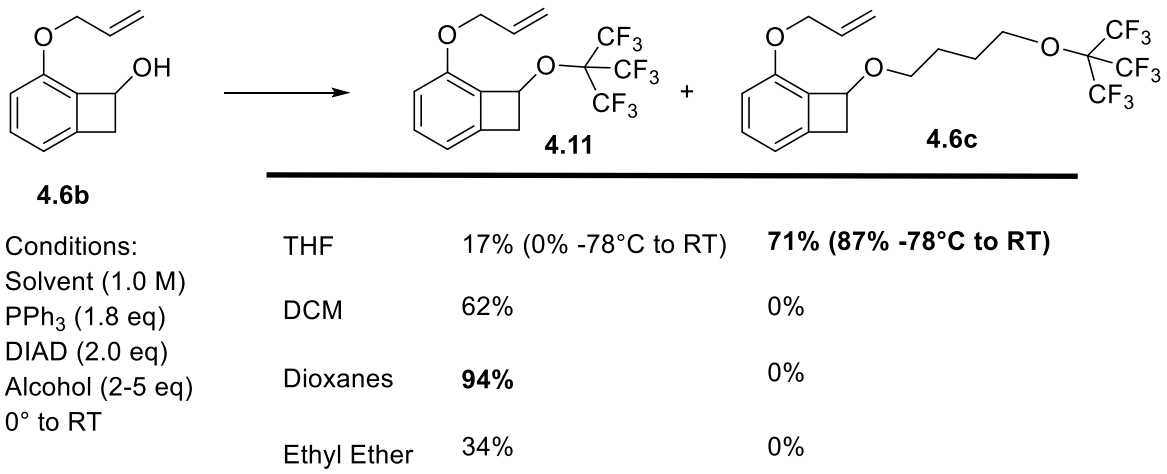

Scheme 4.4: Synthesis of THF-inserted 1-BCB.

The intention was to synthesize the ordinary coupling product **4.11**. However, it was found that when the reaction was run in THF, an unknown product dominated the product mixture. Separation using column chromatography yielded a THF inserted product in 71% yield, a highly unexpected result. Further studies with other cyclic ethereal solvents (Scheme 4.4) showed that only THF produced this type of insertion behavior. Lowering the reaction temperature afforded a higher yield of **4.6c**, suggesting that the solvent insertion is kinetically favored. Hexafluoro-isopropanol (when used as a coupling partner) produced a similar THF inserted product. This was inseparable via chromatography, and was analyzed via proton NMR of the crude reaction mixture.

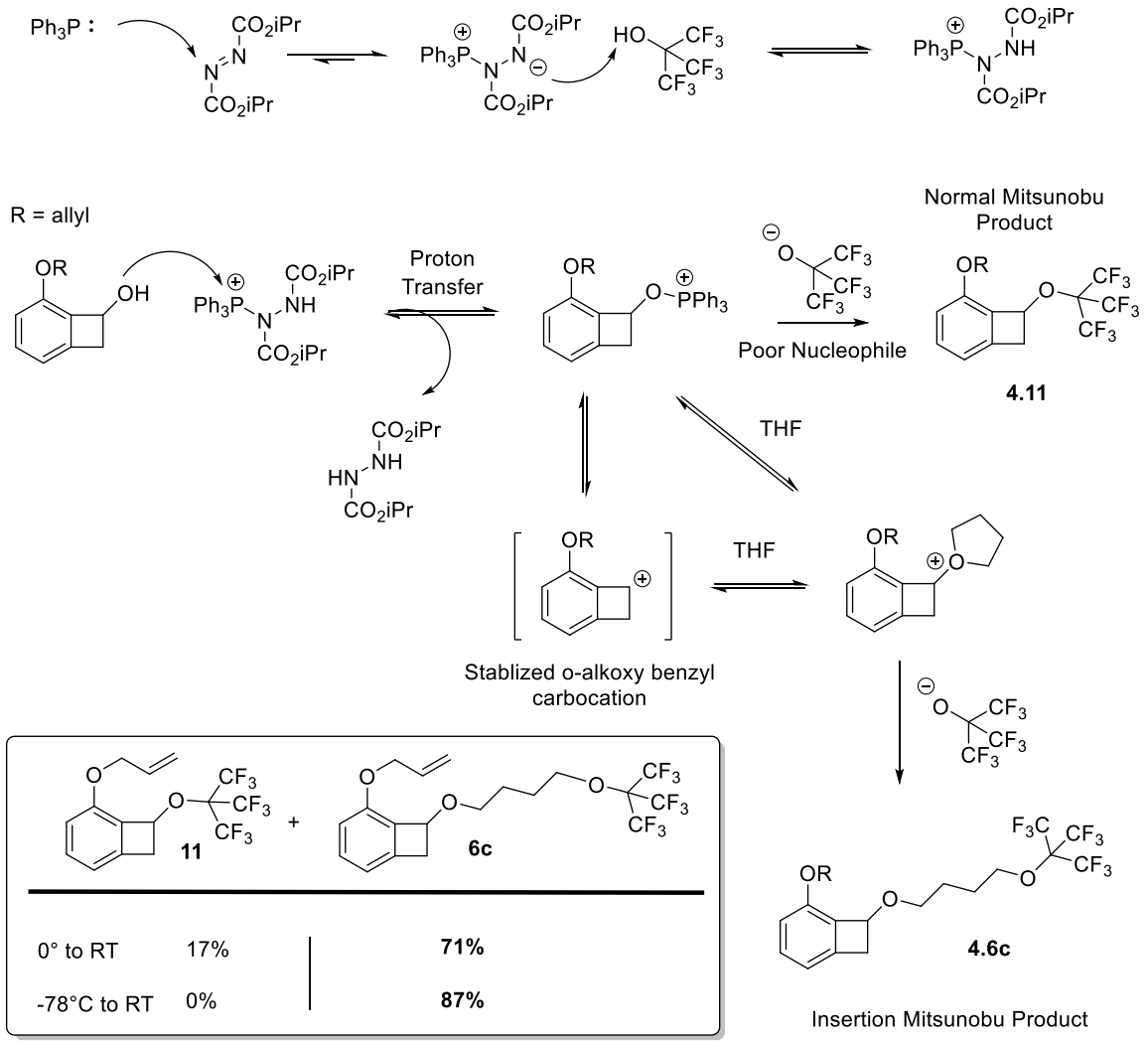

Figure 4.1: Proposed mechanistic pathway of this Mitsunobu variant. An acidic yet exceptionally poor nucleophile, the perfluoro tert-butanol is proposed to bias the reaction pathway in favor of THF as a competitive nucleophile. This reaction is also likely highly S_N1-like in nature due to the highly stabilized o-alkoxy benzyl carbocation.

An explanation for this unusual reactivity has been proposed (Figure 4.1) that is consistent with the experimental results. Perfluoro tert-butanol is sufficiently acidic to push the equilibrium step forward from the diazo zwitterion. Once the activated phosphine has been transferred onto the benzocyclobutanol, it is likely that the resulting

specie has considerable S_N1-like character due to the exceptional leaving group (triphenyl phosphine oxide) and highly stabilized resulting carbocation (o-alkoxy benzyl). The anion of the perfluoro tert-butanol is such a poor nucleophile that competition ensues between the anion and the solvent (THF). When THF inserts, the compound readily undergoes ring opening to form the observed product **4.6c**. Ultimately, this reactivity is the perfect storm of poor nucleophile and extremely stable cationic coupling partner. This reactivity is also likely restricted to benzocyclobutanols since β-hydride elimination is highly disfavored (the resulting product would be anti-aromatic).

The allyl model series of 1-functionalized BCBs was evaluated using differential scanning calorimetry, where a single, large, irreversible exothermic transition is correlated with the thermosetting reaction temperature. The results are presented in Figure 4.2. It should be noted that compound **4.12** was synthesized by Penghao Chen at UT Austin, and compound **4.13** was Cyclotene, donated by Dow Chemical. Firstly, it can be seen that both silyl protected derivatives **4.9** and **4.10** show the exact same exothermic maximum at 260˚C, which suggests that steric factors have little effect as to the ring opening and thermosetting of BCB. Between ketones **4.6a** (231˚C) and **4.12** (238˚C), there is little change, yet what is seen is a small positive effect on reaction temperature. Both of these compounds are still well over the target threshold of 200˚C for next generation packaging applications. Of significant interest is the alcohol, compound **4.6b**, which has an exothermic transition maximum at 176˚C. At first glance a resin with a 1-benzocyclobutenol might appear to be attractive for application in microelectronics, but it ultimately falls short on a few counts. Firstly, the alcohol functional tends to contribute to high dielectric constants and high water absorption, which both lead to parasitic capacitance and cross-talk, killers of electronic device performance. Secondly, there is some literature evidence to suggest that a 1-benzocyclobutenol polymer would

undergo tautomerization to the *o*-methylbenzaldehyde instead of crosslinking. Indeed, the previous synthetic work in this chapter has shown that the isomerization is very fast: it is highly likely that polymers based on **4.6b** would not undergo any cross linking at all.

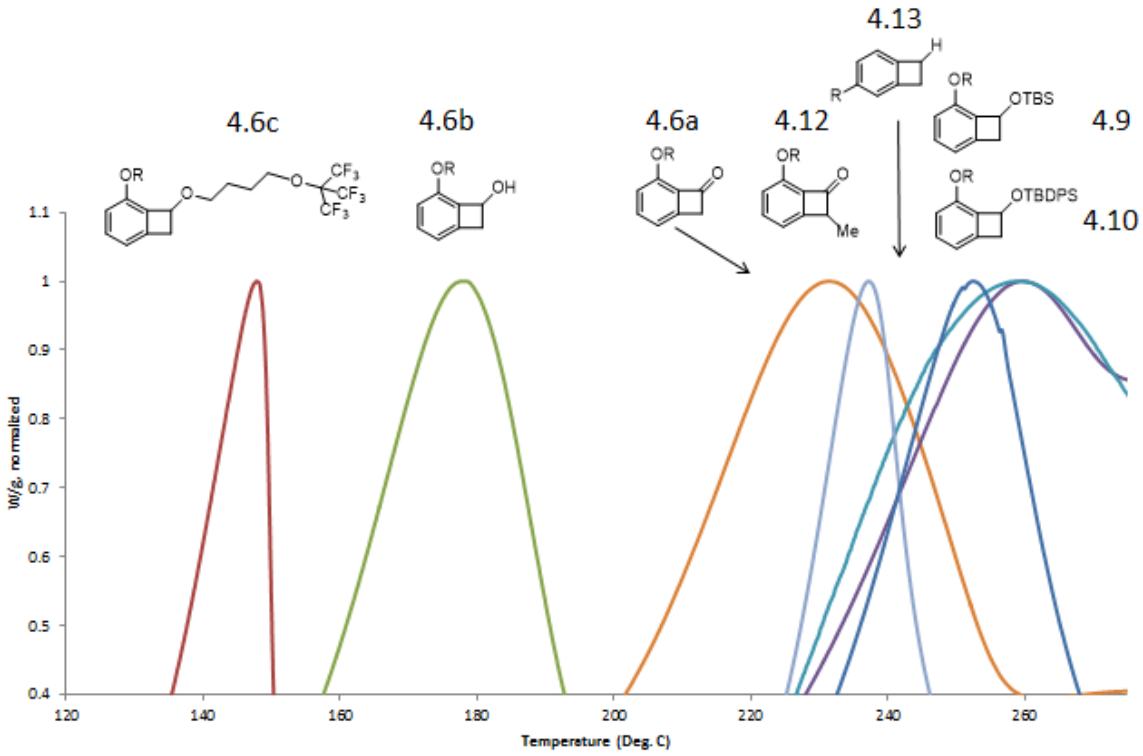

Figure 4.2: Normalized DSC curves of custom BCB compounds from this chapter.

The "winning" derivative, as it were, proved to be the surprise THF-inserted product, **4.6c**, with a DSC exothermic transition at 148˚C. This compound undergoes reaction at temperatures one hundred degrees lower than unsubstituted BCB (**4.13**). It is clear from this study, as well as the studies from Dr. Pugh and Dr. Harth, that 1-alkoxy BCBs undergo ring opening and crosslinking in this temperature regime. However, the DSC evidence does not represent conclusive proof of cross linking, and further studies in NMR solutions and with polymers in thin films were conducted.

Ketone	Reduction Product	Mitsunobu Proudct
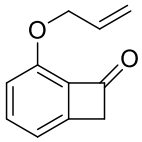 4.6a (99%)	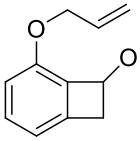 4.6b (92%)	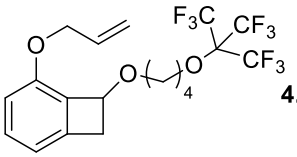 4.6c (71%)
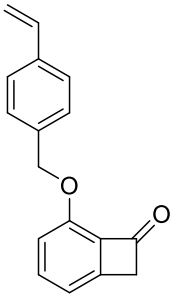 4.7a (68%)	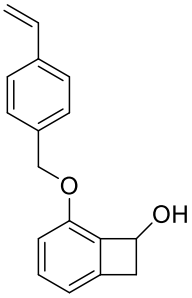 4.7b (87%)	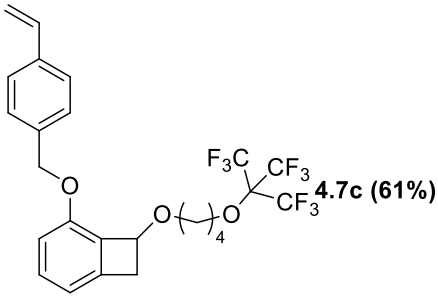 4.7c (61%)
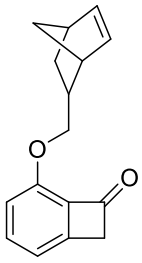 4.8a (52%)	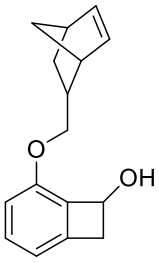 4.8b (93%)	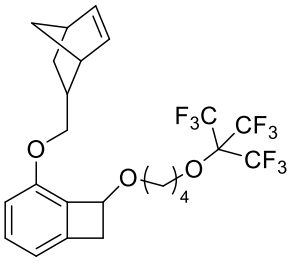 4.8c (69%)

Table 4.1: Synthesis of target monomers for thin film studies.

In order to study the behavior of low temperature BCB polymers in thin films and verify crosslinking, two different monomers were prepared. Using a standard Mitsunobu protocol from the corresponding alcohols, styrenyl and norbornyl benzocyclobutenones **4.7a** and **4.8a** were synthesized. The corresponding reduction products were obtained in high yields using sodium borohydride in methanol, and then the THF inserted Mitsunobu product of each was isolated (**4.7c** and **4.8c**). Using these monomers, twenty percent feed random copolymers were synthesized with styrene and norbornene.

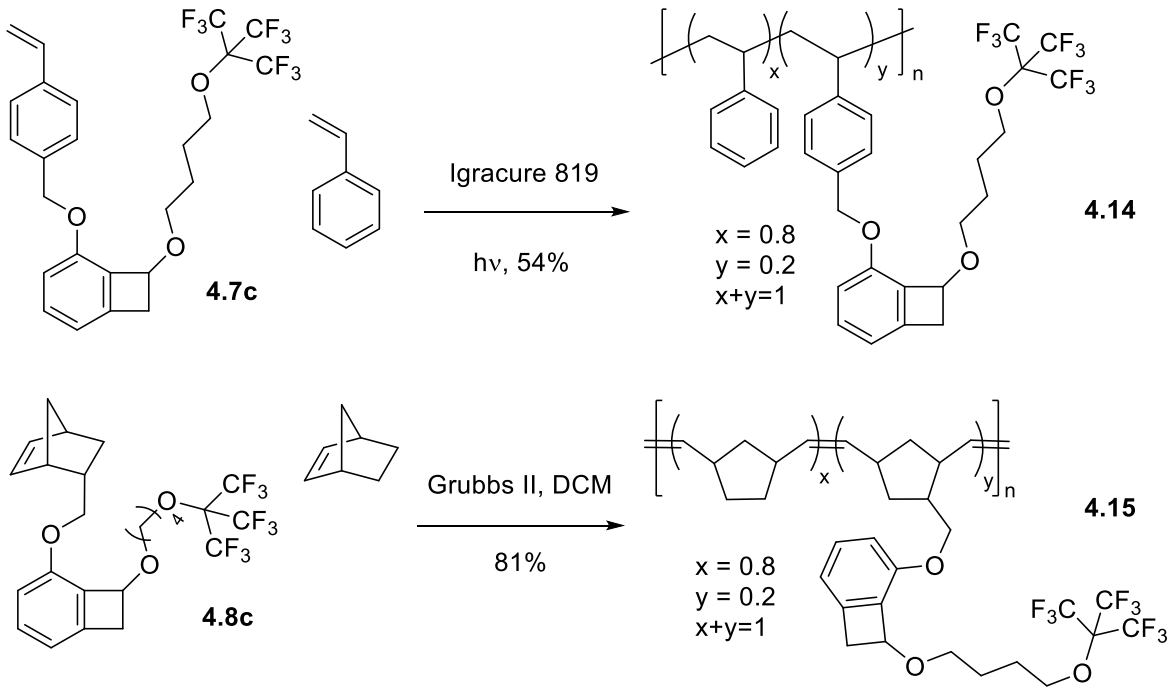

Scheme 4.5: Synthesis of Low T BCB containing copolymers.

The polystyrene copolymer was obtained through free radical polymerization using the commercial photoinitiator Igracure 819. A light based protocol was chosen since thermal polymerization using AIBN (at 60˚C) reliably produced an insoluble gel instead of polymer (which suggests low temperature solution crosslinking). The polynorbornene copolymer was obtained through ring opening metathesis polymerization (ROMP) at room temperature with Grubbs Second Generation catalyst. The composition of the polymers matched the feed of monomers by proton NMR.

Polymers **4.14** and **4.15** were formulated in toluene and spun on silicon wafers to produce thin films varying in thickness from 50-200 nm as measured by spectroscopic ellipsometry. Film thicknesses were measured before curing, after curing and after a toluene wash (2 x 10 second rinse of toluene), which completely stripped control

homopolymers polystyrene and polynorbornene subject to the same curing conditions. Curing was carried out in a vacuum oven which was purged and backfilled with argon gas, and then heated to the requisite temperature and held there for one hour. The results are shown in Figure 4.3.

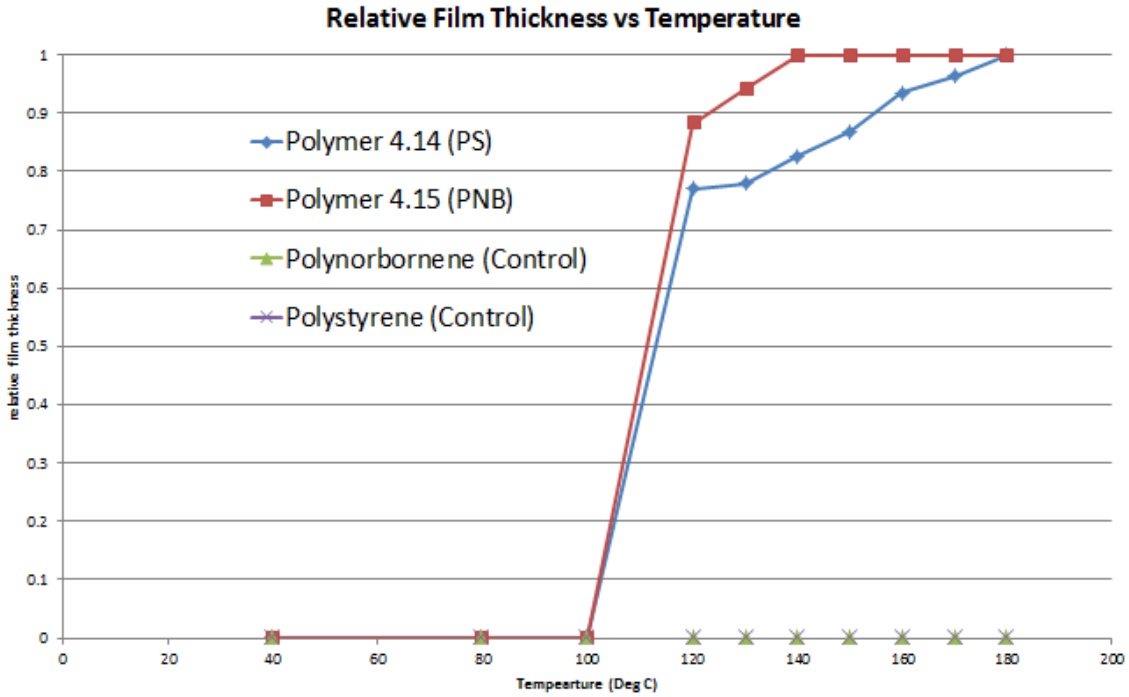

Figure 4.3: Normalized film thickness after toluene wash of studied polymers.

The un-crosslinked polynorbornene and polystyrene polymers were completely dissolved in all temperature conditions, but a sharp onset of film retention began at 120˚C in the experimental polymers **4.14** and **4.15**. By 140˚C, the norbornene-based **4.15** had become completely insoluble, and by 180˚C, the polystyrene polymer had likewise become insoluble. It is possible that polymer **4.15** reached complete insolubility faster due to the high degree of unsaturation in the polymer backbone: alkenes suitable for Diels Alder

addition and therefore crosslinking, as opposed to the case of **4.14**, where each BCB must encounter another BCB in order for a crosslinking event to occur. There may be a dynamic T_g effect at play as well. Uncured polymer **4.15** has a T_g of 52˚C, while uncured polystyrene **4.14** has a T_g of 74˚C. The glass transition rises rapidly over the course of the cure/crosslink, limiting the diffusion of chains in the case of **4.14**, which already has a higher glass transition to start. This is not a problem for **4.15**, however, since readily available double bonds on each polymer unit provide a site for crosslinking whenever the electrocyclic ring opening has occurred. One last plausible explanation is an electrophile effect: the norbornene double bonds may be a better Diels Alder dienophile than the opened BCB itself, slightly lowering the activation barrier for crosslinking. Indeed, evidence for this is seen in Chapter 5.

Solution based H^1 NMR studies were carried out which show that the BCB ring was indeed disappearing as a mechanism of crosslinking. Compound **4.6c** was dissolved in deuterated DMSO and heated in an oil bath at an increasing temperature until a change was observed (120˚C, the same onset in the thin film), and then monitored over time at that temperature with spectra taken intermittently. The spectra are displayed in Figure 4.4.

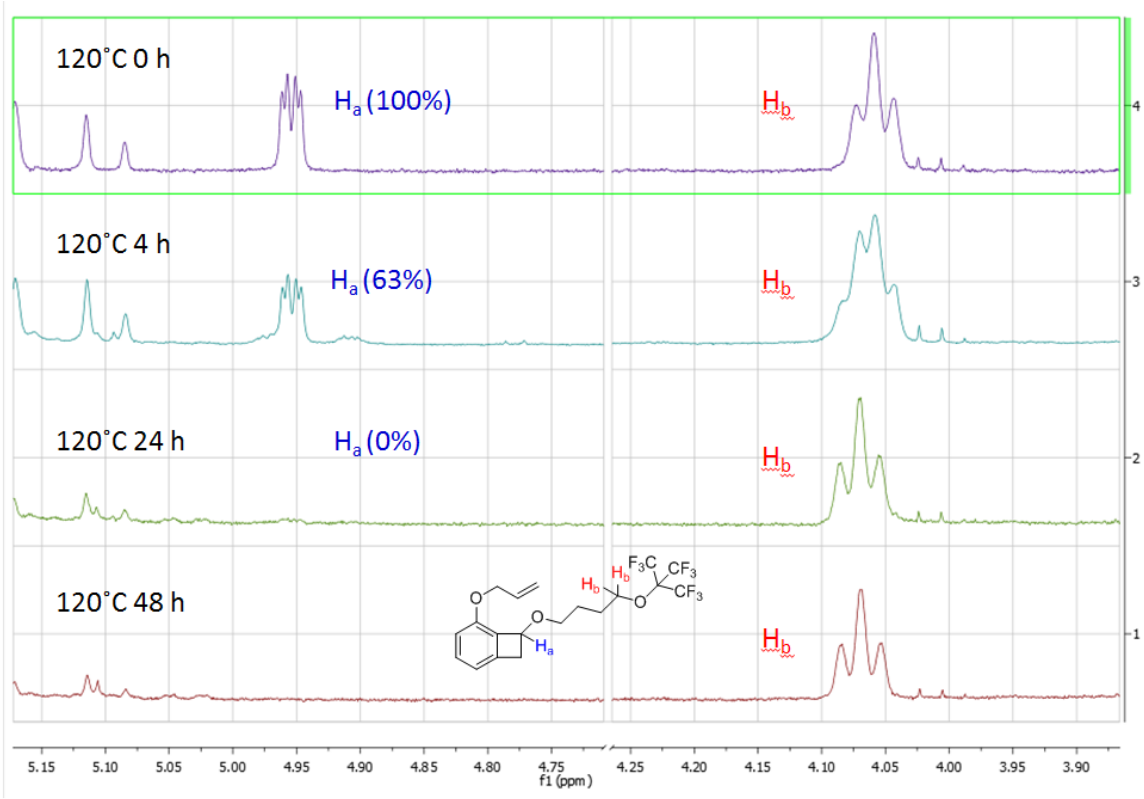

Figure 4.4: Time scale NMRs of 4.6c. Intensity normalized to protons H_b. Spectra show the disappearance of the four membered ring protons overtime, consistent with a thermal decomposition of the cyclobutene ring.

The results highlight proton H_a, the doublet of doublets that is at the benzyl 1-position of the BCB ring, a characteristic resonance of 1-functionalized BCBs. The signal of H_a was normalized to the intensity over time of H_b, the protons adjacent to the perfluoro-tertbutyl functional group. After four hours, the ring protons decreased to 63% intensity. A closer look at the previous triplet H_b reveals that the resonance appears muddled, as perhaps two triplets slightly overlapping. This result is consistent with a partially oligomerized BCB. By hour twenty-four, the ring had completely disappeared. The triplet H_b was now reestablished, albeit at a slightly different resonance, and there was a slight decrease in allyl alkene intensity (resonance around 5.10 ppm), suggesting

some consumption of alkene presumably via Diels Alder. The results strongly suggest that thermal treatment to these BCBs result in a disappearing of the cyclobutene functional group, likely through electrocyclic ring opening and subsequent Diels Alder.

As a control, the compound inert on DSC, compound **4.11**, was subjected the same solution study conditions and **4.6c**, in deuterated DMSO. At all available time points over forty-eight hours, the compound remained completely inert. The resulting spectra are displayed in Figure 4.5.

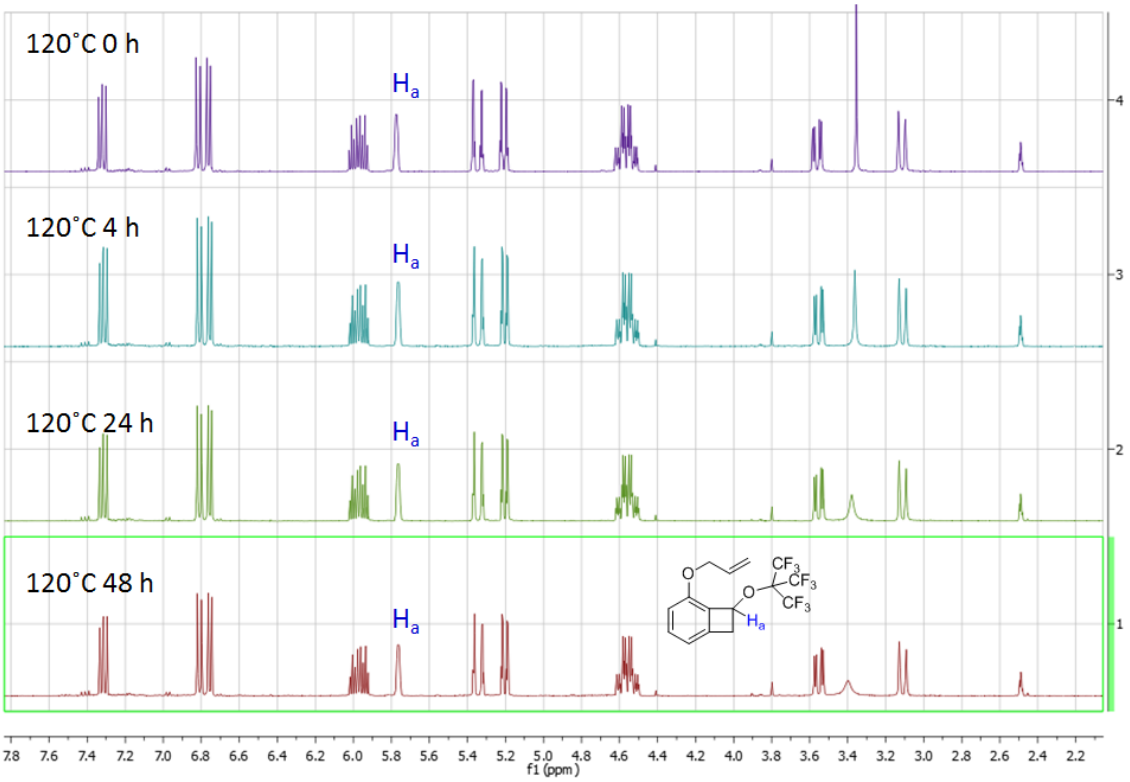

Figure 4.5: Temperature NMR study of compound 4.11 showing no change over time. Results are consistent with the DSC trace of compound 4.11 showing no thermal transition.

No change in relative resonance intensity was observed relative to itself or DMSO. One will notice that the resonance at 3.4 ppm, assigned to water in DMSO, decrease

significantly, as it is slowly volatilized from the DMSO and NMR tube. The results are consistent with the DSC: compound **4.11** is completely inert to reaction at 120˚C.

4.3 CONCLUSION

In this chapter, the synthesis of new 1-functionalized BCBs, their monomers, and polymers have been demonstrated. These compounds have been evaluated using DSC, thin film retention and solution in NMR. The results demonstrate that a 1-alkoxy functionalized BCB is suitable for use as a crosslinking agent at a greatly reduced temperature than unsubstituted BCB.

Furthermore, a unique use of the Mitsunobu reaction was demonstrated. In the presence of the bulky, acidic perfluoro tert-butanol and tetrahydrofuran, the solvent unexpectedly inserted between the coupling partners, producing a 1-alkoxy BCB that proved valuable for application as a low temperature crosslinker. The materials evaluation of the respective polymers derived from this Mitsunobu variant demonstrate great promise for meeting the reduced cure temperature requirements of next generation packaging materials.

In order to fully understand the relationship between functionality and cure temperature, a series of compounds were prepared with the intention of generating a linear free energy relationship (LFER), in order to establish a relationship between electron donating effects and ring opening temperature. A series of 4-functionalized phenols were joined with compound **4.6b** to produce a Hammet-esque series of test compounds. Unfortunately, all of them showed the same exothermic reaction a temperature of 255˚C. Attempts to create 1-aryl BCBs via Kumada couplings and Gilman reactions proved unsuccessful, thus a LFER remains elusive.

In the future, BCB may be actualized as a dynamic, versatile crosslinking functional group with crosslinking available at a variety of desired temperatures. The work in this chapter paves the way for lowering the cure temperature of benzocyclobutene thermosets in a microelectronics packaging application, but the lessons learned here may extend to be a tool with broad application in polymer chemistry.

4.4 EXPERIMENTAL

General Procedures:

Size exclusion chromatography (SEC) data were collected with an Agilent 1100 Series isopump and autosampler with a Viscotek Model 302 TETRA detector platform and THF as an eluent at 23°C. Three I-series mixed bed high-MW columns were calibrated relative to PS standards. A Brewer CEE 100CB Spincoater was used to coat all thin films. Ellipsometry was performed with a J.A. Woollam Co, Inc. VB 400 VASE Ellipsometer withwavelengths from 382 to 984 nm and a 65° angle of incidence. Thermogravimetry and differential scanning calorimetry were performed using a TA Instrument Q500 TGA and TA Q100 DSC, respectively, each with a 50ml flow rate of nitrogen. DSC method used was a constant heating/cooling rate of 10˚C/minute from 25˚C to 300˚C and back to 25˚C for two cycles. TGA samples were ramped to 1000˚C at 10˚C/minute heating rate under nitrogen atmosphere. All thin film samples were placed in a vacuum oven, purged with nitrogen three times, and cured at the specified temperature for one hour.

Reagents:

Triphenyl phosphine and Di-(4-chlorobenzyl)azodicarboxylate were purchased from Combi Blocks. Perfluoro tert-butanol was purchased from Oakwood Chemical. Diisopropyl azodicarboxylate, tert-Butyldimethylsilyl chloride, tert-Butyl(chloro)diphenylsilane, imidazole, styrene, norbornene, THF, DCM, hexanes and ethyl acetate were purchased from Sigma Aldrich.

Synthetic Data:

5-((4-vinylbenzyl)oxy)bicyclo[4.2.0]octa-1,3,5-trien-7-one

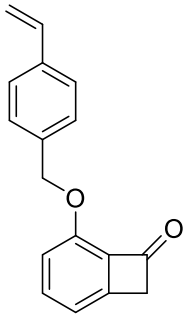

5-hydroxybicyclo[4.2.0]octa-1,3,5-trien-7-one (150mg, 1 eq) and (4-vinylphenyl)methanol (150mg, 1 eq) and triphenyl phosphine (526 mg, 1.8 eq) were dissolved in tetrahydrofuran (6.5ml) in a 100ml rbf equipped with a magnetic stir bar. The mixture was stirred at room temperature at which point diisopropyl azodicarboxylate (DIAD, 439µl, 2.0 eq) was added dropwise. The reaction was stirred at room temperature overnight, at which point reaction was loaded onto silica gel and purified using hexanes and ethyl acetate (9:1) as an elutant. The product was collected and concentrated in vacuo

as a colorless oil in 68% yield (190mg). ^{1}H NMR (400 MHz, $CDCl_3$) δ 7.47 – 7.40 (m, 5H), 7.04 (dd, J = 7.1, 0.5 Hz, 1H), 6.88 (dd, J = 8.4, 0.5 Hz, 1H), 6.72 (dd, J = 17.6, 10.9 Hz, 1H), 5.76 (dd, J = 17.6, 0.9 Hz, 1H), 5.45 (s, 2H), 5.26 (dd, J = 10.9, 0.9 Hz, 1H), 3.94 (t, J = 0.8 Hz, 2H). ^{13}C NMR (101 MHz, $CDCl_3$) δ 185.0, 152.2, 150.5, 137.8, 137.5, 136.4, 135.9, 132.5, 128.1, 126.3, 116.5, 115.3, 114.2, 73.7, 51.2. HRMS: calculated for $C_{17}H_{14}O_2$ (M+H)+ 251.106, found 251.106. FTIR ν = 3081, 3043, 2921, 1760, 1600, 1573, 1473, 1382, 1272, 1128, 1051, 989, 829, 782 cm-1.

5-((4-vinylbenzyl)oxy)bicyclo[4.2.0]octa-1(6),2,4-trien-7-ol

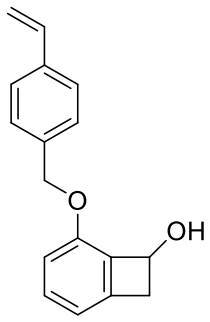

5-((4-vinylbenzyl)oxy)bicyclo[4.2.0]octa-1(6),2,4-trien-7-one (200mg, 1 eq) was dissolved in methanol (15 ml) in a 25ml rbf equipped with a magnetic stir bar at 0˚C. Sodium borohydride (36 mg, 1.2 eq) was added, the reaction was capped with a nitrogen balloon and then warmed to room temperature over two hours. Dilute HCl (0.5M, 10 ml) was added, and the reaction was stirred until a white solid formed (about 30 minutes). The reaction was transferred to a separatory funnel and extracted with ethyl acetate (5 x 15ml). The combined organic extract was washed with brine and dried with magnesium sulfate, filtered and columned on silica gel using hexanes and ethyl acetate (1:1) as an

elutent. The product was collected and concentrated in vacuo to yield a white solid in 87% yield (175 mg, mp = 61-63˚C). ^{1}H NMR (400 MHz, $CDCl_3$) δ 7.43 – 7.22 (m, 4H), 7.19 – 7.09 (m, 1H), 6.72 (d, J = 8.4 Hz, 1H), 6.69 – 6.58 (m, 2H), 5.67 (dd, J = 17.6, 0.7 Hz, 1H), 5.29 – 4.92 (m, 4H), 3.46 (dd, J = 14.5, 4.6 Hz, 1H), 2.89 (dd, J = 14.5, 0.9 Hz, 1H), 2.33 (s, 1H). ^{13}C NMR (101 MHz, $CDCl_3$) δ 153.5, 144.0, 137.2, 137.0, 136.4, 131.4, 131.0, 127.4, 126.4, 115.9, 114.9, 114.0, 70.8, 70.8, 42.4. HRMS: Calculated for $C_{17}H_{16}O_2$ (M+Na)+ = 275.104, found 275.104. FTIR ν = 3261 (broad), 2960, 2925, 1604, 1581, 1471, 1382, 1265, 1045, 993, 831, 773 cm-1.

5-(bicyclo[2.2.1]hept-5-en-2-ylmethoxy)bicyclo[4.2.0]octa-1,3,5-trien-7-one

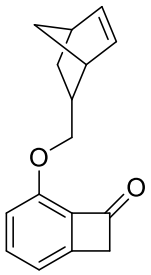

5-hydroxybicyclo[4.2.0]octa-1,3,5-trien-7-one (313mg, 1 eq) and (bicyclo[2.2.1]hept-5-en-2-yl)methanol (289mg, 1eq) and triphenyl phosphine (611 mg, 1 eq) were dissolved in dichloromethane (40ml) in a 100ml rbf equipped with a magnetic stir bar. The mixture was stirred at room temperature at which point a solution of di-(4-chlorobenzyl)azodicarboxylate (DCAD, 856mg, 1 eq) in DCM (10ml) was added

dropwise. The reaction was stirred at room temperature overnight, at which point the white precipitate was filtered and then the filtrate was chromatographed on silica gel using hexanes and ethyl acetate (9:1) as an elutant. The product was collected and concentrated in vacuo as a colorless oil in 52% yield (291mg). ^{1}H NMR (400 MHz, $CDCl_3$) δ 7.37 – 7.28 (m, 1H), 6.90 (dd J = 7.0, 5.5, 1H), 6.72 (td, J = 8.7, 0.6 Hz, 1H), 6.09 (dd, J = 5.7, 3.0 Hz, 1H, endo), 6.02 (ddd, J = 13.2, 5.4, 3.0 Hz, 2H exo), 5.89 (dd, J = 5.7, 2.9 Hz, 1H endo), 4.38 (dd, J = 10.3, 6.2 Hz, 1H exo), 4.18 (dd, J = 10.3, 9.2 Hz, 1H exo), 4.06 (dd, J = 10.2, 6.8 Hz, 1H endo), 3.87 (dd, J = 10.2, 9.2 Hz, 1H endo), 3.81-3.77 (m, 2H), 2.92 (s, 1H), 2.81 – 2.71 (m, 1H), 2.49 – 2.37 (m, 1H), 1.87 – 1.72 (m, 1H), 1.42 – 1.14 (m, 2H), 0.62 (ddd, J = 11.7, 4.4, 2.6 Hz, 1H). ^{13}C NMR (101 MHz, $CDCl_3$) δ 184.7, 152.7, 150.5, 137.6, 136.9, 136.3, 132.3, 116.2 (exo), 116.1 (endo), 114.7 (exo), 114.7 (endo), 76.6 (exo), 75.9 (endo), 51.1, 49.3 (endo), 45.0 (exo), 43.8 (endo), 43.6 (exo), 42.2 (endo), 41.6 (exo), 38.6 (exo), 38.4 (endo), 29.4 (exo), 28.8 (endo). HRMS calculated for $C_{16}H_{16}O_2$ (M+Na)+ 263.104, found 263.104. FTIR ν = 3058, 2969, 2865, 1760, 1604, 1571, 1473, 1456, 1365, 1270, 1216, 1051, 784 cm-1.

5-(bicyclo[2.2.1]hept-5-en-2-ylmethoxy)bicyclo[4.2.0]octa-1(6),2,4-trien-7-ol

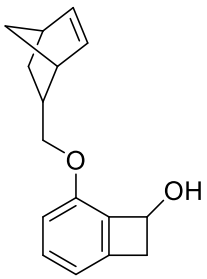

105

5-((bicyclo[2.2.1]hept-5-en-2-yl)methoxy)bicyclo[4.2.0]octa-1(6),2,4-trien-7-one (120mg, 1 eq) was dissolved in methanol (15 ml) in a 25ml rbf equipped with a magnetic stir bar at 0˚C. Sodium borohydride (23 mg, 1.2 eq) was added, the reaction was capped with a nitrogen balloon and warmed to room temperature over two hours. Dilute HCl (0.5M, 10 ml) was added, and the reaction was stirred until a white solid formed (about 30 minutes). The reaction was transferred to a separatory funnel and extracted with ethyl acetate (5 x 15ml). The combined organic extract was washed with brine, dried with magnesium sulfate, filtered and chromatographed on silica gel using hexanes and ethyl acetate (1:1) as an elutent. The product was collected and concentrated in vacuo to yield a colorless oil in 93% yield (112 mg). ^{1}H NMR (400 MHz, $CDCl_3$) δ 7.15 – 7.05 (m, 1H), 6.70 – 6.56 (m, 2H), 5.98 (m, 2H), 5.24 – 5.10 (m, 1H), 4.29 – 3.59 (m, 2H), 3.54 – 3.36 (m, 1H), 2.93 (s, 1H), 2.87 (dd, J = 14.0, 5.5 Hz, 1H), 2.76 (d, J = 7.3 Hz, 1H), 2.46 (s, 1H), 1.90 – 1.64 (m, 1H), 1.44 – 1.09 (m, 2H), 0.55 (ddd, J = 11.8, 7.2, 4.7 Hz, 1H). ^{13}C NMR (101 MHz, $CDCl_3$) δ 153.8, 144.1, 137.5, 136.9, 132.4, 131.3, 115.4, 114.5, 73.7 (exo), 72.9 (endo), 70.9, 49.4, 43.8, 42.3, 38.8, 38.6, 29.6 (exo), 29.0 (endo). HRMS = calculated for $C_{16}H_{18}O_2$ (M+Na)+ 265.120, found 265.120. FTIR ν = 3320 (broad), 3059, 2964, 2933, 2865, 1604, 1583, 1466, 1259, 1045, 769, 721 cm-1.

2-(allyloxy)-8-((1,1,1,3,3,3-hexafluoro-2-(trifluoromethyl)propan-2-yl)oxy)bicyclo[4.2.0]octa-1,3,5-triene

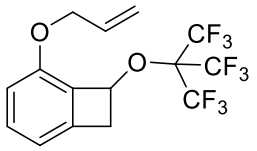

5-(allyloxy)bicyclo[4.2.0]octa-1,3,5-trien-7-ol (152 mg, 1 eq) was dissolved in THF (5.0ml, 1.0M) along with triphenyl phosphine (407mg, 1.8 eq) and perfluorotert-butanol (407mg, 2 eq). The mixture was stirred at 0˚C, and diisopropyl azodicarboxylate (DIAD) was added dropwise (339µl, 2 eq). The reaction warmed to room temperature overnight, at which point the reaction was loaded onto a column of silica gel and chromatographed using a gradient of hexanes to hexanes and ethyl acetate (8:2). As the first compound to elute, the product was concentrated in vacuo and isolated as a colorless oil in 17% yield (58 mg). ^{1}H NMR (400 MHz, $CDCl_3$) δ 7.24 – 7.17 (m, 1H), 6.71 – 6.62 (m, 2H), 5.99 – 5.86 (m, 1H), 5.62 (d, J = 2.5 Hz, 1H), 5.31 (dq, J = 17.3, 1.7 Hz, 1H), 5.17 (dq, J = 10.6, 1.5 Hz, 1H), 4.59 – 4.44 (m, 2H), 3.47 (dd, J = 14.4, 4.0 Hz, 1H), 3.22 (d, J = 14.4 Hz, 1H). ^{13}C NMR (101 MHz, $CDCl_3$) δ 153.7, 143.2, 132.8, 132.6, 127.3, 121.8 (q, J = 290 Hz), 118.9, 117.1, 115.4, 113.6, 75.4, 69.5, 40.8. ^{19}F NMR (376 MHz, $CDCl_3$) δ -70.08 (s). HRMS: calculated $C_{15}H_{11}O_2F_9$ (M+) 394.061, found 394.061.

2-(allyloxy)-8-(4-((1,1,1,3,3,3-hexafluoro-2-(trifluoromethyl)propan-2-yl)oxy)butoxy)bicyclo[4.2.0]octa-1,3,5-triene

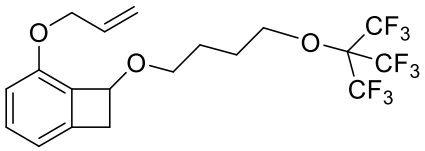

5-(allyloxy)bicyclo[4.2.0]octa-1,3,5-trien-7-ol (152 mg, 1 eq) was dissolved in THF (5.0ml, 1.0M) along with triphenyl phosphine (407mg, 1.8 eq) and perfluorotert-butanol (407mg, 2 eq). The mixture was stirred at 0˚C while diisopropyl azodicarboxylate (DIAD) was added dropwise (339µl, 2 eq). The reaction was warmed to room temperature overnight, at which point the reaction was loaded onto a column of silica gel and chromatographed using a gradient of hexanes to hexanes and ethyl acetate (8:2). The second compound to elute, the product was concentrated in vacuo and isolated as a colorless oil in 71% yield (286 mg). ^{1}H NMR (400 MHz, $CDCl_3$) δ 7.15 (dd, J = 8.4, 7.2 Hz, 1H), 6.66 (dd, J = 7.7, 5.7 Hz, 2H), 5.97 (ddt, J = 17.3, 10.5, 5.2 Hz, 1H), 5.30 (ddd, J = 17.3, 2.9, 1.5 Hz, 1H), 5.17 (ddd, J = 10.5, 2.9, 1.1 Hz, 1H), 4.99 (dd, J = 4.2, 1.8 Hz, 1H), 4.71 – 4.55 (m, 2H), 3.97 (t, J = 5.8 Hz, 2H), 3.60 – 3.49 (m, 2H), 3.31 (dd, J = 14.0, 4.3 Hz, 1H), 3.00 (dd, J = 14.0, 1.1 Hz, 1H), 1.79 – 1.61 (m, 4H). ^{13}C NMR (101 MHz, $CDCl_3$) δ 153.4, 144.1, 133.7, 131.2, 129.3, 121.9 (q, J = 291 Hz), 119.0, 117.0, 115.8, 113.9, 76.1, 69.6, 67.4, 38.0, 26.7, 25.8. ^{19}F NMR (376 MHz, $CDCl_3$) δ -70.43 (s). HRMS: Calculated for $C_{25}H_{23}F_9NaO_3$ (M+Na)+ = 565.140, found 565.139.

8-(4-((1,1,1,3,3,3-hexafluoro-2-(trifluoromethyl)propan-2-yl)oxy)butoxy)-2-((4-vinylbenzyl)oxy)bicyclo[4.2.0]octa-1(6),2,4-triene

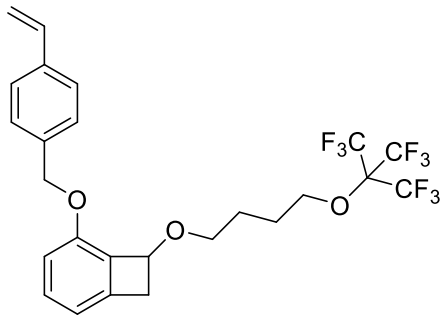

5-((4-vinylbenzyl)oxy)bicyclo[4.2.0]octa-1(6),2,4-trien-7-ol (160mg, 1 eq) was dissolved in THF (5.0ml, 1.0M) along with triphenyl phosphine (297mg, 1.8 eq) and perfluorotert-butanol (175µl, 2 eq). The mixture was stirred at 0˚C, and diisopropyl azodicarboxylate (DIAD) was added dropwise (248µl, 2 eq). The reaction was warmed to room temperature overnight, at which point it was loaded onto a column of silica gel and purified using a gradient of hexanes to hexanes and ethyl acetate (8:2). As the second compound to elute, the product was concentrated in vacuo and isolated as a colorless oil in 61% yield (210 mg). ^{1}H NMR (400 MHz, $CDCl_3$) δ 7.44 – 7.19 (m, 5H), 6.83 – 6.66 (m, 3H), 5.75 (ddd, J = 17.6, 4.7, 0.9 Hz, 1H), 5.30 – 5.07 (m, 3H), 4.93 (dd, J = 4.2, 1.8 Hz, 1H), 4.08 – 3.96 (m, 2H), 3.68 – 3.53 (m, 2H), 3.41 – 3.29 (m, 1H), 3.11 – 2.98 (m, 1H), 1.88 – 1.66 (m, 4H). ^{13}C NMR (101 MHz, $CDCl_3$) δ 153.6, 144.1, 137.2, 136.4, 132.7, 131.3, 129.4, 127.2, 126.3, 121.9 (q, J = 292 Hz), 118.9, 115.9, 114.2, 113.9, 76.2, 70.5, 69.6, 67.6, 38.1, 26.8, 25.9. ^{19}F NMR (376 MHz, $CDCl_3$) δ -70.40 (s). HRMS: calculated for $C_{25}H_{23}F_9O_3$ (M+Na)+ 565.140, found 565.139.

2-(bicyclo[2.2.1]hept-5-en-2-ylmethoxy)-8-(4-((1,1,1,3,3,3-hexafluoro-2-(trifluoromethyl)propan-2-yl)oxy)butoxy)bicyclo[4.2.0]octa-1(6),2,4-triene

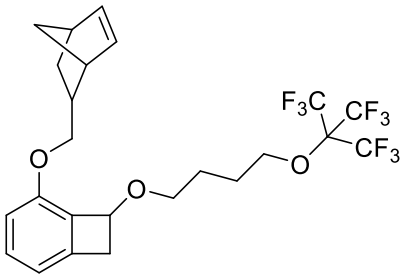

5-(bicyclo[2.2.1]hept-5-en-2-ylmethoxy)bicyclo[4.2.0]octa-1(6),2,4-trien-7-ol (66mg, 1 eq) was dissolved in THF (2.0ml, 1.0M) along with triphenyl phosphine (128mg, 1.8 eq) and perfluorotert-butanol (75µl, 2 eq). The mixture was stirred at 0˚C, and diisopropyl azodicarboxylate (DIAD) was added dropwise (128µl, 2 eq). The reaction was warmed to room temperature overnight, at which point the reaction was loaded onto a column of silica gel and purified using a gradient of hexanes to hexanes and ethyl acetate (8:2). As the second compound to elute, the product was concentrated in vacuo and isolated as a colorless oil in 69% yield (104 mg). ^{1}H NMR (400 MHz, $CDCl_3$) δ 7.25 – 7.08 (m, 1H), 6.69 – 6.56 (m, 2H), 6.13 – 5.80 (m, 2H), 4.98 (dtd, J = 13.5, 4.1, 1.7 Hz, 1H), 4.23 – 3.43 (m, 8H), 3.30 (dt, J = 14.0, 4.1 Hz, 1H), 3.03 – 2.90 (m, 2H), 2.76 (s, 1H), 2.51 – 2.36 (m, 1H), 1.89 – 1.58 (m, 4H), 1.43 – 1.15 (m, 3H), 0.60 – 0.44 (m, 1H). ^{13}C NMR (101 MHz, $CDCl_3$) δ 153.8, 144.1, 137.3, 132.4, 131.2, 129.7, 121.8 (q, J = 292 Hz), 118.9, 115.4, 113.6, 76.3, 72.3, 69.7, 67.6, 49.4, 43.8, 42.2, 38.6, 38.1, 28.9, 26.8, 25.9. ^{19}F NMR (376 MHz, $CDCl_3$) δ -70.43 (s). HRMS: Calculated for $C_{24}H_{25}F_9O_3$ (M+Na)+ 555.154, found 555.155. FTIR ν = 3068, 2956, 2935, 2870, 1604, 1587, 1249 (strong), 1155, 1006, 972, 771, 727 cm-1.

((5-(allyloxy)bicyclo[4.2.0]octa-1,3,5-trien-7-yl)oxy)(tert-butyl)dimethylsilane

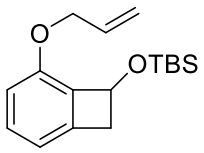

5-(allyloxy)bicyclo[4.2.0]octa-1,3,5-trien-7-ol (89 mg, 1 eq) was dissolved in dimethyl formamide (2ml) in a 5ml rbf equipped with a magnetic stir bar. Imidazole (85 mg, 2.5 eq) was added, then tertbutyldimethyl silyl chloride (92 mg, 1.2 eq) was added. The solution was capped with a nitrogen balloon then stirred for one hour. The reaction mixture was then directly loaded onto a column of silica and chromatographed using hexanes and ethyl acetate (9:1) as an elutent. The product was concentrated in vacuo and isolated as a colorless oil in 95% yield (138 mg). ^{1}H NMR (400 MHz, $CDCl_3$) δ 7.05 (ddd, J = 8.4, 7.1, 0.5 Hz, 1H), 6.64 – 6.48 (m, 2H), 5.91 (ddt, J = 17.3, 10.5, 5.3 Hz, 1H), 5.23 (dq, J = 17.3, 1.4 Hz, 1H), 5.20 – 5.17 (m, 1H), 5.10 (dq, J = 10.5, 1.4 Hz, 1H), 4.71 – 4.48 (m, 2H), 3.32 (ddt, J = 13.8, 4.4, 0.8 Hz, 1H), 2.88 (ddt, J = 13.8, 1.8, 0.8 Hz, 1H), 0.79 (s, 9H), 0.00 (s, 6H). ^{13}C NMR (101 MHz, $CDCl_3$) δ 158.5, 148.6, 138.7, 136.2, 135.9, 122.1, 120.5, 119.7, 75.5, 75.2, 47.1, 30.7, 23.0, 0.5. HRMS: calculated for C17H26O2Si (M+) 290.169, found 290.170.

((5-(allyloxy)bicyclo[4.2.0]octa-1,3,5-trien-7-yl)oxy)(tert-butyl)diphenylsilane

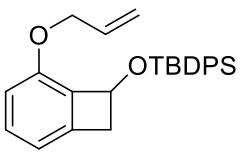

5-(allyloxy)bicyclo[4.2.0]octa-1,3,5-trien-7-ol (61 mg, 1 eq) was dissolved in dimethyl formamide (2ml) in a 5ml rbf equipped with a magnetic stir bar. Imidazole (59 mg, 2.5 eq) was added, then tertbutyldiphenyl silyl chloride (112 mg, 1.2 eq) was added. The solution was capped with a nitrogen balloon then stirred for one hour. The reaction mixture was then directly loaded onto a column of silica and collected using hexanes and ethyl acetate (9:1) as an elutent. The product was concentrated in vacuo and isolated as a colorless oil in 95% yield (134 mg). ^{1}H NMR (400 MHz, $CDCl_3$) δ 7.80 – 7.66 (m, 4H), 7.48 – 7.32 (m, 6H), 7.17 (dd, J = 8.4, 7.1 Hz, 1H), 6.72 (d, J = 8.4 Hz, 1H), 6.61 (d, J = 7.1 Hz, 1H), 5.97 (ddt, J = 17.2, 10.5, 5.4 Hz, 1H), 5.39 (dd, J = 4.3, 2.0 Hz, 1H), 5.31 (dq, J = 17.2, 1.4 Hz, 1H), 5.21 (ddd, J = 10.5, 2.9, 1.4 Hz, 1H), 4.71 (m, 2H), 3.08 (dd, J = 14.0, 4.3 Hz, 1H), 3.01 – 2.93 (m, 1H), 1.09 (s, 9H). ^{13}C NMR (101 MHz, $CDCl_3$) δ 153.4, 143.7, 135.9, 134.0, 133.6, 131.6, 130.9, 129.8, 127.6, 117.4, 115.6, 113.9, 71.0, 70.2, 41.9, 26.9, 19.3. HRMS: calculated for $C_{27}H_{30}O_2Si$ (M+) 414.201 found 414.201.

POLYMER 4.15

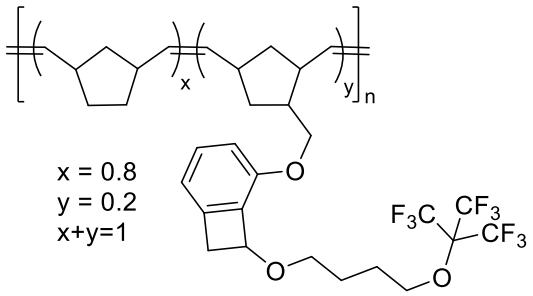

Norbornene (75 mg, 80 eq) and 2-(bicyclo[2.2.1]hept-5-en-2-ylmethoxy)-8-(4-((1,1,1,3,3,3-hexafluoro-2-(trifluoromethyl)propan-2-yl)oxy)butoxy)bicyclo[4.2.0]octa-

1(6),2,4-triene (104mg, 20 eq) were combined in dichloromethane (20ml) in a 50ml rbf with a magnetic stir bar and stirred at room temperature. Second generation Grubbs' catalyst (8.5 mg, 1 eq) was added and the reaction was stirred for one hour at room temperature. Ethyl vinyl ether (2ml) was added, then the reaction was concentrated in vacuo and redissolved in THF (2ml). The reaction was precipitated in methanol, filtered and dried in vacuo to give the corresponding polymer (fibrous solid) in 81% yield (145mg).

Tg = 52˚C. Td5 = 407˚C. GPC Mn = 65.8 kDa, Mw = 115.3 kDa, Đ = 1.75

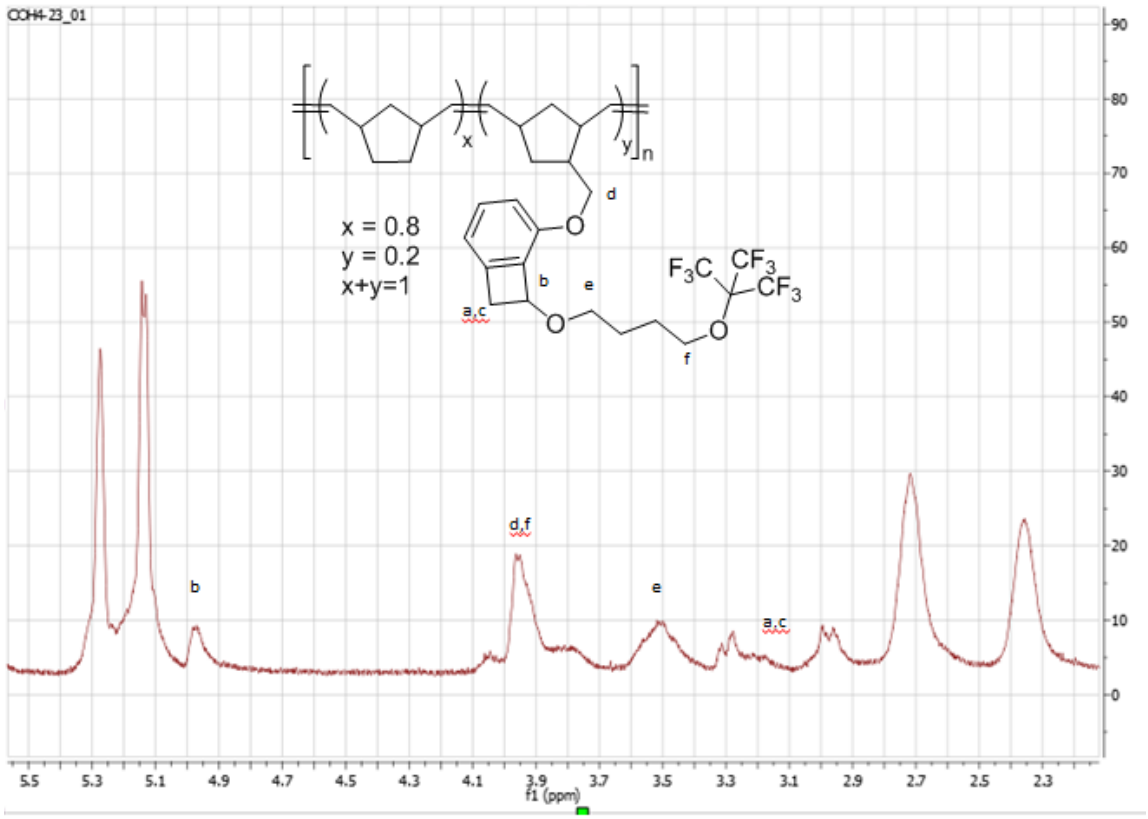

POLYMER 4.14

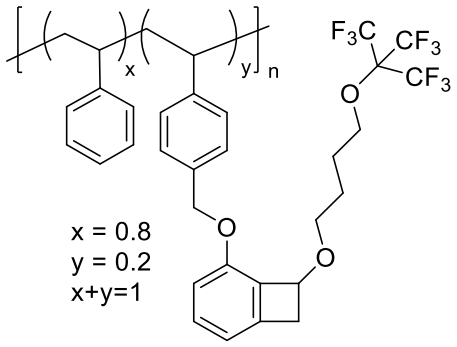

Neat styrene (123mg, 80 eq) and 8-(4-((1,1,1,3,3,3-hexafluoro-2-(trifluoromethyl)propan-2-yl)oxy)butoxy)-2-((4-vinylbenzyl)oxy)bicyclo[4.2.0]octa-1(6),2,4-triene (160mg, 20 eq) were combined in a 5ml rbf with Igracure 819 (6 mg, 1 eq). The mixture was capped and purged with nitrogen gas for 30 minutes, then exposed in a Rayonet Photochemical Reactor with eight 40W broadband UV bulbs for 16h. The reaction was then dissolved in THF (2ml), precipitated in methanol, filtered and dried to give the corresponding polymer (white powder) in 63% yield (173 mg).

Tg = 74˚C. Td5 = 269˚C. GPC Mn = 48.6 kDa, Mw = 100.3 kDa, Đ = 2.06

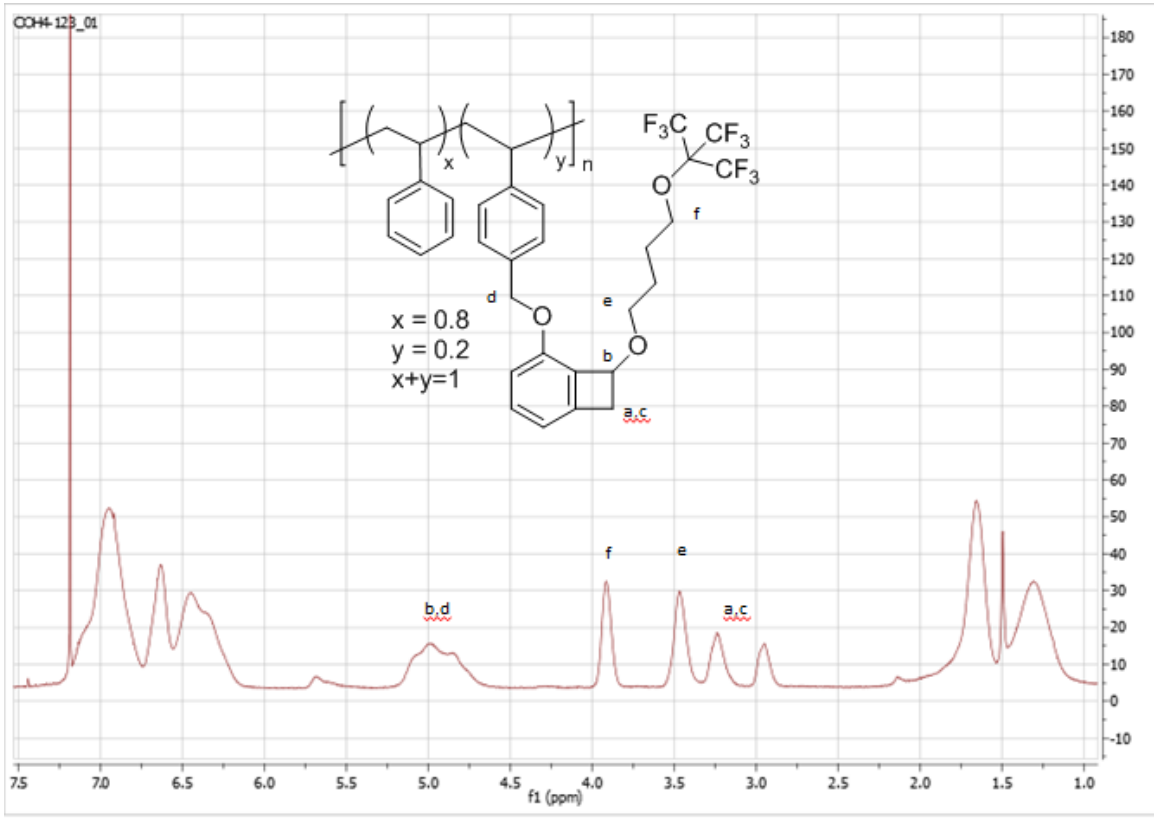
COH4-123_01
x = 0.8
y = 0.2
x+y=1
b,d
f
e
a,c
f1 (ppm)

Chapter 5: Polynorbornene and Benzocyclobutene Dielectric Materials

5.1 INTRODUCTION

Norbornene, a combination of the readily available precursors C5 (cyclopentadiene) and C2 (ethylene) petroleum feedstocks, has found very limited application in the field of organic dielectric materials. There are three major methods for creating isomeric forms of polynorbornene: Ring Opening Metathesis Polymerization (ROMP), radical addition polymers and metal catalyzed vinyl addition polymers.

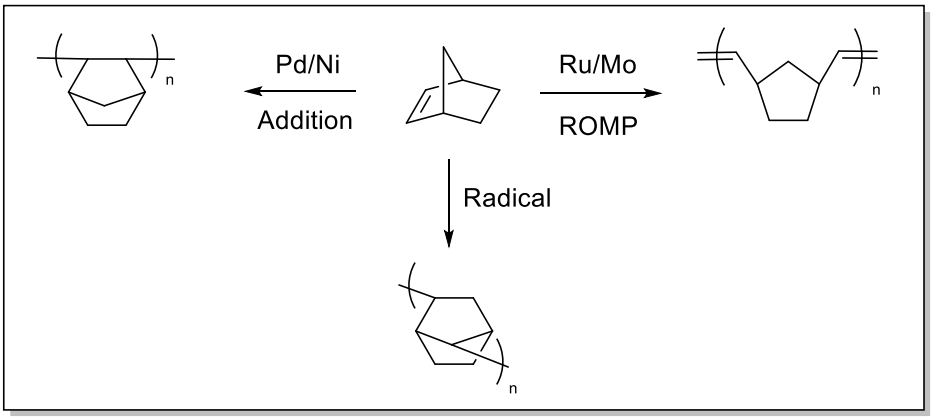

Figure 5.1: General strategy of norbornene polymerization. Three canonical approaches include transition metal catalyzed addition polymerization, Ruthenium (Grubbs) or Molybdenum (Schrock) ring opening metathesis polymerization, and radical initiated polymerization.

Vinyl addition polymers of norbornenes have a long history in electronic materials, notably among chemically amplified resists due to their high transparency, and in spite of their limited monomer scope[49]. These materials have been investigated for applications in microelectronics packaging and will be discussed in more detail in Chapter 6. Radical addition of norbornenes has seen little attention in material science because the polymers have broad dispersity and are difficult to prepare reproducibly. ROMP of norbornenes make excellent materials but have also seen little interest in the

application of dielectric materials due to the low glass transition temperatures (T_g) of the polymers (40-50˚C), which results in a large increase of their CTE at relevant temperatures (25-200˚C)[77].

Nevertheless, these ROMP materials come from cheap petroleum feedstocks and (as hydrocarbons) possess low dielectric constants (2.2-2.4)[47]. ROMP polymers also possess several features that make them attractive for innovation: controlled and living polymerization conditions have been well studied, and the ruthenium based Grubbs catalysts are readily available and are largely insensitive to other functional groups, oxygen and water. Polymerizations typically proceed rapidly and in high yields at room temperature in a variety of solvents. In light of the results described in Chapter 3, where benzocyclobutene (BCB) resins produced excellent material qualities but suffered from a problematic B-stage requirement, a material resin strategy was envisioned in which BCB could be covalently attached to a higher molecular weight polymer backbone to avoid a B-stage. ROMP was chosen for this purpose. A ROMP backbone would provide a large number of available alkenes for crosslinking via Diels Alder reaction. These alkenes could also serve as a crosslinking point for a bis-azide photolithographical strategy. The materials were investigated at a variety of BCB loadings, including two different ROMP norbornene backbones, and with a polystyrene/polynorbornene polymer brush[78]. The materials demonstrated low dielectric constants (2.2-2.4), low coefficients of thermal expansion (CTE = 15 ppm/K in the plane) and direct photopatternability down to five microns half pitch, suggesting these materials are not only prime candidates for next generation packaging materials, but are also highly flexible and versatile polymers that can be adjusted easily to individual engineering applications.

5.2 Results and Discussion: Synthesis

When approaching the problem of how to best join a BCB functional group with polynorbornene, the first fundamental question one must ask is: should the norbornene serve as a nucleophile or an electrophile? Many synthetic chemists might envision a route through 5-bromomethyl norbornene, the easily accessible Diels Alder adduct of cyclopentadiene and allyl bromide. At first glance, a primary bromo-alkane appears to be an excellent electrophile suitable for substitution. However, attempts to alkylate 5-bromomethyl norbornene proved unsuccessful. A closer look via conformational analysis reveals a possible reason for the lack of reactivity. Spartan Semi-Empirical models were built and the energy barriers around the relevant dihedral angle of 5-exo and 5-endo-bromomethyl norbornene were calculated.

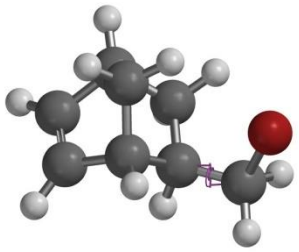

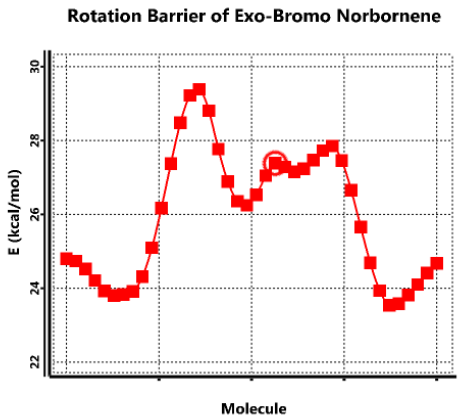

(Figure 5.2 continued on next page)

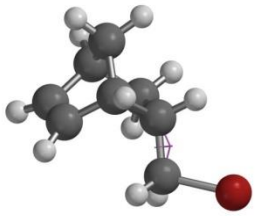

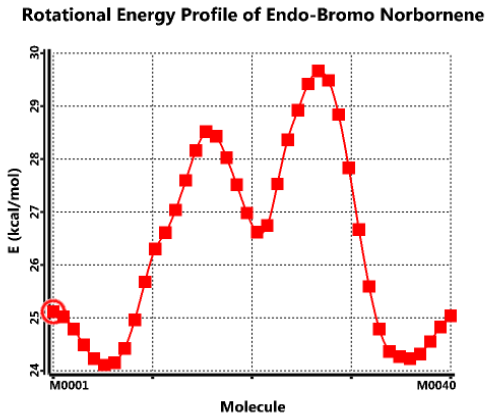

Figure 5.2: Semi-empirical calculations and conformational analysis of 5-bromomethyl norbornene, both exo (above) and endo (below). Both rotational energy profiles demonstrate that the highest energy conformation is also the most reactive: when the bromine is pointed inwards towards the NB cage. Results are consisted with the low S_N2 reactivity observed experimentally.

In both the endo and exo cases, there is a significant rotational barrier to placing the bromine in the reactive position for an S_N2 reaction (pointing under the bridged bicycle). However, a rough 6 kcal/mol barrier between the lowest energy and reactive confirmation doesn't entirely explain this result (after all, the rotation barrier for ethane is about 3 kcal/mol). When the bromine is pointed inward towards the norbornene bicycle, followed by the approach of a nucleophile, the S_N2 transition state involves a bromine gradually moving further away from the reactive carbon—and in this case closer to the norbornene, creating an additional steric repulsion effect. Thus, the combination of

rotation barrier and steric crowding in the resulting transition state suggests the energy is simply too high for substitution to occur.

An alternative approach is to use the norbornene as a nucleophile. A strategy emerged in which a 5-norbornene methanol could be esterified onto BCB. BCB **5.1** was brominated to give arene **5.2**, from which the corresponding Grignard reagent was formed. Addition of CO_2 gas gave the benzoic acid **5.3**, which was purified via column chromatography (unfortunately, attempts to purify by recrystallization were unsuccessful). The requisite norbornene compound was prepared via reduction of the inexpensive acid **5.4** using lithium aluminum hydride, which proceeded nearly quantitatively and required only an aqueous workup to produce the alcohol **5.5**. Finally the target monomer was synthesized in high yield via the Steglich Esterification. A stoichiometric amount of 1-ethyl-3-(3-dimethylaminopropyl)carbodiimide HCl salt (EDC) was added to the two coupling partners along with with a catalytic amount of 4-dimethylamino pyridine (DMAP). Stirring overnight in DCM produced the desired ester after column chromatography as a 4:1 mixture of endo:exo isomers.

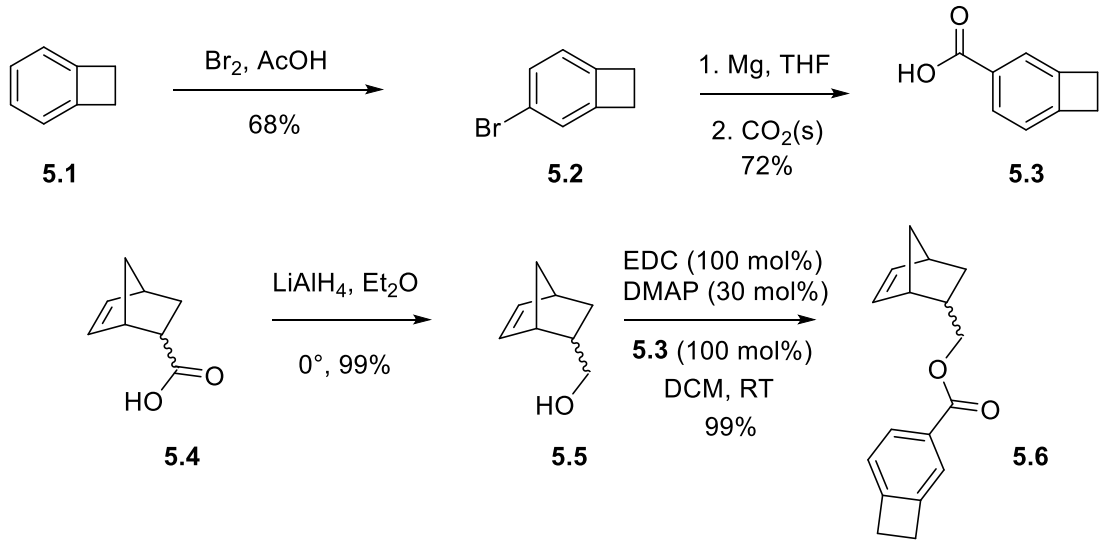

Scheme 5.1: Synthesis of BCB acid and target norbornene-BCB monomer.

A series of copolymers containing norbornene and the custom BCB monomer **5.6** were synthesized. The goal of these experiments was to understand the effect of this monomer's incorporation on material properties and resin performance. Polymerizations were run for one hour in DCM, after which ethyl vinyl ether was added to terminate the polymerization and sequester ruthenium from the resin. The polymers were precipitated in methanol and the composition was found to match the feed by proton NMR.

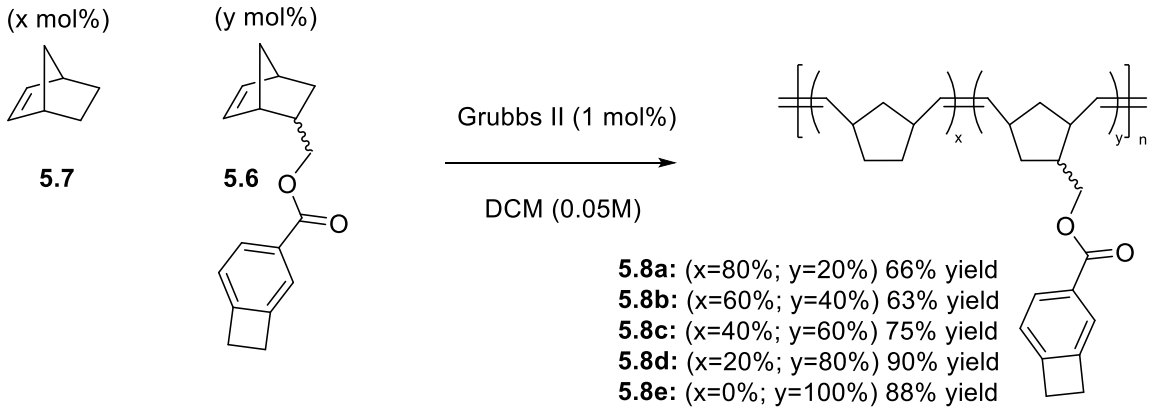

Scheme 5.2: Synthesis of Norbornene-BCB copolymers via ROMP.

Another monomer system was investigated concurrently. Japanese Synthetic Rubber (JSR) Corporation has a proprietary process to synthesize and purify a series of dinorbornenes (DNBs). DNB is the iterative product of another cyclopentadiene Diels Alder reaction on an existing norbornene. These structures were synthesized and investigated as early as 1938 by Alder and Windemuth[79]. Further study of the repeated Diels Alder addition of cyclopentadiene by Soloway suggested that each cyclopentadiene unit adds in a fashion exo from the previous one, and the stereochemistry of the methyl esters is set in the first Diels Alder addition reaction[80]. The methyl ester DNB **5.9** was received as a gift from the JSR corporation as a 55:45 mixture of endo:exo isomers. The Diels Alder adduct of norbornene and methyl acrylate typically produces a 4:1 endo:exo

ratio. The exo product is the thermodynamic product, and the mixture can be driven more in the favor of the exo product upon extended heating. The "up/down" norbornene tetracyclic structure was confirmed through NOESY experiments and crystal structures of the carboxylic acid in previous work in the Willson group[81]. Using a route analogous to that described previously, lithium aluminum hydride reduced the methyl ester to the corresponding alcohol **5.10**. The alcohol **5.10** was submitted to a Steglich Esterification protocol as before, which gave the desired BCB ester product, although in reduced yield from original monomer **5.6**. Also, analysis of the proton NMR revealed that the DNB **5.11** was isolated as a 2:1 mixture of endo:exo isomers, suggesting that the endo product may react slightly faster than the exo in the esterification.

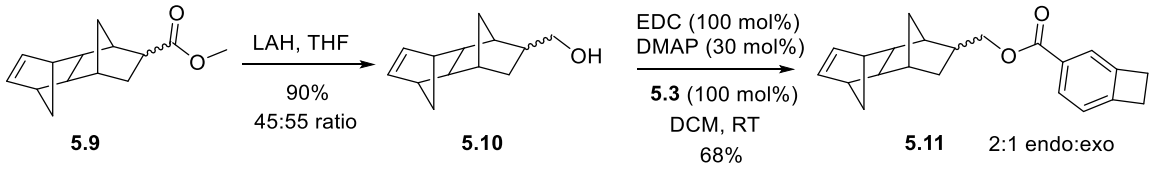

Scheme 5.3: Synthesis of Dinorbornene BCB monomer.

Synthesis of the desired DNB copolymer system provided some unexpected challenges. An analogous copolymer system was proposed using the methyl-tetracyclododecene (MTD) **5.12**, which was also received as a donation from JSR Corporation. Initially, the same reaction conditions used to obtain copolymers **5.8a-e** were tried (THF, Grubbs Second Generation 1 mol%), but no polymer was formed, except in the case of the homopolymer of **5.12**, which proceeded in high yield. As a control experiment, the dinorbornene methyl ester **5.9** was also polymerized in high yield, suggesting that the ester functionality was not unexpectedly poisoning the catalyst. A series of solvents were

tested, and it was found that **5.11** and its monomers polymerized readily in toluene. The resulting copolymers are shown in Scheme 5.4.

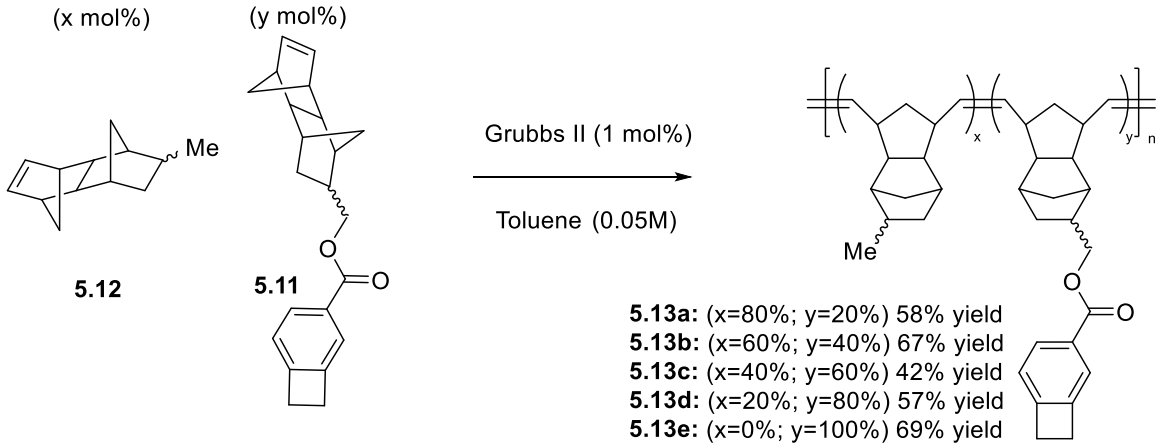

Scheme 5.4: Copolymers of dinorbornene BCB ROMP resin.

An ideal resin would be dry laminated onto a substrate in a solvent free fashion. In order for this to be achieved, a polymer must have a T_g in the range of 90-100˚C. Unfortunately, the polynorbornenes **5.8a-e** possessed T_g on the order of 50-60˚C, while the dinorbornene system T_g's were on the order of 150˚C. It was proposed that a copolymerization between norbornene and dinorbornene monomers could produce a resin of intermediate and controllable T_g. With this in mind, a model system was synthesized to demonstrate the proof of principle. Norbornene **5.7**. and the dinorbornene methyl ester **5.9** were copolymerized to produce a series of copolymers whose composition could be verified by proton NMR integrating the methyl ester protons. The results are shown in Scheme 5.5.

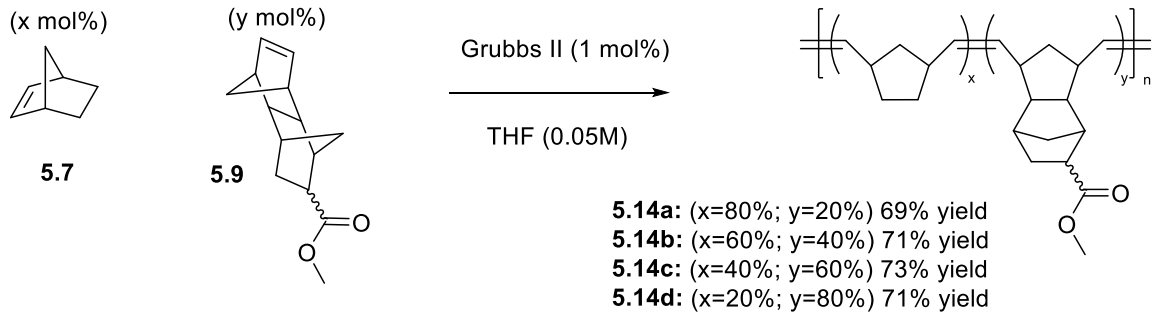

Scheme 5.5: Synthesis of norbornene/dinorbornene copolymers.

Polymerizations were terminated with ethyl vinyl ether and precipitated in methanol to obtain copolymers **5.14a-d**. The copolymer T_g was determined by differential scanning calorimetry and plotted versus dinorbornene percent composition. The results are shown in Figure 5.3.

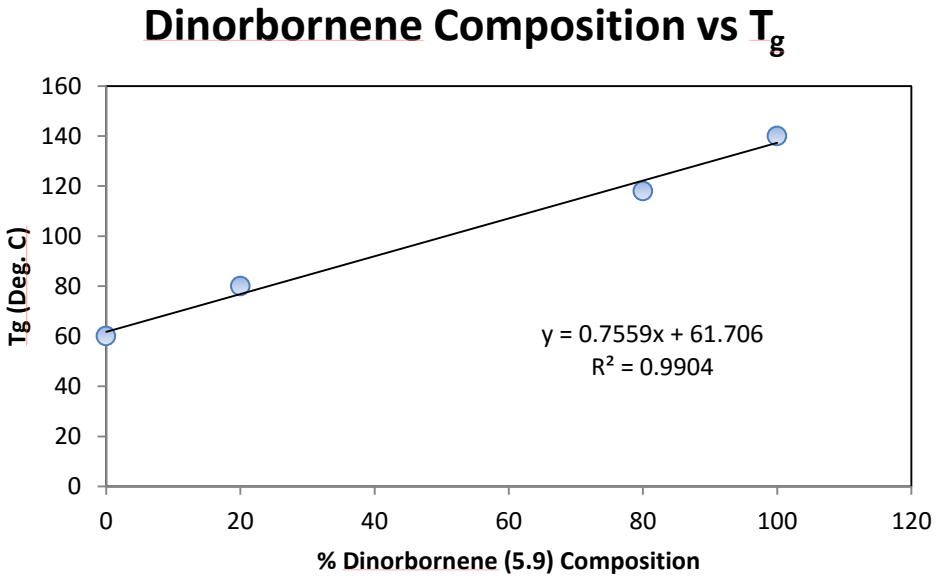

Figure 5.3: Glass transition temperature versus percent dinorbornene (5.9) composition

The results demonstrate that the glass transition temperature of the resin is roughly linear with respect to the feed ratio of monomers. This means that any desired T_g between 60˚C and 140˚C could, in principle be obtained by different combinations of the monomers investigated in this chapter: **5.6**, **5.7**, **5.11** and **5.12**. The results demonstrate the versatility in this resin strategy and are promising for technology transfer.

Another unique polymer architecture has been synthesized in this chapter, a BCB brush polymer. There has been a great deal of progress in the synthesis of styrene norbornene brushes[78,82], and this work was applied to create a unique BCB material. Here, the synthetic strategy has been to click polystyrene onto a norbornene to form an orthogonal macromonomer, as opposed to growing a polymer from a norbornene functional initiator. If the latter strategy is employed, a small but significant portion of chain transfer occurs, creating a bifunctional impurity in the subsequent ROMP step. This leads to high molecular weight chains or gel particles. This strategy does not afford a controlled polymerization or monodisperse product.

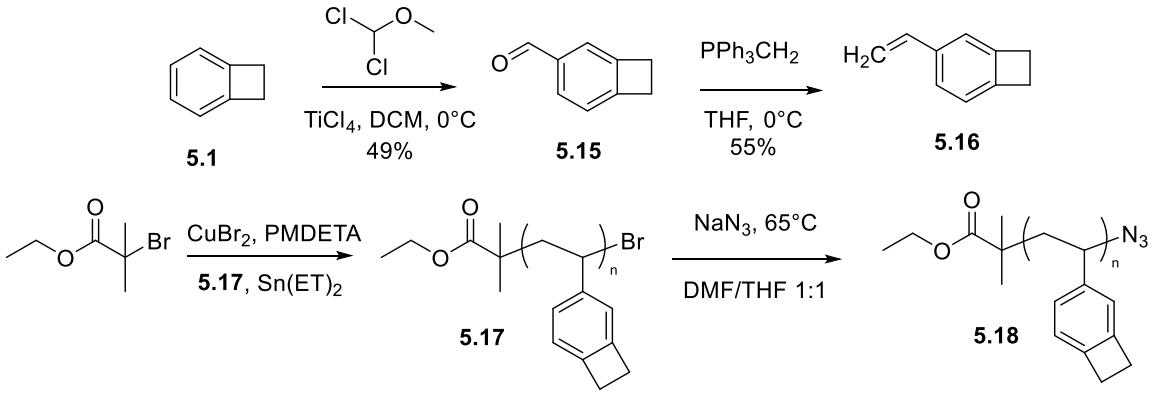

Scheme 5.6: Synthesis of BCB styrene and azide terminated ATRP polymer.

Scheme 5.6 outlines the synthesis of the azide terminated ATRP (atom transfer radical polymerization) polymer. Diverting from BCB **5.1**, the Reiche Formylation was performed using 1,1-dichlorodimethyl ether and the Lewis Acid titanium tetrachloride ($TiCl_4$). The Lewis Acid complex forms the electrophile, which upon hydrolysis gives the desired benzaldehyde **5.15**, and then a Wittig reaction using potassium tert-butoxide to form the active ylide gives the BCB styrene **5.16** in moderate yield. An Activators ReGenerated by Electron Transfer (ARGET) atom transfer radical polymerization (ATRP) procedure was carried out in bulk using ethyl-α isobutyrate as an initiator. As expected, bromine terminated polymer was precipitated from cold methanol as a narrow molecular weight distribution and close to the target molecular weight of 3 kDa. The substitution from bromine terminated to azide terminated was carried out in a DMF/THF solvent mixture, as it was observed that DMF alone could not sufficiently solubilize the polymer. A clear shift in the proton NMR from approximately 4.8 ppm to 4.0 ppm indicated complete conversion into azide terminated polymer **5.18.**

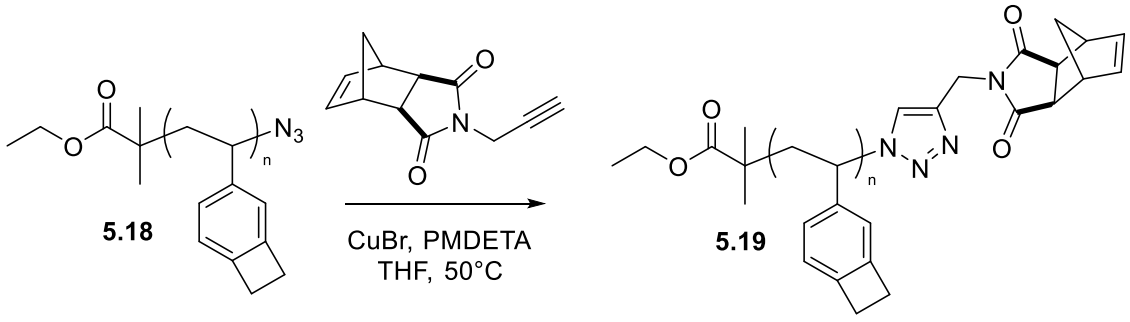

(Scheme 5.7 continued on next page)

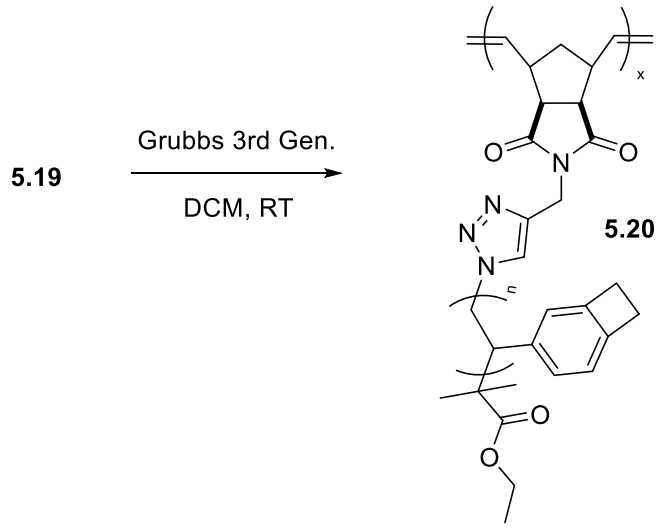

Scheme 5.7: Synthesis of macromonomer and BCB brush polymer.

Synthesis of the macromonomer was completed using the copper catalyzed 1,3-dipolar cycloaddition "Click" reaction. The norbornene was prepared using a literature procedure from exo-carbic anhydride and propargylamine[78]. The resulting polymer **5.19** had only the norbornene end group by proton NMR analysis. Synthesis of the brush was carried out using Grubbs 3rd generation catalyst in DCM at room temperature. GPC traces show a clear shift of the narrow distribution of signal to lower retention volume, signaling a shift to higher molecular weight; this is strong evidence for the formation of brush **5.20**.

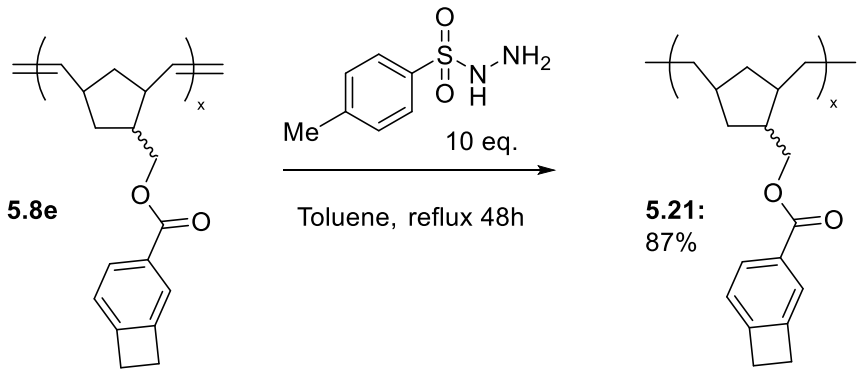

Scheme 5.8: Synthesis of reduced PNB BCB homopolymer. The diimide reduction requires a large excess of hydrazide and extended reaction time.

Lastly, in order to better understand the importance of the role that the unsaturated ROMP backbone might play in BCB crosslinking, a reduced analogue of the homopolymer **5.8e** was prepared. Reducing PNB via a catalytic hydrogenation process is very difficult. Procedures such as palladium on carbon or Rainey Nickel (which can reduce the aromatic polystyrene down to poly-vinylcyclohexane) have no effect on polynorbornene. JSR Corp. has successfully reduced PNB backbones with Ru(II) catalysts. For a lab scale experiment, using a stoichiometric diimide reduction is very effective. Using p-toluenesulfonic hydrazide (Scheme 5.8) in a large excess, diimide was generated in situ and this reagent reduced the backbone of the polymer. Proton NMR showed complete disappearance of alkene resonances. It was found that reaction times shorter than 48 hours often resulted in incomplete or no reduction of the backbone (similarly for using less hydrazide). Purification by precipitation was ineffective as residual 4-methylbenzenesulfinic acid could be seen in the NMR. When the crude reaction mixture was washed three times with sodium bicarbonate and then precipitated, a colorless fibrous solid was obtained as the pure reduced polymer.

5.3 Results and Discussion: Materials Evaluation

In Chapter 3, a thorough discussion of the techniques used to evaluate dielectric materials including nanoindentation, ellipsometry, and wafer bow tests were provided. The materials presented in this chapter have been evaluated using the same methods and equations 3.1 through 3.10.

First generation polynorbornene copolymers were investigated using nanoindentation and heated stage ellipsometry (to measure z-axis CTE α_z). Samples were formulated in toluene then spun onto APTES treated silicon wafers, baked (soft bake at 110˚C) then cured in inert atmosphere at 250˚C for one hour. The resulting samples produced an interesting trend, which is shown in Figure 5.4. At first glance, it is obvious that the data is nonlinear with respect to mole-percent BCB in the polymer. This general materials trend has been observed before. So et al.[83] saw that incorporation of over twenty percent of BCB into polystyrenes showed an exponential increase in T_g of the cured polymer. Herein, a sharp increase in both reduced modulus and z-axis CTE were observed at a BCB content in excess of twenty percent.

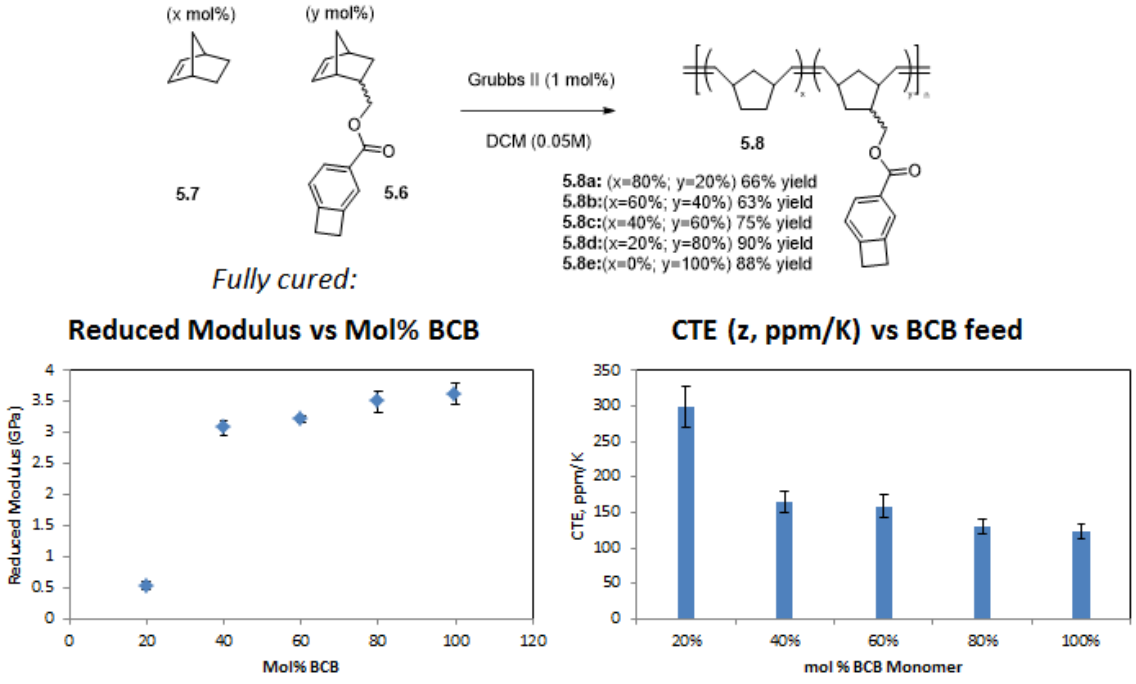

Figure 5.4: Nanoindentation and heated stage CTE data for copolymer series 5.8.

While So et al. do not give an explanation for this phenomenon; it is possible that it is artifact of the chemistry of BCB crosslinking and network formation. Regardless, the results demonstrate something potentially useful for an industrial application: a vendor could achieve 90% of the potential polymer properties with only 40% loading (or less) of the "expensive" BCB crosslinking component, while "diluting" the resin with inexpensive norbornene. The resins demonstrate good materials properties past the key twenty percent loading mark, where reduced moduli reach 3.10 to 3.84 GPa, and most importantly the z-axis CTE ranges from 165 ± 15 ppm/K in polymer **5.8b** to 123 ± 11 ppm/K in the homopolymer **5.8e**. The reader will recall from Chapter 3 that z-axis CTEs of POSS resins were found to be approximately 105, 203 and 216 ppm/K, and the Dow Chemical product Cyclotene has an out of plane CTE on the order of 200-250 ppm/K. All these silicon based resins have good (i.e. low) expansion in the plane of the film

(which is the more important parameter to device fabrication), the results were extremely promising.

In collaboration with Georgia Tech, Jared Schwartz and Dr. Paul Kohl, wafer bow measurements on silicon and germanium were performed on one polymer chosen at random (polymer **5.8d**, 80% BCB). The results were impressive. Two data sets confirmed that the value of the CTE in the plane of the substrate is 15.0 ± 0.3 ppm/K, a factor of two below the goal value of 30 ppm/K. It is especially worth noting that this value is achieved using an all organic, silicon and filler free resin, which is highly advantageous in terms of cost. Unfortunately, the wafer bow instrument broke down shortly after measurements of **5.8d** were complete, so the, data is restricted to this particular entry (although it is verified on the two separate silicon and germanium data sets).

At first glance, one might conclude that these results seem too good to be true. After all, the CTE below the T_g of ROMP polynorbornene is on the order of 100-120 ppm/K (below its T_g), and the CTE of Cyclotene (post-cure) is on the order of 40-50 ppm/K, so it is not obvious why combining these chemistries might produce a lower value rather than give an intermediate value. Fundamentally, things are not always simply the sum of their parts. The CTE of a material is controlled by the average interatomic distance as a function of temperature. This means that the critical means of achieving low CTE is forming many strong (covalent) bonds along a given direction, and in the case of material **5.8**, the bonds being formed during cure are different than Cyclotene; namely, it is likely that BCB engaged in a Diels Alder addition on the backbone of the unsaturated polynorbornene. It is proposed that these bonds are the source of this material's high performance. This is evidence for the "[4+2]" hypothesis introduced in Chapter 3. Just as the [4+2] crosslink product was more dominant in the

case of DF POSS (Figure 3.1) which lead to a lower CTE, here the opportunity for more [4+2] crosslinks has produced data consistent with a lower CTE value than expected.

One way to test this hypothesis is to reduce the backbone of one of the **5.8** series polymers. This was accomplished through a diimide reduction method as discussed in the synthesis section of this chapter. The resulting saturated polymer was formulated, coated and cured in parallel with its "parent" polymer and the z-axis CTEs of the two were compared (Figure 5.5).

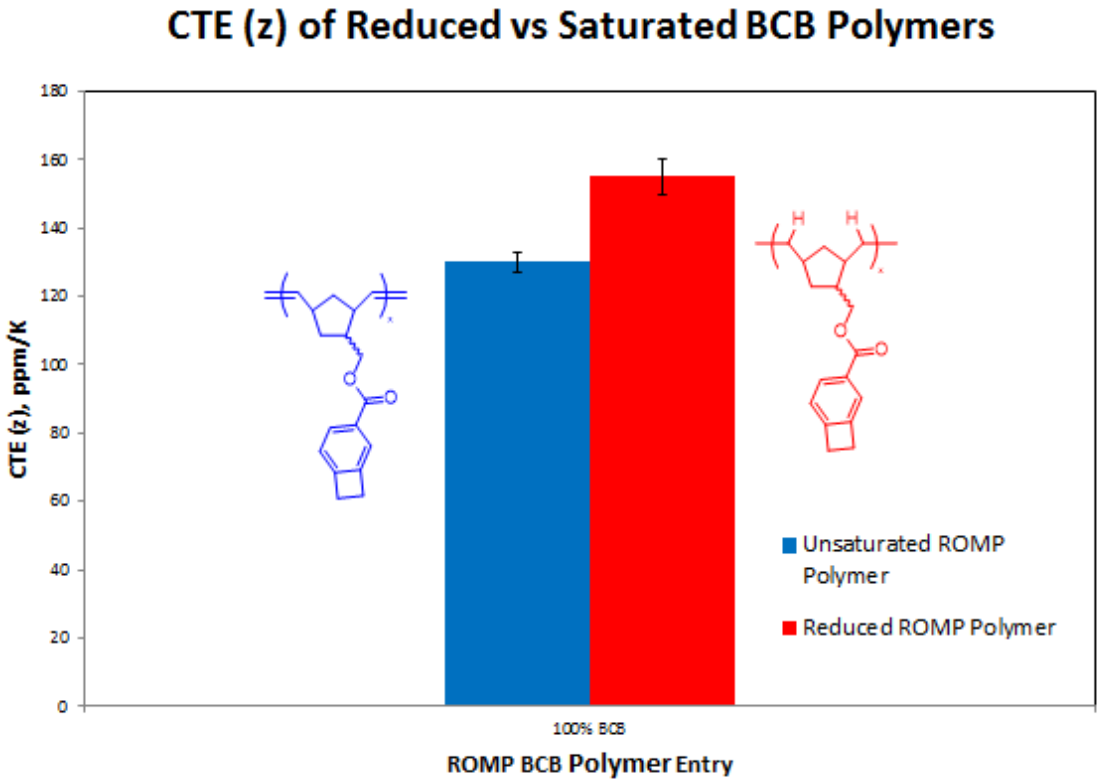

Figure 5.5: Heated stage ellipsometry Z-axis CTE data of both reduced and unsaturated ROMP BCB polymers. Eliminating the double bonds excluded the [4+2] crosslink with the polymer backbone. The result is an increase (about 19% in z-axis CTE).

The results clearly demonstrate the importance of the unsaturated ROMP backbone. In the absence of any double bonds, the [4+2] crosslink (Figure 3.1) is excluded, leaving only other BCB-BCB crosslinks ([4+2] spirocycle, cyclohexene and [4+4] products). A 19% increase in z-axis CTE suggests that the BCB-backbone crosslink is important for minimizing the CTE in these resins. Further evidence for the importance of the unsaturated backbone will be described in Chapter 6 where addition polymerizations of norbornene and their associated materials are discussed.

Dielectric constants were obtained through spectroscopic ellipsometry as the square of the refractive indices of the polymers (the definition of a dielectric constant through Maxwell's Equations). The dielectric constant is often highly dependent on frequency. It was found that many common dielectric materials (ROMP and addition polynorbornene, Cyclotene, polystyrene) where found to have identical dielectric constants in the optical regime (3*10^6 GHz) as in the relevant 1 GHz regime experimentally. It is therefore a relatively safe assumption that optical dielectric data (shown in Table 5.1), are a good estimate of lower frequency data in this case. Dielectric constants for polymer series **5.8** ranged from 2.38 to 2.44, well below the target 3.0 for microelectronics application.

Table 1	M_n (Daltons)	n	n^2	E_r (Gpa)	α(xy) ppm/K
20% BCB	43000	1.55	2.41	0.62	N/A
40% BCB	66700	1.55	2.40	3.10	N/A
60% BCB	97500	1.56	2.43	3.32	N/A
80% BCB	107500	1.56	2.44	3.71	**15.0**
100% BCB	161000	1.55	2.38	3.84	N/A

Table 5.1: Summary material properties of polymer series **5.8**.

While material series **5.8** possessed excellent properties, a second generation material based on dinorbornenes was developed to explore a further decrease in CTE, dielectric constant, and an increase in polymer T_g. As discussed in the synthesis portion of Chapter 5, intermediate ROMP compositions of dinorbornenes and norbornenes can lead to controllable glass transition temperatures, so a dinorbornene dielectric polymer is an ideal candidate for deposition by dry lamination. The copolymers of MTD **5.12** and BCB dinorbornene **5.11** were synthesized to obtain copolymer series **5.13a-e**, and z-axis CTE was obtained through heated stage ellipsometry, as shown in Figure 5.6.

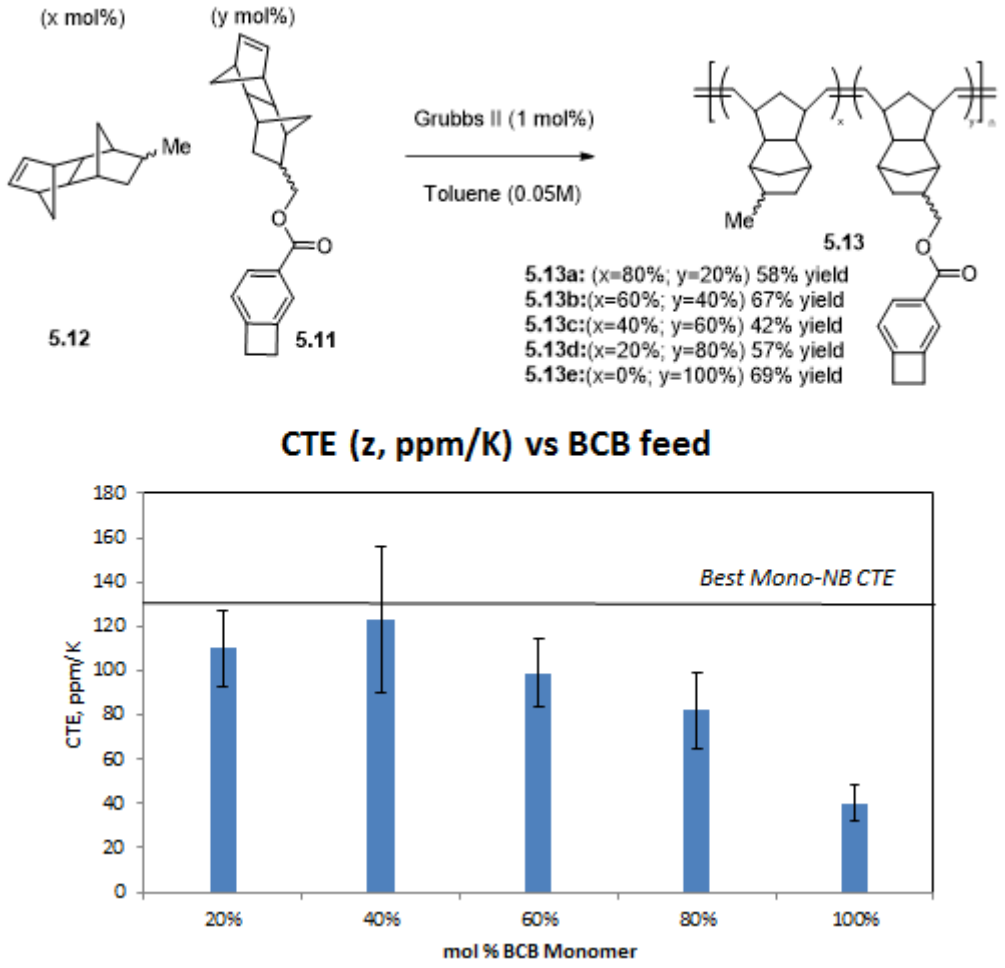

Figure 5.6: Heated stage ellipsometry results showing z-axis CTE of polymer series **5.13**.

The results demonstrate a statistically significant improvement in z-axis CTE over the first generation polynorbornene in four out of five cases. The decrease in CTE is likely due to the rigid nature of monomer unit. Free volume, or functional groups with high degrees of confirmation freedom, is typically associated with a high CTE. Thus, the fused bicyclic monomer is an excellent choice for a low CTE organic material. A particularly promising result is that the CTE of the homopolymer was 40 ± 8 ppm/K, about a factor of three improvement from the corresponding homopolymer **5.8e**.

There is a sharp decrease in CTE (factor of two) between 80% BCB and 100% BCB homopolymer. Further, as shown in Table 5.2, the polymer molecular weight has increased dramatically from approximately 20kDa to 1,170 kDa by GPC (compared to a polystyrene standard). Further, the PDI of the 80% BCB polymer **5.13d** was measured to be 2.6 (similar PDIs were observed for polymers **5.13a-c** as well), while the PDI of the homopolymer **5.13e** was found to be 1.2, using the same catalyst and reaction conditions. These data suggest that the polymerization kinetics of the dinorbornene BCB monomer **5.11** are significantly and surprisingly different from the saturated MTD **5.12**. Namely, the results suggest that in a copolymerization, incorporation of MTD **5.12** creates backbiting and chain transfer side reactions, while BCB monomer **5.11** polymerizes with closer to living-like kinetics. This begs the question: Does a higher PDI increase CTE in these polymers? What exactly is the source and mechanism of this large decrease in CTE? For perspective, out of plane CTEs are typically several factors higher than their in plane counterparts, and a z-axis CTE of 40 ppm/K is remarkably low for an organic material.

Table 2	M_n (Daltons)	n	n^2	α(z) ppm/K
20% BCB	9530	1.53	2.33	110 ± 17
40% BCB	16100	1.53	2.34	123 ± 33
60% BCB	21070	1.50	2.24	99 ± 15
80% BCB	19900	1.47	2.16	82 ± 17
100% BCB	1170000	1.57	2.45	40 ± 8

Table 5.2: Summary of Dinorbornene polymer properties **5.13a-e**.

In order to further probe the source of this attractive decrease in CTE, new syntheses were carried out using the Grubbs 3rd generation catalyst. The pyridine substituted ruthenium compound was synthesized in an equilibrium ligand exchange

reaction from Grubbs 2nd generation catalyst, and this compound has been observed to have much faster initiation and propagation rates in ROMP. The source of this fast initiation is believed to be due to the equilibrium ligand association between the pyridines and the ruthenium metal center. In the case of the Grubbs 2nd generation catalyst, the tricyclohexyl phosphine ligand is in equilibrium between association with the metal (inactive to ROMP) and disassociation from the metal (the active ROMP species). This equilibrium favors the inactive metal center. However, in the case of the Grubbs 3rd generation catalyst, this equilibrium is between the two pyridine species, and the active metal (free of pyridine ligands) is more strongly favored, leading to a faster initiation time, which favors living polymerization kinetics. Thus, switching to the Grubbs 3rd generation catalyst can often produce narrow PDIs and living ROMP kinetics which avoid backbiting or chain transfer.

As an investigation into this effect, polymer **5.13a** was synthesized again, this time using Grubbs 3rd generation catalyst instead of the 2nd generation. The GPC chromatograph in Figure 5.7 compares the results.

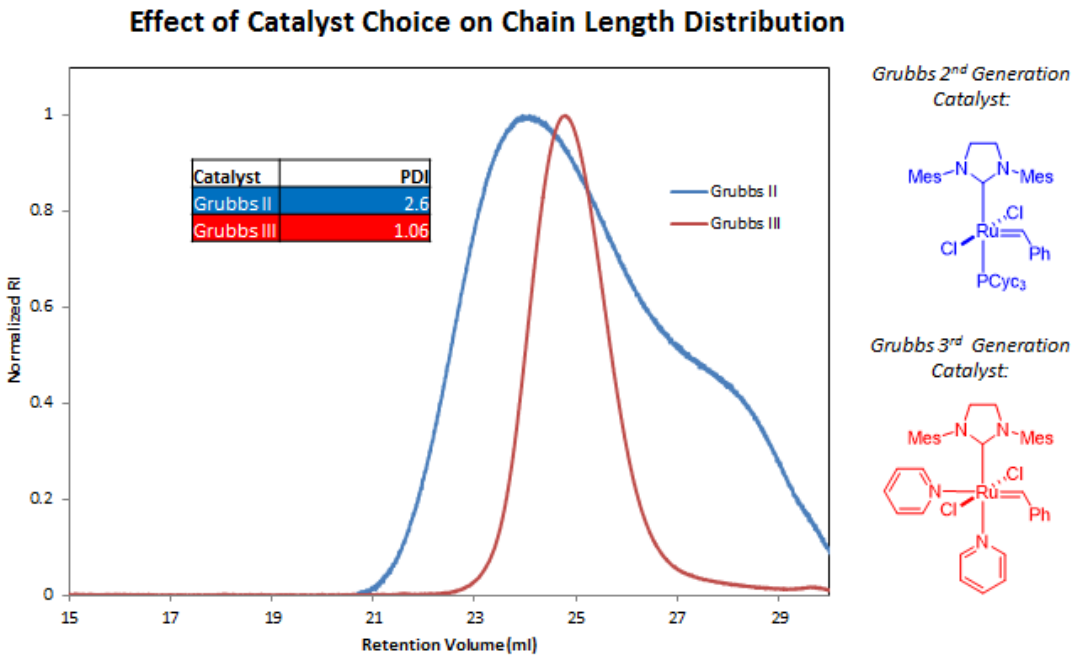

Figure 5.7: GPC chromatographs of polymer **5.13a** synthesized with two different catalysts. The refractive index response reflects the relative distribution of molecular weights. Grubbs 3rd generation catalyst, with much faster initiation and propagation rates, produces a narrow MW distribution characteristic of living kinetics.

The results of the chromatographs are as expected. Using the Grubbs 3rd generation (G3) catalyst, a PDI of 1.06 was obtained, suggestive of living kinetics. The chromatograph of **5.13a** synthesized with Grubbs 2nd generation catalyst shows a much broader molecular weight distribution with a PDI of 2.6. In addition, a shoulder peak at a retention volume of about 28 ml can be observed. It is proposed that this shoulder corresponds to lower molecular weight polymer that has been cleaved as a result of backbiting or chain transfer.

The G3 polymer was isolated, formulated in toluene, spin coated and cured on silicon. The resulting film was subjected to heated stage ellipsometry to obtain the out of plane CTE. The results are shown in Figure 5.8.

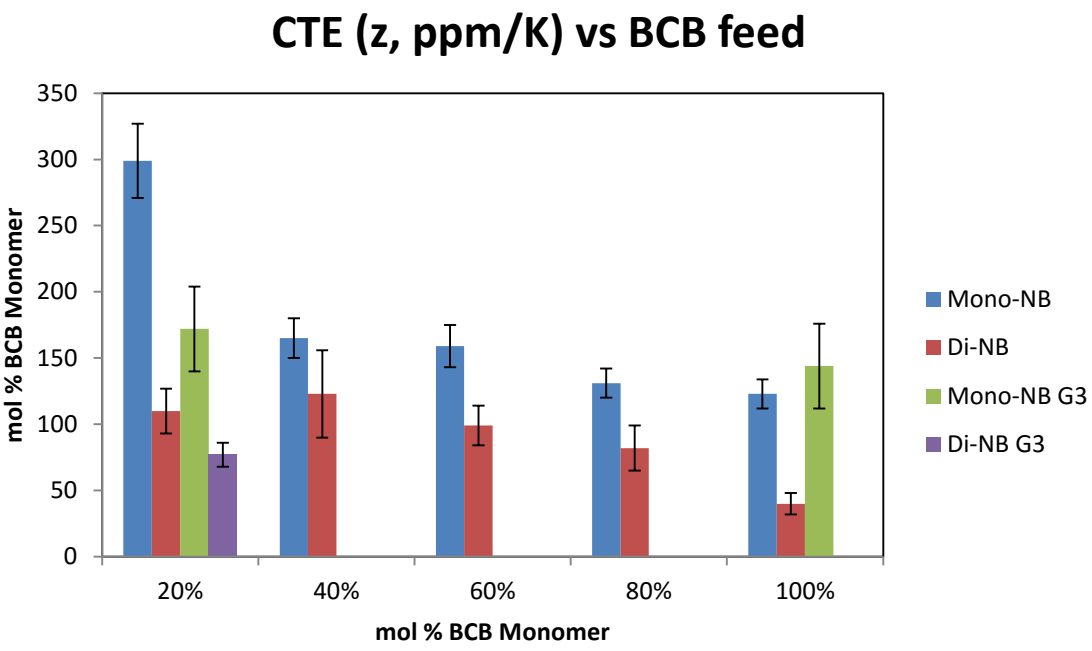

Figure 5.8: Total summary of CTE values including available G3 polymers.

Interestingly: the same polymer, with same BCB composition had a statistically significant lower CTE. The same result (decreased CTE) was observed when the norbornene copolymer **5.8a** was synthesized with Grubbs 3rd generation catalyst. In order to explain these results, it is tempting to rely on the PDI as an indicator, but if this is true, the BCB homopolymers should also have lower CTE. The homopolymer of **5.8e** was remade using G3 (achieving low PDI of 1.1), and the CTE was found not to be statistically different from the corresponding G2 homopolymer. Other G3 copolymers were synthesized, but were not successfully coated onto silicon with sufficient uniformity to obtain good data. Thus, data is unfortunately restricted to entries shown in Figure 5.8.

It is proposed that the two catalysts, G2 and G3, have different reactivity ratios for each monomer. It the case of G2, it is proposed that norbornene **5.7** reacts much faster than BCB norbornene **5.6**, leading to a gradient copolymer. Backbiting would lead to

low molecular weight polymers containing mostly norbornene, which may lead to chains not incorporated in the cured, crosslinked matrix. This in turn results in a significant increase in free volume, and therefore an increase in CTE. It is proposed that the reactivity ratio is less disparate in the case G3, leading to a less gradient like (and therefore more random) copolymer. Also, the absence of backbiting means more chains will be more thoroughly crosslinked in the matrix, leading to less free volume. This more random, linear copolymer is proposed to be the source of lower CTE.

5.4 Results and Discussion: Lithography

While polymer series **5.8** and **5.13** both boast impressive coefficients of thermal expansion and low dielectric constants, next generation packaging materials demand a material that is inherently photopatternable. The strategy that has been developed in this chapter is to use the same bis-azide photopatterning mechanism[84] discussed in Chapter 3. This involves formulating with a low weight percent (5% in this case) with the i-line active molecule BACM (2,6-(bis-4-azidobenzylidene)-4-methylcyclohexan-1-one). Exposure to light forms the triplet nitrene, which can undergo insertion into an alkene to form an aziridine crosslink, forming a three-dimensional network that is insoluble. A patent has been written on the subject of this type of lithography with ordinary ROMP norbornene[85], but since these new resins also contain benzyl carbon-hydrogen bonds which can undergo insertion for an additional crosslink, a full lithographic investigation of these materials is warranted to gauge their potential for packaging applications.

The 20% BCB polymers **5.8a** and **5.13a** were evaluated. Polymers were formulated with bis-azide BACM (5 wt% relative to polymer). The formulation of **5.8a** was then dissolved in toluene (10 wt% total solids) and spun over a four inch silicon wafer and baked at 100˚C for 1 minute to form films about one half micron thick as

measured by spectroscopic ellipsometry. The formulation of **5.13a** was soluble in toluene, but it was found that better (more uniform) coating could be obtained when casting from mesitylene. Thus, a formulation of **5.13a** was dissolved in mesitylene (10 wt% total solids) and spin coated on a four inch silicon wafer. Films were exposed at i-line via contact lithography through a gradient photomask with variable transmission in different regions to obtain different doses on a single wafer. Both films were then developed in toluene for 10 seconds to obtain images.

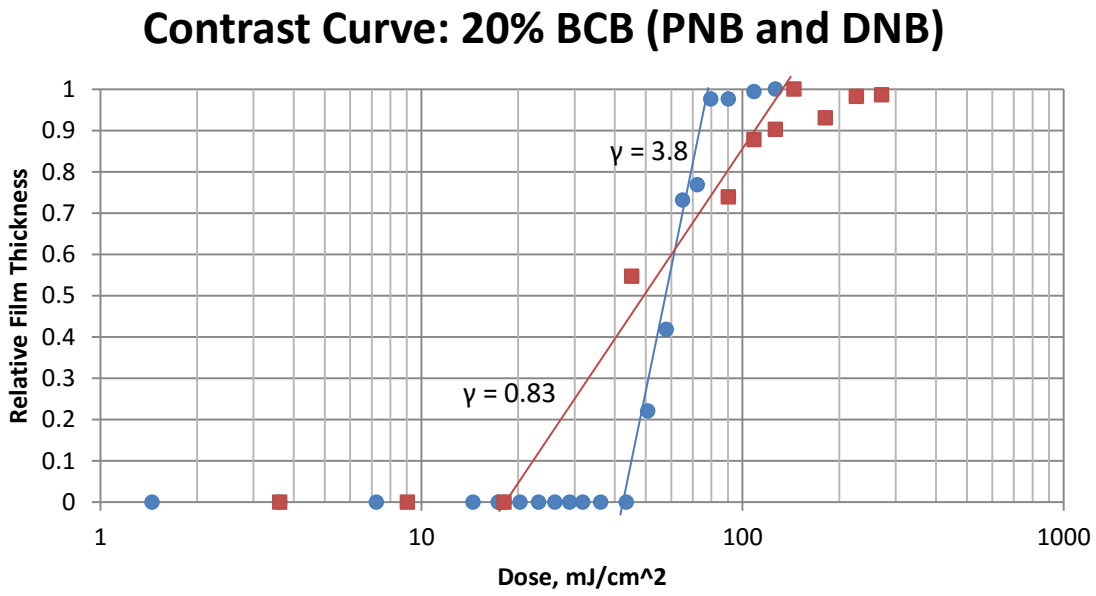

Figure 5.9: Contrast curves for the negative tone style resists of **5.8a** (blue circles) and **5.13a** (red squares) with the bis-azide BACM. The DNB copolymer his significantly lower contrast, likely due to the decrease in concentration of alkenes per unit volume of material.

Figure 5.9 shows the resulting contrast curves. The lithographic contrast (γ), is defined by several terms, and is described in equation 5.1.

$$\gamma = 1/(\log D^0 - \log D^i) \tag{5.1}$$

In this equation, D^0 is the dose (or total energy from light) required to maintain 100% of normalized film thickness after development, and D^i (also known as the interface gel dose), is the dose required to render a minimum amount of polymer insoluble. Taking the difference of the one over the logs of these values produces a value known as the contrast (γ), where higher values are considered to describe "better" resists, capable of resolving smaller features with better aspect ratios.

The results for polymer **5.8a** are particularly promising, with a contrast value of 3.8, which is fairly high for this style of negative tone, network forming resist. However, the dinorbornene based polymer **5.13a** has a significantly lower contrast under identical conditions. These results may be due to the fact that one of the functional groups involved in crosslinking (the alkene), is significantly lower in concentration per unit volume of resist in the case of **5.13a**, due to the highly saturated structure of the dinorbornene. Examination of optical micrographs (Figure 5.10) of line and space patterns reveal that this polymer **5.8a** resist is capable of resolving 2.5 micron half pitch features, a factor of two below the required 5 micron half pitch needed for next generation packaging materials.

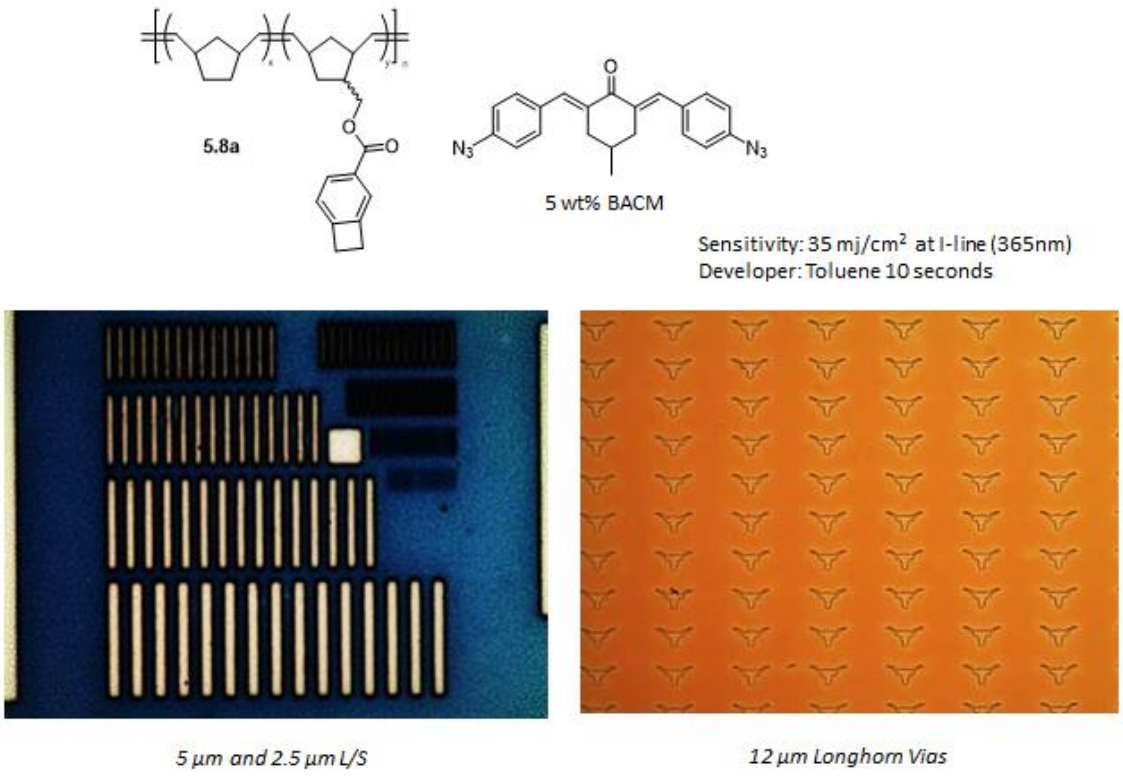

Figure 5.10: Optical micrographs of polymer **5.8a** with bis-azide crosslink and toluene developer. 2.5 µm half pitch resolved (left, top left features) and polymer **5.13a** resolving 12 µm longhorn vias (right, narrowest distance resolved).

These results recorded here surpass the resolution requirement for future packaging, and it should be noted that these results were obtained with little optimization, and were performed with a relatively crude (by today's standards) contact lithography setup open to air (oxidation of the nitrene to the corresponding nitro group is a major side reaction when this chemistry is exposed to oxygen). Under thoroughly controlled conditions, it is proposed that even better resolution and higher aspect ratios might be achieved, suggesting both polymer systems **5.8** and **5.13** have great promise to serve not just as an insulating, low CTE material, but also as a permanent resist, allowing copper circuits to be efficiently and cheaply defined with photolithography.

5.5 CONCLUSION

In order to surpass the current limits of organic low dielectric, low CTE materials, a ROMP polynorbornene and benzocyclobutene system has been designed, synthesized, and evaluated. Chapter 3, reports that POSS based BCB resins demonstrated excellent properties, but suffered from low molecular weight, which required a B-stage in order to produce stable films. In order to solve this problem, a polymer backbone, based on ROMP norbornenes, was chosen. The alkenes in the polymer backbone serve a dual purpose in these resins: they are both a latent aziridine for bis-azide photolithography, and a potential Diels Alder dienophile for BCB thermosetting.

Both polynorbornene-BCB copolymers **5.8** and dinorbornene-BCB copolymers **5.13** have been studied. In both cases, z-axis coefficients of thermal expansion decreased with increasing BCB content in the polymer. The in-plane CTE of polymer **5.8d** was found to be 15.0 ± 0.3 ppm/K, well below the target value of 30 ppm/K. It is presumed that since none of these polymers were observed to have birefringence via spectroscopic ellipsometry, these are more or less isotropic: thus it is very likely that most entries have an in-plane CTE that is very close to polymer **5.8d**. Dielectric constants ranged on the order of 2.2 to 2.4, T_g was controllable based on monomer feed ratio, and photopatternability was demonstrated down to 2.5 μm half pitch lines and spaces: all these values meet or exceed goals for next generation packaging materials.

5.6 EXPERIMENTAL SECTION

Bicyclo[4.2.0]octa-1,3,5-triene-3-carboxylic acid

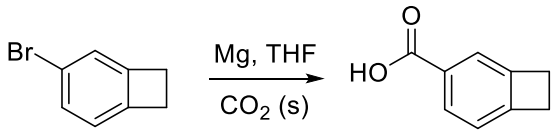

4-Bromobenzocyclobutene (10g, 1 eq), Mg shavings (1.59g, 1.2 eq), and I_2 (139mg, 0.01 eq) were added to a 1 L rbf equipped with a stirbar and the flask flame dried under vacuum. Anhydrous THF (300mL) was then added and the solution cooled to 0˚C. CO_2 in large excess was bubbled into this solution under positive nitrogen pressure for 1 hour, after which the reaction was heated to 45 ˚C. After stirring at 45 ˚C for 3 hours, the reaction was quenched with sequential portions of DI water (25 mL) and 0.5 N aqueous HCl (10 mL) and extracted with ether. The resulting organic fractions were combined, washed with DI water and brine, and dried with $MgSO_4$. Residual magnesium metal and sulfate were filtered off and the filtrate concentrated in vacuo to give 7.4g of crude material. This was purified via column chromatography using 1:1 hexanes and ethyl acetate to yield the product as a white crystalline solid (5.82g, 72% yield). ^{1}H NMR (400 MHz, DMSO) δ 7.81 (d, *J* = 7.7 Hz, 1H), 7.59 (s, 1H), 7.09 (d, *J* = 7.7 Hz, 1H), 3.12 (s, 4H). ^{13}C NMR (101 MHz, DMSO) δ 168.2, 151.2, 145.7, 129.9, 128.9, 123.7, 122.6, 29.8, 29.3. HRMS: C9H8O2 (M)+ calculated: 148.052, found: 148.051.

(Bicyclo[2.2.1]hept-5-en-2-yl)methanol

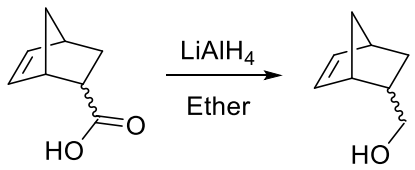

Lithium aluminum hydride (400mg, 1.2 eq) was dissolved in ether (20mL) and cooled to 0 degrees Celsius in a 100mL rbf equipped with a magnetic stirbar. To this stirring mixture was added 5-norbornene-2-carboxylic acid (1.212g, 1 eq) portionwise. The reaction was stirred for 1.5 hours, then quenched with sequential portions of DI water (0.5mL), 1 M aq. NaOH (0.5mL), and DI dwater (1.5 mL). The resulting mixture was dried with sodium sulfate, filtered, and concentrated in vacuo to yield a colorless solid in 99% yield (356 mg). **Endo:** ^{1}H NMR (400 MHz, $CDCl_3$) δ 6.14 (dd, J = 5.7, 3.0 Hz, 1H), 5.96 (dd, J = 5.7, 2.9 Hz, 1H), 3.39 (dd, J = 10.5, 6.5 Hz, 1H), 3.25 (dd, J = 10.5, 8.9 Hz, 1H), 2.93 (s, 1H), 2.81 (s, 1H), 2.36 – 2.21 (m, 1H), 1.81 (ddd, J = 11.6, 9.2, 3.8 Hz, 1H), 1.40 (s, 1H), 0.52 (ddd, J = 11.6, 4.4, 2.6 Hz, 1H). ^{13}C NMR (101 MHz, $CDCl_3$) δ 137.2, 132.2, 66.1, 49.4, 43.5, 42.1, 41.5, 28.7. **Exo:** ^{1}H NMR (400 MHz, $CDCl_3$) δ 6.11 (dd, J = 5.7, 3.0 Hz, 1H), 6.07 (dd, J = 5.7, 2.8 Hz, 1H), 3.70 (dd, J = 10.6, 6.5 Hz, 1H), 3.54 (dd, J = 10.5, 8.8 Hz, 1H), 2.81 (s, 6H), 2.75 (s, 1H), 1.68 – 1.55 (m, 2H), 1.35 – 1.23 (m, 2H), 1.14 – 1.08 (m, 1H). ^{13}C NMR (101 MHz, $CDCl_3$) δ 136.6, 136.4, 67.0, 44.8, 43.2, 41.6, 41.4, 29.5. HRMS: C8H12O (M)+ calculated: 124.089, found: 124.088.

(Bicyclo[2.2.1]hept-5-en-2-yl)methyl bicyclo[4.2.0]octa-1,3,5-triene-3-carboxylate

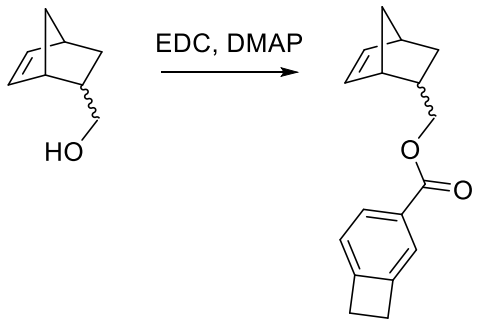

4-Carboxyl Benzocyclobutene (1.9g, 1 eq.), 5-norbornene-2-methanol (1.59g, 1 eq.), 1-ethyl-3-(3-dimethylaminopropyl)carbodiimide hydrochloride (4.9g, 2 eq.), and 80 mL of Dichloromethane were added to a 250ml round bottom flask equipped with a stirbar. When all reagents had dissolved, 4-Dimethylaminopyridine (468mg, 0.3 eq.) was added to the solution in a single portion and the reaction stirred overnight at room temperature. Completion was determined via TLC at 20 hours, at which point the reaction was diluted

with 50 mL of DCM and washed with three sequential portions of DI water. Aqueous waste was back extracted with DCM, and the organic fractions combined, dried with $MgSO_4$, and concentrated in vacuo. The resulting crude material was then purified via column chromatography with 9:1 hexanes and ethyl acetate to yield the product in 99% yield (3.22g). **Endo:** ^{1}H NMR (400 MHz, $CDCl_3$) δ 7.95 (ddd, J = 7.7, 3.9, 1.3 Hz, 1H), 7.72 (s, 1H), 7.09 (d, J = 7.7 Hz, 1H), 6.17 (dd, J = 5.7, 3.0 Hz, 1H), 5.98 (dd, J = 5.7, 2.9 Hz, 1H), 4.09 (dd, J = 10.8, 6.6 Hz, 1H), 3.85 (dd, J = 10.8, 9.6 Hz, 1H), 3.18 (s, 4H), 2.96 (s, 1H), 2.82 (m, 1H), 2.60 – 2.45 (m, 1H), 1.95 – 1.80 (m, 1H), 1.50 – 1.43 (m, 1H), 1.32 – 1.22 (m, 1H), 0.63 (ddd, J = 11.7, 4.4, 2.6 Hz, 1H). ^{13}C NMR (101 MHz, $CDCl_3$) δ 167.1, 151.5, 145.7, 137.6, 132.2, 129.2, 128.8, 123.6, 122.3, 68.1, 49.4, 44.0, 42.2, 37.9, 29.9, 29.3, 28.9. **Exo:** ^{1}H NMR (400 MHz, $CDCl_3$) δ 7.95 (ddd, J = 7.7, 3.9, 1.3 Hz, 1H), 7.72 (s, 1H), 7.09 (d, J = 7.7 Hz, 1H), 6.11 (dd, J = 5.5, 3.0 Hz, 1H), 6.08 (dd, J = 5.5, 2.9 Hz, 1H), 4.37 (dd, J = 10.9, 6.4 Hz, 1H), 4.17 (dd, J = 10.9, 9.2 Hz, 1H), 3.18 (s, 4H), 2.82 (m, 2H), 1.95 – 1.80 (m, 2H), 1.38 (s, 1H), 1.32 – 1.22 (m, 2H). ^{13}C NMR (101 MHz, $CDCl_3$) δ 167.2, 151.5, 145.7, 136.9, 136.2, 129.2, 128.8, 123.6, 122.3, 68.8, 45.0, 43.7, 41.6, 38.1, 29.6, 29.3, 28.9. HRMS: C17H18O2Na (M+Na)+ calculated: 277.120, found: 277.119

(1,2,3,4,4a,5,8,8a-octahydro-1,4:5,8-dimethanonaphthalen-2-yl)methanol

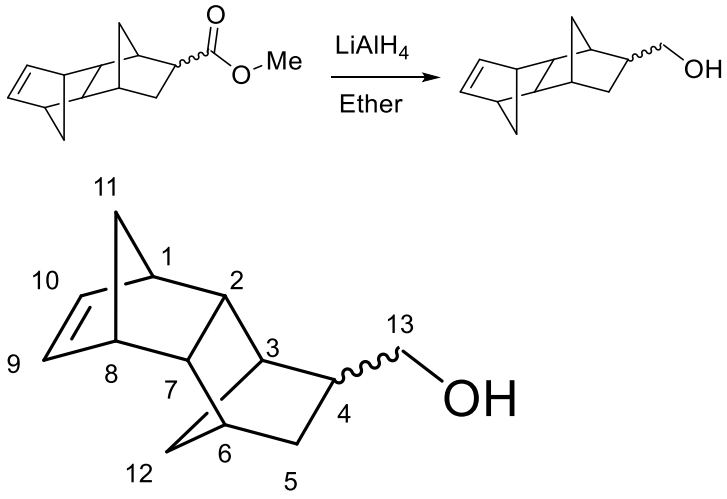

Lithium aluminum hydride (4.07g, 1.2 eq) and ether (100 mL) were added to a 500 mL round bottom flask equipped with a magnetic stir bar and condensing column, and the solution cooled to 0 ˚C. A solution of tetracyclododec-9-en-4-carboxylic acid (17.76g, 1 eq) in ether (150 mL) was then added drop wise over a 60 minute period. The reaction was then allowed to stir at room temperature for one hour, at which point TLC was used to determine completion. Three sequential portions of DI water (4mL), 2.5M NaOH (4 mL), and DI water (16 mL) were then used to quench the reaction. The resulting mixture was extracted with two portions of DI water, and the organic fraction dried with sodium sulfate, filtered, and concentrated in vacuo to yield the product (14.31g, 85% yield, in a 45:55 ratio of isomers in favor of exo). ^{1}H NMR (400 MHz, $CDCl_3$) δ 5.99 – 5.81 (m, 2H-(C9-10)), 3.63 – 3.42 (m, 1H-C(13) endo), 3.35 – 3.16 (m, 1H-C(13) exo), 2.77 (br s, 2H-C(1,8)), 2.58 (s, 1H-C(3)), 2.24 – 1.74 (m, 4H(C2,4,6,7)), 1.62 – 1.54 (m, minor, 1H-($C12_{anti}$), 1.50 – 1.38 (m, major, 1H-(C5) H_b), 1.27 – 1.20 (m, 1H-C(5) H_a), 1.18 – 1.06 (m, 2H-C(11)), 0.83 – 0.76 (m, 2H-C(11)), 0.57 (d, J = 10.2 Hz, 1H-C(12_{syn}) endo), 0.52 (d, J = 10.7 Hz, 1H-C(12_{syn}) exo). ^{13}C NMR (101 MHz, $CDCl_3$) δ (136.2, 135.6, 135.5, 135.2(C9, 10 endo and exo)), (65.6, 63.3 C(13 endo and exo)), (53.0 C(11)), (49.3 C(4 exo)), (48.8, 48.1 C(2,7)), (47.5, 46.9, 46.6, 46.5 C(1,8 endo and exo)), (46.5 C(2)), (44.5

C(7)), (41.1 C(4 exo)), (39.6, 39.0 C(3)), (38.4, 37.7 C(6)), (36.0, 35.8 C(5)), 35.4 C(12,endo), 30.6 C(12,exo). HRMS: C13H18O (M)+ calculated: 190.136, found: 190.135.

(1,2,3,4,4a,5,8,8a-octahydro-1,4:5,8-dimethanonaphthalen-2-yl)methyl bicyclo[4.2.0]octa-1,3,5-triene-3-carboxylate

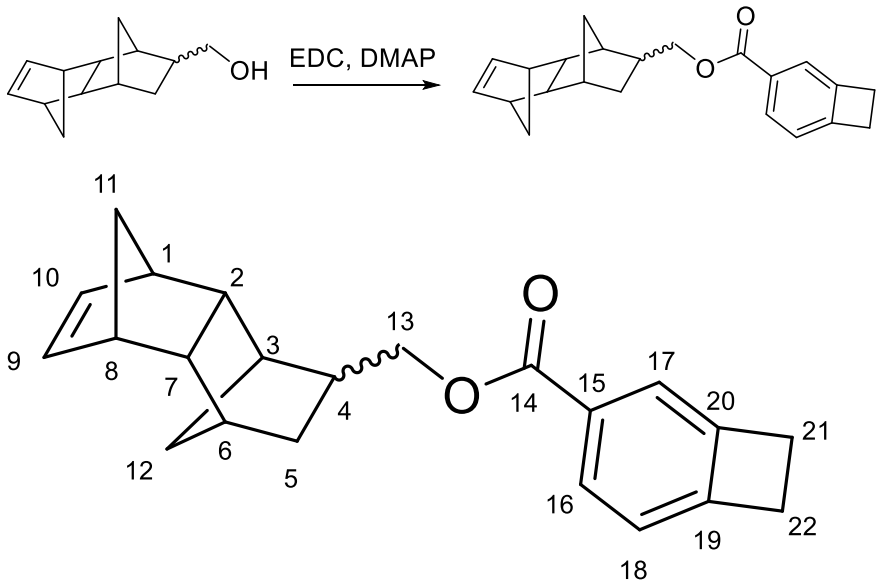

Tetracyclododec-9-en-4-ylmethanol (1.10g, 1.1eq) and 4-Carboxyl Benzocyclobutene (0.94g, 1eq) were dissolved in dichloromethane (80mL) in a 250 mL round bottom flask equipped with a magnetic stirbar. To this stirring solution was added 1-Ethyl-3-(3-dimethylaminopropyl)carbodiimide (1.54g, 1.5eq) and 4-Dimethylaminopyridine (196mg, 0.03eq) sequentially. The reaction was ran overnight at 25˚C and then washed three times with DI water. The organic fraction was then dried over sodium sulfate and concentrated in vacuo. The crude material was purified via column chromatography using hexanes as an eluent to give the product (1.16g, 68% yield). Isolated as a 2:1 mixture of products. The exo product was assigned to be the major product based on the previous work of Rager and Willson where the two diastereomers of methyl ester DNB **5.**9 are isolated and fully characterized.. ^{1}H NMR (500 MHz, $CDCl_3$) δ 7.94 (ddd, J = 7.7, 2.9,

1.3 Hz, 1H-C(16)), 7.72 (s, 1H-C(17)), 7.09 (d, J = 7.7 Hz, 1H-C(18)), 6.03 – 5.89 (m, 2H-C(9,10)), 4.31 (dd, J = 11.1, 7.0 Hz, 1H-C(13), exo), 4.29 – 4.23 (m, 1H-C(13), exo), 4.02 (d, J = 7.8 Hz, 2H-C(13), endo), 3.19 (s, 4H-C(21,22)), 2.93 – 2.76 (m, 2H-C(1,8)), 2.31 – 1.95 (m, 5H-C(3,4,6,2 endo,7, 12_{anti}), 1.92 (dd, J = 8.3, 4.1 Hz, 1H-(C2, exo), 1.82 – 1.67 (m, 1H-C(5b) exo and endo), 1.34 – 1.23 (m, 2H-C(5a) exo and endo), 1.17 (d, J = 7.8 Hz, 1H-C(11) exo+endo), 1.02 (t, J = 4.5 Hz, 1H-C(11) exo), 1.00 (t, J = 4.5 Hz, 1H-C(11), endo), 0.70 (d, J = 10.3 Hz, 1H-C(12_{syn}) endo), 0.67 (d, J = 10.1 Hz, 1H-C(12_{syn}) exo). ^{13}C NMR (126 MHz, $CDCl_3$) δ 167.1 (C(14)), 151.3, 145.6 (C(19, 20)), (136.1, 135.5, 135.4, 135.1 C(9,10) exo and endo), 129.1 (C(15)), 128.7 (C(16)), 123.5 (18), 122.2 (C(17)), 67.2 (C(13) endo), 65.4 (C(13) exo), (52.9 C(11)), (49.1 (C4 exo)), (48.7, 47.9 (C2 C7)), (46.9, 46.6, 46.5, 46.4 (C1-C8 endo and exo)), (43.6 C(2)), (41.2 (C(7)), (40.8 (C4 endo), (40.0, 39.7 (C(3 endo and exo)), (38.5, 37.7 (C6 endo and exo)), (36.1, 35.8 (C5 endo and exo)), (35.3 (C12 endo)), (30.6 (C12exo)), (29.7, 29.2 C(21-22)). HRMS: C22H24O2 (M+) calculated 320.178, found 320.179.

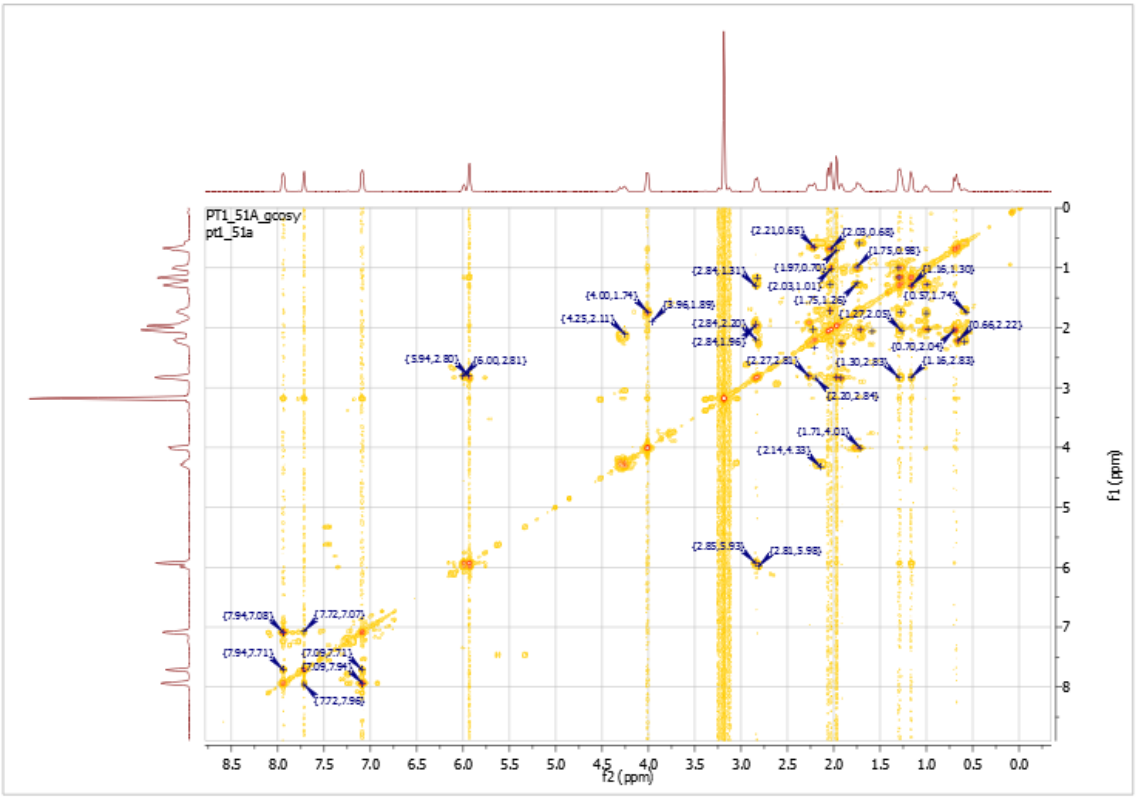

COSY NMR Spectrum of DNB BCB

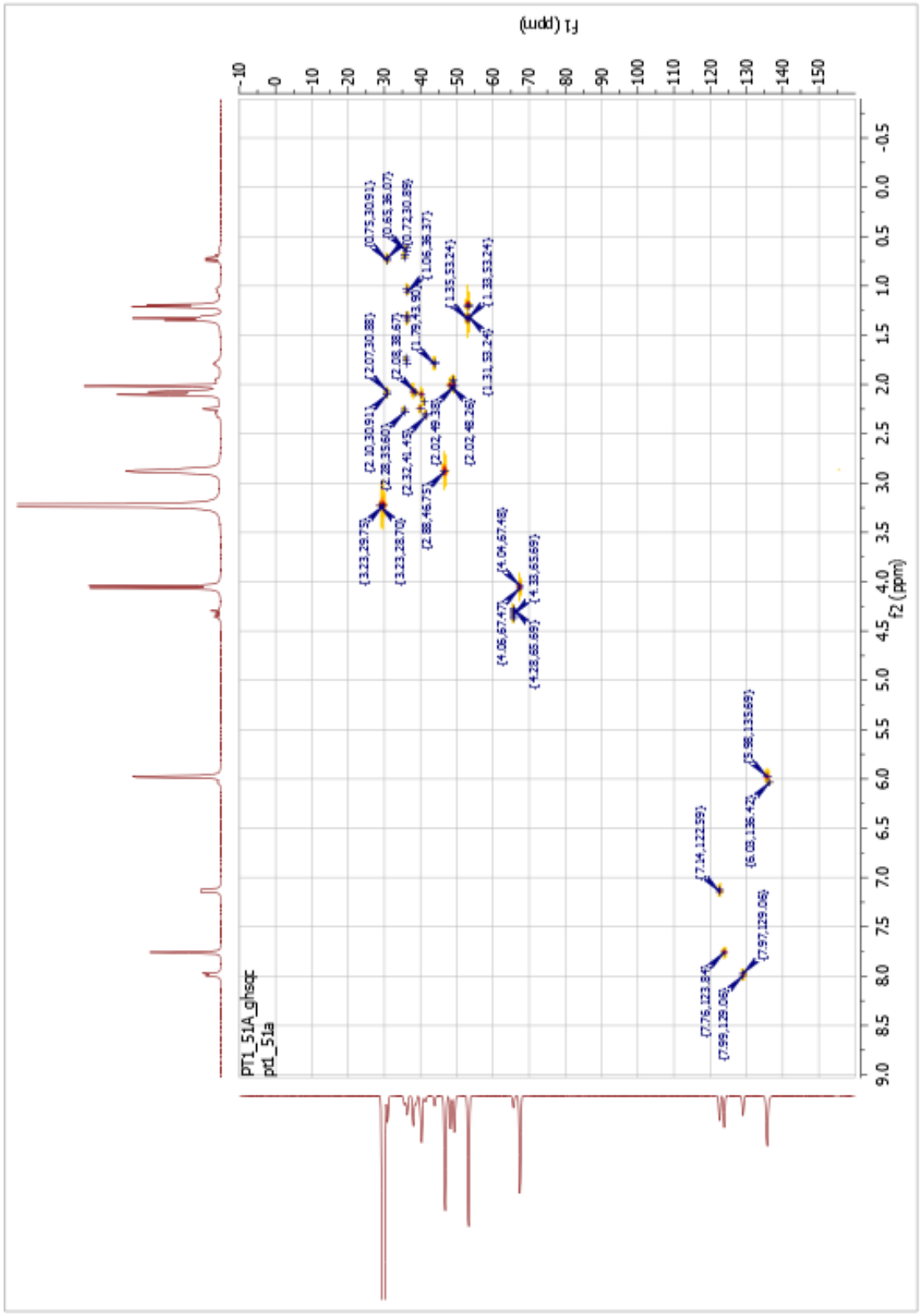
PT1_51A_ghsqc
pt1_51a
f1 (ppm)
f2 (ppm)

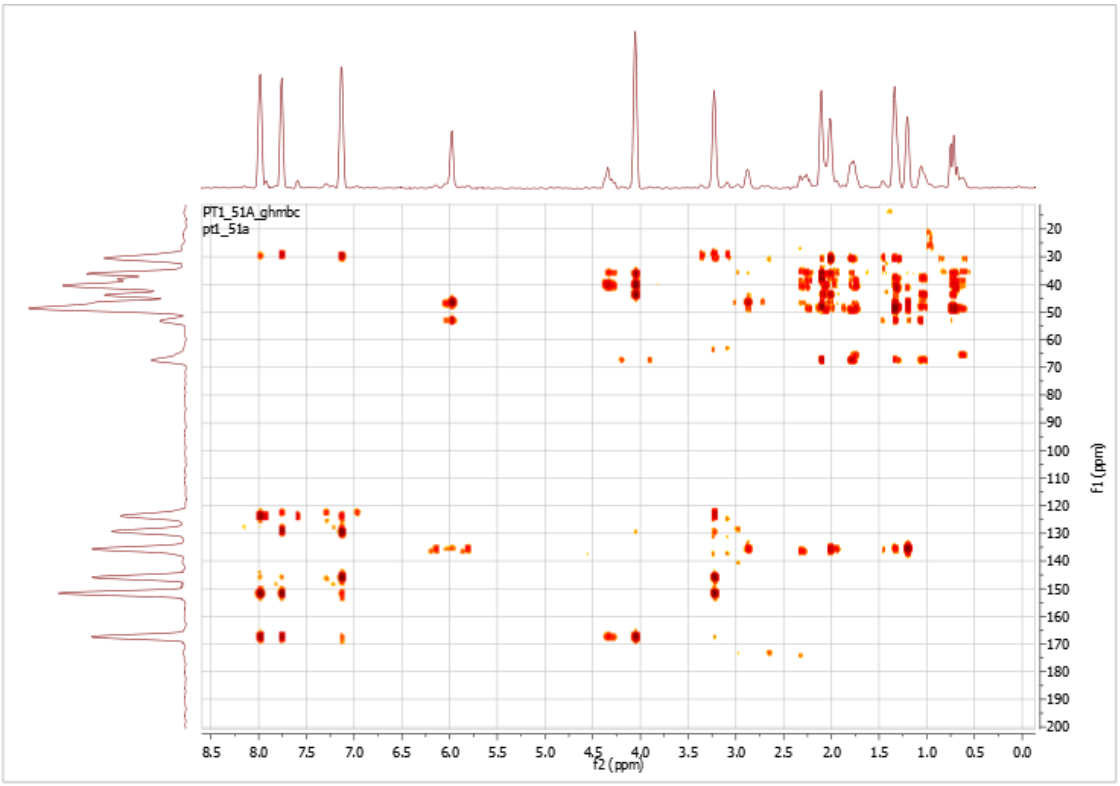

HSQC (top) and HMBC (below) of DNB BCB

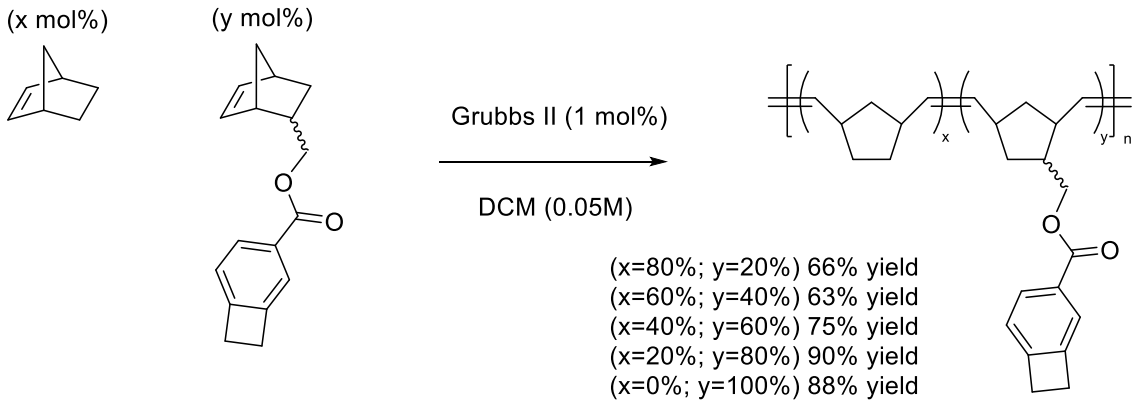

Norbornene BCB copolymers were all synthesized with one standard procedure. As an example, the procedure for copolymer **20** is described. BCB NB monomer **9** (525 mg, 2.06 mmol, 100 eq), was added to a 100 ml round bottom flask equipped with a magnetic stir bar. DCM (41 ml, 0.05 M) was added and the monomer was dissolved. DCM was

used as received without distillation or any additional purification. Open to air, Grubbs Second Generation catalyst (17.5 mg, 0.02 mmol, 1 eq) was added, and the light red reaction mixture was capped with a nitrogen balloon and allowed to stir for one hour at room temperature. After one hour, 1 ml of ethyl vinyl ether was added to terminate the polymerization. After five additional minutes, the reaction was concentrated slightly *in vacuo* until viscosity of the solution had increased noticeably (about 20 ml of 40 ml removed). The reaction mixture was then poured dropwise into vortexing methanol (350 ml). The precipitated polymer was then isolated via vacuum filtration and washed with methanol (2 x 50 ml). The stringy solid was collected in a scintillation vial and dried under high vacuum overnight to remove residual methanol. The polymer was then isolated in 85% yield (445 mg). The following NMR, GPC, DSC and TGA characterization of copolymers in the series is available. The data suggest that the polymerization was run to roughly 100% conversion, as feed matched composition.

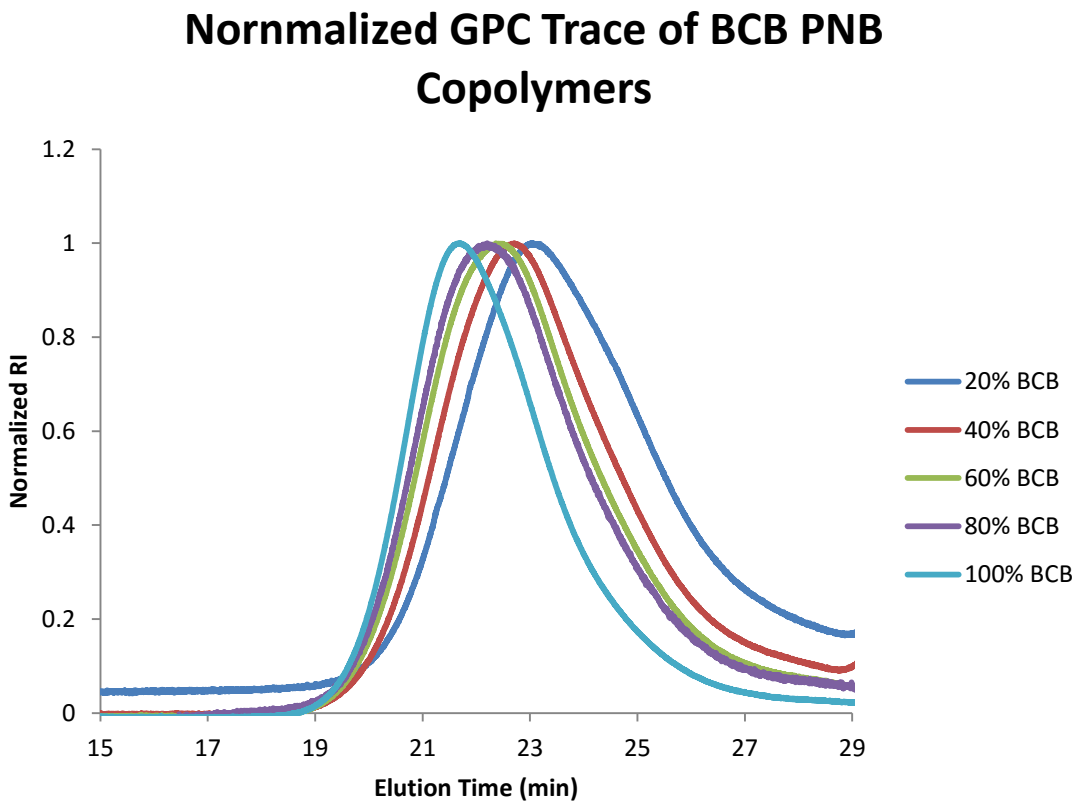

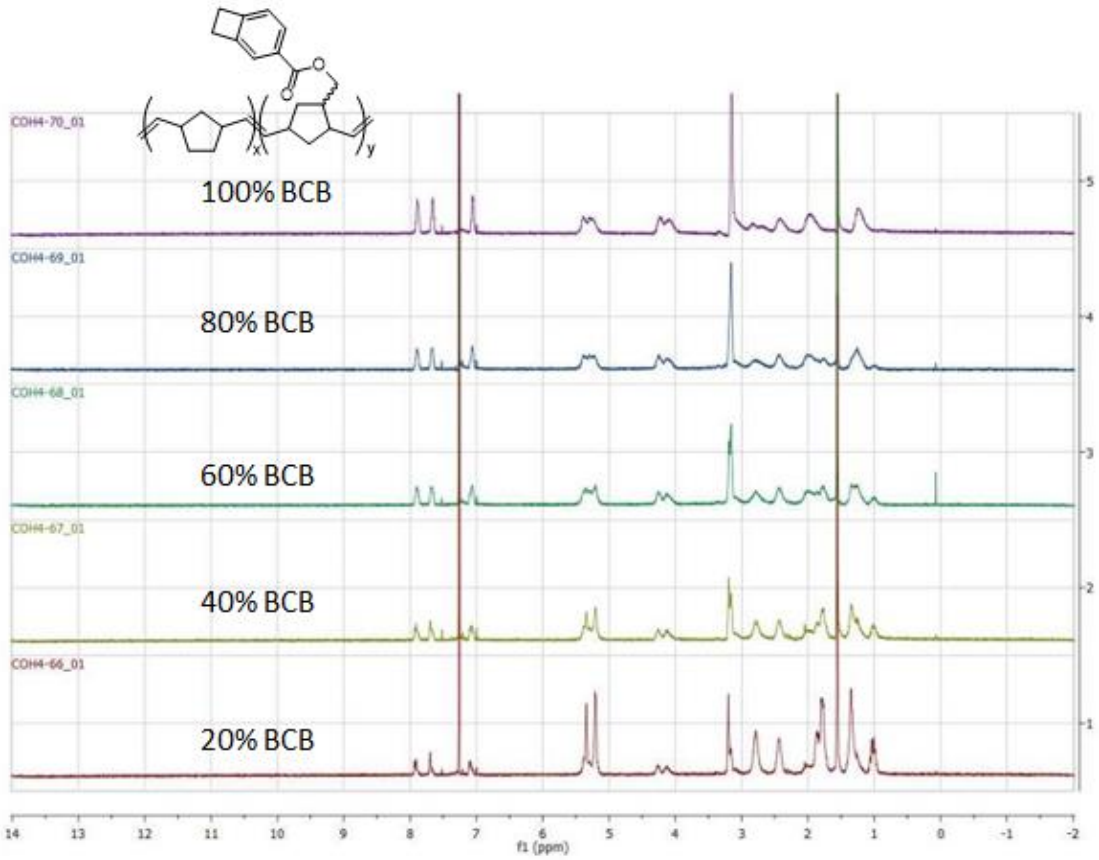

Proton NMR of BCB NB Copolymers.

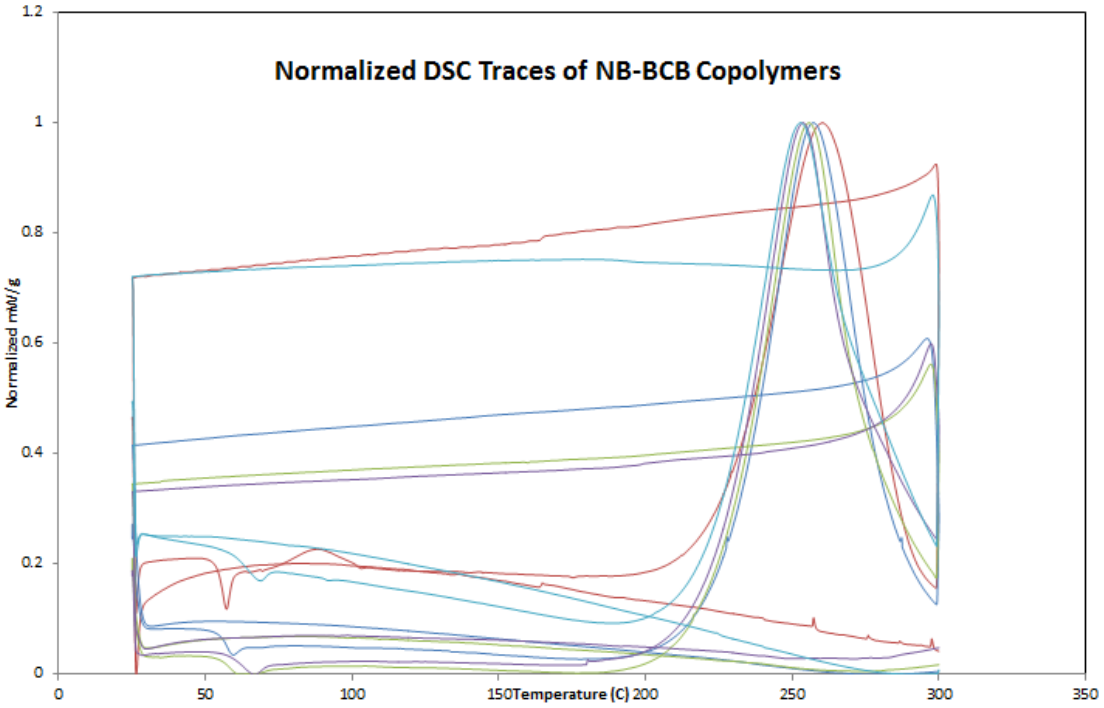
Normalized DSC Traces of NB-BCB Copolymers
Normalized mW/g
Temperature (C)
1.2
1
0.8
0.6
0.4
0.2
0
0
50
100
150
200
250
300
350

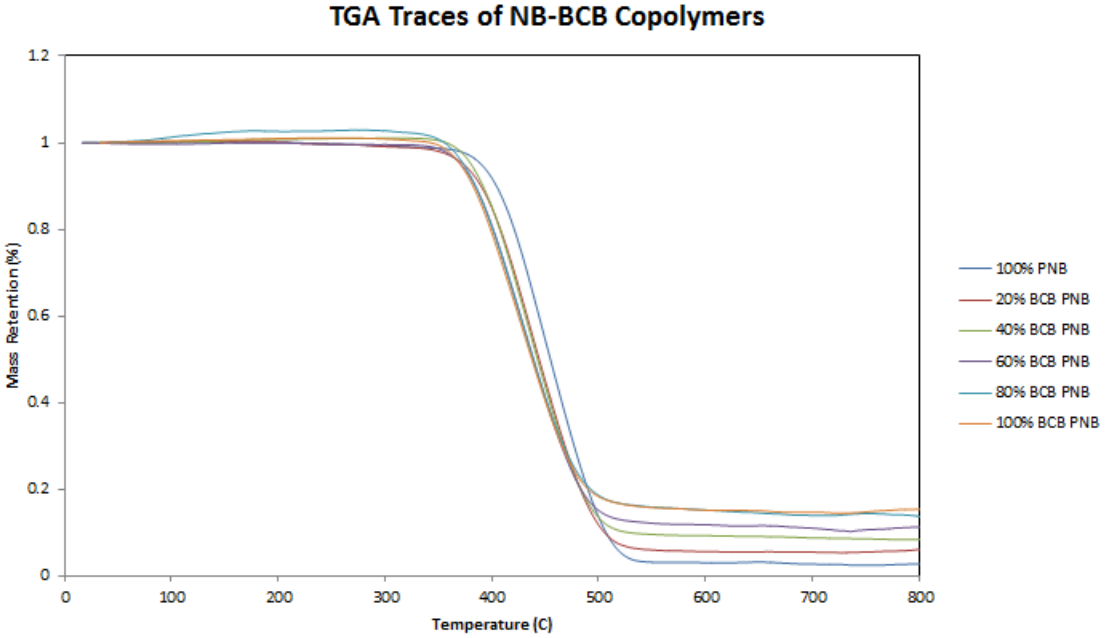
TGA Traces of NB-BCB Copolymers
Mass Retention (%)
Temperature (C)
1.2
1
0.8
0.6
0.4
0.2
0
0
100
200
300
400
500
600
700
800
100% PNB
20% BCB PNB
40% BCB PNB
60% BCB PNB
80% BCB PNB
100% BCB PNB

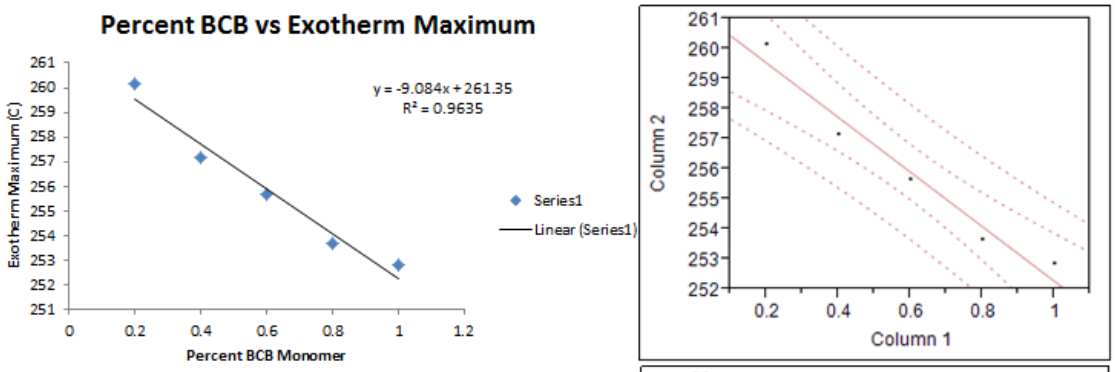

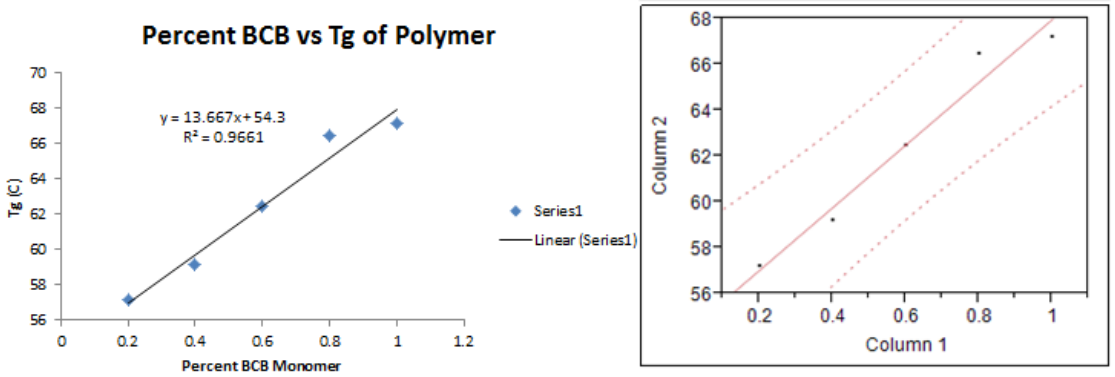

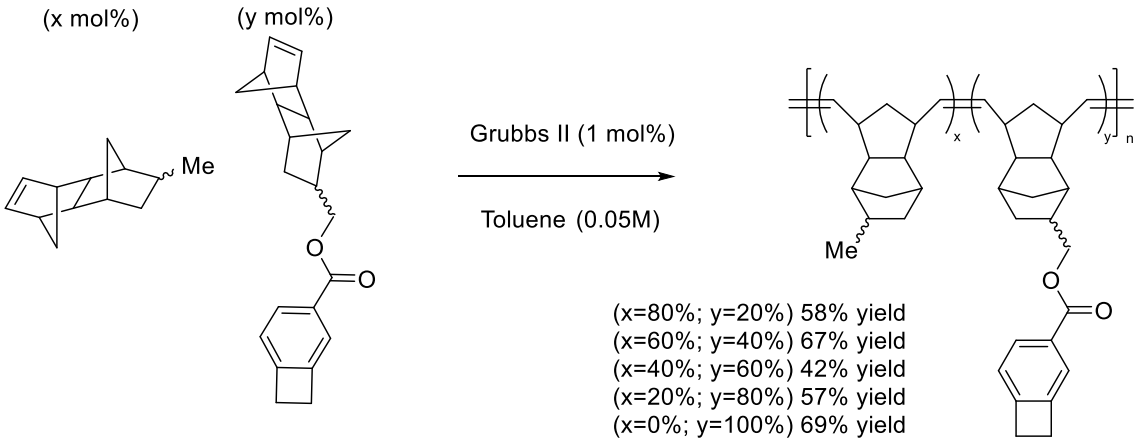

Dinorbornene BCB copolymers were all synthesized with one standard procedure. As an example, the procedure for copolymer **24** is described. BCB DNB monomer **13** (300 mg, 0.94 mmol, 80 eq) and MTD **15** (41 mg, 0.23 mmol, 20 eq), were added to a 100 ml round bottom flask equipped with a magnetic stir bar. Toluene (23 ml, 0.05 M) was

added and the monomers were dissolved. Toluene was used as received without distillation or any additional purification. Open to air, Grubbs Second Generation catalyst (10 mg, 0.012 mmol, 1 eq) was added, and the light red reaction mixture was capped with a nitrogen balloon and allowed to stir for one hour at room temperature. After one hour, 1 ml of ethyl vinyl ether was added to terminate the polymerization. After five additional minutes, the reaction was concentrated slightly *in vacuo* until viscosity of the solution had increased noticeably (about 10 ml of 20 ml removed). The reaction mixture was then poured dropwise into vortexing methanol (250 ml). The precipitated polymer was then isolated via vacuum filtration and washed with methanol (2 x 50 ml). The stringy solid was collected in a scintillation vial and dried under high vacuum overnight to remove residual methanol. The polymer was then isolated in 57% yield (194 mg). The following NMR, GPC and TGA characterization of copolymers in the series is available. The data suggest that the polymerization was run to roughly 100% conversion, as feed matched composition. The scientist who attempts this procedure should note that toluene appears necessary for any ROMP with MTD, be it homopolymer or copolymerization with another monomer. Other solvents such as DCM and THF result in no polymerization when MTD is present.

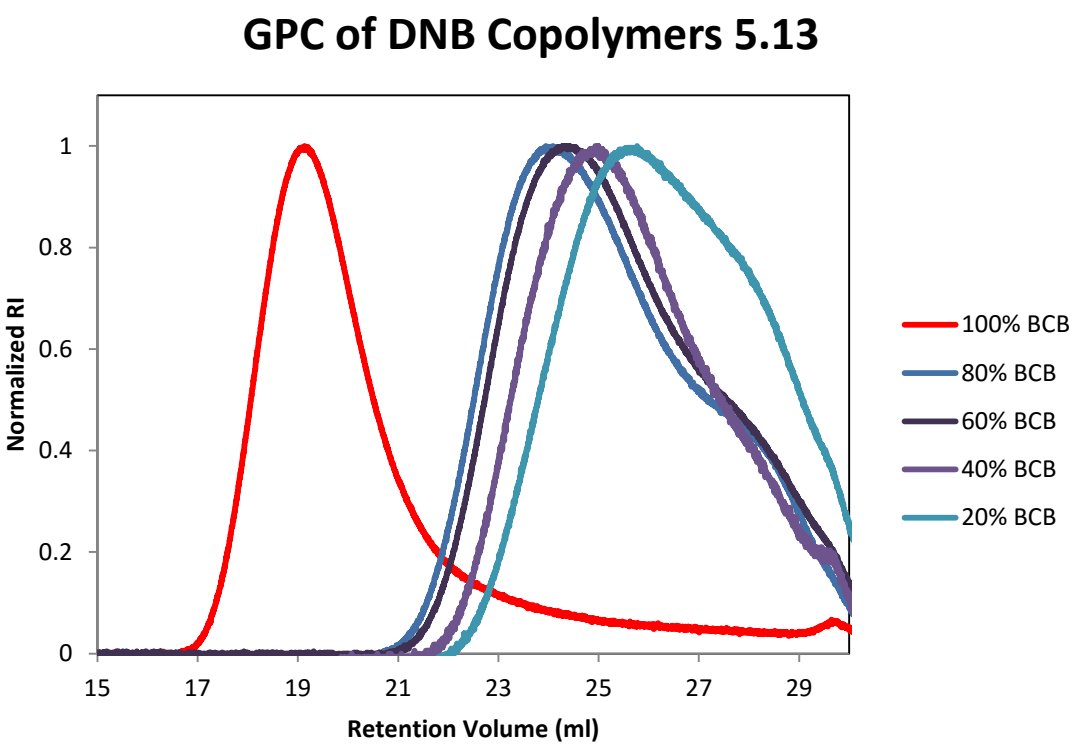
GPC of DNB Copolymers 5.13
Normalized RI
1
0.8
0.6
0.4
0.2
0
15
17
19
21
23
25
27
29
Retention Volume (ml)
100% BCB
80% BCB
60% BCB
40% BCB
20% BCB

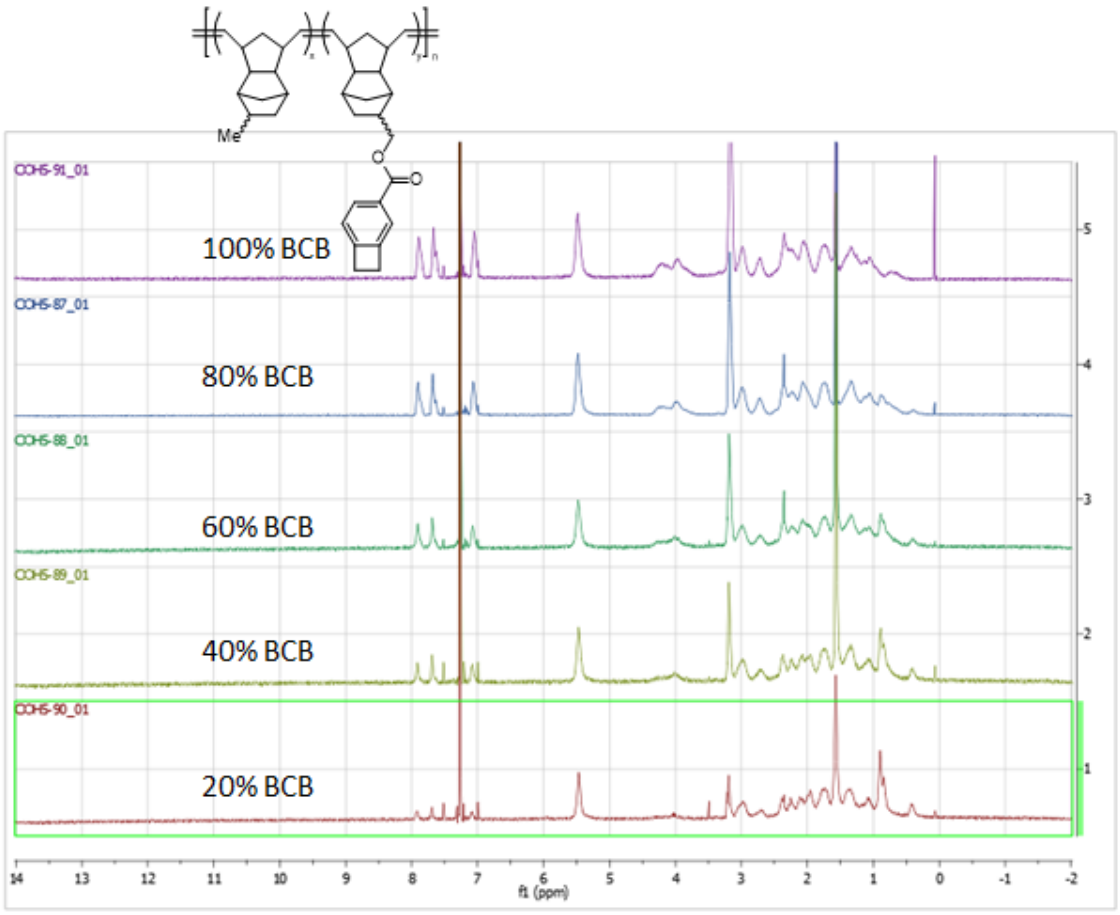

Proton NMR of BCB DNB Copolymers.

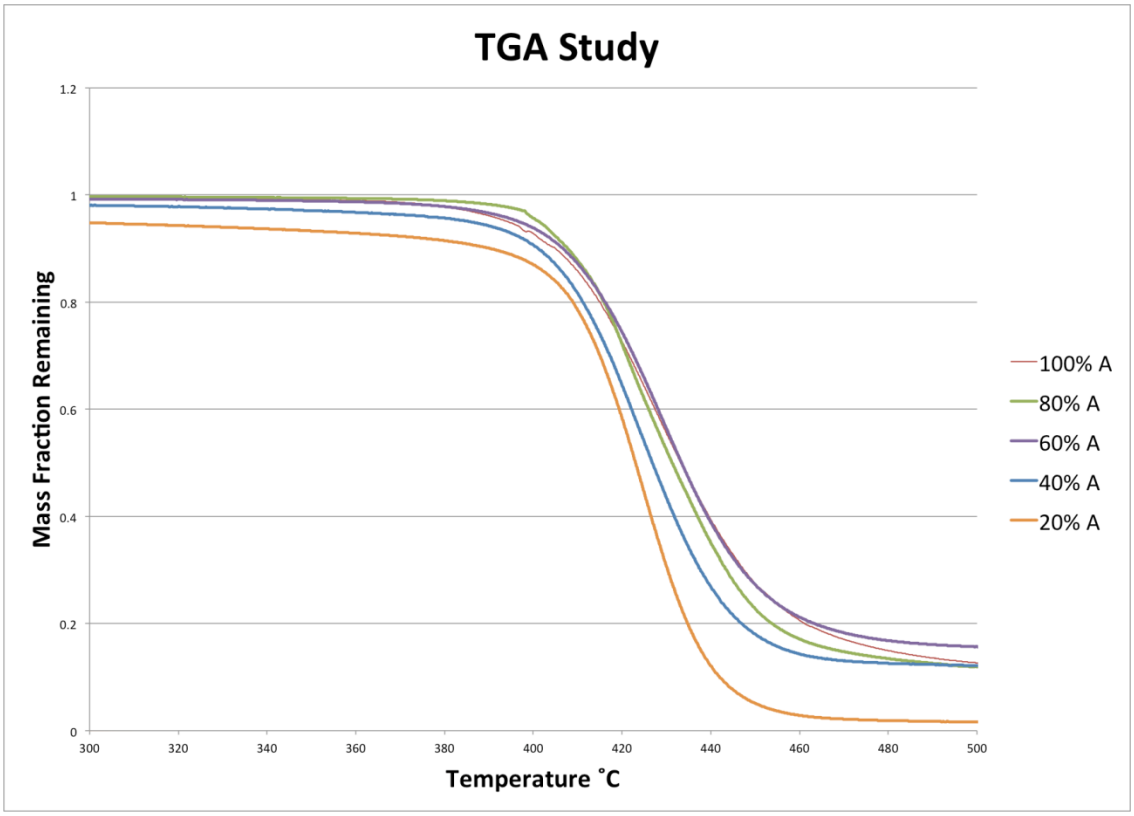

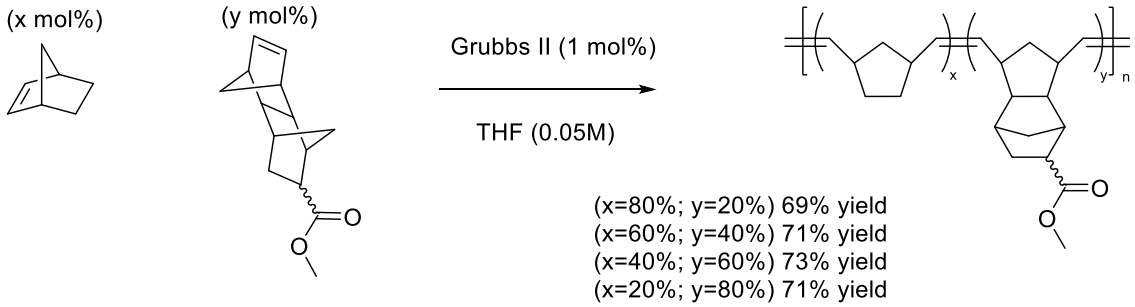

Dinorbornene and norbornene copolymers were all synthesized with one standard procedure. As an example, the procedure for copolymer **27** is described. DNB monomer **10** (436 mg, 2 mmol, 40 eq) and NB **14** (282 mg, 3 mmol, 60 eq), were added to a 250 ml round bottom flask equipped with a magnetic stir bar. THF (100 ml, 0.05 M) was added and the monomers were dissolved. THF was used as received without distillation or any additional purification. Open to air, Grubbs Second Generation catalyst (42 mg, 0.05

mmol, 1 eq) was added, and the light red reaction mixture was capped with a nitrogen balloon and allowed to stir for one hour at room temperature. After one hour, 1 ml of ethyl vinyl ether was added to terminate the polymerization. After five additional minutes, the reaction was concentrated slightly *in vacuo* until viscosity of the solution had increased noticeably (about 50 ml of 100 ml removed). The reaction mixture was then poured dropwise into vortexing methanol (250 ml). The precipitated polymer was then isolated via vacuum filtration and washed with methanol (2 x 50 ml). The stringy solid was collected in a scintillation vial and dried under high vacuum overnight to remove residual methanol. The polymer was then isolated in 57% yield (194 mg). DSC data is presented and discussed during the course of the chapter.

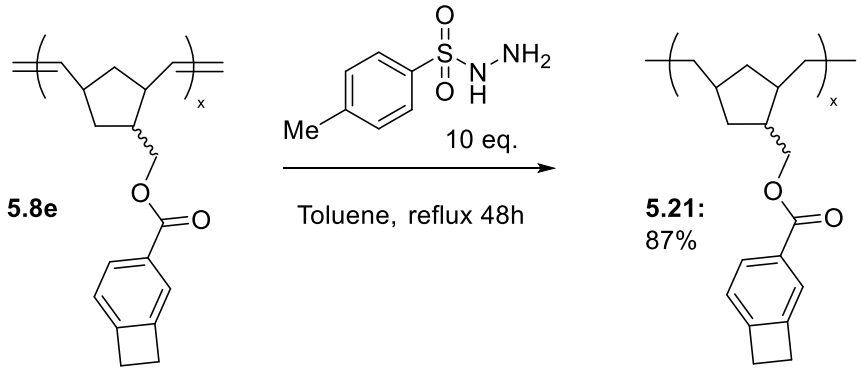

To a solution of ROMP BCB homopolymer (1.2g, 4.72 mmol of alkenes) in toluene (150 ml) was added p-toluenesulfonhydrazide (8.7g, 47.2 mmol, 10 eq with respect to alkenes) portion-wise in air. The mixture was dissolved in a 500 ml rbf equipped with a magnetic stir bar, equipped with a reflux condenser, purged with nitrogen and fitted with a nitrogen balloon. The reactor was then heated to reflux for 48 hours. Upon completion, the reactor was cooled and washed with sodium bicarbonate solution (2 x 100 ml) to remove the 4-methylbenzenesulfinic acid byproduct. The organic layer was then concentrated until viscosity increased noticeably. The reaction mixture was then poured dropwise into vortexing methanol (350 ml). The precipitated polymer was then isolated via vacuum filtration and washed with methanol (2 x 50 ml). The stringy solid was collected in a scintillation vial and dried under high vacuum overnight to remove residual methanol.

The polymer was then isolated in 87% yield (1.04 g). Proton NMR data showed a complete disappearance of alkene functionality, while alkyl-ester protons and aryl-BCB protons remained present. Molecular weight by GPC for unsaturated polymer: M_n = 442 kDa, M_w = 605 kDa, PDI = 1.37. Reduced polymer: M_n = 306 kDa, M_w = 435 kDa, PDI = 1.42. Thermal decomposition data by TGA for unsaturated polymer: T_d5 = 389 ˚C. For reduced polymer: T_d5 = 390 ˚C. DSC data for unsaturated polymer: T_g = 67 ˚C. Exotherm maximum: 253 ˚C, exotherm onset: 219 ˚C. For reduced polymer: T_g = 55 ˚C. Exotherm maximum: 266 ˚C, onset: 224 ˚C.

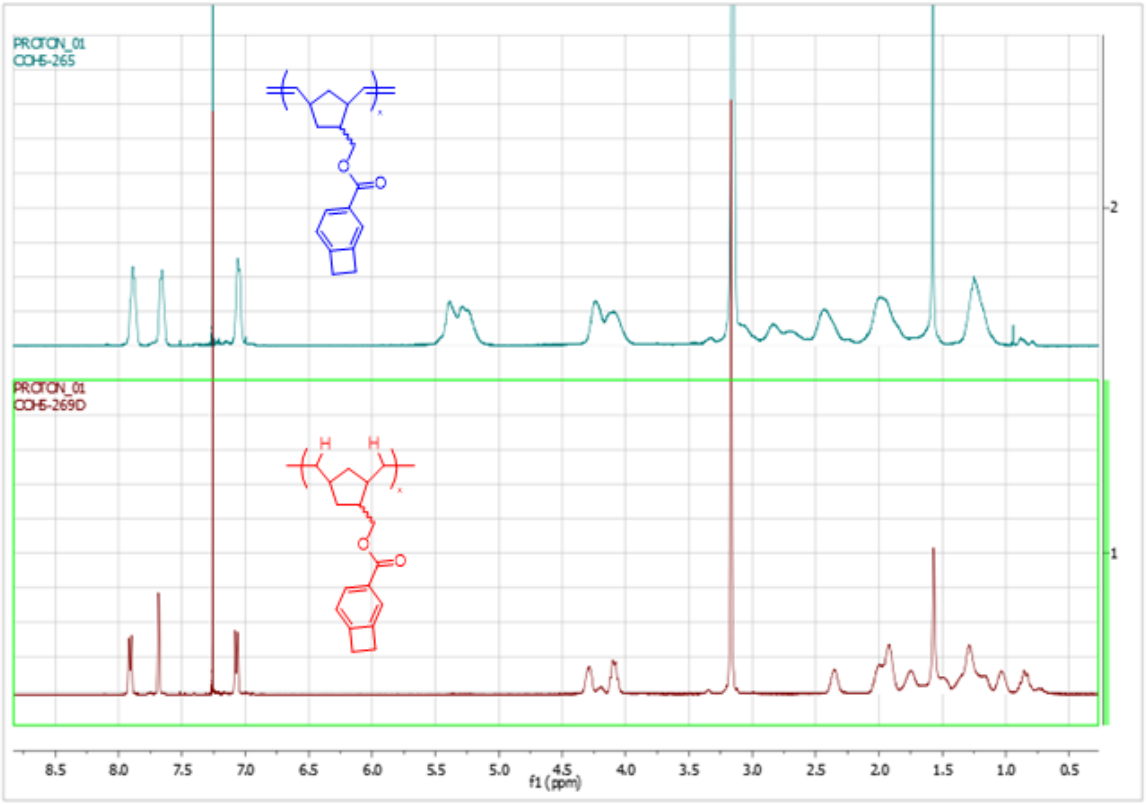

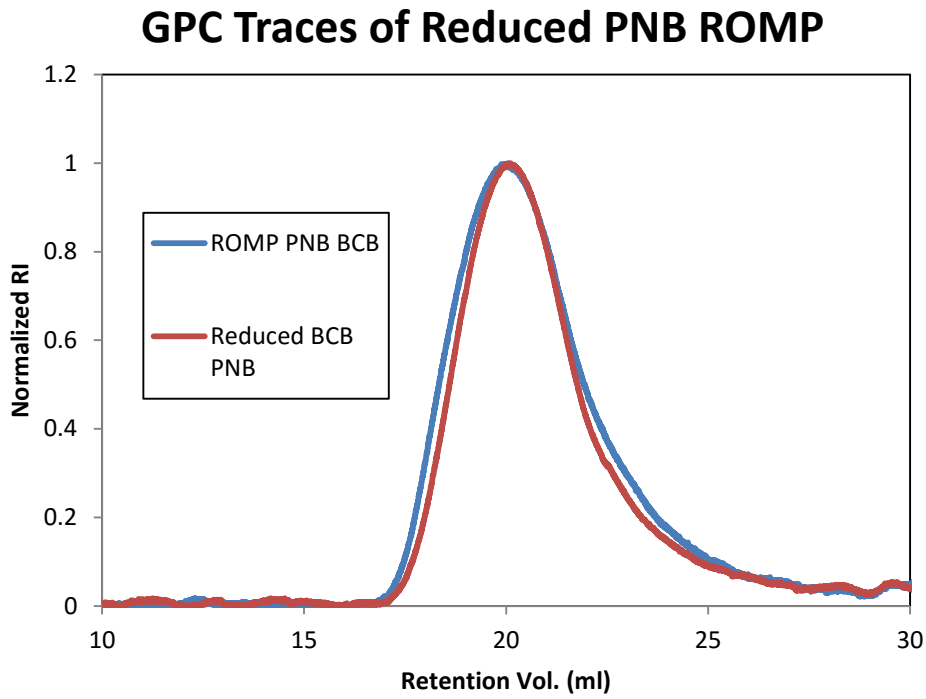
GPC Traces of Reduced PNB ROMP
Normalized RI
Retention Vol. (ml)
ROMP PNB BCB
Reduced BCB PNB
1.2
1
0.8
0.6
0.4
0.2
0
10
15
20
25
30

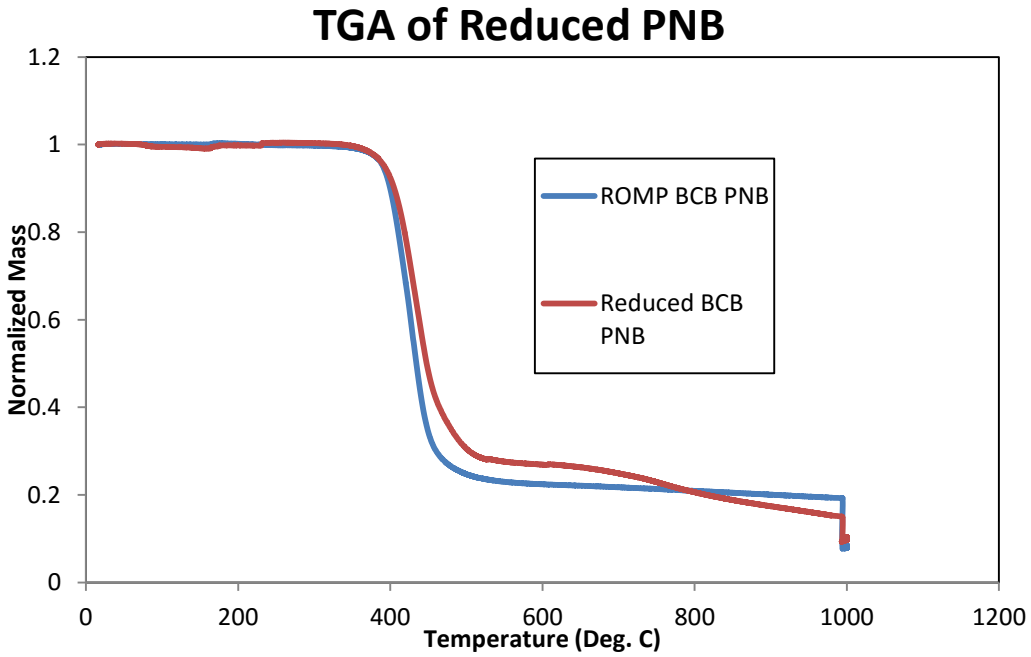
TGA of Reduced PNB
Normalized Mass
Temperature (Deg. C)
ROMP BCB PNB
Reduced BCB PNB
1.2
1
0.8
0.6
0.4
0.2
0
0
200
400
600
800
1000
1200

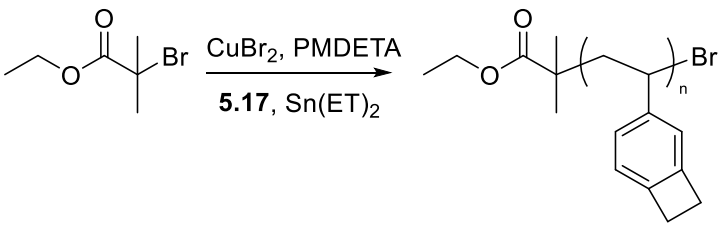

BCB styrene (804 mg, 50 eq) was added to a 25 mlf rbf equipped with a magnetic stir bar and a rubber septum. PMDETA (6.3 µl, 0.3 eq), copper (II) bromide (10 mg, 0.3 eq) and ethyl α-bromoisobutyrate (17.8 µl, 1 eq) were added and the mixture was purged with nitrogen gas for 30 minutes. Once the purge was complete, the reactor was sealed with a nitrogen balloon, and Tin (II) 2-ethylhexanoate was added (11.7 µl, 0.3 eq). The reactor was heated to 90˚C overnight, then precipitated in cold (-78˚C) methanol, isolated via vacuum filtration and dried overnight under vacuum at 60 ˚C. The polymer was isolated as a white powder (329 mg, 61% yield).

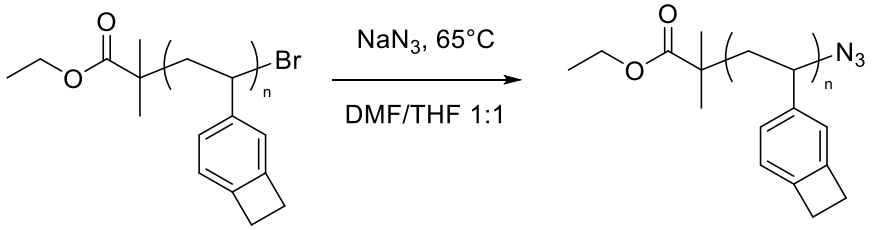

Bromine terminated BCB-PS (MW ~3 kDa, 600 mg, 1 eq) was dissolved in a 1:1 solvent mixture of DMF:THF (6 ml) in a 10 ml rbf equipped with a magnetic stir bar and rubber septum. Sodium azide was added (60 mg, 3 eq) was added and the reactor was heated to 65˚C for 12 hours. Upon completion, the polymer was precipitated in cold (-78˚C) methanol, isolated via vacuum filtration and dried overnight under vacuum at 60 ˚C. The polymer was isolated as a white powder (502 mg, 84% yield). ^{1}H NMR ($CDCl_3$) δ(ppm): PS-Br 4.6–5.0 ppm, PS-N3 3.75–4.25.

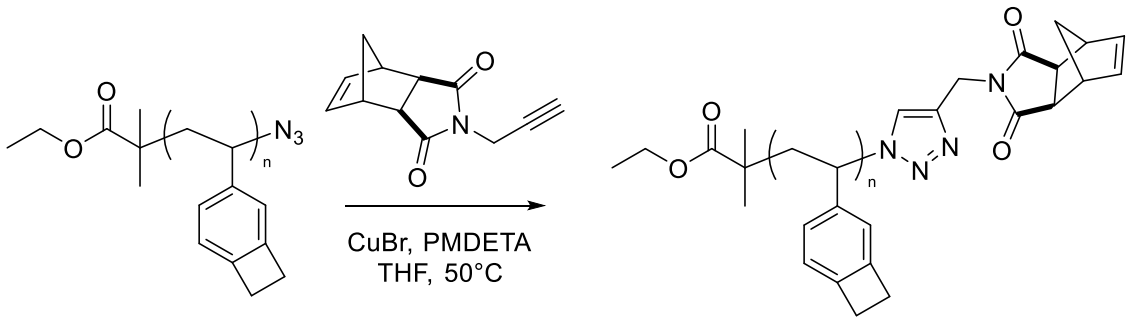

Azide terminated BCB-PS (MW ~3 kDa, 500 mg) was added to exo-NB propargylimide (73 mg, 1.5 eq per chain) in THF (10 ml) in a 25 ml rbf equipped with a magnetic stir bar. Copper bromide (15 mg, 0.4 eq) was added and the reactor was sealed and equipped with a nitrogen balloon. PMDETA (22 µl, 0.4 eq) was added via syringe and the reactor was heated to 50˚C for 12 hours. After which the reaction was concentrated then precipitated in cold (-78˚C) methanol, isolated via vacuum filtration and dried overnight under vacuum at 60 ˚C. The polymer was isolated as a white powder (329 mg, 61% yield). ^{1}H NMR ($CDCl_3$) δ(ppm): PS-N3 3.75–4.25, PS-norbornene 4.89–5.05.

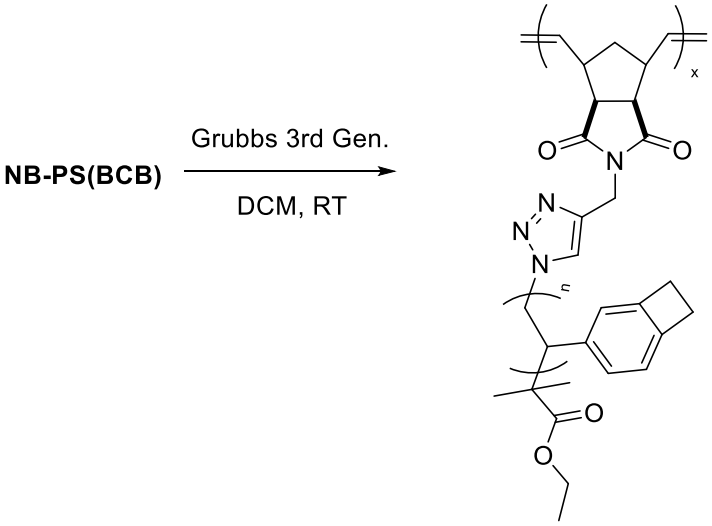

NB-macromonomer (MW ~3.3 kDa, 146 mg, 20 eq) was dissolved in DCM (1.5 ml). Grubbs 3rd Generation catalyst (1.6 mg, 1 eq) was added in air, the reactor was sealed and stirred at room temperature for five hours. After which the reaction was terminated with ethyl vinyl ether and precipitated in methanol (100 ml). The stringy solid was isolated via

vacuum filtration and dried overnight under vacuum at 60 ˚C. The polymer was isolated as a white powder (121 mg, 83% yield).

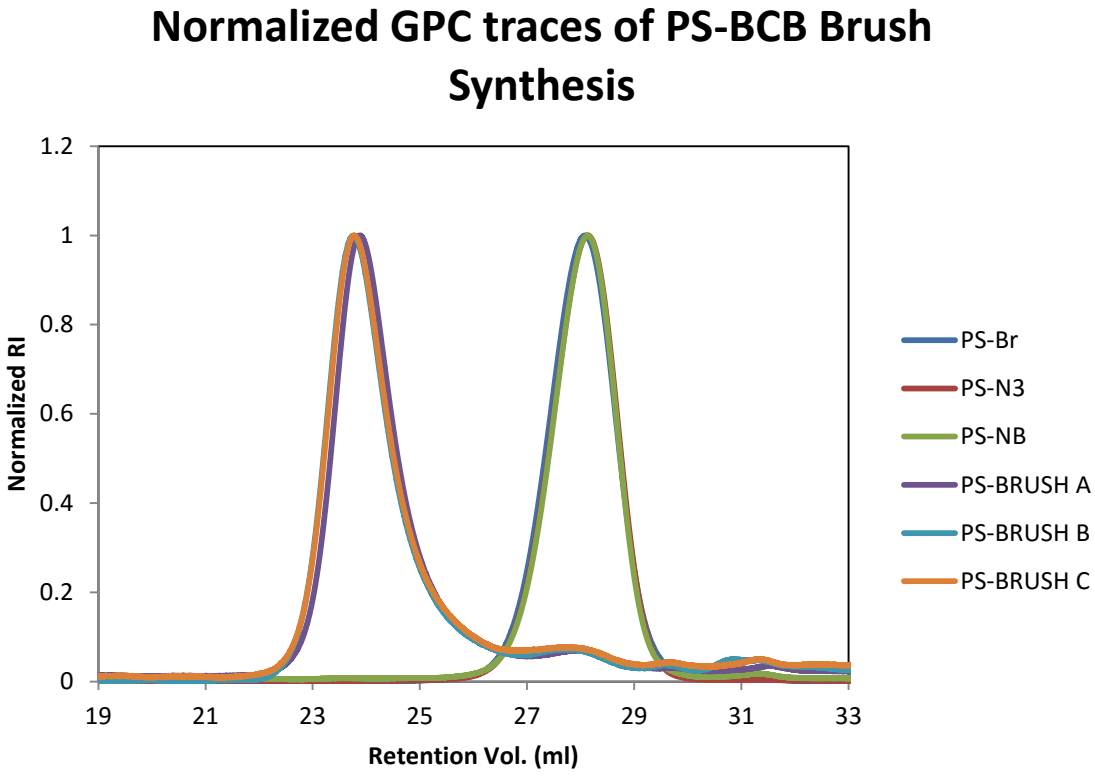

BACM Photobleaching Experiment

The PAC bis-azide BACM was dissolved in spectroscopic grade acetonitrile (97 μM solution). The solution was exposed to broadband UV light at iterative doses, and the UV spectrum was collected after each dose.

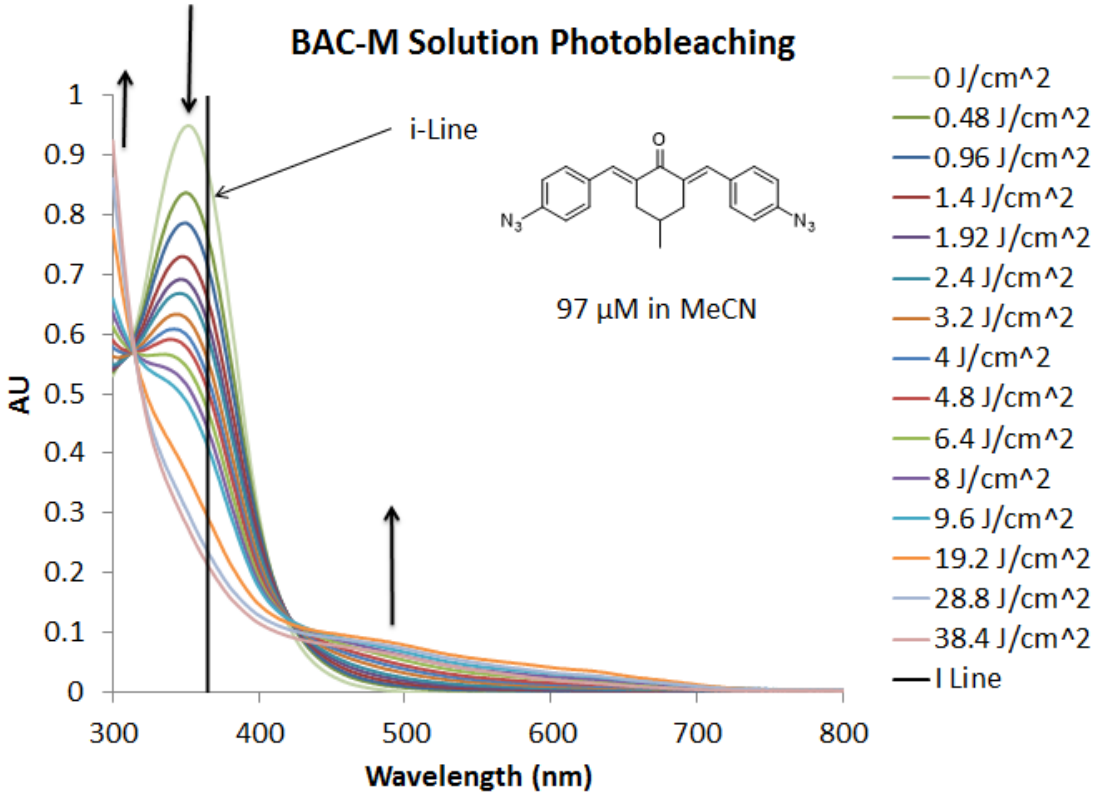
BAC-M Solution Photobleaching
i-Line
97 µM in MeCN
AU
Wavelength (nm)
0 J/cm^2
0.48 J/cm^2
0.96 J/cm^2
1.4 J/cm^2
1.92 J/cm^2
2.4 J/cm^2
3.2 J/cm^2
4 J/cm^2
4.8 J/cm^2
6.4 J/cm^2
8 J/cm^2
9.6 J/cm^2
19.2 J/cm^2
28.8 J/cm^2
38.4 J/cm^2
I Line

Chapter 6: Benzocyclobutene Polynorbornene Materials via Addition Polymerization

6.1 Introduction

The addition polymerization of norbornene is known to produce polymers with high thermal stability (T_{d5} > 400˚C), high T_g (> 300˚C), low dielectric constant (~2.2) and low birefringence[86]. Norbornene monomers are typically synthesized from Diels Alder reactions between cyclopentadiene and a desired olefin in reagent, making them extremely attractive and green feedstocks as a material source[87]. However, despite these attractive features, addition polymerization to form polynorbornenes (PNBs) is often considered undesirable compared to metathesis (ROMP) or controlled free radical polymerizations when it comes to reproducibly synthesizing polymeric materials in high yield and with ease of operation. Addition polymerization of PNB suffers from the following problems: 1) The endo isomer of a substituted norbornene is often unreactive or very slow to react, which requires costly separation of the isomers of the monomers to obtain high polymer yield. Further, in many Diels Alder reactions, the endo isomer is either the dominant or exclusive product, prohibiting use of certain monomers. 2) Lewis acidic catalysts are often required. This often entails preparing a catalyst before every polymerization. Further, these Lewis Acidic cations are capable of reacting with monomer functional groups, eroding the structural integrity of the polymer[88]. 3) Perhaps most importantly of all, most catalyst systems are poisoned by any functional groups on the norbornene monomer, particularly polar functional groups. This greatly inhibits monomer scope and restricts catalyst choice[89].

Little progress in this type of polymerization had been made on any other monomer besides regular, unsubstituted norbornene until Risse et al. successfully performed the living polymerization of 5-exo-norborn-ol, using the catalyst

$Pd(CH_3CN)_4(BF_4)_2$, and later the polymerizations of 5-norbornene methyl ester and carboxylic acid with η^3-allyl palladium (BF_4 and SbF_6 counter anions)[90]. This was a substantial breakthrough on the path to making addition polymerization of norbornene a viable and useful synthetic tool. However this work was still far from "solving" the problem of addition polymerization of norbornenes. With these catalyst systems, many polar norbornenes still have poor or no reactivity, often yields are low unless the polymer is diluted with unsubstituted norbornene or ethylene as a copolymer, high catalyst loadings can be required, and the endo isomer still is often unreactive.

In this chapter, the addition polymerization of PNBs has been explored with the goal of understanding and increasing catalyst activity and applying the polymerization to benzocyclobutene (BCB) norbornene monomers with the goal of creating dielectric polymers for next generation packaging materials.

In the pursuit of understanding catalyst activity, it is clear from the literature that cationic metal centers are ideal, and that early work on the polymerization of olefins has revealed that most metals are often activated by Lewis acids. For this study, the catalyst system η^3-allyl palladium hexafluoro antimonate has been chosen for examination. This catalyst system is prepared from relatively inexpensive and available reagents and has been reported to have respectable monomer scope and high yields. One variable that has been considered but not addressed experimentally in this chapter is the choice of counter-ion for these polymerizations. It is tempting to conclude that an ideal counter-ion would be one that is the largest and least coordinating to the metal, of which there are two likely candidates other than hexafluoro antimonate: 1) fluorinated aryl boron salts (BArF) or 2) hexahalocarboranes[91,92].

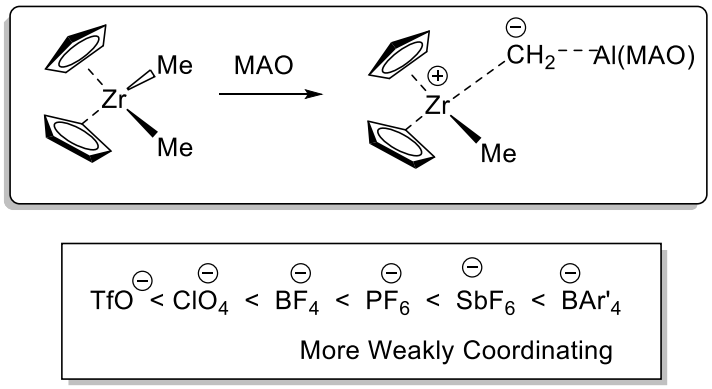

Figure 6.1: (Above) Activation of a Ziegler-Natta catalyst via Lewis Acid. (Below) Ranking of non-coordinating anions from most to least coordinating.

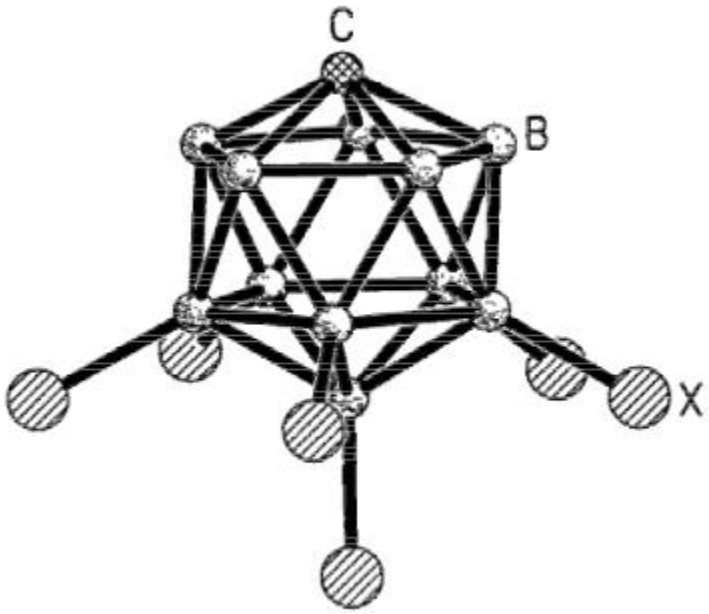

Figure 6.2: Representative structure of a hexahalocarborane.

Unfortunately, in order to prepare the active palladium catalyst, a salt metathesis reaction is required, in which silver chloride (AgCl) is produced as the driving force (AgCl is easily precipitated). Unfortunately, silver BArF salts are not readily available (and often pyrophoric), and carbornanes are often difficult and dangerous to synthesize. Even if one

could obtain the silver carborane salt, there is some evidence to suggest that the salt metathesis might not proceed easily. Thus, in this chapter, the counter-ion variable has been restricted to $AgSbF_6$, which is readily available, very non-coordinating and the active catalyst forms quickly and safely.

In the case of η^3-allyl palladium, the choice of reaction solvent has a tremendous effect on polymerization yields. It has been hypothesized that this is due to solvation of the cationic palladium chain end: in solvents that cannot dissolve the salt-like end groups the polymer precipitates out of solution at low conversion and low molecular weight. However, since crystal structures of palladium and norbornene demonstrate that solvents occupy coordination sites on the metal, it is very plausible that there is also an electronic effect that the solvent contributes to the metal center, and thus the polymerization activity. The literature consensus is that in the case of η^3-allyl palladium hexafluoro antimonate, nitromethane is the best solvent for high yields. In this work, several solvents were screened in addition to the many tried in previous reports. Hexafluoro-isopropanol (HFIPA) has been found to be a reasonable alternative to nitromethane. Further, since phosphine ligands have a well-established affinity for palladium, several ligands were screened *in situ*. It was found that the withdrawing phosphine ligand tris(pentafluorobenzene)phosphine increased catalyst activity but at the cost of greatly decreased molecular weight, which proved to be detrimental to polymer isolation in many cases.

Monomer scope was also examined to a degree. While the η^3-allyl palladium catalyst has been found to have good functional group tolerance, noticeably absent from the literature are results of monomer scope of dinorbornene (DNB) compounds, which were discussed at some length in Chapter 5 because of their interesting and useful properties, particularly for a dielectric application. It has been found that while the

saturated DNB methyl-tetracyclododecene (MTD) demonstrated fast polymerization, high molecular weight and low dispersity, no other DNB monomers produced anything other than low yields of oligomeric products. Perhaps the most unusual result of this chapter is that the η^3-allyl palladium catalyst system has found to be a suitable catalyst for producing polystyrene, a result that is (to the best of the author's knowledge) unprecedented with this system.

BCB containing norbornene monomers were successfully polymerized to form the corresponding addition polymers. These polymers were put through a preliminary evaluation to test their potential as dielectric materials for a microelectronics packaging application. Unfortunately, the results were mixed. While the polymers demonstrated low dielectric constants and good z-axis CTE values compared to their ROMP counterparts, there were statistically no differences in these properties between the BCB containing polymers and the control, regular addition polymerized PNB. The results suggest that one does not gain any benefit in the relevant properties by adding the thermosetting BCB component in this style of polymerization, and thus these resins were not studied further.

6.2 Results and Discussion: Synthesis

In order to optimize and explore new conditions for the addition polymerization of norbornenes, a model system was developed to run many screens on large (gram) scale. The monomer chosen as the model compound was dimethyl bicyclo[2.2.1]hept-5-ene-2,3-dicarboxylate **6.1** ($NB(CO_2Me)_2$). The simple Diels Alder adduct of cyclopentadiene and dimethyl maleate is idea for a few reasons: 1) it is easily synthesized on large scales from available and inexpensive starting materials, 2) it contains the ester functionality relevant to synthesizing BCB containing addition polymers, and 3) it is

isolated as a mixture of endo and exo isomers, also relevant to synthesizing BCB containing addition polymers and addressing the challenge of poor endo polymerization activity.

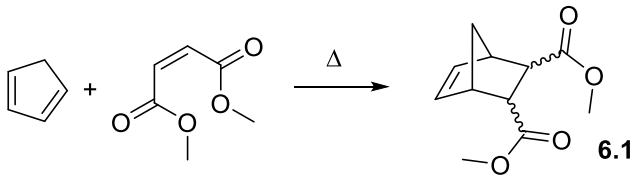

Scheme 6.1: Synthesis of $NB(CO_2Me)_2$ via Diels Alder.

A general method of preparing the catalyst was adapted from the literature. Allyl palladium chloride dimer and silver hexafluoro antimonate were combined under inert atmosphere in a glove box and then nitromethane was added. The solution quickly turned bright yellow and silver chloride precipitated (Scheme 6.2).

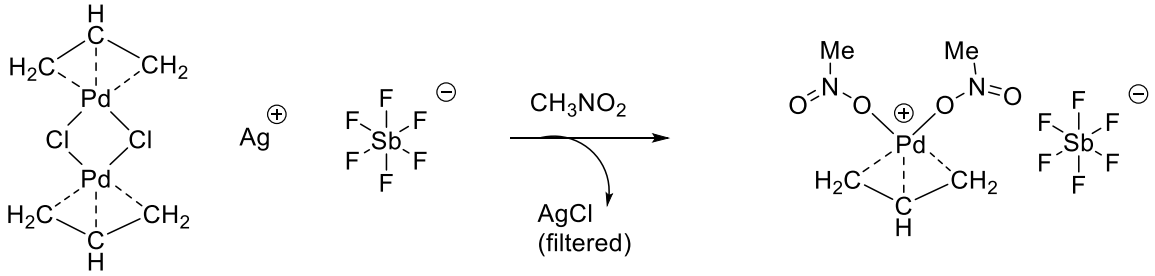

Scheme 6.2: Salt metathesis to form the active catalyst and easily removed silver chloride. In this scheme, the solvent is proposed to coordinate to the palladium. Crystal structures of this catalyst system obtained from oxygen containing solvent consistently demonstrate that two oxygens coordinated to the palladium (in the solid state).

Catalyst stock solutions could then be added to addition polymerization screens as desired. First experiments included polymerizing norbornene **6.2** and the nonpolar DNB methyl-tetracyclododecene (MTD) **6.3**. The polymerization activity of norbornene **6.2**

was found to be very high under standard catalyst conditions: reactions often produced insoluble solids within a few minutes. It was found that higher molecular weight polymer could be isolated when the reaction was diluted to 0.05M in Chlorobenzene. After five minutes the viscous mixture was precipitated in methanol to produce the addition polymer with high T_g (>300˚C) in high yield (80%, Scheme 6.3).

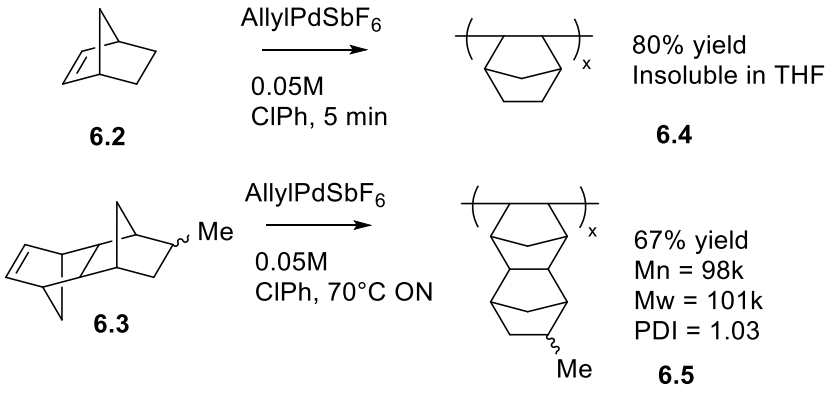

Scheme 6.3: Addition polymerizations of nonpolar norbornenes.

The resulting polymer was insoluble in THF, so molecular weight could not be determined by GPC. The DNB MTD **6.3** was somewhat less active, with high yields only proceeding at elevated (70˚C) temperature. However, **6.3** still produced polymer in good yield and with a very low polydispersity index (PDI) by GPC (see Scheme 6.3). The low dispersity and high molecular weight are consistent with living polymerization kinetics for polymer **6.5**.

While synthesis of addition polymers without polar functional groups proceeded easily in high yields, synthesis of polymers with polar functional groups proved to be much slower and in lower yields. Since prior studies suggest a strong link between solvent choice and polymerization yield, a screen of solvents under standard conditions was performed on monomer **6.1** on gram scale. The results are outlined in Table 6.1.

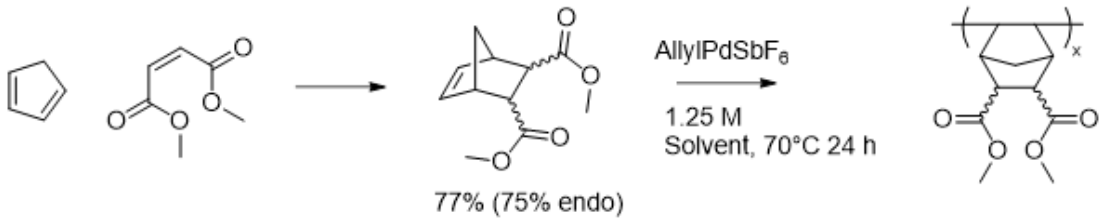

Solvent	Yield (%)	Mn (kDa)	Mw (kDa)	PDI
Perfluoro 15-crown-5	0	0	0	0
Mesitylene	0	0	0	0
HMPA	0	0	0	0
Trichloro trifluoro ethane	0	0	0	0
Nitrobenzene	26	4.04	4.46	1.1
HFIPA	**53**	**7.24**	**8.61**	**1.19**

Table 6.1: Solvent screen of dimethyl ester addition polymer.

Some common reagents known for their ability to solvate certain cations were examined. Hexamethylphosphoramide (HMPA), known for its ability to solvate lithium ions, shut down polymerization activity. Perfluoro 15-crown-5, a known potassium chelating agent, also shut down polymerization activity. The results suggest that the solvents are coordinating the active catalyst to some degree, but the resulting complexes were clearly inert to polymerization. Mesitylene (similar in solvating ability to chlorobenzene, which the reader will note produced polymer in high yields for monomers **6.2** and **6.4**), also produced no polymer, suggesting the importance of chlorine as a site for palladium coordination. Interestingly, nitrobenzene produced a moderate yield of polymer with low dispersity, suggesting that the nitro functional group is important to catalyst activity (nitromethane also produced high yields and low PDI). It also corroborates previously obtained crustal structures that the cationic palladium catalyst is oxophilic (predisposed to occupy its open coordination sites with oxygen functional groups, as observed in THF

and H_2O crystal structures obtained by Claverie et al.). Evidence for the contribution of oxygen containing functional groups further builds as hexafluoro isopropanol (HFIPA) produced polymer in roughly twice the yield and twice the molecular weight as nitrobenzene, with a similarly low dispersity. By contrast, the fluorinated solvent 1,2-trichloro-trifluoro ethane completely shut down polymer activity. It is speculated that a good solvent is one that has the ability to coordinate to the catalyst with a functional group such as oxygen or chlorine, but is also electron withdrawing to some degree to make a more electrophilic catalyst. This follows the observations that in general polyolefin catalysts are more active when they are cationic in nature or coordinating with a Lewis Acid. Inspired by these results, several different phosphine ligands were also screened to see if a strong effect on catalyst activity could be found.

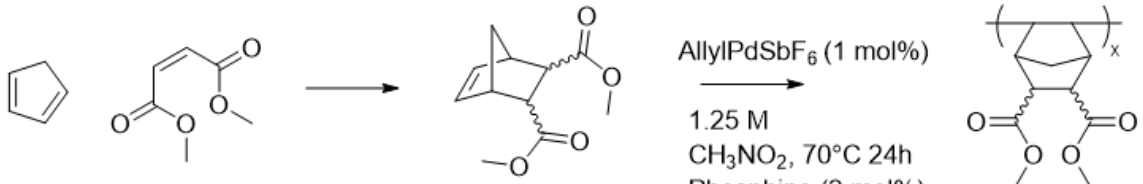

Phosphine (2 mol %)	Yield (%)	Mn (kDa)	Mw (kDa)	PDI
None	31	4.56	5.37	1.18
Triphenyl	0	0	0	0
Tritertbutyl	0	0	0	0
Tricyclohexyl	35	2.1	2.98	1.42
Bis(Pentafluoro benzene) 1, 2 ethane	0	0	0	0
Tris(p-Trifluoromethyl benzene)	12	3.05	3.21	1.05
Tris(1,3-perfluoromethyl benzene)	31	4.3	5.0	1.2
Tris(Pentafluoro benzene)	**62**	**1.25**	**2.48**	**1.97**

Table 6.2: Effect of phosphine choice on dimethyl ester addition polymerization.

Using standard screening conditions and a 2 mol% loading of phosphine relative to monomer (2 equivalents of phosphine per palladium), a few interesting results occurred. First, the electron rich phosphines triphenyl phosphine and tritertbutyl phosphine completely shut down the polymerization. The polymerization proceeded in the presence of tricyclohexyl phosphine in a similar yield as the control (no additives), but provided lower molecular weight. Fluorinated phosphines produced some very interesting results. Tris(*p*-trifluoromethyl benzene) phosphine produced a low yield of polymer but with a very narrow polydispersity. The more electron poor tris(1,3-trifluoromethyl benzene) phosphine produced a higher yield, in the same range as the control.

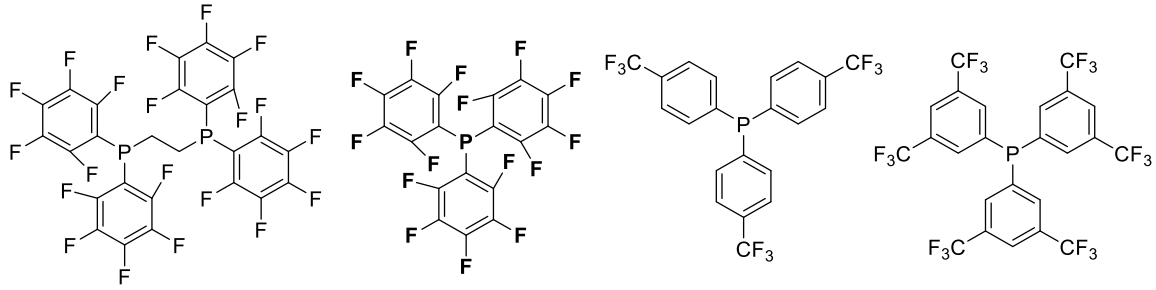

Figure 6.3: Structures of tested fluorinated phosphines.

Tris(perfluoro benzene) phosphine produced a higher yield by about factor of two over the control, albeit at the cost of a much lower molecular weight of polymer. At first glance, the results seem promising, but the significant decrease in molecular weight of the polymer proved to be detrimental when the tris(perfluoro benzene) additive was tested on other monomers, such as MTD and styrene. The resulting materials were low molecular weight oligomers that precipitated poorly in any solvent. The low molecular weight data is very surprising, especially since low (1 mol%) catalyst loadings were used

with respect to monomer, and living like kinetics have been proposed in the literature. In fact, it has often been noted in previous reports that molecular weights were higher than expected assuming living like kinetics. Since low polydispersity was observed, one hypothesis is that the phosphine additive creates some sort of chain transfer agent that contributes to a Reversible Addition-Fragmentation chain Transfer (RAFT) like polymerization. In hope of making this additive useful, more monomer was added in variable amounts once the polymerization appeared to stop (by GPC). Unfortunately, added monomer did not grow onto the end of the chain as observed by GPC. In fact, newly added monomer did not even appear to grow as new chains. Meanwhile, the reaction solution turned from transparent yellow to black (suggesting the termination of active catalyst as palladium black is formed). It was hypothesized that the limiting aspect of the polymerization was catalyst lifetime (i.e. a high rate of termination events). Indeed, if a catalyst solution is left on the benchtop at room temperature for a few hours or days, the solution slowly turns black and becomes ineffective at initiating polymerization.

In polyolefin polymerization, the terminating step is often β-hydride elimination. However, this is unlikely in the case of addition polymerization of norbornenes since the palladium is known to coordinate to the exo face and the fused ring is unable to rotate to reach the required 180˚ dihedral angle required for an anti-periplanar confirmation. Protonation of the palladium species was also proposed as a mechanism of termination. The solvent nitromethane is weakly acidic (pKa ~10), so 1,3-ditertbutyl pyridine was added on various amounts (1-30 mol%) to the polymerization to serve as a sterically bulky, non-metal coordinating proton sponge. Unfortunately, the pyridine shut down all polymerization activity at all additive ratios.

Ultimately, it was decided to abandon the exploration of various solvents and phosphine additives. The results have high variance between solvents and additives, which suggests that there is still a lot of area for development of this style of polymerization. Unfortunately, without a way to reliable quantify the various attributes of solvents or additives, a multidimensional statistical surface design of experiments is not feasible, and trying every possible combination is impractical. However, the possibility of a future where addition polymerization is as easy and robust as ROMP is still not out of the question.

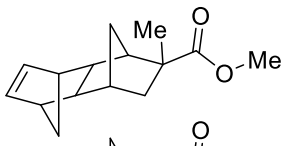	**6.6:** No Reaction	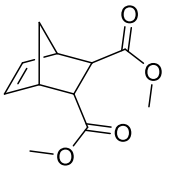	**6.1:** 81% yield[a] Mn = 25k Mw = 31k PDI = 1.24
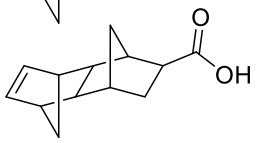	**6.7:** No Reaction	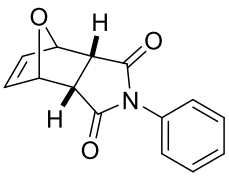	**6.12:** No Reaction
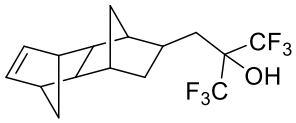	**6.8:** No Reaction	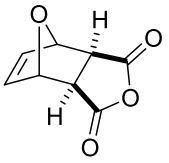	**6.13:** Insoluble Solid
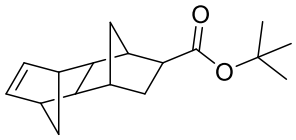	**6.9:** No Reaction	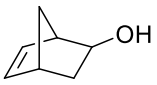	**6.14:** Insoluble Solid
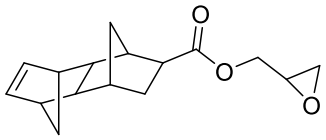	**6.10:** 17% yield of oligomer	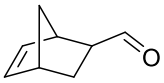	**6.15:** Insoluble Solid
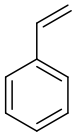	**6.11** 62% yield Mn = 24k Mw = 30k PDI = 1.27	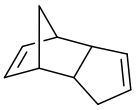	**6.16:** Insoluble Solid
	**6.3:** 67% yield[b] Mn = 98k Mw = 101k PDI = 1.03	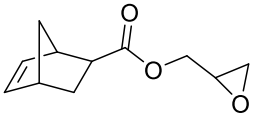	**6.17:** No Reaction
		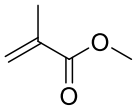	**6.18:** No Reaction

Conditions: 1 mol% Pd catalyst, 1.25M in Nitromethane, 70°C in sealed tubes for 24h. a: run neat, without solvent. b: ClPh 0.05M

Table 6.3: Monomer scope of addition polymerization. Results suggest most polar dinorbornenes are incompatible with the catalyst system.

In order to assess the monomer scope of addition polymerization for dielectric packaging materials, a number of monomers with different relevant functional groups were screened with standard catalyst conditions (Table 6.3). The results reveals a few important trends: 1) Dinorbornene compounds show little to no reactivity with the exception of the nonpolar MTD **6.3**. 2) A number of compounds produced insoluble solids which are likely high molecular weight polymers, as the corresponding addition polymers of **6.14** and **6.15** have been reported in the literature using the same catalyst system. Varying reaction concentration or catalyst loading would likely produce soluble materials. 3) 7-oxanorbornenes show some potential as monomer candidates. The exo-oxanorbornene anhydride **6.13** produced an insoluble solid, but the endo-oxanorbornene n-phenyl imide compound **6.14** proved completely inert. These results are consistent with ordinary norbornene reactivity. 4) Surprisingly, the palladium catalyst polymerized styrene with reasonably high molecular weight.

The inability of the catalyst to polymerize DNBs with any consistency was a highly disappointing result. However, since the reactivity of MTD is quite robust under these conditions, it is clear that the polar functional groups (alcohols, esters, acids) are poisoning the catalyst. What makes these results surprising is that none of the same functional groups shut down catalyst activity in their ordinary norbornene counterparts. There is some precedence that shows that norbornenes with polar functional groups undergo formation of oligomeric macrocycles with a palladium catalyst chelating each monomer unit to each other, which traps active catalyst and inhibits further polymerization. It is possible that dinorbornenes are more susceptible to this trap, but this cannot as of yet be confirmed.

Of interest is this catalyst's ability to polymerize styrene with a low PDI. While there is no shortage of transition metal catalysts that can polymerize styrene, this is

certainly a novel result with this system. Further, in one example, a copolymer between styrene and the NB dimethyl ester **6.1** was produced (Scheme 6.4).

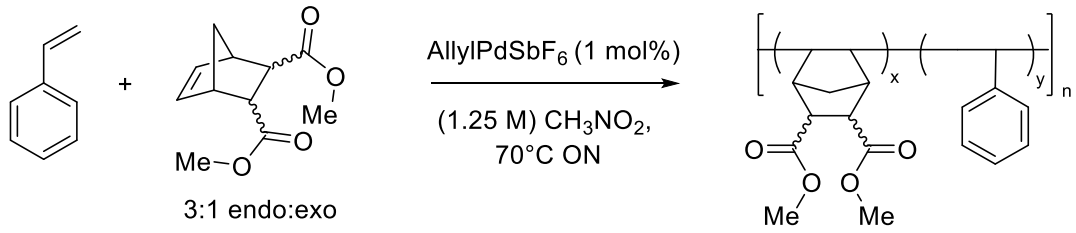

Scheme 6.4: Addition copolymerization of styrene and norbornene.

There are few examples of the reliable addition copolymerization of styrene and norbornenes. While this is not relevant to synthesizing next generation dielectric materials, these copolymers could have very promising properties as a new and unique engineering plastics. Future studies on this type of polymer chemistry are certainly warranted.

In order to assess the viability of benzocyclobutene (BCB) thermosets in norbornene addition polymers, two new addition polymers containing BCB were synthesized. Using monomers **6.19** and **6.21** previously synthesized in Chapter 5, the corresponding addition polymers **6.20** and **6.22** were synthesized and isolated via precipitation into diethyl ether (Scheme 6.5). The two polymers were formulated and thin films were formed via spin coating. Samples were cured under inert atmosphere at 250˚C for one hour, and cure extent was confirmed by differential scanning calorimetry (DSC). Crosslinking was further confirmed as films were rendered insoluble in casting solvents post-cure, whereas pre-cure films and films of norbornene addition polymer **6.4** were dissolved rapidly.

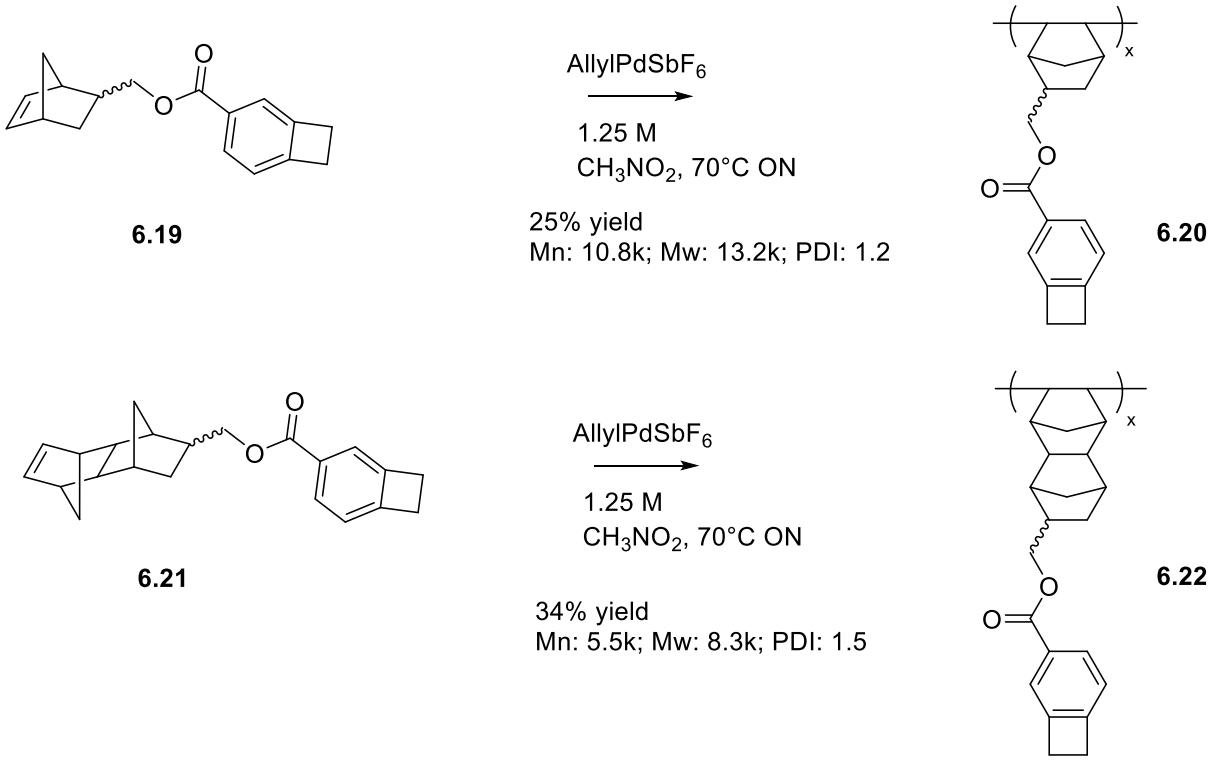

Scheme 6.5: Synthesis of BCB containing addition polymers.

The cured films of polymers **6.20** and **6.22** underwent initial materials evaluation via heated stage ellipsometry as discussed in prior chapters. The out of plane coefficient of thermal expansion (CTE) values were obtained and compared to polymer **6.4** using the same method (Figure 6.2).

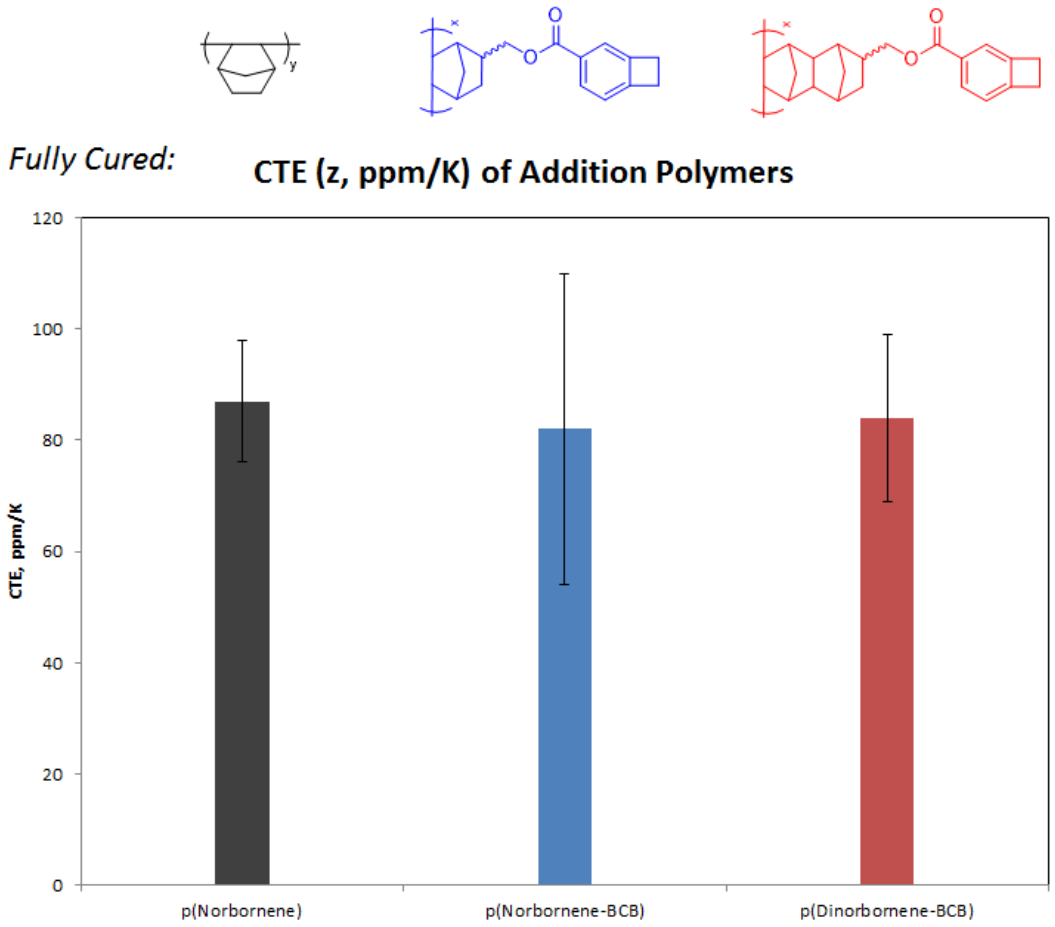

Figure 6.4: CTE values of addition polymers obtained via heated stage ellipsometry.

The results are somewhat disappointing. CTE values obtained were 87 ± 11 ppm/K for PNB **6.4**, 82 ± 28 ppm/K for PNB BCB **6.20**, and 84 ± 17 ppm/K for DNB **6.22**. As one can clearly see in Figure 6.2, there is no statistical difference in these values, although they are almost a factor of two smaller than most ROMP BCB polymers discussed in Chapter 5 and on the order of many of the DNB ROMP BCB polymers also discussed in Chapter 5. What is disappointing is that thermosetting the resin with the relatively costly BCB monomer provided no benefit to CTE values whatsoever. This is consistent with

what has been proposed and observed in Chapters 3 and 5: the [4+2] Diels Alder crosslinking product with BCB and another dieneophile tends to produce the lowest CTE materials, whereas other [4+4] and [4+2] spirocycle products tend to produce higher CTE materials presumably due to an increase of free volume. Ultimately, there appears to be no net benefit to incorporating BCB into addition polymers for next generation packaging materials, especially in light of the low yielding and difficult to optimize nature of addition polymerization.

6.4 CONCLUSIONS

The addition polymerization of norbornene and its derivatives is an interesting and currently underdeveloped tool in polymer chemistry. Currently, the polymerization is restricted by catalysts that have limited shelf life and poor functional group tolerance. Some efforts are reported in this chapter to contribute to the understanding of how the canonical catalyst, η^3-allyl palladium hexafluoro antimonate, could be optimized to increase yields and improve functional group tolerance. As reported in the literature, the catalyst is extremely sensitive to choice of solvent, with nitromethane being the prototypical choice. Previous works have reasoned that the solvent functions solely to solvate the cationic palladium chain end, but it is proposed in this chapter that solvent choice may also have a significant electronic effect on the reaction, as crystal structures have shown solvent coordination to the palladium center. Further, addition solvents were screened that were not reported in the literature. It was found that HFIPA made a suitable alternative solvent to nitromethane.

Further evidence that the electronics of the metal center influence this reaction was found during a study of various phosphine additives. Adding a variety of phosphines produced huge variances in yield, with the highest yield obtained by tris(pentafluoro

benzene) phosphine. Unfortunately, this additive significantly decreased the molecular weight of polymer obtained, even in other monomers besides the model compound **6.1**. While it is clear that phosphine additives have significant effects on the polymerization, it is unclear from these data what the trends are, as none of these additives significantly improve the utility of this catalyst.

Monomer scope was also investigated. Results in this chapter suggest that the majority of norbornenes with polar functional groups can be polymerized, but conditions must be altered significantly for each case in order to obtain useable material. Dinorbornenes were largely inactive with the palladium catalyst, with the exception of MTD and (fortuitously) the BCB containing DNB **6.21**. Since MTD polymerized very rapidly and produced a high molecular weight, low dispersity polymer, the data suggest that polar functional groups are particularly a problem with DNBs. DNBs could be susceptible to forming oligomeric ladders and macrocycles with a palladium in each repeat unit, although this hypothesis cannot be confirmed without the relevant crystallographic data.

Lastly, BCB containing addition polymers were synthesized to compare the effect of incorporating BCB in addition polymers on relevant values to packaging materials, such as CTE. Two successful BCB thermosets were synthesized and crosslinked, however they showed no improvement in CTE compared to non-crosslinked PNB addition polymer. The results can be explained in light of work reported in Chapters 3 and 5. Without any dienophiles other than BCB itself, crosslinking produces very little of the [4+2] crosslink product that is believed to be the lowest CTE crosslink. Addition polymers clearly have low CTE due to their low torsional energy contribution (highly rigid polymers), but without any dienophiles like the ROMP PNB backbone or alkene groups in the POSS resins, the benefit of additional crosslinking is marginalized, as other

[4+4] and [4+2] spirocycle products create free volume in each crosslink. Further, since these types of materials are typically brittle, they are likely to be susceptible to cracking and device failure. In summary, incorporation of BCB into PNB addition polymers does not improve material properties relevant for microelectronics packaging, and other classes of materials should be prioritized for this application.

6.5 Experimental Section

General Procedures:

Size exclusion chromatography (SEC) data were collected with an Agilent 1100 Series isopump and autosampler with a Viscotek Model 302 TETRA detector platform and THF as an eluent at 23°C. Three I-series mixed bed high-MW columns were calibrated relative to PS standards. Thermogravimetry and differential scanning calorimetry were performed using a TA Instrument Q500 TGA and TA Q100 DSC, respectively, each with a 50ml flow rate of nitrogen. DSC method used was a constant heating/cooling rate of 10˚C/minute from 25˚C to 300˚C and back to 25˚C for two cycles. TGA samples were ramped to 1000˚C at 10˚C/minute heating rate under nitrogen atmosphere. All NMR experiments were performed on a Varian 400 MHz spectrometer at ambient temperature. For PNB(dimethyl ester) GPC experiments, a dn/dc of 0.03 was used. Reagents were used as received from Sigma Aldrich or as a donation from JSR. Allyl palladium chloride dimer $[PdCl(C_3H_5)]_2$ and silver hexafluoroantimonate ($AgSbF_6$) were both stored in a glovebox under argon atmosphere. A Brewer CEE 100CB Spincoater was used to coat all thin films. Ellipsometry was performed with a J.A. Woollam Co, Inc. VB 400 VASE Ellipsometer withwavelengths from 382 to 984 nm and a 65° angle of incidence.

Z-axis CTE data was processed using a variable temperature silicon substrate model in CompleteEase software. The data was fit with an ordinary least squares regression and the error bars represent the 95% confidence intervals of the slope of the curve.

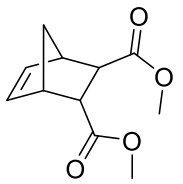

Dimethyl-bicyclo[2.2.1]hept-5-ene-2,3-dicarboxylate: The synthesis of the model compound dimethyl ester was adapted from the literature. Dimethyl maleate (1.05 eq) was placed in a round bottom flask equipped with a stir bar and reflux condenser. Freshly cracked cyclopentadiene (1.0 eq) was added dropwise at room temperature, then the mixture was refluxed for 12 hours. The resulting mixture was distilled under vacuum and the product was isolated as a colorless liquid (bp 150˚C at 5 mmHg, 74% yield.) Compound isolated as 3:1 mixture of endo to exo isomers, and was used as the model compound for all subsequent polymerization studies. ^{1}H NMR (400 MHz, $CDCl_3$) δ 6.26 (t, J = 1.8 Hz, 1H), 6.21 (t, J = 1.9 Hz, 1H), 3.65 (s, 3H exo), 3.61 (s, 3H endo), 3.30 – 3.28 (m, 2H endo bridgehead), 3.16 (dt, J = 3.3, 1.6 Hz, 2H endo α carbon), 3.11 – 3.08 (m, 2H exo bridgehead), 2.62 (d, J = 1.9 Hz, 2H exo α carbon), 2.11 (d, J = 9.1 Hz, 1H exo), 1.47 (m, 1H endo + exo), 1.33 (d, J = 8.6 Hz, 1H endo).

Representative catalyst preparation: Allyl palladium chloride dimer $[PdCl(C_3H_5)]_2$ (100 mg, 1 eq Pd) and silver hexafluoroantimonate ($AgSbF_6$) (230 mg, 1.24 eq Sb) were weighed out under inert argon atmosphere in a glove box, placed in a 20 ml glass vial and removed from the box. To the vial was added nitromethane (10 ml, 0.027 M solution) or chlorobenzene (10 ml, 0.027 M solution); upon addition of solvent silver chloride salt

could be seen precipitating out of solution. A flea Teflon coated stir bar was added to the vial and the solution was stirred for five minutes. The solution was then filtered into a new vial through a 0.2 μm syringe filter to remove the silver chloride, and then the transparent yellow solution was used immediately for polymerization.

Representative Polymerization Procedure:

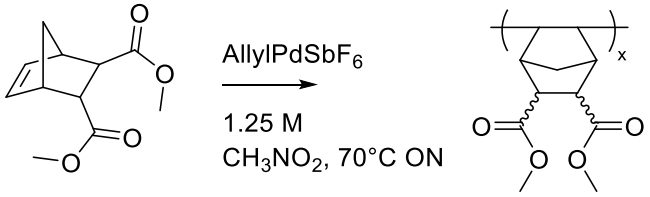

A stock solution of catalyst was prepared as described above. A quartz tube with a magnetic stir bar was charged with monomer (100 eq), nitromethane or desired solvent (1.25 M with respect to monomer), and catalyst solution (0.027 M, 1 eq of Pd). The reaction vessel was then sealed and stirred in an oil bath kept at 70˚C for 24 hours. The polymer was then precipitated by pouring the reaction mixture dropwise into either diethyl ether or methanol. The polymer was filtered, washed with precipitation solvent and then dried under vacuum at 60˚C overnight.

Sample F^{19} NMR Phosphine Ligand Experiment:

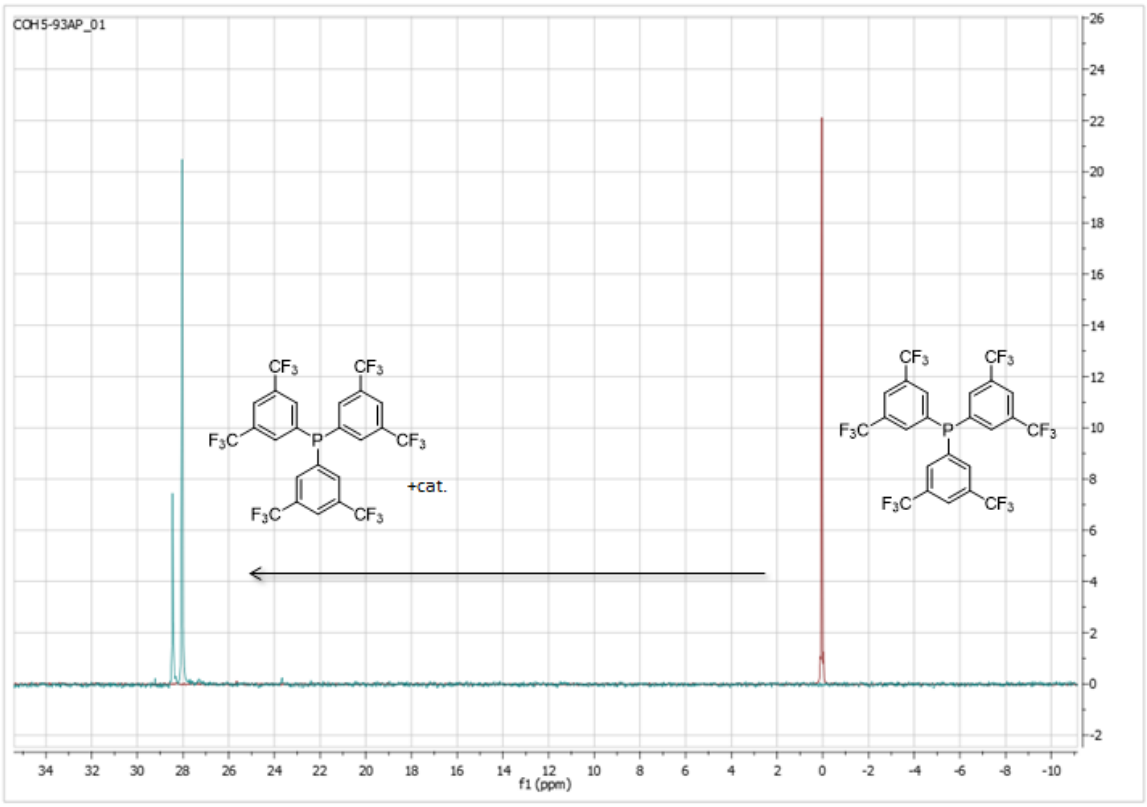

Tris(1,3-trifluormethyl benzene) phosphine was dissolved in CD_3NO_2 and a spectrum was taken (red NMR trace) and a single singlet was observed. The solution was then added to allyl palladium chloride and silver hexafluoro antimonate as per the typical catalyst preparation procedure (see above). The solution was filtered to remove the silver chloride precipitate and the spectrum was taken again. The previous singlet had disappeared and had shifted downfield completely. Also seen is a new singlet, corresponding to the hexafluoro antimonate cation. Results qualitatively support the evidence that the phosphine ligands are interacting with the catalyst.

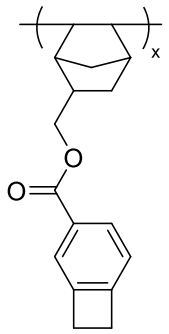

To a 10 ml sealable reaction tube was added a magnetic stir bar and monomer **6.19** (373 mg, 100 eq) and 1 ml of chlorobenzene. Catalyst stock solution (0.49 ml at 0.03M in chlorobenzene) was added and the tube was sealed. The vessel was heated in an oil bath at 70˚C for 12 hours. The tube was then removed from heat and precipitated dropwise into vortexing methanol (100 ml). The polymer was collected via vacuum filtration and dried overnight under vacuum at 60˚C. The polymer was isolated in 25% yield. M_n: 10.8 kDa, M_w: 13.2 kDa, PDI: 1.22. No T_g observed by DSC up to 300˚C.

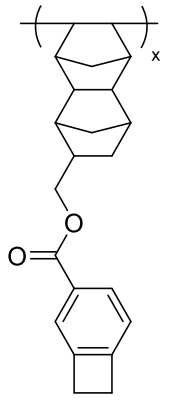

To a 10 ml sealable reaction tube was added a magnetic stir bar and monomer **6.21** (433 mg, 100 eq) and 1 ml of nitromethane. Catalyst stock solution (0.49 ml at 0.03M in nitromethane) was added and the tube was sealed. The vessel was heated in an oil bath at 70˚C for 12 hours. The tube was then removed from heat and precipitated dropwise into vortexing methanol (100 ml). The polymer was collected via vacuum filtration and dried

overnight under vacuum at 60˚C. The polymer was isolated in 34% yield. M_n: 5.5 kDa, M_w: 8.3 kDa, PDI: 1.51. No T_g observed by DSC up to 300˚C.

Chapter 7: High T_g Top Coats for Block Copolymer Lithography

7.1 Introduction

Block copolymer (BCP) self-assembly offers a variety of accessible morphologies[93] with periodicities (L_o) on the order of 10-100 nm[94,95]. BCP self-assembly is an attractive technology for next generation lithography[96], since current 193nm immersion lithography has a resolution limit on the order of about 35 nm. While the prototypical example of a self-assembling BCP is polystyrene-block-polymethylmethcarylate (PS-b-PMMA)[97], a great deal of work has been done recently on the assembly of silicon containing BCPs in order to impart etch selectivity, and therefore make BCPs lithographically useful[98]. The greatest challenge of silicon containing BCP self-assembly is that silicon containing blocks preferentially wet the air interface in thin films, creating parallel morphologies (instead of the lithographically useful perpendicular morphologies)[99]. Thus, Bates et al. designed a methodology of polarity switching top coats which were able to access a range of interfacial energies[100]. These polymers were spin coat-able from methanol as the trimethylammonium (TMA) salts of their ring open anhydrides, thus not disturbing the BCP film stack. Once deposited, the anhydrides underwent ring closing during the high temperature anneal to evaporate TMA and form the polymer of desired interfacial energy. Maher et al. also developed a fast throughput screening method of top coat interfacial behavior through the "Island and Hole" test using a BCP film of thickness incommensurate with its L_o and evaluating morphology using atomic force microscopy (AFM)[101]. Using this method, Maher et al. have been able to orient a variety of silicon containing BCPs of various L_os and high chi (χ).

The top coat work has paved the way for a lithographically useful methodology for processing BCPs, but much work needs to be done before they are the method of choice for manufacturing. Current methods produce the required perpendicular

orientation, but the overall pattern after etching looks like a random fingerprint. Long range orientation of lines and spaces in exact locations will be required for next generation fabrication. Thus, the field of BCP directed self-assembly (DSA) has the goal of combining standard 193nm lithographic techniques with precise thin film engineering in order to surpass the current resolution limits. Current methodology could produce three to six lines on a wafer for every one printed with 193 nm light, a density multiplication of 3-6x.

While DSA looks very promising, challenges are associated with optimizing the process to minimize defects. Current conditions can produce many straight lines and spaces with high density multiplication, but defects are often rampant and their causes are not necessarily understood. Unpublished data obtained by Greg Blachut at Imec in Belgium suggests a strong correlation between higher annealing temperature and high image quality. Unfortunately, current generation top coats de-wet from BCP films when annealing temperature surpasses their T_g (~220˚C), and BCPs intermix with the film stack, causing the DSA process to fail. Thus, a completely new generation of top coats was designed in order to increase T_g while maintaining the required interfacial energy and a polarity switching functional group.

Building off the work described in Chapter 6, this chapter investigates the use of the addition polymerization of norbornene (NB) to form high T_g (>300˚C) copolymers with a polarity switching functionality[102]. In addition, the ring opening metathesis polymers (ROMP) of exo-carbic anhydride and assorted exo-imides were found to have high T_gs (250-280˚C) are were also evaluated to determine their wetting behavior. Results show great difficulty in revamping the materials system: cracking and de-wetting were common occurrences. Only one monomer (MTD) was found to wet the silicon containing block. Unfortunately, creating reproducible copolymers of MTD and a

polarity switching NB proved a challenge due to the highly disparate kinetics of polymerization between monomers.

7.2 Results and Discussion

In order for a high T_g polymer system to work in current thin film processes, polarity switching monomers had to be evaluated. This means that either an anhydride or an acid ester must be able to form a TMA salt, and the resulting polymer must be soluble in methanol. The norbornene selected must also be readily polymerizable and compatible with other "nonpolar" monomers in order to tune interfacial surface energy. The catalyst system used for addition polymerization of norbornenes in this chapter was η^3-allyl palladium hexafluoro antimonate, prepared via the salt metathesis from allyl palladium chloride dimer and silver hexafluoro antimonate. It was chosen due to its relatively low cost, high activity and functional group tolerance. Four candidate monomers were chosen for study based on the aforementioned criteria (Figure 7.1).

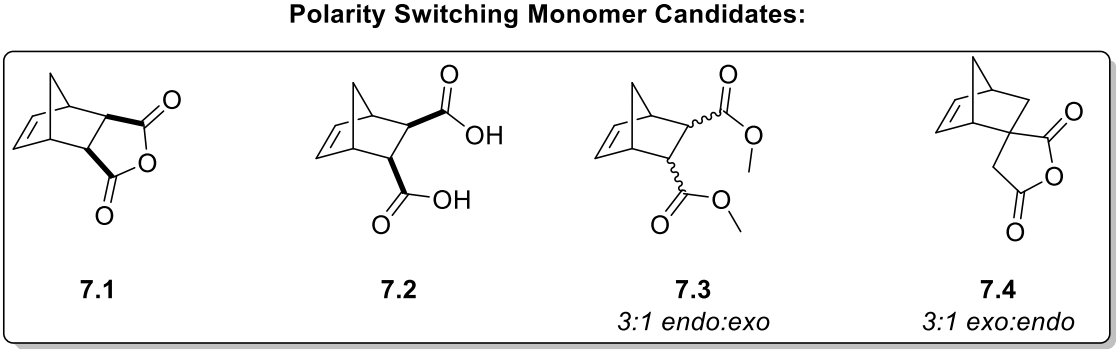

Figure 7.1: Polarity switching monomer candidates for high T_g top coats.

The most obvious candidate is carbic anhydride, the abundant and cheap Diels Alder adduct of cyclopentadiene and maleic anhydride. Unfortunately, the Diels Alder reaction produces exclusively the endo product, which is completely inactive to addition

polymerization. Fortunately the exo product (compound **7.1**) is reactive. Exo carbic anhydride is the thermodynamically favored product of the Diels Alder cycloaddition, whereas the endo compound is the heavily favored kinetic product. Heating molten endo carbic anhydride for an extended period of time (18-24 hours) produces a crude mixture of the exo and endo products. Fortuitously, the exo carbic anhydride can be isolated in large quantities after successive (3 times) recrystallization in benzene (Figure 7.2).

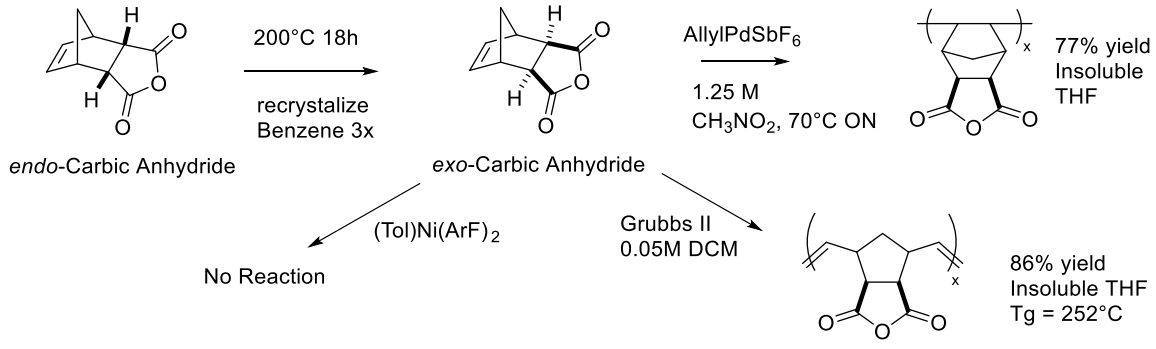

Figure 7.2: Synthesis and reactions of exo carbic anhydride.

Exo carbic anhydride **7.1** proved to be readily polymerizable using palladium catalyzed addition polymerization. The ring opening metathesis polymerization of **7.1** yielded a surprisingly high T_g polymer that also appears potentially suitable for top coat application. Other addition polymerization conditions, such as the popular $(Tol)Ni(ArF)_2$ catalyst, produced no polymer. Addition polymers obtained with a palladium based system, however, could be isolated in high yield and showed no T_g up to 300˚C, making them excellent candidates for high T_g top coats.

Other monomers evaluated included the exo diacid hydrolysis product of exo carbic anhydride (compound **7.2**) and the dimethyl ester **7.3**. The addition polymers of both monomers were synthesized, but their TMA salts were not readily soluble in

methanol (further, the TMA salt of the addition polymer of **7.3** often did not form). Consequently, these monomers which are basic and theoretically capable of a polarity switch, were not investigated further.

The Diels Alder product of cyclopentadiene and itaconic anhydride **7.4** proved to be a very interesting candidate for polarity switching top coats. The monomer is readily synthesized in a ratio of 3:1 exo to endo isomers, and the addition polymerization proceeds in high yields[103]. The TMA salt is easily formed and very soluble in methanol; methanol solutions also spin coat very well, producing uniform films with relative ease. Due to the high quality of films obtained, the NB itaconic anhydride addition polymer was chosen for a thin film transmission FTIR study of the polarity switching behavior and the data are shown in Figure 7.3.

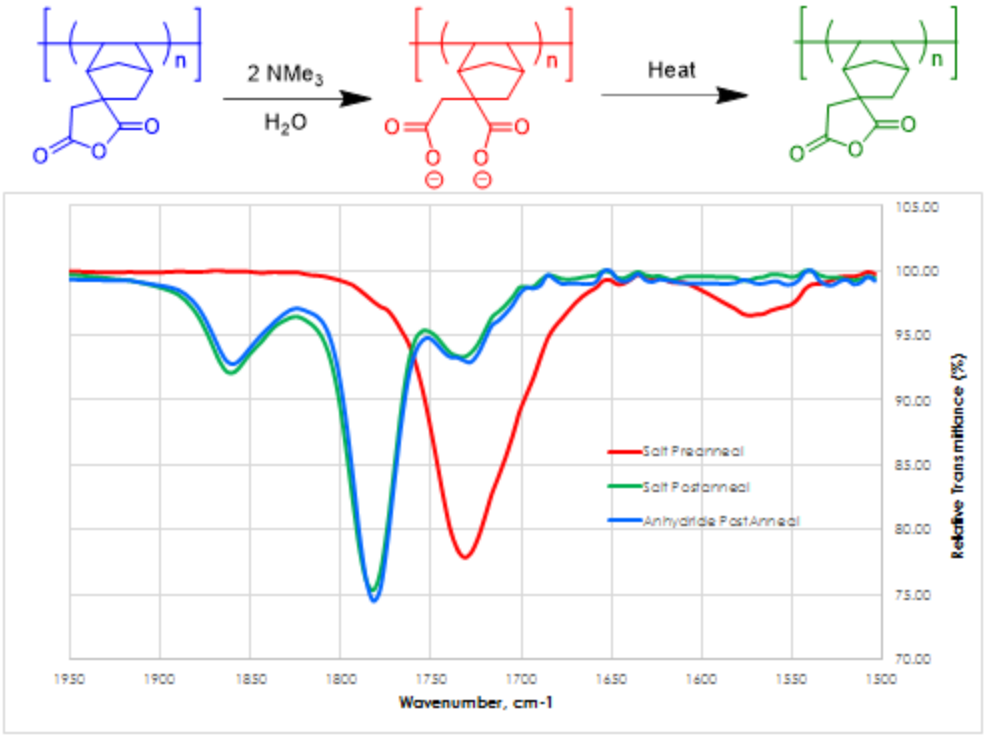

Figure 7.3: Thin film FTIR study (transmittance) of the homopolymer of NB itaconic anhydride (blue), the TMA salt (red, TMA counter-ions omitted for clarity) and the TMA salt after a post bake.

The FTIR spectrum of the homopolymer clearly shows both the carbonyl C=O stretch at around 1780 cm^{-1} and the distinctive anhydride asymmetric stretch at about 1860 cm^{-1}. The TMA salt shifts the carbonyl C=O stretch to 1730 cm^{-1} while (importantly) the asymmetric stretch that designates the presence of an anhydride functionality is completely gone. Upon heating, the anhydride is reformed and TMA is evaporated, and the resulting green trace in Figure 7.3 overlaps with the homopolymer and shows the reappearance of the asymmetric anhydride stretch. From these results, one can conclude that the NB itaconic anhydride addition polymer is a suitable polarity switching candidate for a top coat application.

Next, it is important to determine the wetting behavior of the NB itaconic anhydride addition polymer. A comprehensive analytic method for determining which block wets a surface was developed by Maher et al.[100] That work shows that thin films of block copolymers of thicknesses incommensurate with their L_0 form microstructures aptly named islands (for bumps) and holes (for depressions) in the thin films when annealed. In all experiments in this chapter, a crosslinked polystyrene mat was used as the surface treatment (preferring to wet the polystyrene block). PS-b-TMSS block copolymer (22 nm L_0 spun at approximately 1.2 L_0 thickness), and unless otherwise noted a confined island/hole test was performed by coating the TMA salt of the top coat in question, annealed to close the anhydride and orient the BCP. The top coat was then stripped in TMA and island or hole topology was confirmed by optical microscopy or atomic force microscopy (AFM). Conditions produced holes (white dotes on optical microscope), suggested that the polymer preferred to form a surface with the polystyrene block, rather than the silicon containing block. If the test produced islands (dark spots on optical microscope), this suggested that the polymer in question preferred to wet the silicon containing block. Generally speaking, it has been observed that more polar

monomers tend to favor interaction with styrene, while more nonpolar monomers tend to favor interaction with the silicon containing block.

The polar anhydride containing monomers were expected to wet the more polar polystyrene block. As expected, when the addition polymer of NB itaconic anhydride was tested, the BCP produced holes, indicating a preference for PS (Figure 7.4).

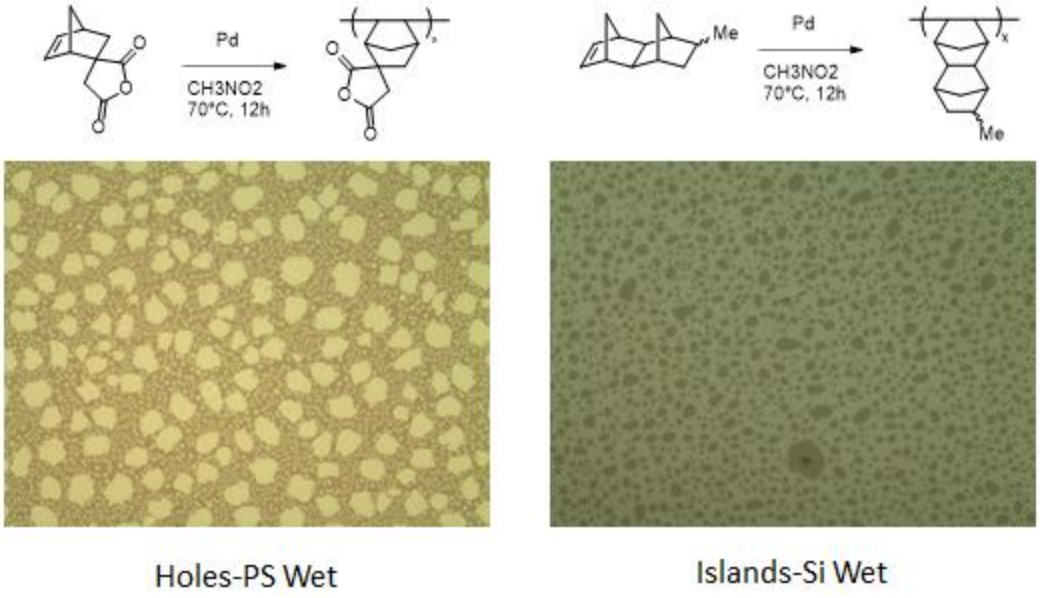

Figure 7.4: Optical micrographs of annealed BCP using both NB itaconic anhydride and MTD addition polymers as surface treatments. The tests were performed at 1.2 L_0 of BCP, annealing for ten minutes at 190˚C.

The addition polymer of MTD was found to wet the silicon containing block (Figure 7.4, right). To the best of this author's knowledge, this is the only norbornene derived monomer known to wet the silicon containing block of a BCP.

An ideal surface treatment would be some copolymer of the NB itaconic anhydride and the nonpolar MTD. In theory, some intermediate composition would produce a neutral surface: an interface at which neither block of the BCP prefers to wet

the surface, resulting in a perpendicular orientation useful for BCP lithography and DSA (Figure 7.5).

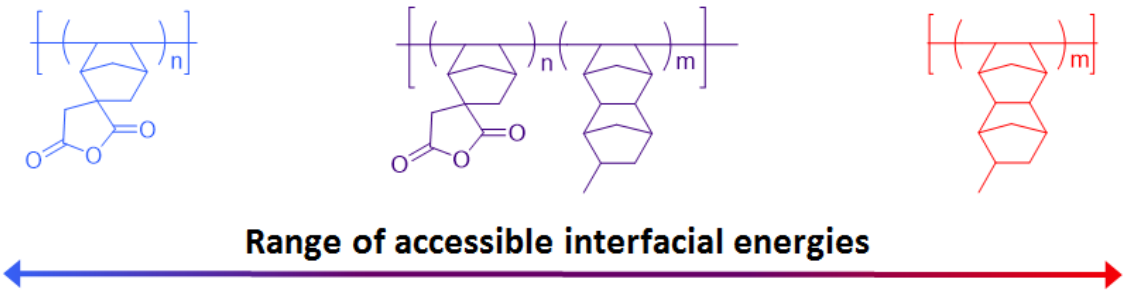

Figure 7.5: Visualization of surface energy composition. Whereas homopolymers of NB itaconic anhydride (left, blue) and MTD (right, red) represent polar and nonpolar surfaces, a copolymer (middle, purple), should have an intermediate, neutral energy at the surface.

The next phase of the project involved attempting to synthesize and characterize copolymers of MTD with a polar anhydride capable of undergoing a solubility switch. Attempts were made to compolymerize MTD and the NB dimethyl ester **7.3**. The results were disappointing, as GPC traces of the resulting polymers revealed a bimodal distribution, suggesting two homopolymers were synthesized instead of one copolymer.

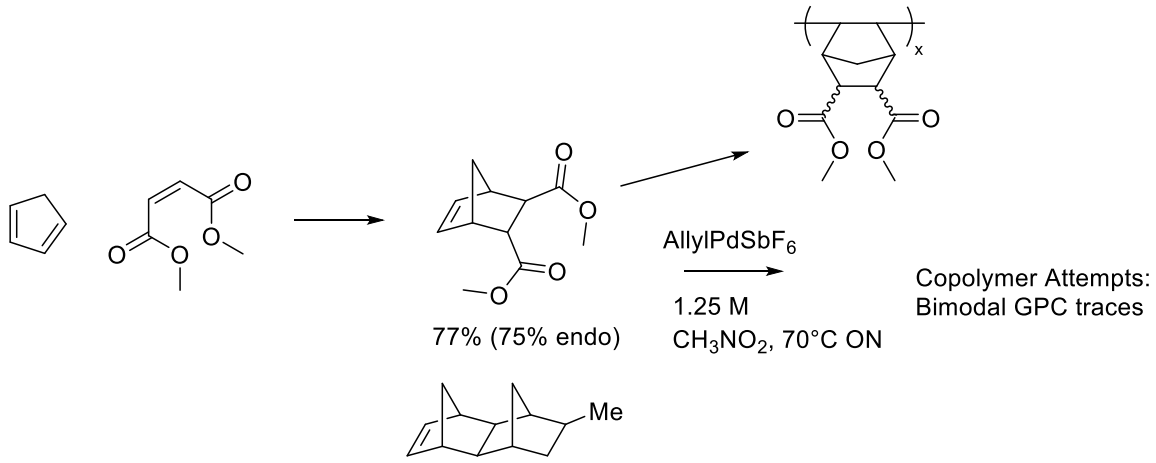

Scheme 7.1: Synthesis of NB dimethyl ester and attempted copolymerization.

Attempts to synthesize a copolymer between MTD and the NB itaconic anhydride **7.4**, however the reactions were not successful. Whenever polymerization was attempted, the resulting crude mixture contained unreacted **7.4** and homopolymer of MTD (Scheme 7.2).

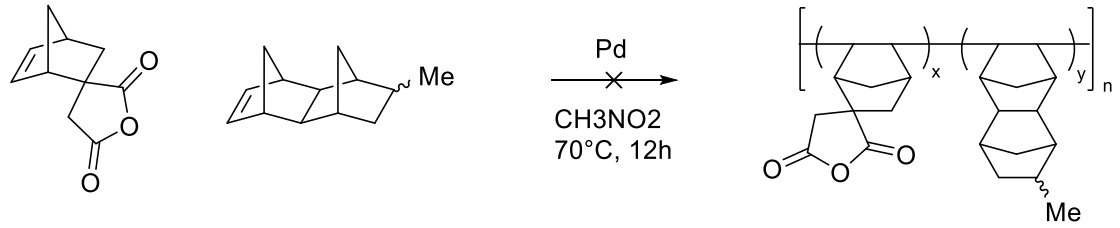

Scheme 7.2: Attempted synthesis of MTD and NB itaconic copolymers. Only MTD homopolymer was isolated.

Individually, homopolymer of NB itaconic anhydride can be obtained in high yields. The lack of reactivity in the copolymerization may stem from the fact that the MTD monomer reacts significantly faster than itaconic monomer, resulting in Pd-terminated MTD homopolymer chains. These data suggest the rate of reaction between MTD terminated polymer and itaconic monomer is also very slow. Otherwise, one

would expect some consumption of itaconic anhydride to form a sort of block copolymer. Indeed, in experiments where MTD homopolymer was synthesized, complete conversion was often observed on timescales of less than one hour, whereas the homopolymerization of NB itaconic anhydride required 12-24 hours to reach yields greater than 50%.

It is known that in order to reproducibly produce top coats that align BCPs, a controlled microstructure is needed (the best systems are styrene-maleic anhydride radical copolymerizations, where it is well known that styrenes and maleic anhydrides produce a polymer with an alternating microstructure. It was found that random copolymerizations that produce more gradient like microstructures could not reproducibly generate useful materials). This necessitates a brief discussion of reactivity ratios.

7.3 The Terminal Model of Copolymerization

A polymerization between two monomers M_1 and M_2 (in this chapter MTD and an anhydride containing monomer, respectively) has four different propagating reactions one must consider and four rate constants for each as follows.

$$-M_1* + M_1 \xrightarrow{k_{11}} -M_1M_1* \tag{7.1}$$

$$-M_1* + M_2 \xrightarrow{k_{12}} -M_1M_2* \tag{7.2}$$

$$-M_2* + M_1 \xrightarrow{k_{21}} -M_2M_1* \tag{7.3}$$

$$-M_2* + M_2 \xrightarrow{k_{22}} -M_2M_2* \tag{7.4}$$

Each equation (7.1-4) describes a scenario where a reactive end of the polymer chain (in this case, a palladium terminated end) with a certain monomer reacts differently with itself or another monomer at two distinctive rates. This model is called the Terminal Model (also referred to as the Mayo-Lewis equation), in which the last monomer on the chain controls the rates of the next propagation step. The notable exception is referred to

as the Penultimate Model, where the monomer unit prior to the reactive end (the penultimate monomer, if you will) has a significant effect on the rates of propagation. For example, equation 7.1 would become:

$$-M_1M_1* + M_1 \xrightarrow{k_{111}} -M_1M_1M_1* \tag{7.5}$$

This is only significant in a few cases. Using the terminal model is often sufficient. While there are four different rate constants for propagation, ultimately the relative amounts of monomer incorporated into the polymer involves only two pairs of these constants. These are referred to as the reactivity ratios.

$$r_1 = \frac{k_{11}}{k_{12}} \tag{7.6}$$

$$r_2 = \frac{k_{22}}{k_{21}} \tag{7.7}$$

This leads to the following scenarios:

1. If $r_1 \approx r_2 \gg 1$, the monomers prefer to only react with themselves and this results in a mixture of two homopolymers.
2. If $r_1 \approx r_2 > 1$, then the homopolymerization of M_1 (and M_2) is favored but in the event of chain transfer will give rise to a block copolymer.
3. If $r_1 \approx r_2 \approx 1$, then M_1 will react as fast with itself as M_2 and vice versa, resulting in a random copolymer.
4. If $r_1 \approx r_2 \approx 0$, then both monomers prefer to react with each other rather than themselves, resulting in an alternating polymer. Maleic anhydride (r_1 = 0.01) and styrene (r_2 = 0.02) is a classic example of this case.
5. If $r_1 \gg 1 \gg r_2$, then in the early stages of the polymerization M_1 is incorporated much faster than M_2. When M_1 gets depleted, the end of the chains mostly become composed of M_2 resulting in a gradient polymer.

Ultimately an ideal chemistry would have either $r_1 \approx r_2 \approx 0$ or $r_1 \approx r_2 \approx 1$. The challenge of reproducible top coats is in the last case (#5) where a gradient polymer is produced. If the chemistry produces a gradient, it may be possible to use a semi-batch reactor and carefully tailored rates of addition in order to create a random copolymer, but this complicates the operation significantly.

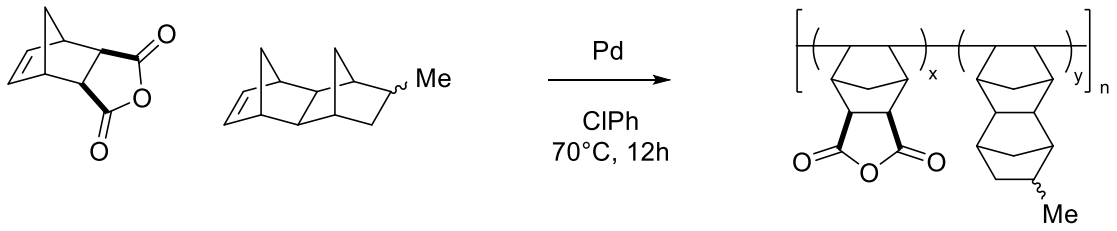

Scheme 7.3: Synthesis of a CA and MTD addition copolymer.

A batch copolymerization of the exo carbic anhydride **7.1** and MTD run in chlorobenzene produced a copolymer that contained some of the CA monomer by FTIR. CA **7.1** also has the potential advantage for this application of being isolated as one isomer (for the NB itaconic anhydride, the endo and exo isomers cannot be separated easily, and it is well known that addition polymerization rates are vastly different, complicating the model kinetics and semi-batch equations greatly). In order for reactivity ratios to be estimated, there must be a reliable and accurate way of determining the relative composition of monomer in the final monomer, which is this case proved to be challenging.

Proton NMR was the first and most obvious analytical method, but spectra obtained had no easily resolved peaks to provide a reliable quantification. Carbon NMR provided some promise. The anhydride peaks of **7.1** are easily resolved in the downfield region of the spectra, and while MTD is obtained in a 2:1 isomer ratio of endo and exo

methyl groups, the methyl shifts are well resolved and far upfield in the spectrum (~20 ppm), and are highlighted in Figure 7.6 (the C^{13} spectrum of MTD).

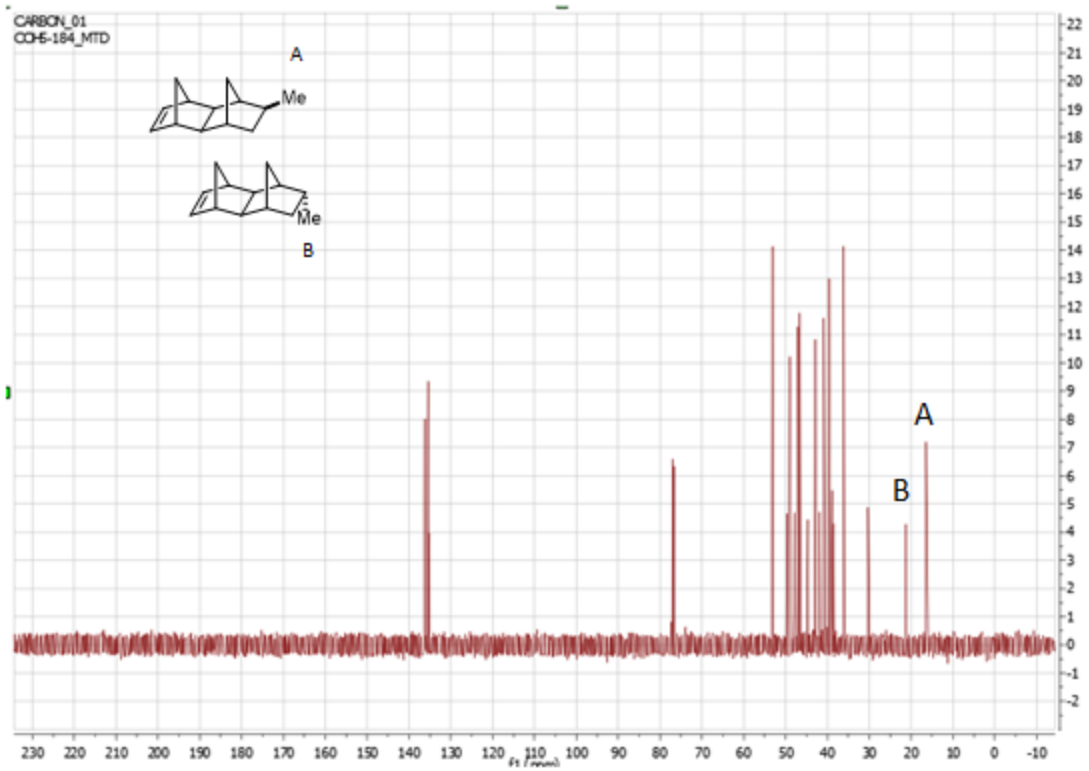

Figure 7.6: Carbon NMR spectrum of MTD monomer. Methyl resonances are highlighted (relative isomers are proposed). Methyl resonances assigned were consistent with a 2:1 ratio in the proton NMR and HSQC.

These data appeared promising at first, but ultimately the approach suffered from the poor solubility of the addition polymers of MTD and exo CA in common NMR solvents. Saturated solutions of the addition polymers produced weak signals in the carbon NMR, not enough signal to measure the relaxation delay required for a quantitative carbon NMR experiment. Ultimately, this method was not viable for determining monomer composition.

Further attempts at quantification of monomer incorporation included combustion analysis, but the samples run at UT Austin and Midwest Microlabs did not produce data that provided interpretation of monomer ratio. Unfortunately, the polymers with CA feed ratios of 80, 50 and 20 percent failed to dissolve in TMA even at high temperatures (100˚C) for extended times (24-48 hours). These results suggest that whatever the degree of incorporation of CA was in the polymer, it was insufficient to render the material soluble in orthogonal solvents, meaning that there is little chance that these MTD containing polymers could be viable materials for BCP top coats.

One additional attempt was employed to make a viable addition polymer top coat. Since it is well established that silicon containing blocks often wet surfaces containing tertiary butyl groups, and tertiary butyl imides have been successfully incorporated in prior top coat systems, a new polymer was proposed consisting of CA **7.1**, and the corresponding tertiary butyl imide **7.5** (synthesized in one step from CA). It was proposed that since both compounds are chemically similar (in the sense that they are both contain exclusively exo polar five membered rings), they would have similar rates of propagation, and the reactivity ratios of this system might resemble case #3 where $r_1 \approx r_2 \approx 1$ producing close to a random copolymer without having to resort to a semi-batch reactor preparation. The synthesis of tert-butyl imide monomer and the addition copolymers are outlined in Scheme 7.4.

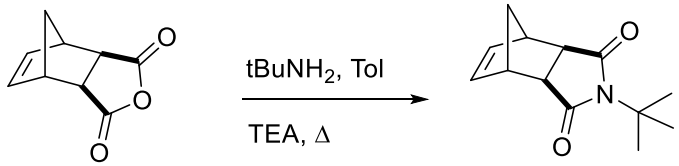

7.1 **7.5**

(Scheme 7.4 continued on next page)

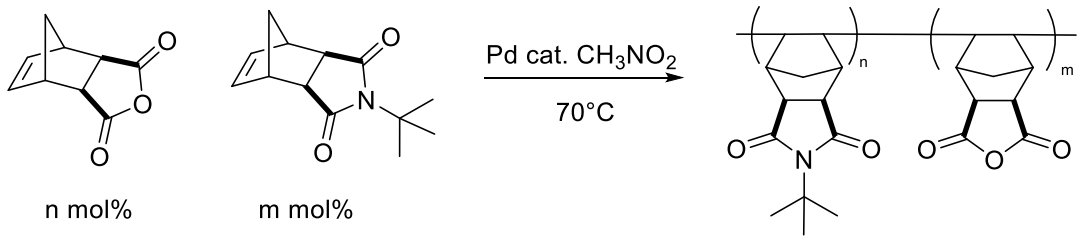

Scheme 7.4: Synthesis of the nonpolar tert-butyl imide analogue of CA and the resulting addition copolymers.

Several addition copolymers readily dissolved in TMA and methanol. These top coats were cast over a standard silicon containing BCP (L_0 = 22 nm) and the confined island/hole test was performed to determine wetting behavior (Table 7.1).

Imide Feed (mol%)	Anhydride Feed (mol%)	Which Block Wets (PS/TMS)	T_g
20	**80**	**Dewet/Cracking**	**>300˚C**
30	**70**	**Dewet/Cracking**	**>300˚C**
40	**60**	**Dewet/Cracking**	**>300˚C**
80	**20**	**Insoluble in TMA**	**>300˚C**
100	**0**	**Insoluble in TMA**	**>300˚C**

Table 7.1: Evaluation of addition polymer topcoats for BCP lithography. TMA salt top coats did not produce discernable island or hole features in thin films, behavior consistent with dewetting.

Unfortunately, neither islands nor holes formed when the BCPs were annealed at 190˚C. The top coats appeared to dewet and crack (Figure 7.7).

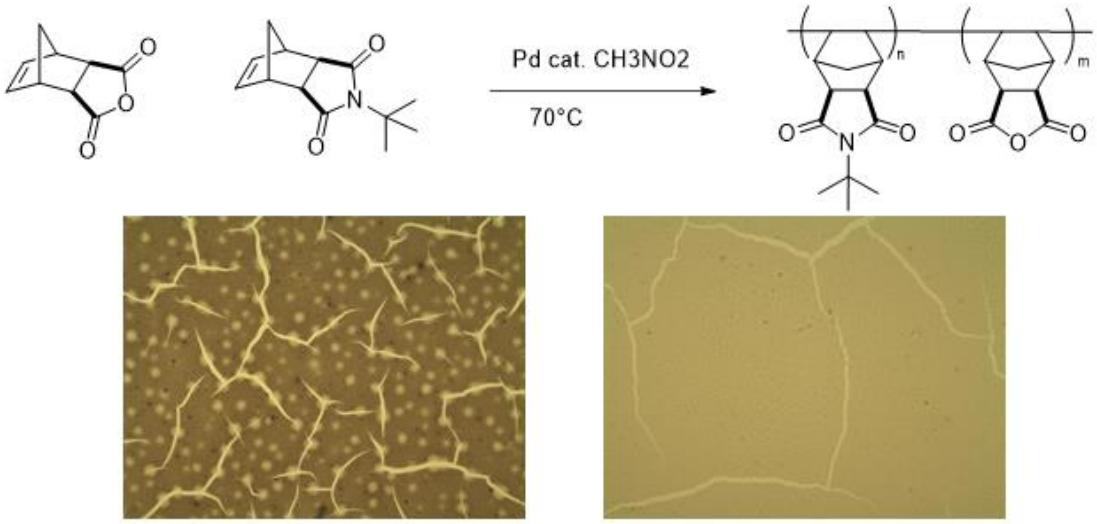

Figure 7.7: Optical micrographs of the confined island/hole test using addition polymer top coats. Cracking throughout the film is readily observed.

The cracking is not too surprising, in light of the fact that addition polymers of norbornene typically have low elongation to break. In conclusion, addition polymerization top coats have attractive properties for a lithographical application including high T_gs and the ability to spin coat out of methanol. There are still problems that remain to be overcome, however. This chemistry tends to rarely produce a controlled microstructure. Work on the kinetics of this polymerization is still required. Another challenge is that the elongation to break of these materials remains substandard for the annealing step.

7.4 High T_G ROMP Top Coats for BCP Lithography

Ring opening metathesis polymerization (ROMP) is a well-established method of creating high molecular weight, kinetically living polynorbornenes. This style of polymerization has been discussed in previous chapters. One might overlook ROMP as a method for synthesizing high T_g top coats since the most common ROMP polymers of

PNB have T_gs on the order of 50-60˚C, well below the current generation styrene-maleic anhydride top coats that have T_gs on the order of 200-220˚C. However, it was found that the ROMP product of exo CA **7.1** produced an unexpectedly high T_g polymer (~250˚C, refer back to Figure 7.2). In light of this result, two new top coat systems were synthesized based on this observation.

The first system is the ROMP analogue of the previous addition polymer. It was produced by copolymerizing **7.5** with **7.1** using Grubbs Second Generation catalyst in dimethylformamide (DMF) as shown in Scheme 7.5.

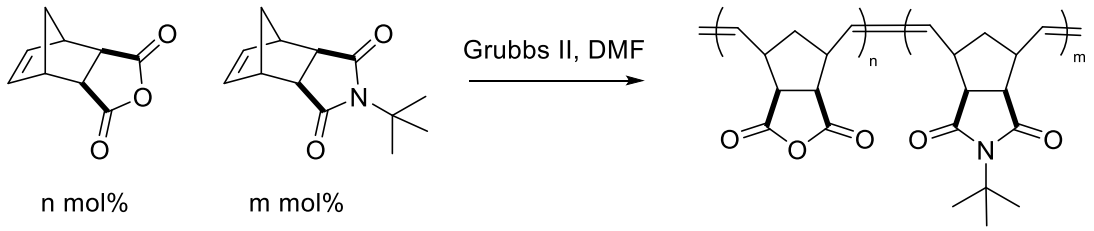

Scheme 7.5: Synthesis of first ROMP high T_g top coats.

Imide Feed (mol%)	Anhydride Feed (mol%)	Which Block Wets (PS/TMS)	T_g
20	**80**	**PS**	**302˚C**
50	**50**	**PS**	**274˚C**
80	**20**	**PS**	**233˚C**

Table 7.2: Top coat evaluation of first ROMP high T_g top coats.

These ROMP top coats dissolved in TMA solution. They were concentrated down to a plastic transparent solid, and then re-dissolved in methanol. These solutions were spun onto BCPs and the confined island/hole test was performed, the results of which are

displayed in Table 7.2. The copolymers possessed T_gs as high as 302˚C, but the T_g was strongly a negative function of **7.5** incorporated in the polymer (needed to attempt to wet the silicon containing block). When the amount of **7.5** in the feed reached 80%, the T_g had dropped precipitously to 233˚C, making any benefit in increased annealing temperature marginal at best. Furthermore, all three top coats synthesized were found to universally wet the more polar polystyrene surface via the confined island/hole test. Non were sufficiently "non-polar" to wet the silicon containing block.

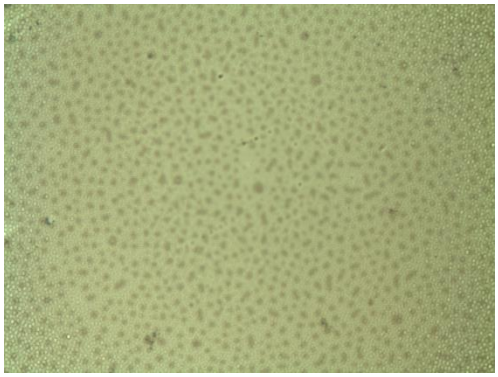

Figure 7.8: Sample micrograph of confined island/hole test for first ROMP top coat series. With 1.2 L_0 BCP thickness on SiO_2: confined islands suggest preferential PS wetting behavior.

These results suggest that the ROMP top coats have largely solved the problem of dewetting and cracking, but they lack the ability to wet the silicon block and polymer T_gs are both high and highly variable.

In order to better wet the silicon block (and thus access an energetically neutral top coat), a second series of ROMP top coats were synthesized. While tertiary butyl groups have been found in top coats that wet the silicon containing block, the 3,5(ditertbutyl benzene) functionality has been found to be even more preferential for

silicon than ordinary tertbutyl groups. In an attempt to produce a more "nonpolar" ROMP top coat, a new exo CA imide analogue was synthesized (**7.6**, Scheme 7.6).

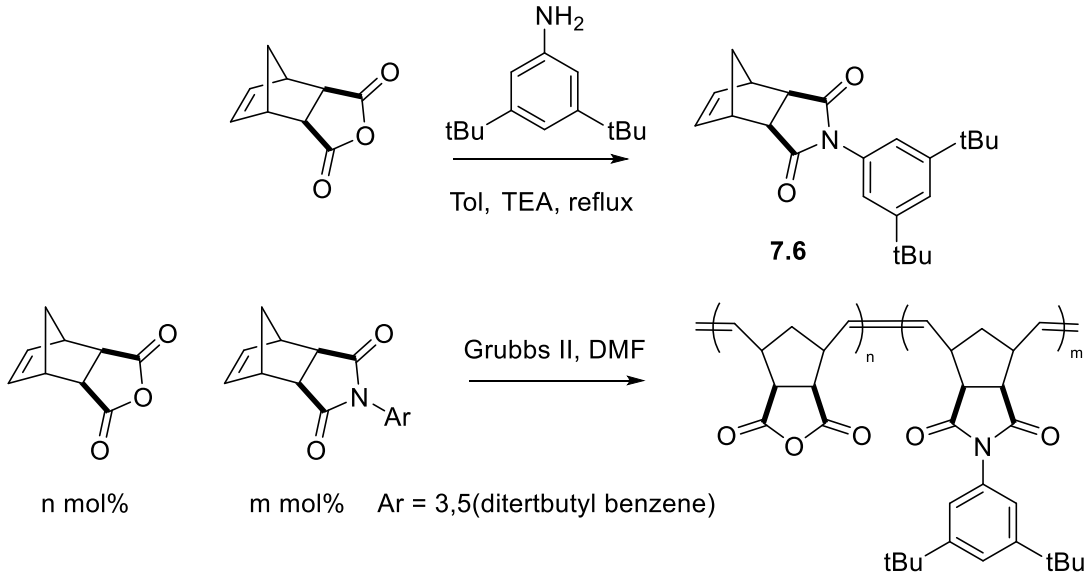

Scheme 7.6: Synthesis of the 3,5-(ditertbutyl benzene) analogue of exo CA, and the corresponding ROMP top coat polymers.

The second attempt at a high T_g ROMP top coat suffered from nearly the same problems as the previous entry. This time the nonpolar monomer component decreased the T_g of the polymer even more than the previous tertiary butyl imide ROMP polymers.

Imide Feed (mol%)	**Anhydride Feed (mol%)**	**Which Block Wets (PS/TMS)**	**T_g**
20	**80**	**PS**	**284˚C**
30	**70**	**PS**	**274˚C**
50	**50**	**PS**	**243˚C**
100	**0**	**N/A**	**226˚C**

Table 7.3: Evaluation of diteributyl imide ROMP copolymers. High T_gs were largely observed, but unfortunately no top coat could wet the silicon containing block.

The evaluation of the ditertibutyl top coat system is shown in Table 7.3. Once more high T_gs could be obtained (up to 284˚C) but with increasing amounts of monomer **7.6**, the T_g was depressed significantly. Polymer containing 50% feed of **7.6** has a T_g of only 243˚C, and still was not "nonpolar" enough to wet the silicon block. At this point, any polymer that incorporated more of **7.6** in an attempt to wet the silicon block would have a T_g too low to provide any DSA benefit over current generation top coats.

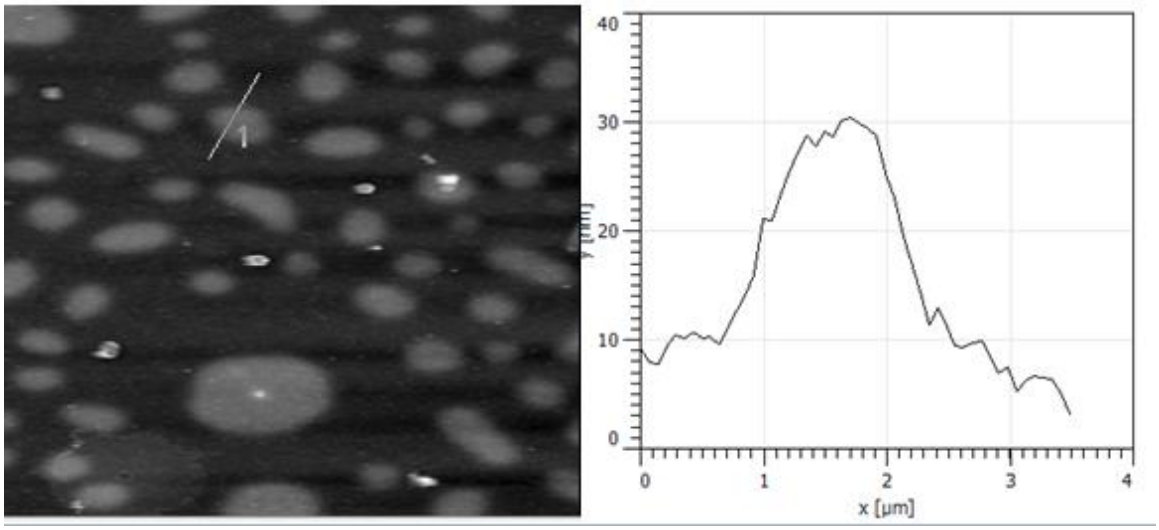

Figure 7.9: AFM data of confined island hole test of second series of ROMP high T_g top coat. At a BCP thickness of 1.2 L_0 on SiO_2 island features correspond to a PS preferential top coat.

7.5 CONCLUSION

Ultimately, the quest to synthesize high T_g top coats for block copolymer lithography was an endeavor fraught with unexpected challenges. There are several variables to juggle: 1) reliable chemistry to synthesize polymers with high T_gs, 2) incorporation of a polarity switching anhydride functionality, 3) incorporation of a monomer that wets the silicon containing block of a BCP, 4) solubility in a spin coating solvent orthogonal to the BCP, and 5) batch to batch reproducibility. As one goes down

the list, the options available to a polymer chemist dwindle rapidly. In this chapter, two different "flavors" of polarity switching high T_g top coats have been evaluated, both derived from norbornene: addition polymers and ROMP polymers.

At first glance, it appeared that addition polymerization of norbornenes would be an excellent method to approach high T_g top coats. After all, norbornene addition polymers typically have T_g's in excess of 300˚C, and often don't melt up to their thermal decomposition. Further, a plethora of monomers are available commercially and more can be synthesized via Diels Alder reactions. However, very quickly it became apparent that there was a lack of silicon wetting "nonpolar" norbornene derived compounds. In fact, only one norbornene compound in Chapter 7 was able to wet the silicon surface: MTD. At first glance, it seemed victory was assured: after all, at least two polarity switching norbornenes (the carbic and itaconic anhydrides **7.1** and **7.4**, respectively) could be readily polymerized with the allyl palladium catalyst system.

But alas, results described in this chapter suggest that the kinetics of propagation between MTD and its polar norbornene counterparts are so disparate that it is improbable that semi-batch procedures can be employed to reproducibly create a more random copolymer. Even if one could control the kinetics of the polymerization, addition polymers with high feeds of carbic anhydride were still insoluble in TMA, meaning so little anhydride is incorporated into the polymer that there is not enough salt per chain to render the material soluble. Unfortunately, this likely excludes MTD copolymers as a viable top coat candidate.

The other addition polymer synthesized successfully formed the TMA salt, but cracked when annealed on top of BCP in a film stack. Addition polymers of norbornenes, while known for their high modulus, are also brittle. So brittle, in fact, that

cracking was even observed in this thin film application. The results suggest that cracking may be a critical failure point of this type of chemistry for top coat application.

An alternative approach to the addition polymers, ROMP top coats based on exo carbic anhydride **7.1** had surprisingly high T_gs and were investigated to overcome the cracking issue. While ROMP top coats didn't crack, no monomers were found that could successfully wet the silicon block (MTD-co-CA ROMP polymers were found to have T_gs too low to be useful). While these materials ultimately came up short, they make excellent TMA salts and are synthesized easily. If a silicon wetting monomer can be found that does not significantly depress the T_g of these ROMP polymers, this system has the best success of synthesizing a useable top coat in the future.

7.6 Experimental Section

General Procedures:

Size exclusion chromatography (SEC) data were collected with an Agilent 1100 Series isopump and autosampler with a Viscotek Model 302 TETRA detector platform and THF as an eluent at 23°C. Three I-series mixed bed high-MW columns were calibrated relative to PS standards. A Brewer CEE 100CB Spincoater was used to coat all thin films.. Thermogravimetry and differential scanning calorimetry were performed using a TA Instrument Q500 TGA and TA Q100 DSC, respectively, each with a 50ml flow rate of nitrogen. DSC method used was a constant heating/cooling rate of 10˚C/minute from 25˚C to 300˚C and back to 25˚C for two cycles. TGA samples were ramped to 1000˚C at

10˚C/minute heating rate under nitrogen atmosphere. Thin film IR transmission spectra were collected on a Nicolet Avatar 360 FT-IR.

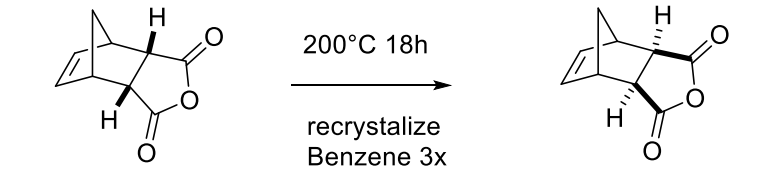

endo-Carbic Anhydride *exo*-Carbic Anhydride

A 500 ml rbf was half filled with the commercially available endo-carbic anhydride (200 g), fitted with a refux condenser and heated to 200˚C for 16 hours. The resulting yellow molten material was allowed to cool to about 75˚C and benzene was then added until dissolution was complete. The mixture was recrystallized at room temperature. The crystals were collected via vacuum filtration, and the process was repeated twice to yield a colorless crystalline solid as the pure exo compound (about 30 g isolated, 15% yield). H^1 NMR ($CDCl_3$): δ (ppm): 6.31 (2H, t), 3.43 (2H, s), 2.99 (2H, s), 1.65 (1H, m), 1.42 (1H, m).

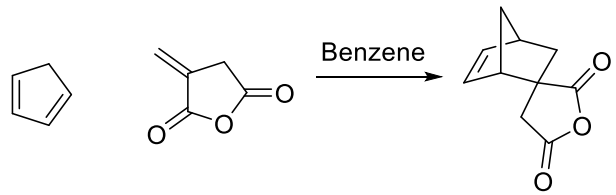

Cyclopentadiene was collected by cracking dicyclopentadiene at 180˚C (36.3g, 1.5 eq) and was added to itaconic anhydride (41g, 1 eq) in benzene (80 ml) at room temperature

in a 250 ml rbf equipped with a magnetic stir bar. The flask was sealed with a rubber septum and nitrogen balloon and stirred overnight. The crude mixture was precipitated from petroleum ether to obtain the desired product (52.8 g, 81%) as a colorless solid, a 3:1 mixture of exo to endo. MP: 53-54˚C. ^{1}H NMR (400 MHz, CDCl3): 6.46 (1H, dd, 5.8 Hz, 3.1 Hz), 6.40 (1H, dd, 5.8 Hz, 3.1 Hz), 6.20 (1H, dd, 5.8 Hz, 3.1 Hz), 6.07 (1H, dd, 5.8 Hz, 3.1 Hz), 3.16 (1H, d, 18.6 Hz), 3.11 (1H, m), 3.10 (1H, m), 2.96 (3H, m), 2.82 (1H, d, 19.2 Hz), 2.65 (1H, d, 19.2 Hz), 2.52 (1H, dd, 11.9 Hz, 3.7 Hz), 2.15 (1H, d, 9.2 Hz),1.92–1.85 (2H, m), 1.68–1.66 (1H, m), 1.56–1.53 (1H, m), 1.44 (1H, d, 8.9 Hz), 1.31 (1H, dd, 11.9 Hz, 3.1 Hz).

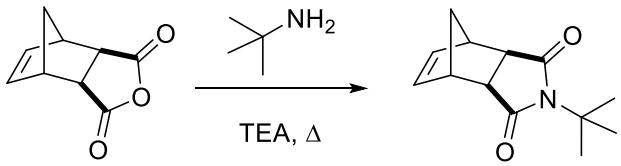

To a 50 ml rbf equipped with a magnetic stir bar was added toluene (18 ml), exo-carbic anhydride (2.539 g, 1 eq), tert-butyl amine (1.63 ml, 1 eq), and triethylamine (0.224 ml, 0.1 eq). The reactor was equipped with a reflux condenser and sealed with a nitrogen balloon and a rubber septum, then refluxed for 3 hours. The reaction was concentrated *in vacuo* and then recrystallized in ethanol to produce a slightly off yellow crystalline solid (1.6 g, 47%). MP: 124-126˚C ^{1}H NMR (400 MHz, $CDCl_3$) δ 6.33 (m, 2H), 3.41 – 3.37 (m, 2H), 2.83 (d, J = 1.3 Hz. 2H), 1.65 – 1.58 (m, 1H), 1.50 (m, 1H), 1.31 (s, 9H). ^{13}C NMR (101 MHz, $CDCl_3$) δ 179.3, 137.8, 58.4, 47.4, 45.7, 42.6, 28.4.

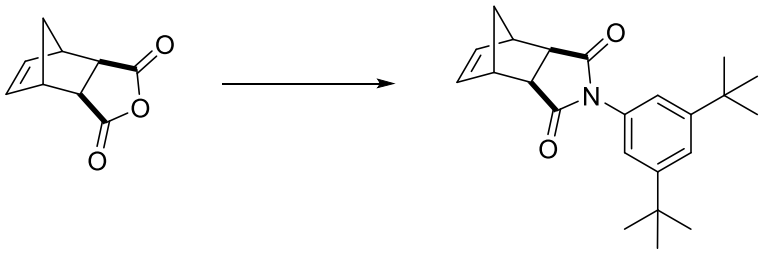

To a 50 ml rbf equipped with a magnetic stir bar was added toluene (15 ml), exo-carbic anhydride (3.137 g, 1 eq), ditert-butyl aniline (3.9 g, 1 eq), and triethylamine (0.28 ml, 0.1 eq). The reactor was equipped with a reflux condenser and sealed with a nitrogen balloon and a rubber septum, then refluxed for 3 hours. The reaction was concentrated *in vacuo* and then recrystallized in ethanol at -78˚C (for about 1 hour) to produce a slightly off yellow crystalline solid (3.49 g, 52%). MP: 96-98˚C ^{1}H NMR (400 MHz, $CDCl_3$) δ 7.42 (t, J = 1.8 Hz, 1H), 6.99 (d, J = 1.8 Hz, 2H), 6.33 (t, J = 1.8 Hz, 2H), 3.41 – 3.35 (m, 2H), 2.84 (t, J = 7.7 Hz, 2H), 1.64 – 1.58 (m, 1H), 1.52 – 1.46 (m, 1H), 1.32 – 1.28 (m, 18H). ^{13}C NMR (101 MHz, $CDCl_3$) δ 177.3, 151.7, 138.0, 131.2, 123.0, 120.6, 47.9, 45.7, 43.1, 35.0, 31.3.

Addition Polymerization General Procedure:

A stock solution of catalyst was prepared as described in Chapter 6. A quartz tube with a magnetic stir bar was charged with monomer (100 eq. relative to Pd), nitromethane or desired solvent (1.25 M with respect to monomer), and catalyst solution (0.027 M, 1 eq of Pd). The reaction vessel was then sealed and stirred in an oil bath kept at 70˚C for 24 hours. The polymer was then precipitated by pouring the reaction mixture dropwise into

either diethyl ether or methanol. The polymer was filtered, washed with precipitation solvent and then dried under vacuum at 60˚C overnight.

ROMP General Procedure:

ROMP polymers were made from the following general procedure. Monomers (100 eq. total) were added to a suitable round bottom flask equipped with a magnetic stir bar and rubber septum. DMF (10 ml/g of monomer) was added. When dissolution was complete, Grubbs second generation catalyst (1 eq) was added. The reaction was stirred at room temperature for one hour. After which ethyl vinyl ether (0.5 ml) was added to terminate the reaction. The viscous liquid was then precipitated in vortexing methanol. Polymer was collected via vacuum filtration and dried *in vacuo* overnight at 60˚C to produce a stringy solid.

General Procedure for TMA Salts:

In a 10 mL scintillation vial, a given sample of polymer was added to 10 mL of 50% aqueous trimethylamine. The vial was sealed and stirred until the polymer was completely dissolved. Isolation of the salt was achieved by rotary evaporation. The solution of polymer in aq. TMA was diluted with 200 mL of THF and the solvent was removed *in vacuo*, yielding the TMA salt of the polymer.

General Thin Film Procedures (Island/Hole Test)

A ~1 wt% solution of top coat salt in methanol/TMA solution was spin coated onto the BCP film at ca. 2500 rpm, which produced a 15-25 nm thick film. For both BCPs, the confined island and hole test produced identical results with top coat film thicknesses between 10-100 nm (even thicker top coat films were not tested). Samples were annealed on a Thermolyne HP-11515B hot plate between 170 °C and 190 °C for about ten minutes and quickly cooled to room temperature on a solid metal block. Samples stripped with trimethylamine and methanol (one to three times). Stripped samples generally contained little (<2 nm) residual top coat as measured by ellipsometry. Optical microscope or AFM were then used to assess topography.

Appendix A: Thianaphthene Oxime Crystallography Data

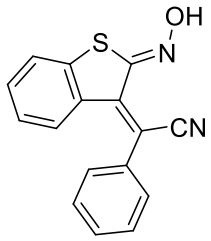

Figure A.1: View of **3.6** showing the atom labeling scheme. Displacement ellipsoids are scaled to the 50% probability level.

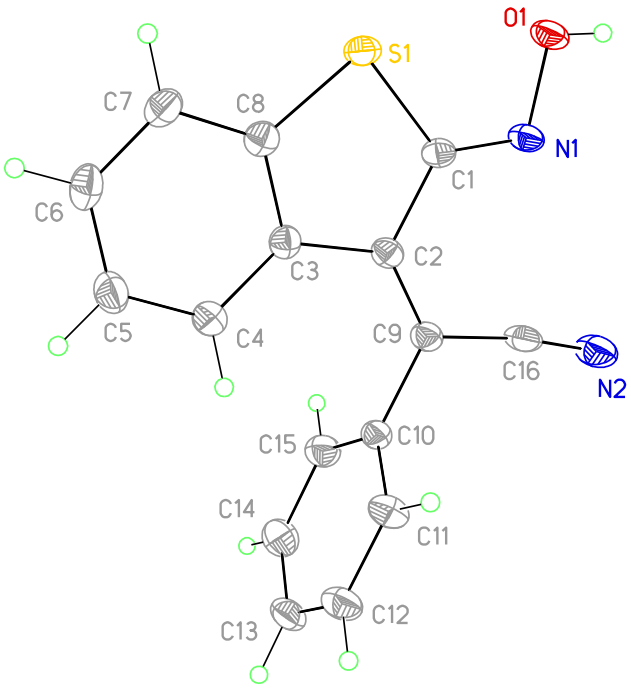

X-ray Experimental for $C_{16}H_{10}N_2OS$: Crystals grew as large, yellow prisms by slow evaporation from toluene. The data crystal was cut from a larger crystal and had approximate dimensions; 0.41 x 0.35 x 0.28 mm. The data were collected on a Rigaku

SCX-Mini diffractometer with a Mercury CCD using a graphite monochromator with MoKα radiation (λ = 0.71075Å). A total of 422 frames of data were collected using ω-scans with a scan range of 1° and a counting time of 12 seconds per frame. The data were collected at 153 K using a Rigaku XStream low temperature device. Details of crystal data, data collection and structure refinement are listed in Table 1. Data reduction were performed using the Rigaku Americas Corporation's Crystal Clear version 1.40.[1] The structure was solved by direct methods using SIR97[2] and refined by full-matrix least-squares on F^2 with anisotropic displacement parameters for the non-H atoms using SHELXL-97.[3] Structure analysis was aided by use of the programs PLATON98[4] and WinGX.[5] The hydrogen atoms on carbon were calculated in ideal positions with isotropic displacement parameters set to 1.2xUeq of the attached atom (1.5xUeq for methyl hydrogen atoms). The hydrogen atom bound to O1 was observed in a ΔF map and refined with an isotropic displacement parameter. The function, $\Sigma w(|F_o|^2 - |F_c|^2)^2$, was minimized, where $w = 1/[(\sigma(F_o))^2 + (0.0581*P)^2]$ and $P = (|F_o|^2 + 2|F_c|^2)/3$. $R_w(F^2)$ refined to 0.126, with R(F) equal to 0.0488 and a goodness of fit, S, = 1.03. Definitions used for calculating R(F), $R_w(F^2)$ and the goodness of fit, S, are given below.[6] The data were checked for secondary extinction effects but no correction was necessary. Neutral atom scattering factors and values used to calculate the linear absorption coefficient are from the International Tables for X-ray Crystallography (1992).[7] All figures were generated using SHELXTL/PC.[8] Tables of positional and thermal parameters, bond lengths and angles, torsion angles and figures are found elsewhere.

Empirical formula	C16 H10 N2 O S	
Formula weight	278.32	
Temperature	153(2) K	
Wavelength	0.71075 Å	
Crystal system	Triclinic	
Space group	P-1	
Unit cell dimensions	a = 6.857(4) Å	α= 99.571(14)°.
	b = 8.647(5) Å	β= 92.484(12)°.
	c = 11.426(7) Å	γ = 91.042(15)°.
Volume	667.2(7) $Å^3$	
Z	2	
Density (calculated)	1.385 Mg/m^3	
Absorption coefficient	0.238 mm^{-1}	
F(000)	288	
Crystal size	0.41 x 0.35 x 0.28 mm	
Theta range for data collection	2.39 to 27.50°.	
Index ranges	-8<=h<=8, -7<=k<=11, -14<=l<=14	
Reflections collected	5436	
Independent reflections	2984 [R(int) = 0.0493]	
Completeness to theta = 27.50°	97.7 %	
Absorption correction	Semi-empirical from equivalents	
Max. and min. transmission	1.00 and 0.691	
Refinement method	Full-matrix least-squares on F^2	
Data / restraints / parameters	2984 / 0 / 185	
Goodness-of-fit on F^2	1.033	
Final R indices [I>2sigma(I)]	R1 = 0.0488, wR2 = 0.1239	
R indices (all data)	R1 = 0.0530, wR2 = 0.1265	
Largest diff. peak and hole	0.321 and -0.382 $e.Å^{-3}$	

Table A.1: Crystal data and structure refinement for 3.6.

	x	y	z	U(eq)
C1	6350(2)	4019(2)	887(1)	18(1)
C2	5204(2)	4900(2)	1846(1)	18(1)
C3	3455(2)	3948(2)	2018(1)	18(1)
C4	1927(2)	4329(2)	2790(2)	24(1)
C5	401(2)	3253(2)	2810(2)	27(1)
C6	349(2)	1800(2)	2067(2)	27(1)
C7	1833(2)	1398(2)	1285(2)	25(1)
C8	3362(2)	2481(2)	1272(1)	20(1)
C9	5744(2)	6338(2)	2462(1)	19(1)
C10	4700(2)	7231(2)	3484(1)	19(1)
C11	3277(2)	8296(2)	3281(1)	25(1)
C12	2348(2)	9128(2)	4237(2)	28(1)
C13	2844(2)	8931(2)	5389(1)	28(1)
C14	4268(3)	7877(2)	5591(1)	30(1)
C15	5198(2)	7028(2)	4639(1)	25(1)
C16	7437(2)	7205(2)	2186(1)	24(1)
N1	7935(2)	4530(2)	498(1)	20(1)
N2	8712(2)	8041(2)	2059(1)	35(1)
O1	8618(2)	3376(2)	-394(1)	26(1)
S1	5341(1)	2138(1)	329(1)	23(1)

Table A.2: Atomic coordinates (x 10^4) and equivalent isotropic displacement parameters ($Å^2$x 10^3) for 3.6. U(eq) is defined as one third of the trace of the orthogonalized U^{ij} tensor.

References (for Appendix A)

1) DENZO-SMN. (1997). Z. Otwinowski and W. Minor, Methods in Enzymology, **276**: Macromolecular Crystallography, part A, 307 – 326, C. W. Carter, Jr. and R. M. Sweets, Editors, Academic Press.
2) SIR97. (1999). A program for crystal structure solution. Altomare, A., Burla, M. C., Camalli, M., Cascarano, G. L., Giacovazzo, C., Guagliardi, A., Moliterni, A. G. G., Polidori, G. and Spagna, R. J. Appl. Cryst. 32, 115-119.
3) Sheldrick, G. M. (2008). SHELXL97. Program for the Refinement of Crystal Structures. Acta Cryst., A64, 112-122.
4) Spek, A. L. (1998). PLATON, A Multipurpose Crystallographic Tool. Utrecht University, The Netherlands.
5) WinGX 1.64. (1999). An Integrated System of Windows Programs for the Solution, Refinement and Analysis of Single Crystal X-ray Diffraction Data. Farrugia, L. J. J. Appl. Cryst. 32. 837-838.
6) $R_w(F^2) = \{\Sigma w(|F_o|^2 - |F_c|^2)^2/\Sigma w(|F_o|)^4\}^{1/2}$ where w is the weight given each reflection.
   $R(F) = \Sigma(|F_o| - |F_c|)/\Sigma|F_o|\}$ for reflections with $F_o > 4(\sigma(F_o))$.
   $S = [\Sigma w(|F_o|^2 - |F_c|^2)^2/(n - p)]^{1/2}$, where n is the number of reflections and p is the number of refined parameters.
7) International Tables for X-ray Crystallography (1992). Vol. C, Tables 4.2.6.8 and 6.1.1.4, A. J. C. Wilson, editor, Boston: Kluwer Academic Press.
8) Sheldrick, G. M. (1994). SHELXTL/PC (Version 5.03). Siemens Analytical X-ray Instruments, Inc., Madison, Wisconsin, USA.

Bibliography

(1) Moore, G. "Cramming More Components Onto Integrated Circuits." *1965* **1965**.
(2) Mack, C. "Fundamental Principles Of Optical Lithography: The Science Of Microfabrication." 2008.
(3) Willson, C.; Ito, H.; Fréchet, J.; Tessier, T. "Approaches To The Design Of Radiation Sensitive Polymeric Imaging Systems With Improved Sensitivity And Resolution." *Journal of the Electrochemistry Society* **1986**, *133*, 181.
(4) Crivello, J. V. "The Discovery And Development Of Onium Salt Cationic Photoinitiators." *Journal of Polymer Science: Part A: Polymer Chemistry* **1999**, *37*, 4241-4254.
(5) Willson, G. C.; Frechet, J. M. J.; Eichler, E.; Ito, H. Poly(P-Tert-Butoxycarbonyloxystyrene): "A Convenient Precursor To P-Hydroxystyrene Resins." *Polymer 24*, 995-1000.
(6) Jeng, S.; Havemann, R.; Chang, M. "Process Integration And Manufacturasility Issues For High Performance Multilevel Interconnect." *MRS Proceedings* **1994**.
(7) Jensen, K. H.; Hanson, J. E. Synthesis And Photochemistry Of Tertiary Amine Photobase Generators. *Chemistry of Materials* **2002**, *14*, 918-923.
(8) Cameron, J.; Frechet, J. "Photogeneration Of Organic Bases From O-Nitrobenzyl-Derived Carbamates." *Journal of the American Chemical Society* **1991**, *113*, 4303-4313.
(9) Cameron, J.; Willson, C. "Photogeneration Of Amines From A-Keto Carbamates: Photochemical Studies." *Journal of the American Chemical Society* **1996**, *118*, 12925-12937.
(10) Frechet, J. M. "Amine Catalyzed Intramolecular Lmidization Of Alkyl And Aryl Phthalamates. Kinetics And Mechanism In Deuteriated Chloroform." *J. Chem. Soc. Perkin Trans.* **2003**, *2*, 2329-2333.
(11) Thompson, L.; Chin, T.; Kanga, R. "Characterization Of Novel Sulfonic Acid Photogenerating 2-Nitrobenzyl Ester Derivatives." *Journal of Vacuum Science and Technology B* **1990**, *8*, 1461.
(12) Merrifield, R. "Solid-Phase Peptide Synthesis." *Advances in Enzymology and Related Areas* **2006**, *85*, 2150.
(13) Houlihan, F.; Shugard, A.; Gooden, R. "Nitrobenzyl Ester Chemistry For Polymer Processes Involving Chemical Amplification." *Macromolecules* **1988**, *21*, 2001-2006.
(14) Davis, R.; Pizzini, L. "Condensation Of Aromatic Nitro Compounds With Acrylacetonitriles." 1, 2 II. Some P-Substituted Nitrobenzenes. *The Journal of Organic Chemistry* **1960**, *82*, 2913-2915.
(15) Hagiwara, Y.; Mesch, R. A.; Kawakami, T.; Okazaki, M.; Jockusch, S.; Li, Y.; Turro, N. J.; Willson, C. G. "Design And Synthesis Of A Photoaromatization-Based Two-Stage Photobase Generator For Pitch Division Lithography." *The Journal of Organic Chemistry* **2013**, *78*, 1730-1734.

(16) Isidro-Llobet, A.; Alvarez, M.; Albericio, F. "Amino Acid-Protecting Groups." *Chemical Reviews* **2009**, *109*, 2455-2504.
(17) Suyama, K.; Shirai, M. "Photobase Generators: Recent Progress And Application Trend In Polymer Systems." *Progress in Polymer Science* **2009**, *34*, 194-209.
(18) Smith, W. "Removal Of Chlorine From Aromatic Nitrochloro Compounds. Preparation Of 1, 3-Dinitronaphthalene." *Journal of the American Chemical Society* **1949**, *71*, 2855.
(19) Smith, W.; Campanaro, L. "Removal Of Halogen From Aromatic Nitrohalo Compounds." *Journal of the American Chemical Society* **1953**, *75*, 3602.
(20) Asakura, T.; Yamato, H.; Ohwa, M. "Novel Photoacid Generators." *Journal of Photopolymer Science and Technology* **2000**, *13*, 223-230.
(21) Suyama, K.; Araki, H.; Shirai, M. "Quaternary Ammonium Salt As DBU-Generating Photobase Generator." *Journal of Photopolymer Science and Technology* **2006**, *19*, 81-84.
(22) Duncan, J.; Silversmith, E. "Stereospecific Thermal Cycloadditions And Catalyzed Isomerizations: An Organic Laboratory Project." *Journal of Chemical Education* **1974**, *51*, 277.
(23) Asakura, T.; Yamato, H.; Tanaka, K.; Takahashi, R. "Studies On Photodecomposition Of An Oxime Sulfonate." *Journal of Photopolymer Science and Technology* **2014**, *27*, 227-230.
(24) Schiedler; Vellucci, J.; Beaudry, C. "Formation Of Carbon–Carbon Bonds Using Aminal Radicals." *Organic Letters* **2012**, *14*, 6092-6095.
(25) Schiedler, D. A.; Vellucci, J. K.; Lu, Y.; Beaudry, C. M. "The Development Of Carbon-Carbon Bond Forming Reactions Of Aminal Radicals." *Tetrahedron* **2015**, *71*, 1448-1465.
(26) E.; Russel, D. J. B. "The Evolution Of Build-Up Package Technology And Its Design Challenges." *IBM J. Res. & Dev.* **2005**, *49*, 641-21.
(27) Wan, X.; Jiang, X.; Wang, Q.; Yin, J. "A Nanoimprint Lithography Hybrid Photoresist Based On The Thiol–Ene System." *Advanced Functional Materials* **2011**, *21*, 2960-2967.
(28) Li, G.; Wang, L.; Ni, H.; Pittman, C. U., Jr. "Polyhedral Oligomeric Silsesquioxane (POSS) Polymers And Copolymers: A Review." *Journal of Inorganic and Organometallic Polymers* **2002**, *11*, 1-32.
(29) Tegou, E.; Bellas, V.; Gogolides, E.; Argitis, P.; Eon, D.; Cartry, G.; Cardinaud, C. "Polyhedral Oligomeric Silsesquioxane (POSS) Based Resists: Material Design Challenges And Lithographic Evaluation At 157 Nm." *Chemistry of Materials* **2004**, *16*, 2567-2577.
(30) Palmieri, F. Dissertation, University of Texas, 2008, pp. 1-230.
(31) Ho, P. S.; Lee, K.; Yoon, S.; Lu, X.; Ogawa, E. T. "Effect Of Low K Dielectrics On Electromigration Reliability For Cu Interconnects." *Materials Science in Semiconductor Processing* **2004**, *7*, 157-163.

(32) Kudo, T.; Machida, K.; Gordon, M. S. "Exploring The Mechanism For The Synthesis Of Silsesquioxanes." 4. The Synthesis Of T. *The Journal of Physical Chemistry A* **2005**, *109*, 5424-5429.
(33) Oyama, T.; Iijima, T.; Tomoi, M. "New Concept Of Positive Photosensitive Polyimide: Reaction Development Patterning (RDP)." *Journal of Polymer* **2001**.
(34) Jen, W. "Materials And Processes For Advanced Lithography Applications," University of Texas, 2009.
(35) Jacobsson, B. "Materials Development For Step And Flash Imprint Lithography," University of Texas, 2011.
(36) Long, B.; Keitz, B.; Willson, C. "Materials For Step And Flash Imprint Lithography (S-FIL®)." *Journal of Materials Chemistry* **2007**, *17*, 3565-3656.
(37) Fritz, N.; Saha, R.; Allen, S.; Kohl, P. "Photodefinable Epoxycyclohexyl Polyhedral Oligomeric Silsesquioxane." *Journal of Electronic Materials* **2010**, *39*, 149.
(38) Kohl, P. A. "Low–Dielectric Constant Insulators For Future Integrated Circuits And Packages." *Annual Review of Chemical and Biomolecular Engineering* **2011**, *2*, 379-401.
(39) Kehagias, N.; Zelsmann, M.; Chouiki, M. "Low Temperature Direct Imprint Of Polyhedral Oligomeric Silsesquioxane (POSS) Resist." *Microelectronic Engineering* **2011**, *88*, 1997-1999.
(40) Laine, R. M. "Nanobuilding Blocks Based On The [Osio1.5]X (X= 6, 8, 10) Octasilsesquioxanes." *Journal of Materials Chemistry* **2005**, *15*, 3725.
(41) Zuo, X.; Yu, R.; Shi, S.; Feng, Z.; Li, Z. "Synthesis And Characterization Of Photosensitive Benzocyclobutene-Functionalized Siloxane Thermosets." *Journal of Polymer Science Part A: Polymer Chemistry* **2009**, 6246-6258.
(42) Zuo, L. F. X. "Synthesis And Characterization Of Siloxane Resins Derived From Silphenylene-Siloxane Copolymers Bearing Benzocyclobutene Pendant Groups." *Journal of Polymer Science: Part A: Polymer Chemistry* **2008**, *46*, 7868-7881.
(43) Yang, J.; Cheng, Y.; Xiao, F. "Synthesis, Thermal And Mechanical Properties Of Benzocyclobutene-Functionalized Siloxane Thermosets With Different Geometric Structures." *European Polymer Journal* **2012**, *48*, 751-760.
(44) Harth, E.; van Horn, B.; Lee, V. Y.; Hawker, C. J. "A Facile Approach To Architecturally Defined Nanoparticles Via Intramolecular Chain Collapse." *Journal of the American Chemical Society* **2002**, *124*, 8653-8660.
(45) Ryu, D. Y. "A Generalized Approach To The Modification Of Solid Surfaces." *Science* **2005**, *308*, 236-239.
(46) Jensen, F.; Coleman, W.; Berlin, A. "Ring Opening Reactions Of Benzocyclobutene And Derivatives." *Tetrahedron Letters* **1962**.
(47) Volksen, W.; Miller, R. D.; Dubois, G. "Low Dielectric Constant Materials." *Chemical Reviews* **2010**, *110*, 56-110.
(48) Loke, A.; Wetzel, J.; Townsend, P.; Tanabe, T.; Vrtis, R.; Zussman, M.; Kumar, D.; Ryu, C.; Wong, S. "Kinetics Of Copper Drift In Low-K Polymer Interlevel Dielectrics." *IEEE Transactions on Electronic Devices* **1999**, *46*, 2178-2187.
(49) Maier, G. "Low Dielectric Constant Polymers For Microelectronics." *Progress in Polymer Science* **2001**, *26*, 3-65.

(50) Hodge, T.; Allen, S.; Kohl, P. A. "In Situ Measurement Of The Thermal Expansion Behavior Of Benzocyclobutene Films." *Journal of Polymer Science: Part A: Polymer Chemistry* **1999**, *37*, 311-321.
(51) Kohl, P. A.; Hodge, T. C.; Bidstrup, S. A. "An In-Situ Measurement Technique For Through-Plane Thermal Properties Of Thin Dielectric Films." *MCM Proceedings* **1994**, 344-349.
(52) Bidstrup, S.; Hodge, T.; Lin, L.; Kohl, P. "Anisotropy In Thermal, Electrical And Mechanical Properties Of Spin-Coated Polymer Dielectrics." *Materials Research Symposium* **1994**.
(53) Pye, J. E.; Roth, C. B. "Physical Aging Of Polymer Films Quenched And Measured Free-Standing Via Ellipsometry: Controlling Stress Imparted By Thermal Expansion Mismatch Between Film And Support." *Macromolecules* **2013**, *46*, 9455-9463.
(54) Briscoe, B.; Fiori, L.; Pelillo, E. "Nano-Indentation Of Polymeric Surfaces." *Journal of Physics D: Applied* **1998**, *31*, 2395.
(55) Oliver, W.; Pharr, G. "An Improved Technique For Determining Hardness And Elastic Modulus Using Load And Displacement Sensing Indentation Experiments." *Journal of materials Research* **1992**, *7*, 1564.
(56) Moran, M.; Casado, C. M.; Cuadrado, I. "POSS Synthesis." *Organometallics* **1993**, *12*, 4327-4333.
(57) Lewis, L. N.; Stein, J.; Gao, Y.; Colborn, R. E.; Hutchins, G. "Platinum Catalysts Used In The Silicones Industry: Their Synthesis and Activity in Hydrosilylation." *Platinum Metals Review* **1997**, *41*, 66-75.
(58) Marciniec, B.; Maciejewski, H.; Pietraszuk, C.; Pawluc, P. "Hydrosilylation." Springer, 2009.
(59) Schmid, G.; Stewart, M.; Wetzel, J.; Palmieri, F.; Hao, J.; Nishimura, Y.; Jen, K.; Kim, E.; Resnick, D.; Liddle, J. "Implementation Of An Imprint Damascene Process For Interconnect Fabrication." *Journal of Vacuum Science and Technology B* **2006**, *24*, 1283.
(60) Zhang, C.; Laine, R. M. "Hydrosilylation Of Allyl Alcohol With : Octa(3-Hydroxypropyldimethylsiloxy)Octasilsesquioxane And Its Octamethacrylate Derivative As Potential Precursors To Hybrid Nanocomposites." *Journal of the American Chemical Society* **2000**, *122*, 6979-6988.
(61) Denmark, S.; Wang, Z. "Highly Stereoselective Hydrocarbation Of Terminal Alkynes Via Pt-Catalyzed Hydrosilylation/Pd-Catalyzed Cross-Coupling Reactions." *Organic Letters* **2001**, *3*, 1073-1076.
(62) Berthon-Gelloz, G.; Schumers, J.; de Bo, G.; Markó, I. E. "Highly-Selective Hydrosilylation Of Terminal And Internal Alkynes Catalyzed By A (Ipr)Pt(Diene) Complex." *The Journal of Organic Chemistry* **2008**, *73*, 4190-4197.
(63) Mehta, G.; Kotha, S. "Recent Chemistry Of Benzocyclobutenes." *Tetrahedron* **2001**.
(64) Bosman, A.; Horn, B.; Hawker, C. "Production Of Crosslinked, Hollow Nanoparticles By Surface-Initiated Living Free-Radical Polymerization." *Journal of Polymer Science: Part A: Polymer Chemistry* **2002**, *40*, 1309-1320.
(65) Sadana, A. K.; Saini, R. K.; Billups, W. E. "Cyclobutarenes And Related Compounds." *Chemical Reviews* **2003**, *103*, 1539-1602.

(66) Hickenboth, C. R.; Moore, J. S.; White, S. R.; Sottos, N. R.; Baudry, J.; Wilson, S. R. "Biasing Reaction Pathways With Mechanical Force." *Nature* **2007**, *446*, 423-427.
(67) Baker, J. S. "Synthesis Of Functional Vinylbenzocyclobutenes For Use As Crosslinkers In The Preparation Of Amphiphilic Nanoparticles," University of Akron, 2011, pp. 1-238.
(68) Pugh, C.; Baker, J. S.; Storms, W. K. "Synthesis Of A Polymerizable Benzocyclobutene That Undergoes Ring-Opening Isomerization At Reduced Temperature." *Synlett* **2013**, *24*, A-E.
(69) Dobish, J. N.; Hamilton, S. K.; Harth, E. "Synthesis Of Low-Temperature Benzocyclobutene Cross-Linker And Utilization." *Polymer Chemistry* **2012**, *3*, 857.
(70) Stevens, R.; Bisacchi, G. "An Efficient And Remarkably Regioselective Synthesis Of Benzocyclobutenones From Benzynes And 1, 1-Dimethoxyethylene." *The Journal of Organic Chemistry* **1982**, *47*, 2393-2396.
(71) Skorcz, J.; Robertson, J. "New 1-Aminomethylbenzocyclobutenes." *Journal of Medicinal Chemistry* **1965**, *8*, 255-257.
(72) Tadross, P. M.; Stoltz, B. M. "A Comprehensive History Of Arynes In Natural Product Total Synthesis." *Chemical Reviews* **2012**, *112*, 3550-3577.
(73) Chen, P.; Savage, N.; Dong, G. "Concise Synthesis Of Functionalized Benzocyclobutenones." *Tetrahedron* **2014**, *70*, 4135-4146.
(74) Chino, K.; Takata, T.; Endo, T. "Polymerization Of O-Quinodimethanes Bearing Electron-Donating Groups In Situ Formed By Thermal Isomerization Of Benzocyclobutenes." *Macromolecules* **1997**, *30*, 6715-6720.
(75) Chino, K.; Takata, T.; Endo, T. "Polymerization Of O-Quinodimethanes. III. Polymerization Of O-Quinodimethanes Bearing Electron-Withdrawing Groups Formed In Situ By Thermal Ring-Opening." *Polymer Science Part A: Polymer* **1999**, *37*, 1555-1563.
(76) Swamy, K.; Kumar, N.; Balaraman, E. "Mitsunobu And Related Reactions: Advances And Applications." *Chemical Reviews* **2009**, *109*, 2551-2651.
(77) Bielawski, C. "Tailoring Polymer Synthesis With Designer Ruthenium Catalysts," California Institute of Technology, 2002.
(78) Bates, C.; Chang, A.; Momčilović, N.; Jones, S. "ABA Triblock Brush Polymers: Synthesis, Self-Assembly, Conductivity, And Rheological Properties." *Macromolecules* **2015**, *48*, 4967-4973.
(79) Alder, K.; Windemuth, E. *Chemische Berichte* **1938**, *71B*, 2409.
(80) Alder, K.; Stein, A. *Justus Liebigs Ann. Chem.* **1932**, *496*, 204.
(81) Rager, T.; Willson, C. "Synthesis And Characterization Of Diastereoisomerically Pure Tetracyclo [6.2.1.13, 6.2.7] Dodec-9-Ene-4-Carboxylic Acid Derivatives." *Helvetica Chimica Acta* **2000**.
(82) Teo, Y.; Xia, Y. "Importance Of Macromonomer Quality In The Ring-Opening Metathesis Polymerization Of Macromonomers." *Macromolecules* **2015**, *48*, 5656-5662.
(83) So, Y.; Hahn, S.; Li, Y. "Styrene 4-Vinylbenzocyclobutene Copolymer For Microelectronic Applications." *Journal of Polymer Science Part A: Polymer Chemistry* **2008**, *46*, 2799-2806.

(84) Ohba, K. "Overview Of Photo-Definable Benzocyclobutene Polymer." *Journal of Photopolymer Science and Technology* **2002**, *15*, 177-182.
(85) Benedikt, G. "Ring-Opened Polynorbornene Negative Photoresist With Bisazide," US Patent 4571375. February 18, 1986.
(86) Janiak, C.; Lassahn, P. "The Vinyl Homopolymerization Of Norbornene." *Macromolecular Rapid Communications* **2001**, *22*, 479-492.
(87) Okoroanyanwu, U.; Byers, J.; Shimokawa, T. "Alicyclic Polymers For 193 Nm Resist Applications: Lithographic Evaluation." *Chemistry of Materials.* **1998**.
(88) Walter, M. D.; Moorhouse, R. A.; Urbin, S. A.; White, P. S.; Brookhart, M. "Γ-Agostic Species As Key Intermediates In The Vinyl Addition Polymerization Of Norbornene With Cationic (Allyl)Pd Catalysts: Synthesis And Mechanistic Insights." *Journal of the American Chemical Society* **2009**, *131*, 9055-9069.
(89) Commarieu, B.; Claverie, J. P. "Bypassing The Lack Of Reactivity Of Endo-Substituted Norbornenes With The Catalytic Rectification–Insertion Mechanism." *Chem. Sci.* **2015**, *6*, 2172-2181.
(90) Reinmuth, A.; Melia, J.; Swords, N.; Risse, W. "(H3-Allyl) Palladium (II) And Palladium (II) Nitrile Catalysts For The Addition Polymerization Of Norbornene Derivatives With Functional Groups." *Macromolecules* **1996**, *29*, 2755-2763.
(91) Reed, C. A. Carborane Acids. "New Strong Yet Gentle Acids For Organic And Inorganic Chemistry." *Chemical Communications* **2005**, 1669.
(92) Reed, C. "Carboranes: A New Class Of Weakly Coordinating Anions For Strong Electrophiles, Oxidants, And Superacids." *Accounts of Chemical Research* **1998**.
(93) Hustad, P. D.; Marchand, G. R.; Garcia-Meitin, E. I.; Roberts, P. L.; Weinhold, J. D. "Photonic Polyethylene From Self-Assembled Mesophases Of Polydisperse Olefin Block Copolymers." *Macromolecules* **2009**, *42*, 3788-3794.
(94) Cen, C.; Thiel, S.; Mannhart, J.; Levy, J. "Oxide Nanoelectronics On Demand." *Science* **2009**, *323*, 1026-1030.
(95) Zheng, W.; Wang, Z. "Morphology Of ABC Triblock Copolymers." *Macromolecules* **1995**, *28*, 7215-7223.
(96) Bates, F.; Hillmyer, M.; Lodge, T.; Bates, C. "Multiblock Polymers: Panacea Or Pandora's Box?" *Science* **2012**.
(97) Mansky, P.; Russell, T.; Hawker, C.; Pitsikalis, M. "Ordered Diblock Copolymer Films On Random Copolymer Brushes." *Macromolecules* **1997**, *30*, 6810-6813.
(98) Bates, C. M.; Seshimo, T.; Maher, M. J.; Durand, W. J.; Cushen, J. D.; Dean, L. M.; Blachut, G.; Ellison, C. J.; Willson, C. G. "Polarity-Switching Top Coats Enable Orientation Of Sub-10-Nm Block Copolymer Domains." *Science* **2012**, *338*, 775-779.
(99) Bates, C. "Advanced Materials For Block Copolymer Lithography," University of Texas, 2013.
(100) Maher, M. J.; Bates, C. M.; Blachut, G.; Sirard, S.; Self, J. L.; Carlson, M. C.; Dean, L. M.; Cushen, J. D.; Durand, W. J.; Hayes, C. O. "Interfacial Design For Block Copolymer Thin Films." *Chemistry of Materials* **2014**, *26*, 1471-1479.
(101) Walton, D.; Kellogg, G.; Mayes, A.; Lambooy, P. "A Free Energy Model For Confined Diblock Copolymers." *Macromolecules* **1994**, *27*, 6225-6228.

(102) Chen, C. "Synthesis Of Top Coat Surface Treatments For The Orientation Of Thin Film Block Copolymers," University of Texas, 2013.
(103) Li, J.; Kato, J.; Kudo, K.; Shiraishi, S. "Synthesis And Properties Of Novel Soluble Polyimides Having An Unsymmetric Spiro Tricyclic Dianhydride Unit." *Chemistry and Physics* **2000**.